

“Smart” Hydrogels based on Trishydrophilic Triblock Terpolymers

DISSERTATION

zur Erlangung des akademischen Grades eines Doktors der
Naturwissenschaften (Dr. rer. nat.) im Fach Chemie der Fakultät für
Biologie, Chemie und Geowissenschaften der Universität Bayreuth

vorgelegt von

Stefan Reinicke

Geboren in Halle an der Saale

Bayreuth 2010

Die vorliegende Arbeit wurde in der Zeit von November 2006 bis September 2010 in Bayreuth am Lehrstuhl Makromolekulare Chemie II unter Betreuung von Herrn Prof. Dr. Axel H. E. Müller angefertigt.

Vollständiger Abdruck der von der Fakultät Biologie, Chemie und Geowissenschaften der Universität Bayreuth genehmigten Dissertation zur Erlangung des akademischen Grades eines Doktors der Naturwissenschaften (Dr. rer. nat.).

Promotionsgesuch eingereicht am:	28.09.2010
Zulassung durch die Promotionskommission:	27.10.2010
Wissenschaftliches Kolloquium:	01.03.2011

Amtierender Dekan: Prof. Dr. Stephan Clemens

Prüfungsausschuss:

Prof. Dr. Axel H. E. Müller (Erstgutachter)
Prof. Dr. Thomas Hellweg (Zweitgutachter)
Prof. Dr. Andreas Fery (Vorsitzender)
Prof. Dr. Jürgen Senker

*I think perhaps the most important problem is that
we are trying to understand the fundamental
workings of the universe via a language devised for
telling one another when the best fruit is.*

Terry Pratchett

*Dedicated to Carina
and my family*

Summary/ Zusammenfassung	1
1 Introduction	6
1.1 Stimuli-responsive polymers	6
1.1.1 Temperature- and pH-sensitivity	7
1.1.2 Additional stimuli	9
1.2 Magnetic nanoparticles	11
1.3 Structural definition and classification of gels	13
1.4 Stimuli-responsive (“smart”) hydrogels	16
1.4.1 Temperature- and pH-responsive hydrogels	17
1.4.2 Magneto-responsive hydrogels	19
1.4.3 Application fields for “smart” hydrogels	20
1.5 Experimental part	22
1.5.1 Block copolymer synthesis	22
1.5.2 Synthesis of magnetic nanoparticles and nanoparticle/ polymer hybrid structures	26
1.5.3 Rheology	27
1.5.4 Small angle neutron scattering (SANS)	32
1.5.5 Dynamic light scattering (DLS)	35
1.6 Objective of the thesis	37
1.7 References	39
2 Overview of the thesis	45
2.1 One-pot synthesis of polyglycidol-containing block copolymers with alkyllithium initiators using the phosphazene base <i>t</i> -BuP ₄	46
2.2 Smart hydrogels based on double responsive triblock terpolymers	48

2.3	Flow induced ordering in cubic gels formed by P2VP- <i>b</i> -PEO- <i>b</i> -P(GME- <i>co</i> -EGE) triblock terpolymer micelles: A rheo-SANS study	50
2.4	Combination of “living” anionic polymerization and ATRP via “click” chemistry as a versatile route to multiple responsive triblock terpolymers and corresponding hydrogels	52
2.5	Magneto-responsive hydrogels based on maghemite/triblock terpolymer hybrid micelles	56
2.6	Individual contributions to joint publications	58
3	One-pot synthesis of polyglycidol-containing block copolymers with alkyl lithium initiators using the phosphazene base <i>t</i>-BuP₄	61
4	Smart hydrogels based on double responsive triblock terpolymers	77
5	Flow induced ordering in cubic gels formed by P2VP-<i>b</i>-PEO-<i>b</i>-P(GME-<i>co</i>-EGE) triblock terpolymer micelles: A rheo-SANS study	107
6	Combination of “living” anionic polymerization and ATRP via “click” chemistry as a versatile route to multiple responsive triblock terpolymers and corresponding hydrogels	134
7	Magneto-responsive hydrogels based on maghemite/triblock terpolymer hybrid micelles	167
8	Appendix	205
8.1	Thermo-sensitive polymers with tunable LCST based on modified polyglycidol	205
8.2	List of publications	208
8.3	Contributions to national and international conferences	210
	Glossary	212
	Acknowledgements	216

Summary

The work presented in this thesis focuses on the synthesis of double stimuli-responsive, trishydrophilic triblock terpolymers and their utilization for the construction of “smart” hydrogel systems, responding to a variety of external stimuli. The central focus was put on ABC triblock terpolymers composed of a pH-sensitive A block, a water soluble B block and a thermo-sensitive or multi-responsive C block. This concept was used for the construction of hydrogels responding independently to pH, temperature, and UV light. It was further applied to the formation of polymer/nanoparticle hybrid micelles suitable for the formation of magneto-responsive hydrogels (ferrogels).

At first, a new route for the synthesis of block copolymers, containing ethylene oxide and glycidol derivatives, was developed. The crucial aspect of this procedure, based on sequential anionic polymerization, was the utilization of the phosphazene base *t*-BuP₄, enabling the anionic polymerization of epoxide monomers in the presence of lithium counterions. It was shown, that ethoxyethyl glycidyl ether polymerizes easily under the established polymerization conditions without unwanted termination. Hence, we were able to synthesize well-defined block copolymers containing vinyl and epoxide monomers in a one-pot reaction, without performing additional intermediate steps.

This new synthetic route was then utilized to synthesize a series of poly(2-vinylpyridine)-*block*-poly(ethylene oxide)-*block*-poly(glycidyl methyl ether-*co*-ethyl glycidyl ether) (P2VP-*b*-PEO-*b*-P(GME-*co*-EGE)) triblock terpolymers suitable for pH and temperature dependent hydrogel formation. The reversible gelation for this particular system relies on two distinct mechanisms. Under conditions, where only one outer block is insoluble, core-shell-corona (CSC) micelles are formed, resulting in gelation via close cubic packing of the micelles. On the other hand, the micelles are also able to crosslink through their corona when both outer blocks are insoluble. As a direct consequence, a temperature triggered gel-sol-gel transition occurred at pH = 7, accompanied by a unique gel strengthening. Solubility and gelation studies were performed by DLS, rheology and SANS. The influence of polymer concentrations and block lengths on the gelation behavior and gel properties was studied.

In order to derive information about the exact structure of the cubic lattice formed in the low temperature gel phase (simple cubic or body centered cubic), a 19 wt% aqueous solution of P2VP₅₆-*b*-PEO₄₁₀-*b*-P(GME₄₈-*co*-EGE₄₈) at pH = 7 was further investigated using SANS

under steady shear. By application of shear stress, the irregularly arranged polydomains of the sample oriented macroscopically along a preferred direction, which led to highly defined, strongly anisotropic 2D scattering patterns. The interpretation of these patterns confirmed the presence of a body centered cubic packing. The gel-sol transition upon temperature increase can be explained by a shrinkage of the shell of the CSC micelles.

To increase the versatility of the established hydrogel concept, we further synthesized ABC triblock terpolymers with different responsive polymers as C blocks. This required an alternative synthetic route, combining anionic polymerization and ATRP via “click” chemistry. After optimization of each synthetic step, exemplary poly(2-vinylpyridine)-*block*-poly(ethylene oxide)-*block*-poly(oligo(ethylene glycol) methacrylate) (P2VP-*b*-PEO-*b*-POEGMA) and poly(2-vinylpyridine)-*block*-poly(ethylene oxide)-*block*-poly(dimethylaminoethyl methacrylate) (P2VP-*b*-PEO-*b*-PDMAEMA) triblock terpolymers were synthesized, respectively, and characterized regarding their solubility and gelation behavior. At pH > 5, P2VP₅₆-*b*-PEO₃₇₀-*b*-PDMAEMA₇₀ forms CSC micelles with a P2VP core, and a pH- as well as thermo-sensitive PDMAEMA corona. This particular structure represents a hydrogel, whose temperature dependent response can be easily changed from a gel-sol to a sol-gel transition by increasing the pH from 8 to 9. At pH = 7.5 on the other hand, gel formation is induced by the addition of hexacyanocobaltate(III) ([Co(CN)₆]³⁻) ions due to electrostatic interactions between the [Co(CN)₆]³⁻ ions and the charged DMAEMA units, causing a physical crosslinking of the CSC micelles. The gel can subsequently be disintegrated by an exposure to UV-light, based on a UV-catalyzed aquation of the [Co(CN)₆]³⁻ ions to [Co(CN)₅H₂O]²⁻.

In the last part, a new approach was developed to create a novel type of magnetic field-responsive hydrogels (ferrogels), in which the nanoparticles are tightly bound to the polymer matrix. The P2VP block of the previously synthesized P2VP-*b*-PEO-*b*-P(GME-*co*-EGE) triblock terpolymers was quaternized to a low extent and complexed with negatively charged, citrate stabilized maghemite (γ -Fe₂O₃) nanoparticles. Using different analytical methods it was shown that well-defined CSC hybrid micelles were obtained with cores formed by a complex of P2VP and 3-4 nanoparticles per core. Concentrated solutions of these micelles are able to form gels depending on temperature, as revealed by rheology measurements. Due to the presence of the maghemite particles, it is possible to induce gelation via remote heating using AC magnetic fields, which was demonstrated by high frequency magnetocalorimetry.

Zusammenfassung

Die vorliegende Arbeit befasste sich mit der Synthese von doppelt stimuli-sensitiven, trishydrophilen Triblockterpolymeren und deren Einsatz zur Herstellung "intelligenter" Hydrogelsysteme, welche auf verschiedene externe Stimuli reagieren. Der Schwerpunkt der Arbeit lag dabei auf ABC Triblockterpolymeren bestehend aus einem pH-sensitiven A-Block, einem wasserlöslichen B-Block und einem thermo- oder multi-sensitiven C-Block. Dieses Konzept wurde sowohl für die Herstellung von Hydrogelen angewendet, die unabhängig auf pH- und Temperaturänderungen sowie UV-Licht reagieren, als auch zur Synthese von Polymer/Nanopartikel-Hybridmizellen, die sich zur Herstellung von Ferrogelen eignen.

Zu Beginn wurde ein Syntheseweg für die Herstellung von Blockcopolymeren, welche Ethylenoxid und Glycidolderivate enthalten, entwickelt. Der entscheidende Punkt dieses auf sequentieller anionischer Polymerisation basierenden Synthesewegs war der Einsatz der Phosphazenenbase $t\text{-BuP}_4$, da diese die anionische Polymerisation von Epoxidmonomeren auch in der Gegenwart von Lithiumgegenionen ermöglicht. Es konnte gezeigt werden, dass Ethoxyethylglycidylether unter den gewählten Bedingungen ohne unerwünschte Abbruchreaktionen polymerisiert. Dadurch konnten definierte Blockcopolymere, die sowohl Vinyl- als auch Epoxidmonomere enthalten, in einer Ein-Topf-Reaktion hergestellt werden, ohne weitere Zwischenschritte durchführen zu müssen.

Die neue Syntheseroute wurde anschließend genutzt, um eine Serie von Poly(2-vinylpyridin)-*block*-polyethylenoxid-*block*-poly(glycidylmethylether-*co*-ethylglycidylether) (P2VP-*b*-PEO-*b*-P(GME-*co*-EGE)) Triblockterpolymeren zu synthetisieren, die pH- und temperaturabhängig Hydrogele bilden. Die reversible Gelierung des gewählten Systems basiert dabei auf zwei verschiedenen Mechanismen. Wenn nur einer der beiden Außenblöcke unlöslich ist, bilden sich Kern-Schale-Korona (CSC) Mizellen, die sich in einer kubisch-dichtesten Packung anordnen. Der zweite Gelierungsmechanismus beruht auf der Möglichkeit, die Mizellen über ihre Korona zu vernetzen, indem der zweite Außenblock ebenfalls unlöslich geschaltet wird. Als direkte Konsequenz konnte bei $\text{pH} > 5$ und entsprechender Temperaturerhöhung ein Gel-Sol-Gel Übergang beobachtet werden, welcher mit einer ungewöhnlichen Gelverfestigung einhergeht. Untersuchungen zur Löslichkeit und zum Gelierungsverhalten wurden mittels DLS, Rheologie und SANS durchgeführt. Desweiteren wurde der Einfluss der Blocklängen und Konzentrationen auf die Geleigenschaften studiert.

Im Anschluss wurde eine 19 %ige Lösung von P2VP₅₆-*b*-PEO₄₁₀-*b*-P(GME₄₈-*co*-EGE₄₈) bei pH = 7 weiter untersucht um die exakte Struktur der kubisch-dichtesten Mizellpackung (kubisch primitiv oder kubisch raumzentriert) innerhalb des Gels bei niedriger Temperatur zu bestimmen. Dazu wurden SANS Messungen unter dem Einfluss von Scherung durchgeführt. Durch das Anlegen einer Scherkraft orientieren sich die zunächst irregulär angeordneten Polydomänstrukturen makroskopisch entlang einer Vorzugsrichtung, was zu hochdefinierten, anisotropen 2D-Streubildern führt. Die Interpretation dieser Muster ergab, dass es sich um eine kubisch raumzentrierte Packung handelt. Der bei Temperaturerhöhung stattfindende Gel-Sol Übergang kann mit einem Schrumpfen der Mizellschale erklärt werden.

Um die Vielseitigkeit unseres Hydrogelkonzeptes zu erhöhen, haben wir es in einem nächsten Schritt auf ABC Triblockterpolymere mit anderen stimuli-sensitiven Polymeren als C-Blöcke erweitert. Dieses Anliegen verlangte jedoch eine alternative Syntheseroute, welche anionische Polymerisation mit ATRP über „Click“-Chemie kombiniert. Nach der Optimierung der einzelnen Syntheseschritte wurden exemplarische Poly(2-vinylpyridin)-*block*-polyethylenoxid-*block*-poly(oligoethylenglykol)methacrylat (P2VP-*b*-PEO-*b*-POEGMA) und Poly(2-vinylpyridin)-*block*-polyethylenoxid-*block*-polydimethylaminoethylmethacrylat (P2VP-*b*-PEO-*b*-PDMAEMA) Triblockterpolymere synthetisiert und bezüglich ihres Löslichkeits- und Gelierungsverhaltens charakterisiert. Bei pH > 5 bilden sich aus P2VP₅₆-*b*-PEO₃₇₀-*b*-PDMAEMA₇₀ CSC Mizellen mit einem P2VP-Kern und einer pH- und thermo-sensitiven PDMAEMA Korona. Diese spezielle Struktur führt zu einem Hydrogel, dessen thermo-sensitives Verhalten sich durch einfache Erhöhung des pH-Werts von 8 auf 9 von einem Gel-Sol- zu einem Sol-Gel-Übergang umschalten lässt. Bei pH = 7.5 dagegen kann eine Gelbildung durch die Zugabe von Hexacyanocobaltat(III)-ionen induziert werden, bedingt durch einen Vernetzungseffekt basierend auf elektrostatischen Wechselwirkungen zwischen [Co(CN)₆]³⁻ Ionen und geladenen DMAEMA Einheiten. Dieses Gel lässt sich anschließend durch eine UV-katalysierte Hydratation der [Co(CN)₆]³⁻ Ionen zu [Co(CN)₅H₂O]²⁻ (Photo-Aquation) wieder zerstören.

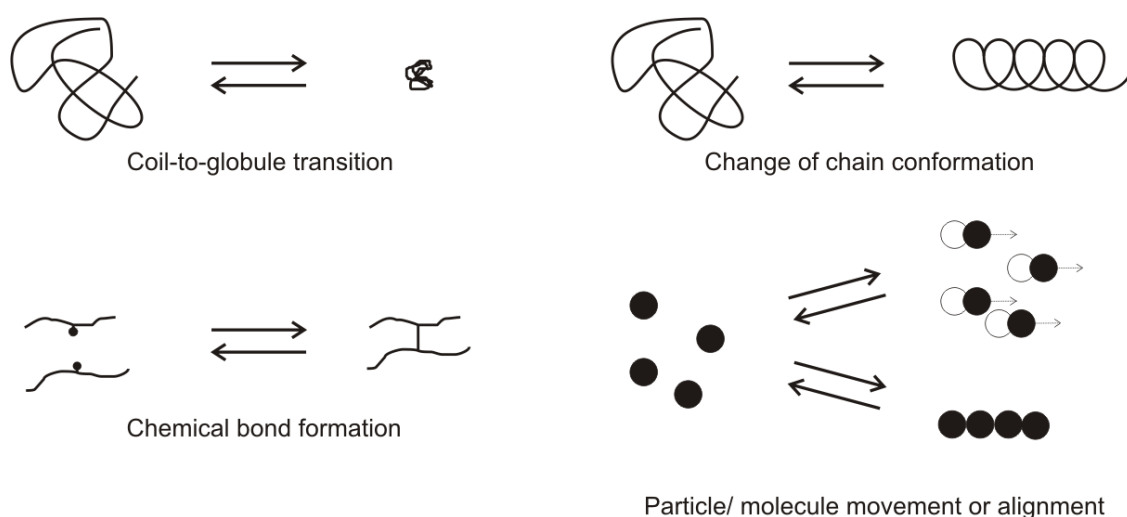
Im letzten Teil der Arbeit wurde ein neues Konzept zur Herstellung neuartiger magnetfeldsensitiver Hydrogele (Ferrogele), in denen die entsprechenden Nanopartikel fest an die Polymermatrix gebunden sind, entwickelt. Der P2VP-Block der zuvor synthetisierten P2VP-*b*-PEO-*b*-P(GME-*co*-EGE) Triblockterpolymere wurde zu einem geringen Grad quaternisiert und mit negativ geladenen, citratstabilisierten Maghemitnanopartikeln (γ -Fe₂O₃) komplexiert. Mittels verschiedener Analysemethoden konnte gezeigt werden, dass dieses Verfahren zu

wohldefinierten CSC-Hybridmizellen führt, deren Kern aus einem Komplex aus quaternisiertem P2VP und je 3-4 Nanopartikeln besteht. Konzentrierte Lösungen dieser Mizellen sind in der Lage temperaturabhängig zu gelieren, was mittels Rheologiemessungen demonstriert wurde. Durch die Anwesenheit der Maghemitpartikel ist es zudem möglich, eine Gelbildung zu induzieren, welche auf Hitzeentwicklung durch das Anlegen eines magnetischen Wechselfelds basiert. Dies konnte durch Hochfrequenz-Magnetokalorimetriemessungen gezeigt werden.

1 Introduction

1.1 Stimuli-responsive polymers

Stimuli-responsive or “smart” materials are defined as materials that respond with a large property change on small changes in their physical and/ or chemical environment. There are numerous external stimuli which have to be considered, such as light, electric and magnetic fields, changes in ionic strength, solvent quality and so on. The two by far most important stimuli though are pH and temperature. One can distinguish between materials, where stimuli-responsiveness originates from one single component (e.g. a stimuli-responsive polymer) and such ones where the responsiveness is provided by interplay between several components (e.g. polymers in combination with special nanoparticles or salts). The primary response mechanism mostly relies on a change of solvent quality of the surrounding medium of the polymer, i.e. a transition of the polymer chains from a dissolved, highly swollen state to a more or less collapsed state. Other types of response are changes in chain conformation, reversible formations of chemical bonds, or response to mechanical stress within a polymer matrix induced by molecule/ particle movements (Scheme 1.1). These mechanisms can be “translated” into a variety of secondary or phenomenological response types depending on the nanoscopic and macroscopic structure and composition of a material. The coil-to-globule transition of a polymer chain for instance, can be utilized for the formation, deformation and/ or contraction of micellar aggregates^{1,2} or three-dimensional networks^{1,3,4}, the alternation of surface properties^{2,5} or simply a precipitation of a material. The reversible formation of chemical bonds on the other hand is mostly used for network formation or stabilization of aggregates.⁶ In the following, typical stimuli are introduced with the help of common examples.



Scheme 1.1. Primary response mechanisms to external stimuli.

1.1.1 Temperature- and pH-sensitivity

Thermo-sensitive polymers undergo a coil-to-globule transition upon a change of temperature. Most thermo-sensitive polymers exhibit a lower critical solution temperature (LCST), which means that they become insoluble in water upon temperature increase. In such a case, the polymer is solubilized through hydrogen bonds below the transition point. These bonds break up when the LCST is reached, causing a collapse of the insoluble polymer backbone. The by far most important thermo-sensitive polymer showing an LCST is poly(N-isopropyl acrylamide) (PNIPAAm),⁷⁻⁹ since it exhibits a sharp and quick coil-to-globule transition at 32 °C, which is favorable for many applications. The chemical structures of PNIPAAm and other thermo-sensitive polymers are shown in Figure 1.1. Recently, polymers like polyoxazolines^{10,11} and poly(oligo(ethylene glycol) methacrylate)s^{12,13} attracted growing interest, since their LCST can be tuned within a wide temperature range just by copolymerizing different oxazoline or OEGMA monomers, respectively. In general, the LCST of a thermo-sensitive polymer can be tuned by incorporating comonomers, either increasing (high polarity of comonomer) or decreasing (low polarity of comonomer) the LCST.

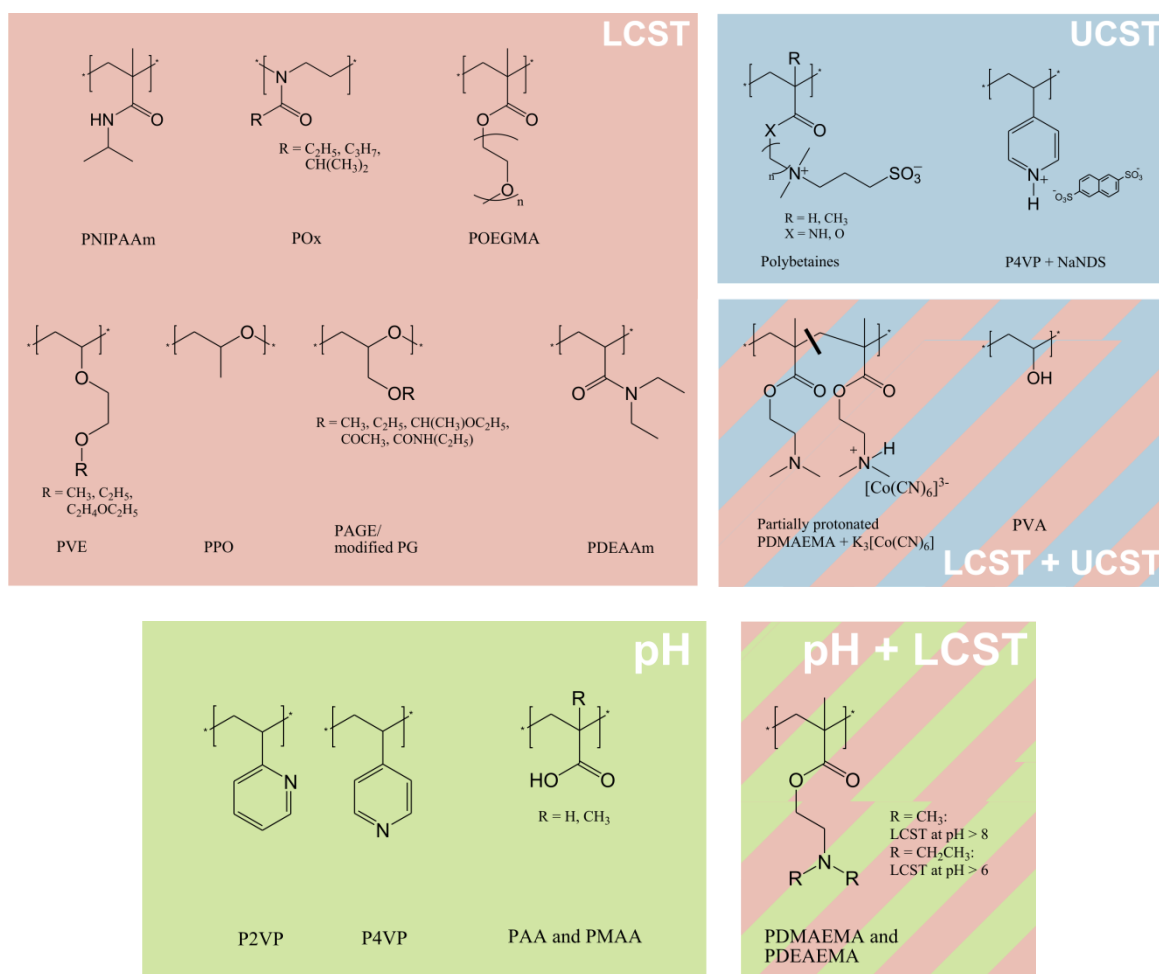


Figure 1.1. Chemical structures of temperature- and pH-sensitive polymers.

Polymers can also become soluble upon temperature increase. In such a case the polymer exhibits an upper critical solution temperature (UCST). In contrast to polymers showing an LCST, the number of polymers with a water-based UCST is limited. Most UCST-systems reported in literature deal with polymers dissolved in organic solvents or solvent combinations, as for instance poly(2-oxazoline)s in ethanol/ water mixtures¹⁴, or PNIPAAm in bis(2-methoxyethyl) ether (diglyme).¹⁵ Polymers, showing a UCST in water, are almost exclusively based on polybetaines, polymers exhibiting zwitterionic side groups.¹⁶⁻¹⁸ The driving force for the abrupt dissolution of the polybetaine at its UCST is based on a disintegration of zwitterionic clusters, formed via coulombic interactions. Temperature dependent coulombic interactions are also responsible for the occurrence of a UCST in the case of polycations interacting with multivalent counterions.^{19,20} Some rare examples are known showing both, a UCST and an LCST in aqueous solution, as for instance poly(vinyl alcohol) (PVA)²¹ and PDMAEMA in combination with hexacyanocobaltate at a suitable pH.¹⁹ As a concluding remark, it is noted that the transition temperatures do not only depend on the

chemical nature of the polymer. Usually the transition temperatures can be tuned within relatively narrow temperature ranges by adjusting parameters like polymer architecture, chain lengths, ionic strength, concentration and nature of end groups.

The class of pH-sensitive polymers is constituted by polybases and polyacids.^{1,3,22} Upon protonation or deprotonation of functional groups along the polymeric backbone, the pH-sensitive polymer changes from a charged, hydrophilic to an uncharged, less hydrophilic or completely hydrophobic state. The structures of the most frequently used polymers are shown in Figure 1.1. In some cases, polymers are thermo-responsive beyond a critical pH. PDMAEMA and PDEAEMA for instance exhibit LCST's at $\text{pH} > 8$ and $\text{pH} > 6$ respectively.^{23,24}

Polymers, being sensitive to pH and temperature at the same time can further be obtained by copolymerizing monomers, responding to different stimuli.^{25,26} NIPAAm for instance was copolymerized with *tert*-butyl acrylate, yielding a PNIPAAm-*co*-PAA copolymer after polymerization and deprotection.²⁷ The LCST of such a copolymer depends strongly on the pH.

1.1.2 Additional stimuli

The solubilization of several polar polymers can be manipulated via ionic strength adjustment. An increasing salt concentration for instance influences hydrogen bonding to PNIPAAm and therefore lowers the LCST to a considerable extent.²⁸ A very strong effect is observed for certain polyelectrolytes like poly(styrene sulfonic acid), due to a charge screening effect.²⁹ A strong effect occurs further in the case of polymers capable of complexing ions. A strong response to several cations for instance is reported for polymers which carry crown ether side groups, known to have a strong coordination effect for particular alkaline and alkaline earth metal cations.³⁰ Cyclodextrine substituents on the other hand interact with a variety of compounds via host-guest complexation.³¹ In some cases, polymers respond selectively to the presence of a specific compound in the solution. Polymers, carrying phenylboronic acid derivatives for instance respond to the presence of glucose.⁶ Specific binding sites in general are used to obtain systems which respond to certain proteins or other biomolecules.^{6,32}

Another stimulus is based on redox reactions and related to that, electric fields. Such a stimulus is expressed for instance by a reversible formation of chemical bonds through a

redox mechanism. A particular example is the formation of disulfide bonds from thiol groups.⁶ Another mechanism includes the chemical modification of multivalent counterions interacting with polyelectrolytes. The counterions change their valency through the redox process, which in turn causes the transition of the polymer from a collapsed to a swollen state or vice versa.³³ Response to electric fields finally is also based on the movement of ions or ionic moieties in such fields. Such a movement induces mechanical stress to which the polymer responds to either in a direct manner (if ionic groups are integral part of the polymer chains) or by changes in osmotic pressure due to movement of free ions.^{6,32}

Light sensitivity is expressed by numerous mechanisms. A phototriggered isomerization of polymeric substituents for instance can cause a change of chain conformation and/ or polarity. Such substituents are mostly based on azobenzene structures.^{6,32,34} Other substituents get ionized (e.g. spiropyran) or dimerized (e.g. cinnamate groups) upon irradiation.^{32,35} An indirect response to light is possible in the case of polyacids/ -bases when using them in combination with photoacid generators.³⁶ This approach however has not been tried so far. Finally, the valency of counterions of polyelectrolytes can be affected by exposure to light, such as UV-sensitive hexacyanocobaltate(III)-ions.¹⁹ Photoswitchable surfactants can be utilized as well.³⁷

The last group of stimuli-responsive materials is based on such responding to magnetic fields. In this case, responsiveness originates not from the polymer itself, but rather from inorganic, magnetic nanoparticles in the vicinity of polymer chains or networks which either orient or move within a magnetic field which in turn induces mechanical stress within a polymeric matrix.^{38,39} An indirect response is obtained when polymers are thermo-sensitive and the nanoparticles used are able to develop heat upon exposure to alternating magnetic fields.^{40,41} Since magneto-responsive systems are almost exclusively based on hydrogels, they will be discussed in more detail in section 1.4.2.

As a concluding remark, it is mentioned, that electro-, light- and magneto-responsive systems exhibit sensitivity to a field. Field-sensitivity has the great benefit to come along with no diffusion or heat transfer restrictions retarding the response to the stimulus.

1.2 Magnetic nanoparticles

Colloidal magnetic materials are mostly based on ferrimagnetic iron oxides, namely γ - Fe_2O_3 (maghemite) and Fe_3O_4 (magnetite) or mixed ferrites with the general composition $\text{Me}^{\text{II}}\text{Fe}^{\text{III}}_2\text{O}_4$ (Me = Co, Zn). Besides, also the ferromagnetic metals iron, cobalt and nickel are used.⁴² To preserve the colloidal stability, such nanoparticles are mostly surrounded by a protecting surfactant or polymer layer.⁴³

Downsizing the dimensions of a ferri- or ferromagnetic material from the macroscopic to the nanoscopic scale (diameter: 1–1000 nm) causes a dramatic change of its magnetic properties.^{44,45} Bulk materials exhibit nano- or micrometer sized magnetic domains, characterized by a parallel alignment of the magnetic moments within one domain, which in consequence causes a net magnetization even in the absence of outer fields (hysteresis). Below a certain critical size however, single domains are formed, whose magnetic field induced orientation is easily destroyed by thermal fluctuation. In such a case, the magnetization curves follow a symmetrical sigmoidal shape with no hysteresis (Fig. 1.2), analogous to the behavior of bulk paramagnetic materials, in which a magnetic moment is induced by an independent orientation of single atoms.

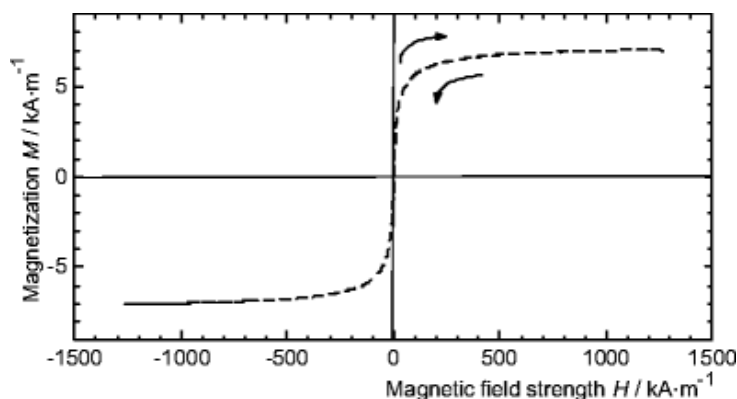
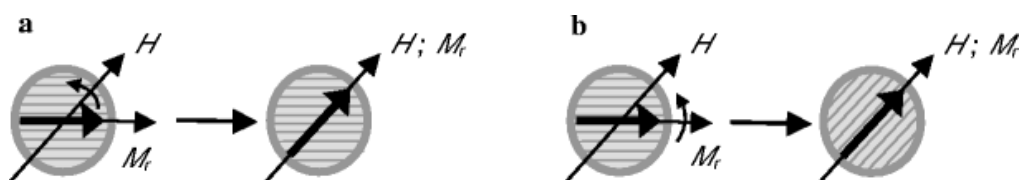


Figure 1.2. Magnetization curve of an electrostatically stabilized Fe_3O_4 -based magnetic colloid in water (1.8 vol% Fe_3O_4).⁴²

The magnetic moment of a single domain magnetic nanoparticle however appears to be three to four orders of magnitude higher than the corresponding moment in conventional paramagnetic materials. Such a behavior is termed as “superparamagnetic”. The critical diameter for superparamagnetic behavior is for instance 150 nm for Fe_3O_4 and 14 nm for cobalt and iron.⁴⁶

The remagnetization of magnetic nanoparticles can occur via two distinct mechanisms, Brownian motion or internal (Néel) relaxation (Scheme 1.2). In the first case, the ability to reorient, i.e. the relaxation time, depends mostly on the viscosity of the dispersing medium. In the case of Néel relaxation, activation against a crystal anisotropy barrier is necessary. The particle dimensions also have a great impact (Fig. 1.3).⁴⁷ Néel relaxation is influenced by the size of the magnetic core, whereas Brownian rotation strongly depends on the hydrodynamic diameter of the particle. Above a certain threshold particle size, Brownian rotation starts to dominate, since the crystal anisotropy barrier becomes too high to facilitate Néel relaxation. If such “blocked” particles are further immobilized within a polymeric matrix, magnetization can be preserved on a long time scale. A material, commonly used for such purposes is CoFe_2O_4 (cobalt ferrite), since the critical diameter for CoFe_2O_4 is only 7 nm.



Scheme 1.2. Schematic depiction of the Néel (a) and Brownian (b) remagnetization mechanism.⁴²

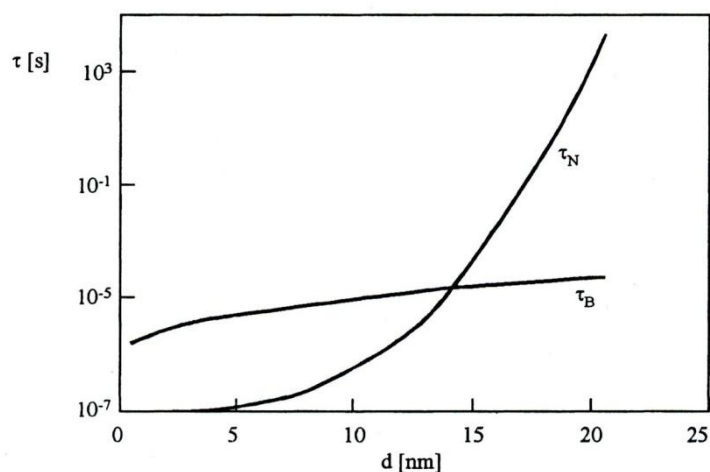


Figure 1.3. Brownian and Néel relaxation time for the magnetization of a magnetite ferrofluid with kinematic viscosity $\nu = 100 \text{ mm}^2/\text{s}$ as a function of particle size.⁴⁷

Magnetic nanoparticles are able to align themselves in uniform DC magnetic fields or move in the direction of the field gradient of non-uniform fields. In the presence of AC fields, heat is developed, due to a permanent reorientation of the particles. All these features are utilized for a variety of applications, including nanomotors and actuators, magnetic sensing and drug

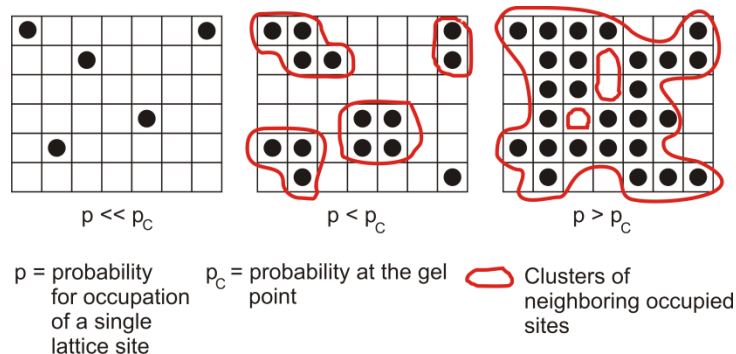
targeting, hyperthermia and by far most important: vacuum sealing rotary feedthroughs (e.g. in hard disk drives).^{48,49}

1.3 Structural definition and classification of gels

The word “gel” is frequently used not only in natural sciences but also in the normal life. Many industrial products or ingredients of such, especially in the food and cosmetics market, are labeled with the term “gel”. It is obvious that this term is often misused, especially - but not exclusively - outside the scientific world. This leads to the question, in which case the use of the word “gel” is reasonable and in which case not. In general, a gel can be defined by structural and rheological features. A rheological definition will be given in section 1.5.3, a quick structural definition shall be given here. In 1926, Jordan Lloyd defined gels as self-supporting materials which are composed of two different components, one of which is liquid and the other one solid.⁵⁰ A more exact structural definition considers gels as three-dimensional networks, swollen in a solvent to a certain, finite extent.⁵¹ This definition however accounts only for real networks, but not for structured liquids, also acting as gels from a rheological point of view. Furthermore, a swollen rubber for instance should be called a gel as well according to these definitions, even if the amount of liquid is very low and the rubber acts more like a solid. Almdal and Kramer added, that the liquid should be present in substantial quantity.⁵² This quantity was not clearly defined, but the authors stated at least, that liquid-like materials (which obviously contain a huge amount of liquid) could be gels as well. In a recent review, Nishinari concluded that a gel is a system consisting of molecules, particles, chains, etc., which are partially connected to each other in a fluid medium by crosslinks to the macroscopic dimensions.⁵³ It should be added, that the crosslinks can be real (e.g. in covalent networks) or apparent (e.g. in jammed micellar solutions).

The phenomenological picture of the gel point is rather clear. De Gennes and Stauffer pointed out the analogy between gelation and the percolation theory.^{54,55} The percolation theory utilizes a regular lattice in which each cavity is occupied by a structure building block with a certain probability p . If p increases, bigger and bigger clusters of building blocks occur. The critical probability p_c finally is the value, at which the cluster reaches a size which extends through the whole lattice (Scheme 1.3). With the words of Winter et al. a gel point is defined as the point where the weight-average molar mass of the apparent network diverges into

infinity (infinite sample size) or where the network first expands continuously throughout the whole sample volume (finite sample size).⁵⁶



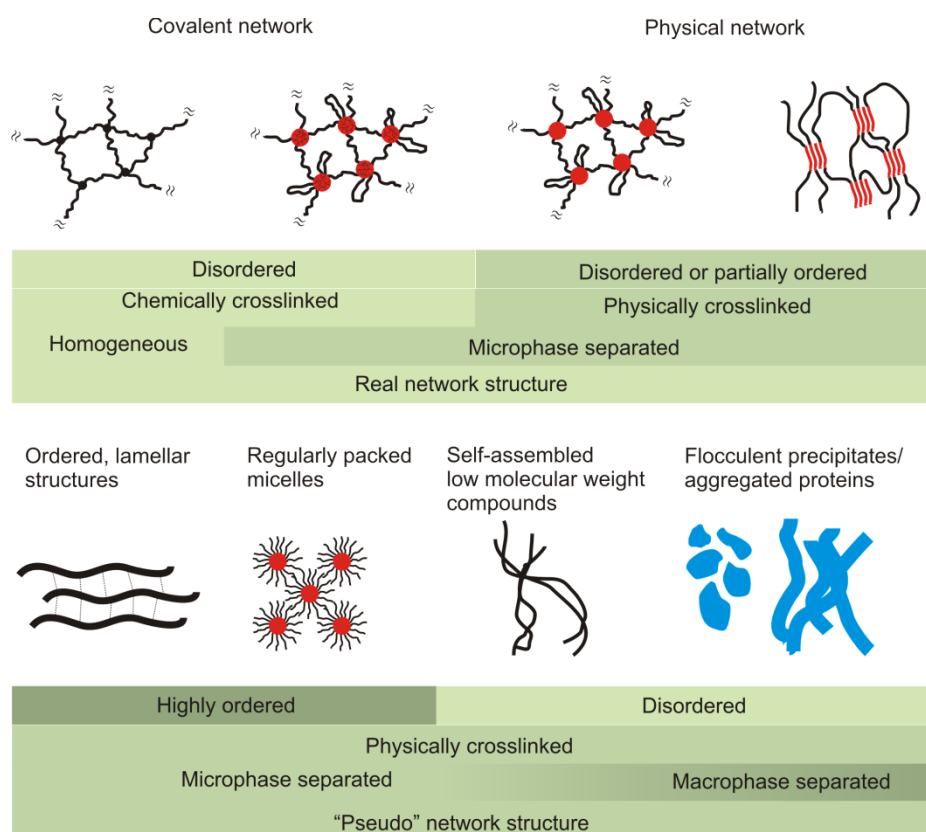
Scheme 1.3. Schematic depiction of the gelation process according to the percolation theory.

The structural classification of gels can be done with the help of several criteria like nature of the network junctions, structural order, homogeneity, and so on. In 1974, Flory defined four different gel classes:⁵⁷

1. Covalent polymeric networks; completely disordered
2. Polymer networks formed through physical aggregation; predominantly disordered, but with regions of local order
3. Well-ordered lamellar structures, including gel mesophases
4. Particulate, disordered structures

A schematic overview of the different gel classes is given in Scheme 1.4. The first class is constituted by gels composed of chemically crosslinked (covalent) networks, like polysiloxane based networks, polystyrene gels or vulcanized rubber. Such covalent networks exhibit punctual network junctions with no extension in space and a rather low functionality. The gel is homogeneous and no structural order is present. Furthermore, a covalent network can be considered as a single molecule of infinite size. However, a network can also consist of many molecules interacting through supramolecular (physical) aggregation (class 2). The network junctions in such a case are not punctual and have a rather high functionality. Due to the partial aggregation of the chains through crystallization or hydrophobic interactions, such a network can be considered as microphase separated. Depending on the particular nature of the physical crosslinks (crystalline or amorphous), the gel is either partially ordered or, analogous to the covalent networks, completely disordered. Networks of this type are for instance constituted of ABA type triblock copolymers, where only the B block is soluble in the liquid component. Most thermoplastic elastomers are based on such polymers.⁵⁸ Another

important class of polymers being able to form such networks are proteins like gelatin⁵⁹ or collagen⁶⁰. In such cases, the network junctions are formed by small crystalline domains. In some cases, physical networks can be subsequently transferred into covalent networks, if the aggregated chain sequences are chemically crosslinked after the network formation. Such a gel would consist of a covalent, microphase separated network.



Scheme 1.4. Basic structural classification of gels according to the degree of order, type of crosslinks, homogeneity and type of network.

The first two gel classes introduced so far include structures which can be considered as real networks. Gels, however, can also be composed of highly ordered structures, forming pseudo-networks due to attracting forces like hydrogen bonding, van-der-Waals or electrostatic forces. Such systems are often referred to as “structured liquids” (class 3) and consist of lamellar structures formed by a variety of surfactants⁶¹, phospholipids⁶² and clays like montmorillonite⁶³, and of other regularly packed micellar aggregates. The most common polymer-based gel of this type is formed by poly(ethylene oxide)-*block*-poly(propylene oxide)-*block*-poly(ethylene oxide) (PluronicTM) triblock copolymers.⁶⁴

It has to be noted, that the apparent network junctions of physical networks (class 2) and highly ordered structures (class 3) are often much weaker and much more dynamic than in the

case of covalent networks. Gel strengths therefore appear to be somewhat lower in most cases and gel like behavior occurs on shorter time scales and only on relatively weak mechanical deformation.

The fourth class of gels involves macrophase separated systems. Such systems are usually composed of particles with large geometric anisotropy, like needles, fibrils or networks of fibers such as in V_2O_5 gels.⁶⁵ Globular or fibrillar aggregates of proteins are also included in this class.⁶⁶ Fibrillar aggregates formed by certain low molecular weight compounds via supramolecular self assembly on the other hand mostly exhibit fibril diameters located on the submicrometer scale.⁶⁷ Therefore, it is reasonable to consider these systems as microphase rather than macrophase separated. It is further noted that also covalent networks can be macrophase separated (inhomogeneous network structure).⁶⁸ Such systems form an intermediate between class 1 and 4.

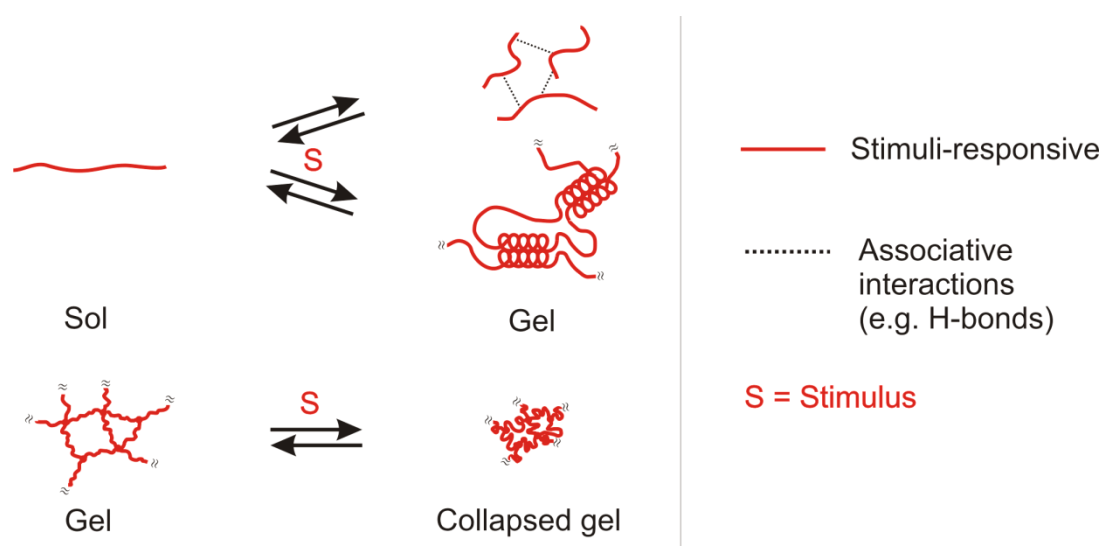
1.4 Stimuli-responsive (“smart”) hydrogels

Hydrogels are defined as gels, where the solid component of the gel is swollen in water. They are either obtained from natural sources like tissue and other biomaterials or from synthetic polymers. Gels belonging to the first class are mostly protein based (collagen, fibrin or polypeptides) or derived from polysaccharides (alginate, agarose, hyaluronic acid, dextran).^{60,69} Synthetic hydrogels are composed of chemically crosslinked poly(hydroxyethyl methacrylate) (PHEMA), poly(vinyl alcohol) (PVA), poly(ethylene oxide) (PEO), and several other water soluble polymers.^{60,68}

The term “smart” or stimuli-responsive in the special case of gels means the formation/ disintegration, swelling/ contraction, alteration of mechanical properties or deformation of such a gel upon small changes in its physical and chemical environment. Stimuli-responsive hydrogels are commonly based on synthetic polymers. A few natural polymers however, like cellulose derivatives, gelatin or chitosan can form “smart” hydrogels as well without the incorporation of additional stimuli-responsive polymers.⁵⁹ Most systems reported so far respond to pH and/ or temperature^{3,4,70} or alternatively to magnetic fields.^{38,39,41}

1.4.1 Temperature- and pH-responsive hydrogels

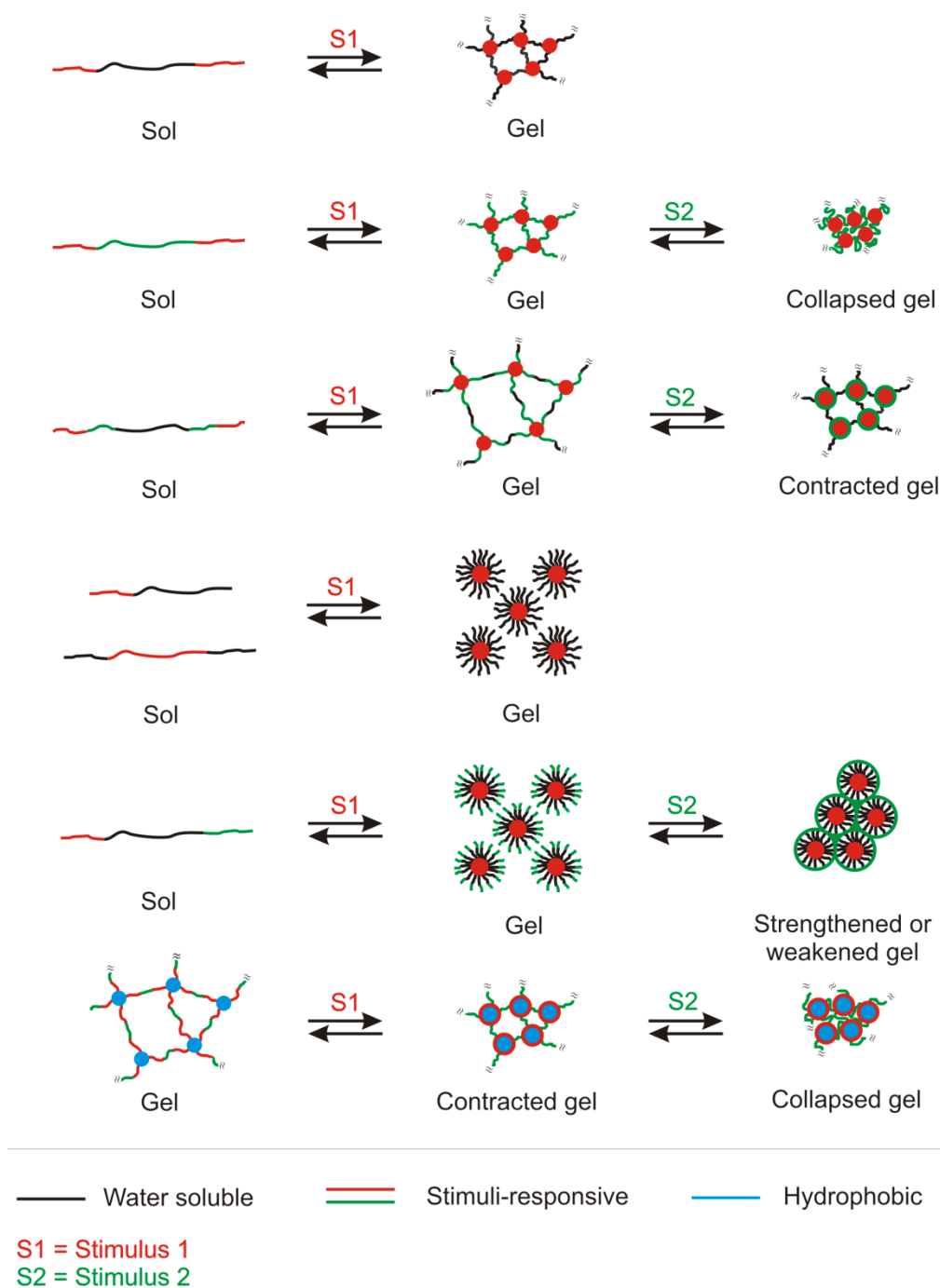
Temperature- and pH-responsive hydrogels are best classified by considering their polymer architecture and composition. Both criteria are strongly correlated to the particular response mechanism. Homo- and statistical copolymers are included in class 1 and 2 (Scheme 1.5) whereas block copolymer structures are summarized in the third class (Scheme 1.6). Class 1 involves all linear homopolymers which form physical networks through hydrogen bonding or partial crystallization upon a stimulus.^{59,60,69,71} The second class on the other hand considers chemically crosslinked polymers, which mostly respond via reversible contraction or deformation.^{3,72} Multi-responsive hydrogels can be obtained by copolymerizing monomers responding to different stimuli²⁵⁻²⁷ or by creating interpenetrating networks.⁷³ For some special purposes, the dimensions of such a network are limited to several hundred nanometers or a few micrometers. Such systems are called nano- or microgels and are commonly obtained through emulsion polymerization processes.^{26,27,74}



Scheme 1.5. “Smart” hydrogel systems based on linear and crosslinked homopolymers and statistical copolymers.

The third class includes a variety of block copolymer structures which exhibit an amphiphilic nature only at suitable conditions (Scheme 1.6).^{3,4,70} Depending on the particular block sequence, such block copolymers form either physical networks or micelles, which pack regularly above a certain critical volume fraction. By suitable combinations of different blocks, it is possible to create hydrogels which respond in a multi-step manner or can be addressed independently by different stimuli. ABC triblock terpolymers composed of poly(alkyl vinyl ether) blocks with different LCST’s for instance show a reversible gel

formation and a subsequent gel strengthening upon temperature increase⁷⁵, whereas a PDEAAm-*b*-PAA-*b*-PDEAAm triblock copolymer forms a gel upon temperature change which subsequently contracts when reaching a critical pH.⁷⁶ Block copolymer based hydrogels might also be permanently crosslinked, which is the case when network junctions are formed by hydrophobic blocks like PMMA⁷⁷ or PS⁷⁸, or a subsequent chemical crosslinking is carried out.⁷⁹ In such cases, the response of the gel is limited to a reversible contraction and/or collapse.



Scheme 1.6. A selection of “smart” hydrogels based on block copolymers.

1.4.2 Magneto-responsive hydrogels

Magneto-responsive hydrogels consist of stimuli-responsive or water soluble polymers in combination with magnetic nanoparticles.^{6,38,39} In the majority of all cases, the nanoparticles are entrapped within a three-dimensional, covalent network. Consequently, the response mechanisms are limited to a reversible contraction or deformation. The particular response is mainly determined by the type of magnetic field applied. Non-uniform DC magnetic fields cause a movement of the particles towards the region of highest field strength, which in turn deforms the polymer matrix. A cylindrical shaped PVA-based gel, loaded with magnetite particles, for instance showed an uniaxial contraction along the field gradient direction (Fig. 1.4).³⁸ The extent of contraction was tunable by an adjustment of the field strength. Uniform magnetic fields on the other hand do not cause such a particle/ field interaction but rather a particle/ particle interaction due to the creation of induced magnetic dipoles. The consequence is an alignment of the nanoparticles within the polymer matrix, again causing enormous mechanical stress which leads to an alteration of the gel properties. Zrinyi et al. synthesized small gel beads of PNIPAAm loaded with magnetite nanoparticles, which aggregated into clusters in a non-uniform field and aligned along the magnetic field direction of a uniform field.⁸⁰ Particle alignment prior to the crosslinking of the surrounding polymer on the other hand leads to gels with anisotropic swelling properties.⁸¹ AC magnetic fields finally cause heat development due to a permanent reorientation of the entrapped nanoparticles. In combination with thermo-responsive polymers, this feature can be utilized to construct reversibly forming or at least contracting hydrogels. It is noted, that gels which form/ disintegrate within a magnetic field rarely exist so far.

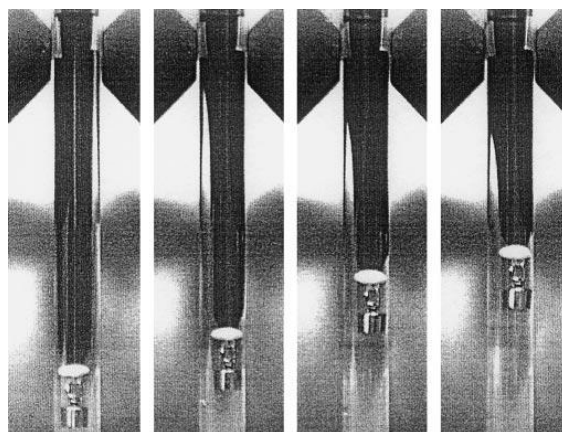
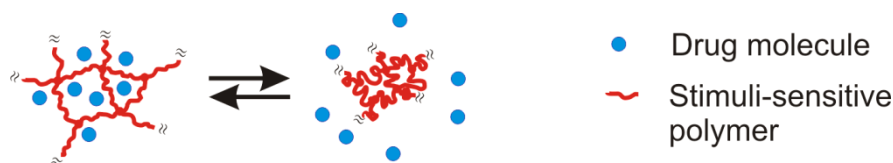


Figure 1.4. Active deformation of a magnetic-field-sensitive gel under a load.³⁸

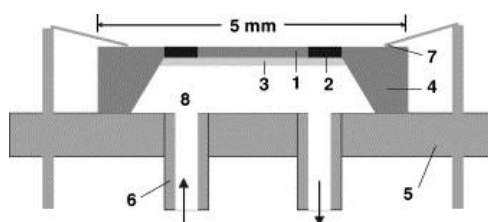
1.4.3 Application fields for “smart” hydrogels

Common non-stimuli-responsive hydrogels find already widespread use, especially in medicine, due to their unique mechanical properties in combination with biocompatibility and degradability. The best known application of a hydrogel is probably the utilization of crosslinked PHEMA as soft contact lense. Hydrogel scaffolds are furthermore ideal for tissue engineering purposes.^{69,82} They can replace cartilages and damaged skin and act as wound dressing, sealant and adhesive.⁶⁰ Another important feature is the ability to entrap drug molecules and release them slowly within the body. “Smart” hydrogels expand the opportunities of hydrogels in medical applications, since the use of such gels helps to avoid a number of difficulties. The injection of conventional hydrogels into the body for instance is a challenge, since gels hardly flow. Thermo-sensitive gels, exhibiting gel properties only under physiological conditions, can be injected as easily flowing sols and build up the demanded gel properties only within the body.⁸³ Furthermore, the stimuli-responsiveness of hydrogels helps to control drug release, since the release can be triggered on demand in that case (Scheme 1.7).⁵⁹ Magneto-responsive gels could be used further for hyperthermia applications since they are suitable for non-invasive heat development within a certain tissue.⁸⁴



Scheme 1.7. Sketch of a triggered drug release from a “smart” polymeric network applying an external stimulus.

However, medicine is not the only field in which “smart” hydrogels play an important role. Their response to external stimuli is further useful for sensing applications, in actuating systems, and microfluidic devices.⁸⁵ A pH- and cation sensor for instance was constructed with the help of a hydrogel composed of NIPAAm and 2VP.⁸⁵ The sensing principle relied on a translation of the volume change of the hydrogel into a voltage via bending of a piezoelectric stripe (Scheme 1.8). Recently, the construction of a colorimetric glucose sensor by arranging micron-sized hydrogel particles within an inverse polystyrene opal, was reported.⁸⁶ By a contraction of the hydrogel particles, incident light was partially scattered causing a decrease of the intensity of reflected light (Fig. 1.5).



Scheme 1.8. Operational principle of a hydrogel-based sensor: (1) bending plate; (2) piezoresistive bridge; (3) swellable hydrogel stripe; (4) Si-chip; (5) socket; (6) tube; (7) interconnect; (8) solution.⁸⁵

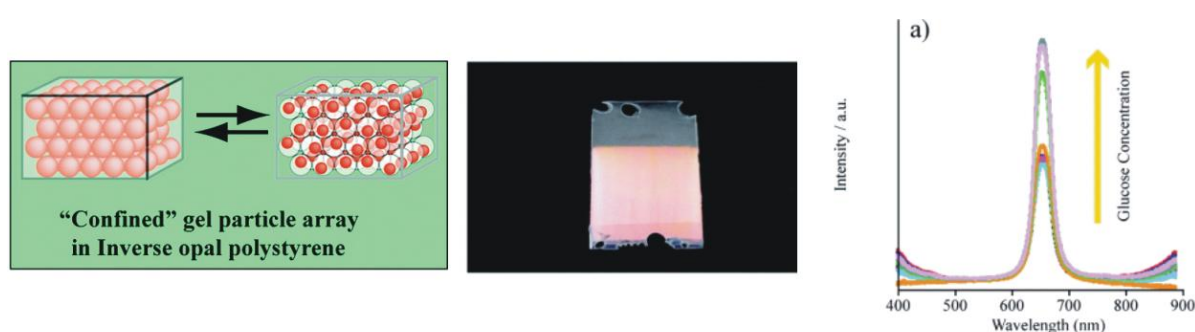


Figure 1.5. Working principle of a colorimetric glucose sensor based on “smart” hydrogels: left: Schematic depiction of small hydrogel beads confined in an inverse opal polystyrene array; middle: Optical microscope image of the inverse opal polystyrene; right: Glucose concentration dependence of the reflection spectra of the gel confined in the inverse opal at 30 °C in CHES buffer solution.⁸⁶

Microfluidic devices mostly rely on small gel beads, which can close microchannels reversibly and thus control flow within these channels (Fig. 1.6).⁸⁷

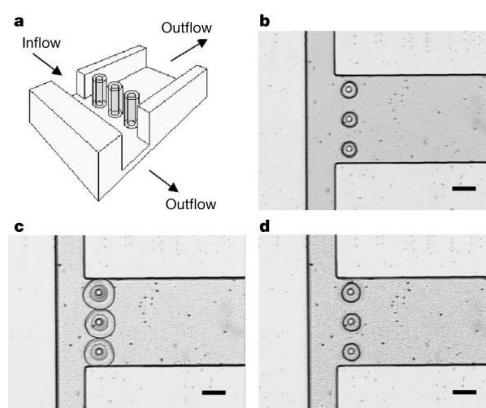


Figure 1.6. A microfluidic device utilizing a P(AA-co-HEMA) gel: a) Scheme of a microchannel with prefabricated posts surrounded by hydrogel jackets; b) Top view of the posts right after polymerization; c) Top view of the expanded hydrogel jackets blocking the channel; d) Top view of the contracted hydrogel jackets allowing flow.⁸⁷

For actuating systems, especially electric- and magnetic-field-responsive hydrogels are used, since these systems respond mainly via contraction or shape deformation (Fig. 1.4). A special type of deformation was reported for silicon/ iron nanoparticle composite materials, which were able to coil under the influence of a magnetic field.⁸⁸ Figure 1.7 finally shows an

example of a ferrogel with anisotropic swelling properties.⁸⁹ All these features are potentially useful for directed movements which are required to construct actuators for robots, artificial muscles, micromachines, and so on.

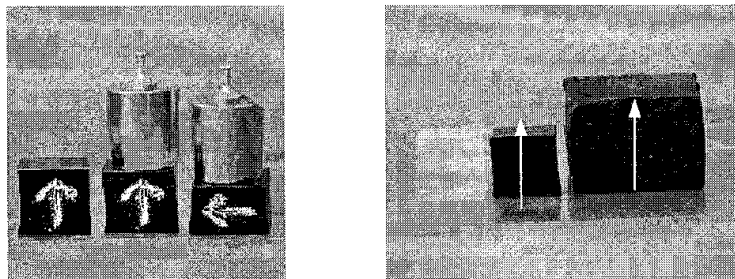


Figure 1.7. Anisotropic mechanical (left image) and swelling (right image) properties.⁸⁹

1.5 Experimental Part

1.5.1 Block copolymer synthesis

Block copolymer structures are accessible through a variety of “living” and/ or controlled polymerization techniques, including anionic and cationic polymerization, controlled radical polymerization (ATRP, RAFT, NMP) and ring opening (methathesis) polymerization (ROP, ROMP).^{90,91} All these methods have in common that the ability of the polymer chains to grow is preserved at any time, which in turn opens the principle opportunity to grow a second block from the first one. By using multifunctional initiating sites (grafting-from) or macromonomers (grafting-through), one has further access to brush- or star-like architectures. Additional techniques like post polymerization modification and coupling reactions finally give access to a great variety of block copolymer structures and sequences. In the following, a short introduction to ATRP, anionic polymerization with special focus on epoxide polymerization, and common coupling reactions will be given.

1.5.1.1 Atom transfer radical polymerization (ATRP)

The principle of all controlled radical polymerization procedures is a significant decrease of the concentration of active, propagating radicals compared to free radical polymerization, which in consequence suppresses typical radical involving side reactions like recombination or disproportionation.⁹¹⁻⁹³ In ATRP, this is achieved by keeping the vast majority of

propagating chains in a dormant state. (Re-)activation occurs via homolytic cleavage of a functional group from the chain end (mostly a halogen atom), with the help of complexed Cu(I) salts or other transition metal complexes. The general reaction mechanism is shown in Figure 1.8.

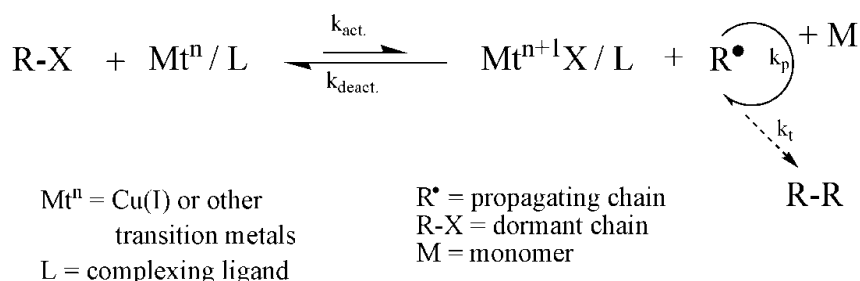


Figure 1.8. Reaction mechanism of the atom transfer radical polymerization (ATRP).

The main advantage of ATRP is its insensitivity to a huge number of functional groups, which renders ATRP a very versatile polymerization method. Furthermore, ATRP initiators are easily accessible or even commercially available. Some monomers, however, interfere with the catalyst system, for instance by complexing Cu(I) (e.g. 2-vinylpyridine). In such cases, one has to use strong ligands competing with the complexing monomer.⁹³ Acidic monomers on the other hand, tend to oxidize Cu(I) and/ or protonate the ligand. Such monomers can only be polymerized in a protected state. Other problems occurring in ATRP are inadequate blocking efficiencies and sequence limitations. Propagating acrylate radicals for instance are not able to add methacrylate monomers.⁹⁴

1.5.1.2 Anionic polymerization

The propagating chain ends in anionic polymerization carry a negative charge, which excludes termination reactions, due to electrostatic repulsion. Consequently, the chain ends stay active at any time. Since system immanent termination reactions cannot take place at all, achievable polydispersities are usually very low and follow a POISSON distribution.⁹⁵ Another advantage is the ease of chain end functionalization, since carb- or oxyanions readily react with a number of compounds such as acids or alkyl halides. A negative aspect is the necessity of a strict purification of monomers and solvents, since carbanions are very sensitive to air and moisture. The choice of polymerizable monomers is limited with respect to radical polymerization techniques and the block sequences are determined by the nucleophilicity of

the active chain ends of the involved monomers. Due to the high basicity of the active chain ends, transfer reactions to solvent molecules or to the monomer might further take place.

The polymerization of epoxide monomers constitutes a special field within anionic polymerization. Monomer addition occurs here simultaneously with a ring opening (Fig. 1.9A). This ring opening is the driving force for the addition, since it causes a release of ring strain. The “living” chain ends are constituted by oxyanions, which are generally more stable than carbanions, but can still be considered as strong bases which are able to react with a variety of acidic compounds. Especially protic solvents should be excluded, since residual water or alcohol molecules can serve as additional initiating sites, due to a proton exchange equilibrium between these molecules and the propagating oxyanion chain ends.⁹⁶

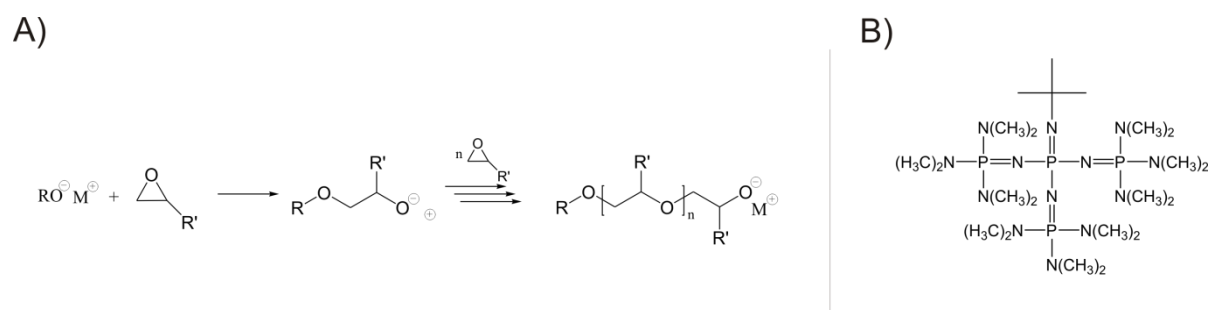


Figure 1.9. A) Reaction mechanism of the anionic ring opening polymerization of epoxide derivatives; B) Chemical structure of the phosphazene base *t*-BuP₄.

The type of counterion of the propagating oxyanion chain end has a strong impact on the polymerization behavior. Depending on the size and polarizability of the distinct cation used, different degrees of association of the active chain ends occur, which influences the propagation rate and stereoregularity of the resulting polymer.^{97,98} Li⁺ is the least favorable counterion since it causes the formation of unreactive associates. Yet, its utilization is a key step towards new block sequences involving certain vinyl and epoxide monomers at the same time.⁹⁹ The discovery of the phosphazene base *t*-BuP₄ (Fig. 1.9B) as a very effective complexing agent for Li⁺ finally solved that problem, rendering Li⁺ a suitable counterion for epoxide polymerization.^{99,100} The structure of *t*-BuP₄, with the inner amino groups, and the outer non-polar methyl groups, fulfils the criterium for a cryptand-like behavior. The inner free volume of the molecule is suitable for complexing the rather compact Li⁺-ion. It is noted, that this coordination step consumes a rather long time period as expressed by an induction period at the beginning of the polymerization.⁹⁹

A last crucial point is the occurrence of transfer reactions in the anionic polymerization of ethylene oxide derivatives of the general structure depicted in Figure 1.10, which limits the maximum achievable molar masses.¹⁰¹ So far, no suitable anionic initiating system based on alkoxides is known leading to high molar mass polyglycidol derivatives.

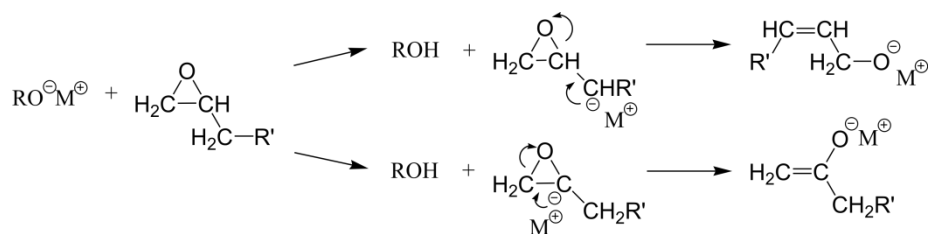


Figure 1.10. Mechanisms of transfer reactions occurring during the anionic ring opening polymerization of epoxide derivatives using alkoxide initiators.

1.5.1.3 Coupling methods

As pointed out, common polymerization techniques for the synthesis of block copolymers come along with several restrictions, limiting the possibilities with respect to block architectures and sequences. To overcome such limitations, it might be suitable to first synthesize a variety of polymer precursors and couple them subsequently, using suitable coupling agents. Figure 1.11 shows linking reactions which are commonly used for such purposes.^{90,102} Especially highlighted is the copper(I)-catalyzed 1,3-dipolar Huisgen cycloaddition, better known as “click” reaction. This reaction is known to take place under ambient conditions, proceeds fast and is quantitative.^{103,104} Its success is well documented by a huge amount of publications dealing not only with the synthesis of various block copolymer architectures but also with the functionalization of chain ends, particles and surfaces.¹⁰⁵⁻¹⁰⁷ It is further emphasized that “click” chemistry is easily combinable with ATRP. Common ATRP initiating sites, which are mostly preserved after finishing the polymerization, can be easily transformed into “click”-components by a simple nucleophilic substitution of the halogen end group by an azide moiety.^{108,109} Another combined polymerization/ coupling method worth to be mentioned is the recently developed RAFT hetero-Diels-Alder addition (RAFT-HDA), also known as “clack” reaction. Here, a RAFT chain transfer agent moiety, situated at the chain end of a previously synthesized polymer is directly reacted with a diene, attached to a second polymer chain (Fig. 1.11).

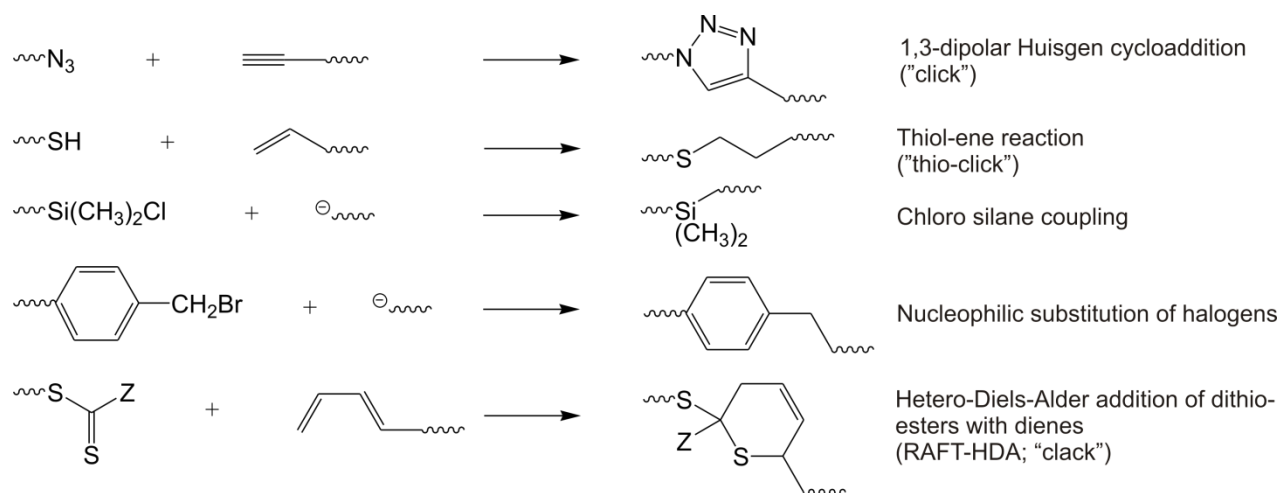


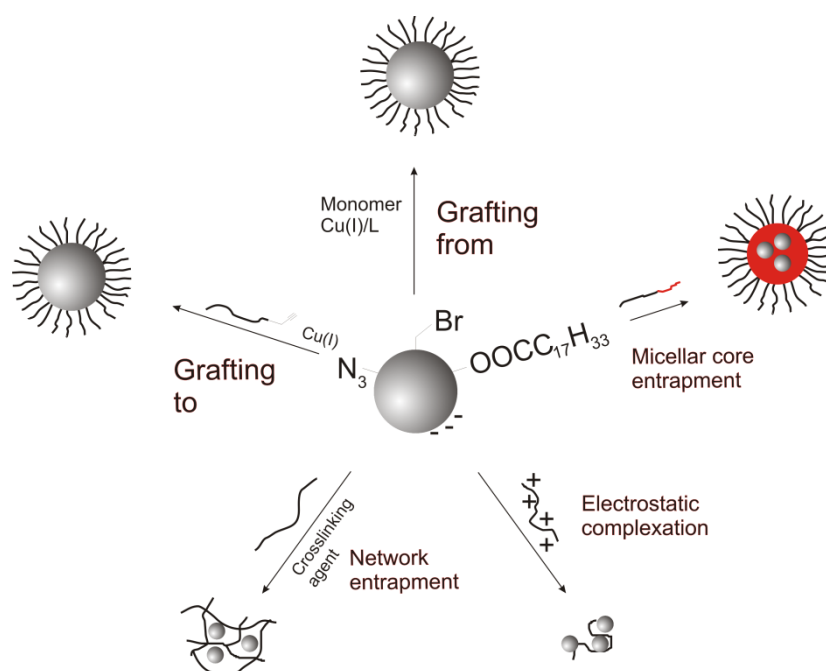
Figure 1.11. Selection of coupling methods applied in block copolymer synthesis.

1.5.2 Synthesis of magnetic nanoparticles and nanoparticle/polymer hybrid structures

Nanoparticles in general can be synthesized by two principle strategies, the "top-down" and the "bottom-up" approach. In the first case, bulk or micrometer sized material is disintegrated into nanosized objects with the use of mills or by plasma treatment. A better control of size and size distribution, however, is reached with the "bottom-up" approach. Common procedures for metal and metal oxide nanoparticles are the coprecipitation of ferrous salts, the thermal decomposition of metal carbonyls and other complexes, or the reduction of metal salts.^{42,43} Sometimes, template assisted procedures involving for instance the use of gels are employed, in order to achieve a better size control. Alternatively, microemulsions are utilized.⁴³

A crucial point in nanoparticle synthesis is the stabilization step. Usually, surfactants or polymers are employed, introducing colloidal stability through ionic or steric repulsion. Size controlling surfactants might serve as stabilizing layer at the same time. The choice of stabilizing agents strongly influences the chemical and physical properties of the nanoparticles. By using oleic acid as the stabilizing surfactant for instance, hydrophobic particles are obtained. Citrate stabilized nanoparticles on the other hand are hydrophilic due to the presence of negative surface charges. Another way of stabilizing nanoparticles is a surface passivation under mild oxidation conditions.⁴³ Stabilization of nanoparticles and further processing to fabricate hybrid structures often goes hand in hand. Stabilizing agents for

nanoparticles can be functionalized with moieties, initiating polymerizations or being suitable for linking reactions. Consequently, polymer chains can be introduced via a “grafting-from” or “grafting-to” approach.^{41,42} (Scheme 1.9) Another way of constructing polymer/nanoparticle hybrid structures is the entrapment of hydrophobically modified nanoparticles within the core of block copolymer micelles.⁴¹ Nanoparticles with a surface charge on the other hand can be complexed with polyelectrolytes.⁴¹ An entrapment of particles within a polymeric network can be simply achieved by dispersing or creating the particles in a polymer solution followed by a chemical crosslinking of the polymer chains.⁴¹



Scheme 1.9. Examples for the synthesis of polymer/nanoparticle hybrid structures representing the five principle strategies.

1.5.3 Rheology

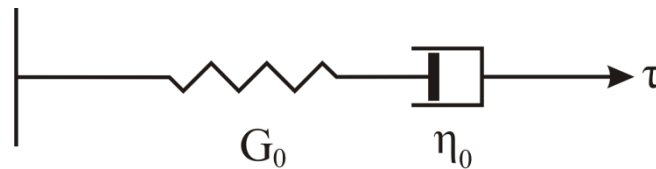
Rheology describes the flow properties of a material. In order to measure these properties, the material is disturbed by applying shear forces and its response is monitored. There are two ideal cases, one of which is the fully elastic (Hookean) solid and the other one the flowing (viscous) fluid. In the first case, the sample will only relax, if the applied stress is released. The shear stress in that case is proportional to the shear strain according to:

$$\tau = G \cdot \gamma \quad \text{Eq. 1.1}$$

G is the shear modulus. A fluid on the other hand will relax immediately by viscous flow. In that case, τ is proportional to the shear rate $\dot{\gamma} = d\gamma/dt$ but independent of shear strain according to Newton's law:

$$\tau = \eta \cdot \dot{\gamma} \quad \text{Eq. 1.2}$$

η is the viscosity of the sample. The mechanical properties of polymers and polymer solutions constitute an intermediate state between both cases. They are called viscoelastic, which means in practice, that their response to stress is time-dependent. For low stresses, Maxwell proposed a model considering the sample as a series connection of a spring and a dashpot, representing the elastic and the viscous part, respectively (Scheme 1.10).¹¹⁰



Scheme 1.10. Spring and dashpot representation of a Maxwell element.

Systems represented by this model are called linear viscoelastic. The time dependence of G is expressed by

$$G(t) = G_0 \cdot e^{-t/\lambda} \quad \text{Eq. 1.3}$$

G_0 is the equilibrium shear modulus. λ is the characteristic relaxation time and is expressed by:

$$\lambda = \frac{\eta}{G_0} \quad \text{Eq. 1.4}$$

Most materials behave linear viscoelastic only at low shear strains. At higher deformations, where the sample is prone to higher stresses, η often becomes shear rate and G shear strain dependent. If viscosity drops with increasing shear rate, shear thinning takes places, if it increases, shear thickening occurs. For highly structured liquids, such as gels based on regular packings of micelles, shear thinning occurs already at relatively low shear rates, which is due to structural reorganization processes.

The rheological characteristics of a sample can be determined with the help of rotational rheometers by establishing a desired shear rate and measuring the shear stress (strain

controlled mode) or vice versa (stress controlled mode). Independent on the particular cell geometry of the measuring system, the shear stress τ is proportional to the torque M , which is directly detectable. Furthermore, the shear rate $\dot{\gamma}$ does only depend on the cell dimensions within the linear viscoelastic regime. Figure 1.12 summarizes the most frequently used geometries.

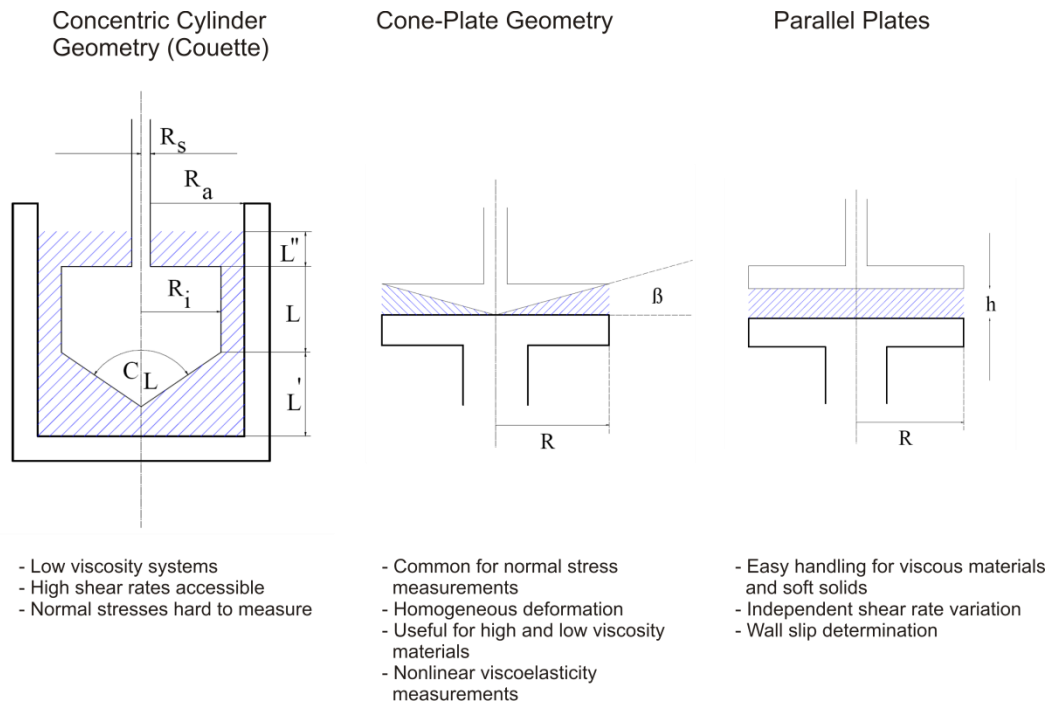


Figure 1.12. Commonly applied measuring cell geometries for rheology.¹¹¹

In order to derive important information about the dynamics of a viscoelastic sample, it is reasonable to apply oscillatory shear.¹¹² In this experiment, the applied strain and in consequence the detected shear stress change periodically according to:

$$\begin{aligned}\gamma &= \gamma_0 \sin \omega t \\ \tau &= \tau_0 \sin(\omega t + \delta)\end{aligned}\quad \text{Eq. 1.5 and 1.6}$$

As can be seen, τ oscillates at the same frequency as γ however with a phase shift expressed by the phase angle δ . The more the shear stress is oscillating out of phase, the higher is the viscous contribution to the response. The stress wave can be divided into two waves of the same frequency, one in phase with the strain wave, one out of phase by an angle of 90° :

$$\tau = \tau' + \tau'' = \tau'_0 \sin \omega t + \tau''_0 \cos \omega t \quad \text{Eq. 1.7}$$

Having in mind, that $G = \frac{\tau_0}{\gamma_0}$, it follows:

$$\frac{\tau}{\gamma_0} = G'(\omega) \sin \omega t + G''(\omega) \cos \omega t \quad \text{Eq.1.8}$$

$$\text{with } G'(\omega) = \frac{\tau_0}{\gamma_0} \cos \delta \quad \text{and } G''(\omega) = \frac{\tau_0}{\gamma_0} \sin \delta$$

G' is the in-phase or elastic modulus (also called storage modulus), being a measure of the elastic response of the system and G'' is the out-of-phase or loss modulus, being a measure of the viscous response of the system. The ratio $G''/G' = \tan \delta$ is called loss factor. G' and G'' are the real and the imaginary part of a complex modulus G^* according to:

$$G^* = G' + iG'' \quad \text{Eq. 1.9}$$

From the complex modulus, the magnitude of a complex viscosity can be calculated by:

$$|\eta^*| = \frac{1}{\omega} |G^*| = (\eta'^2 + \eta''^2)^{1/2} = \left[\left(\frac{G''}{\omega} \right)^2 + \left(\frac{G'}{\omega} \right)^2 \right]^{1/2} \quad \text{Eq. 1.10}$$

It is finally noted, that, besides steady and oscillatory shear experiments, samples can be further characterized rheologically within the linear viscoelastic regime by creep or stress relaxation experiments.

1.5.3.1 Rheological definition of a gel

A gel combines liquid like and solid like behavior due to its multicomponent nature and therefore exhibits, analogous to polymer solutions in general, viscoelastic behavior. Some materials appear to be very close to one of the two limiting cases (liquid or solid), although they still can be treated as gels, according to structural definitions. However, it is hard to recognize such systems intuitively as gels. For the term “solid like gel”, Almdal and Kramer defined⁵²:

- Absence of an equilibrium modulus
- The storage modulus G' should be independent of frequency at least in the order of seconds

- The loss modulus G'' should be considerably smaller than the storage modulus

However, not every system acts unambiguously as gel according to these criteria. Some systems for instance do not follow the criterion of the frequency independent moduli and have a G' which is only slightly higher than G'' , although they still appear as free-standing gels. Such a system is often called a “weak” gel.¹¹³ That term however is not accepted by everyone.

In conclusion no strict definition of a gel can be postulated, regardless of the definition criterion. It is the best solution to search for operational definitions, most suitable for the practical handling of gels. Nishinari concluded, that a gel might be present, if it does not flow under gravitational forces.⁵³ Furthermore, the storage modulus G' should be frequency independent at least within a range of 10^{-3} to 10^2 rad/s, which is accessible by most conventional rheometers. Last but not least, the loss factor should be low ($\tan\delta < 0.1$), meaning, that the elastic part of the response dominates.

The definition of the gel point is also relatively controversial. The easiest way to determine a gel point is to find the point at which the storage and the loss modulus intersect, or in other words, at which $G''/G' = \tan\delta = 1$. This definition however is rather problematic since this criterion is not valid in every case.¹¹⁴ This is obvious if one takes into account, that the dynamic moduli and therefore $\tan\delta$ are frequency dependent also in the vicinity of the gelation point. Winter et al. defined the sol-gel transition as the point where both $G'(\omega)$ and $G''(\omega)$ follow a power law with the same exponent^{115,116}:

$$G'(\omega) \sim G''(\omega) \sim \omega^n \quad \text{Eq. 1.11}$$

It follows, that $\tan\delta$ is time (or frequency) independent at the gel point according to equation 1.12:

$$\tan \delta = \frac{G''(\omega)}{G'(\omega)} = \tan\left(n \frac{\pi}{2}\right) \quad \text{Eq. 1.12}$$

A time dependent gel point for instance, could then be determined by recording $\tan\delta$ / time curves at different frequencies. The time at which all $\tan\delta$ curves intersect marks the gel point. However, Winter et al. themselves observed also systems, where the $\tan\delta$ curves do not intersect in one single point.¹¹⁷ Other authors also found this criterion invalid for several cases.¹¹⁸⁻¹²¹ It gets even more difficult when dealing with systems, which behave rheologically as a “weak” gel even if they flow under gravitational forces. In such a case, it is

reasonable to determine the gel point as a point, where G' increases rapidly or rises above a certain threshold value.

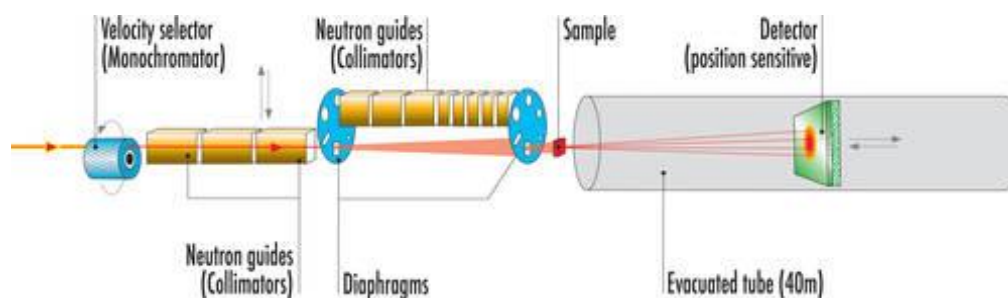
1.5.4 Small angle neutron scattering (SANS)

Scattering techniques are powerful tools for structure determination in micellar solutions. It includes scattering of visible light, neutrons and x-rays. Characteristic for each method is the covered range of the scattering vector q , which determines the length scale on which structural investigations can be carried out. The scattering vector depends on the wavelength of the scattered photons and is defined as:

$$q = \frac{4\pi}{\lambda} \sin \frac{\theta}{2} \quad \text{Eq. 1.13}$$

λ is the wavelength of the scattered waves and θ the scattering angle.

Light scattering and SANS/SAXS appear to be complementary since light covers a range of rather low q -values whereas x-rays and neutrons enable structural studies on a local length scale in the range of atomic or molecular distances. Consequently, it is a powerful tool for structural investigations of micellar solutions. The setup of a neutron scattering device is shown in Scheme 1.11.¹²²



Scheme 1.11. Setup of a SANS experiment.¹²²

For scattering purposes, cold neutrons are needed ($E = 0.1-10$ MeV, $\lambda = 30-3$ Å), which are commonly generated by a nuclear reactor and subsequently decelerated using moderating systems.¹²³ The monochromator provides a neutron beam with a wavelength dispersity of $\Delta\lambda/\lambda \approx 10$ % and the collimation setup focuses the beam before passing the sample to be investigated. Detection occurs via gaseous substances like BF_3 , emitting ionizing particles upon neutron impact.¹²³ The detecting unit is a two-dimensional multi-detector which can be moved along the neutron flight direction in order to cover a q -range as broad as possible.

The primarily recorded data are two-dimensional scattering images. By a radial averaging of these images, one obtains the q -dependent intensity profile $\langle I(q) \rangle$, which is defined as follows:

$$\langle I(q) \rangle = \Delta\rho NP(q)S(q) + I_{incoherent} \quad \text{Eq. 1.14}$$

$\Delta\rho$ is the difference in scattering length density between the scattering objects and the surrounding medium, N is the number of scattering particles, $P(q)$ the form factor and $S(q)$ the structure factor. For diluted samples where no interactions between the scattering particles take place, $S(q) \approx 1$ applies and the intensity profile exclusively contains information about the particle dimensions. By using a variety of fit models for the form factor, one obtains useful information, such as shape, diameter and consistency of the scattering objects.^{124,125} In semi-diluted and concentrated solutions, the influence of the structure factor becomes important. At sufficiently high concentration, an intensity maximum occurs, whose position provides information about the center-to-center distance of the scattering objects. If ordered domains are present, additional higher order reflections are visible at defined q values. These values, normalized to the position of the structure factor maximum, provide information about the type of crystal lattice present in the sample (Table 1.1).

Table 1.1. Common crystal lattice types and their crystallographic specifications occurring in concentrated micellar solutions.¹²⁶⁻¹²⁸

Lattice type	Allowed values for $n = h + k + l$	Relative peak positions in $I(q)$
Simple cubic	Any	$1:2^{1/2}:3^{1/2}:2 \dots$
Body centered cubic	n even	$1:2^{1/2}:3^{1/2}:2 \dots$
Face centered cubic	h,k,l all odd or all even	$1:4/3^{1/2}:8/3^{1/2}:11/3^{1/2} \dots$
Cylindrical hexagonal	l even, $h + 2k \neq 3n$	$1:3^{1/2}:2:7^{1/2}:9^{1/2} \dots$

When dealing with concentrated, ordered micellar solutions, the primarily recorded 2D diffraction patterns provide additional useful information. In principle, three kinds of patterns are observable (Fig. 1.13). A pattern can be fully isotropic, i.e. the intensity does not depend on the azimuthal angle (Fig. 1.13A), which points to the presence of randomly oriented domains with a local order, like in powder diffraction experiments. Smearred Bragg reflections, as shown in Figure 1.13B, point to the presence of randomly oriented, ordered

domains with a weak preferred orientation. The presence of fully aligned monodomains (i.e. macroscopically oriented sample), finally leads to patterns with sharp Bragg spots as shown in Figure 1.13C. Such a pattern either stands for one single macroscopic orientation (“single crystal”), or represents a superposition of patterns originating from a set of different macroscopic orientations. In general a higher degree of order in micellar solutions, allowing for a detailed investigation of packing characteristics, can be achieved by applying shear to the sample.¹²⁹

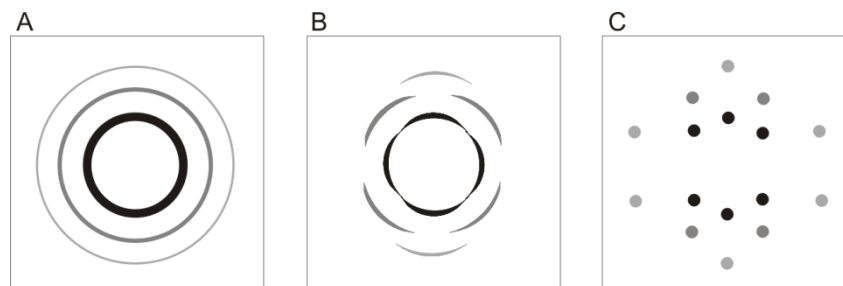


Figure 1.13. Sketches of 2D-scattering patterns obtainable from SANS experiments: A) isotropic pattern; B) anisotropic pattern with smeared Bragg reflections; C) strongly anisotropic pattern with sharp Bragg spots.

A detailed interpretation of patterns from fully aligned domains, including indexation of the reflections, is commonly achieved with the help of reticular planes.¹²⁸ These are planes at which an incident beam is refracted under the condition angle of incidence = angle of reflection. The orientation of these planes relative to the crystal lattice is expressed by so called Miller indices (hkl) (Fig. 1.14).

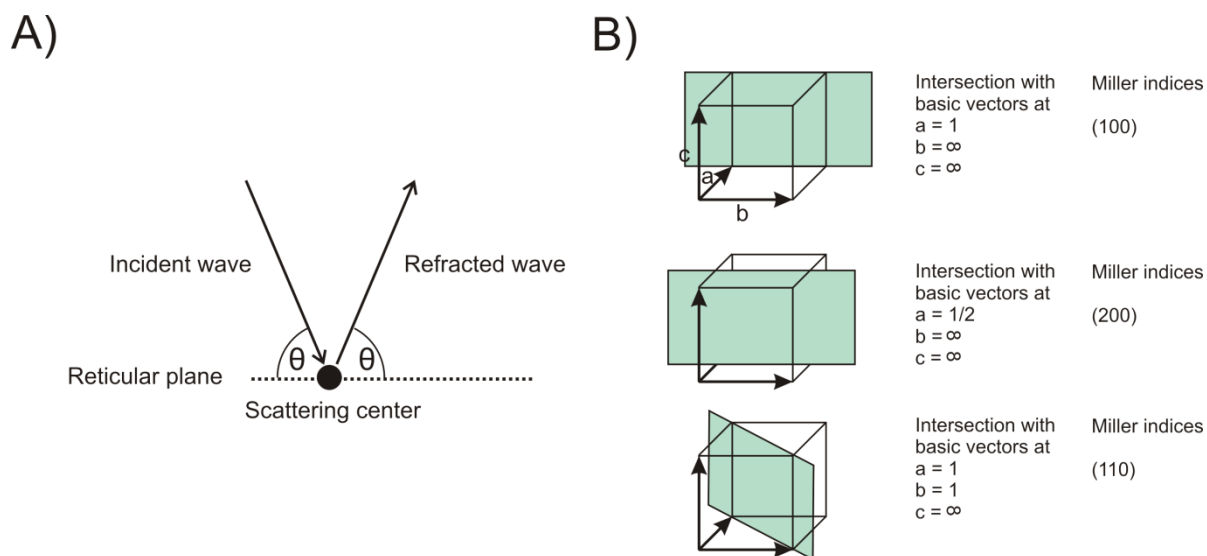


Figure 1.14. A) Schematic depiction of the definition of a crystallographic reticular plane; B) reticular planes and their corresponding Miller indices.

In general, only reflections are allowed, for which the Bragg relation is fulfilled:

$$n\lambda = 2d_{hkl} \sin \theta \quad \text{Eq. 1.15}$$

d_{hkl} is the distance between two particular $\{hkl\}$ planes. For symmetry reasons, the Miller indices h, k, l , and their sum n , has to adopt characteristic values for each lattice. These values are summarized in Table 1.1. The different spots in the 2D pattern lie on concentric circles. Those located on the same circle have the same scattering angle, which means that they originate from identical $\{hkl\}$ planes. Reflections from planes of the same order n on the other hand lie on a vertical axis within the pattern starting with $n = 0$ in the center¹³⁰. With these predictions, an easy indexation of the observed reflections can be carried out giving the opportunity to determine the lattice type of the sample. The positions of the indexed reflections allows for further conclusion about the preferred orientation of the crystal domains relative to the incident neutron beam. Finally, it is also possible to derive quantitative information from 2D patterns, in particular lattice spacings. For a simple cubic packing for instance the lattice spacing a can be calculated according to the relation:

$$d_{hkl} = \frac{a}{(h^2 + k^2 + l^2)^{1/2}} \quad \text{Eq. 1.16}$$

d_{hkl} is obtained from the Bragg relation. For other lattice types, such a calculation can be carried out as well, though the corresponding equations are much more complicated.

1.5.5 Dynamic light scattering

Particles in solution, as for instance micellar aggregates, always undergo brownian motion. The characteristics of these motions, i.e. the time scale on which they are occurring and their particular nature (translational or rotational motion, segment relaxation) potentially provide useful information about the particle shape and size. Dynamic light scattering relies on the analysis of temporal intensity fluctuations of light scattered by the dissolved particles, caused by their motion. Due to the temporal fluctuations the recorded quantity can be analyzed by an intensity time autocorrelation formalism. In a commonly performed homodyne-experiment, where the scattered light is directly directed to the photon detector, the output signal is proportional to intensity $I(t)$ and is autocorrelated with time according to¹³¹⁻¹³³:

$$g_2(t) = \frac{\langle I(0) \cdot I(t) \rangle}{\langle I(0) \rangle^2} \quad \text{Eq. 1.17}$$

with $g_2(t)$ being the normalized intensity autocorrelation function (ICF). The field autocorrelation function (ECF) $g_1(t)$, describing the electric field fluctuations of the scattered light, is obtained from $g_2(t)$ with the help of the Siegert-relation¹³⁴:

$$g_1(t) = \frac{\langle E(0) \cdot E(t) \rangle}{\langle E(0) \rangle^2} = \sqrt{\frac{g_2(t) - A}{B}} \quad \text{Eq. 1.18}$$

with A, being a baseline parameter and B accounting for deviations from the ideal correlation. For the simplest case of monodisperse hard spheres $g_1(t)$ is expressed by:

$$g_1(t) = e^{-\Gamma t} \quad \text{Eq. 1.19}$$

Γ is the decay rate from which the translational diffusion coefficient D_T and in consequence the hydrodynamic radius R_h can be calculated as follows:

$$\Gamma = D_T q^2 \quad \text{Eq. 1.20}$$

$$R_h = \frac{kT}{6\pi\eta D_T} \quad \text{Eq. 1.21}$$

Equation 1.21 is the Stokes-Einstein relation. η is the viscosity of the solvent. If rotational motions contribute to the decay of the autocorrelation function (which is the case for anisotropic particles), Γ changes to:

$$\Gamma = q^2 \cdot D_T + 6D_R \quad \text{Eq.1.22}$$

with D_R being the rotational diffusion coefficient. In consequence, one can derive useful information about the particle shape by plotting Γ vs. q^2 . Spherical particles for instance should lead to a straight line, which intersects with the point of origin, whereas cylinders yield a curve with decreasing slope and an intersection with the ordinate. Since most investigated particles exhibit a certain polydispersity, the determined decay rate only represents a mean value. In order to account for the polydispersity of the system, $g_1(t)$ has to be described as a weighted sum of exponentials according to:

$$g_1(t) = \int_0^{\infty} G(\Gamma) e^{(-\Gamma t)} d\Gamma \quad \text{Eq. 1.23}$$

where $G(\Gamma)$ is the distribution function of the decay rates. $G(\Gamma)$ can be analyzed by two principle methods. One is the cumulant method, which relies on a polynomial fitting procedure of $\ln(g_1(t)) = A + Bt + Ct^2 + Dt^3$ giving the average hydrodynamic radius of the particles along with their polydispersity. Alternatively, the CONTIN analysis can be carried out which relies on an inverse Laplace transformation and is suitable for multimodal size distributions.

1.6 Objective of the thesis

The importance of “smart” hydrogels is manifested in the huge number of already realized and potential applications, especially in medicine. Consequently, the research interests of many groups were and still are focused on “smart” hydrogels. The German science foundation started a priority program on “smart” hydrogels (SPP 1259) in 2006¹³⁵, which was motivated by the fact, that many aspects in hydrogel synthesis and characterization were still quite unexplored and in consequence many potential applications not realizable until then.

We recognized in particular, that the number of block copolymer based hydrogels, which can be addressed independently by different external stimuli, is still limited. The few examples reported so far exhibited rather high polydispersities and only fairly defined block lengths.

Another unsolved problem was that most magneto-responsive hydrogels (ferrogels) have the disadvantage, that nanoparticles, providing the sensitivity to magnetic fields, are not tightly bound to the polymer matrix, which gives rise to particle aggregation and/ or leaching. Besides, most ferrogel systems are responding via contraction/ deformation but not reversible formation/ disintegration.

The intention of this work, which is also part of the SPP 1259, was to contribute to the solution of these particular problems. The central focus was put on ABC triblock terpolymers, which are composed of a pH-sensitive A block, a water soluble B Block, and a thermo-sensitive C block. With this novel concept, I was aiming at the construction of block copolymer based hydrogels, which respond independently to pH and temperature. By a slight modification of the A block, introducing the ability to complex magnetic nanoparticles, this

concept could be further extended to the formation of polymer/ nanoparticle hybrid micelles suitable for the formation of ferrogels, which do not exhibit the aforementioned disadvantages.

Tasks to be accomplished within this work mainly included the development of suitable synthetic routes yielding the desired ABC triblock terpolymers and the corresponding hydrogels and a detailed investigation of the aggregation and gelation behavior of the synthesized systems.

As a perspective for future research, the employed ferrogel approach might be used to incorporate blocked nanoparticles, which gives the opportunity to reversibly freeze in a magnetization in a gel matrix and in turn obtain hydrogels with anisotropic, mechanical and magnetic properties.

1.7 References

- [1] Tsitsilianis, C. Design of responsive, water-soluble block copolymers. In *Responsive Polymer Materials: Design and Applications*; Minko, S., Ed.; Blackwell Publishing: Ames, Iowa 2006; pp 27.
- [2] Gohy, J.-F. Stimuli-responsive block copolymer assemblies. In *Block Copolymers in Nanoscience*; Lazzari, M.; Liu, G.; Lecommandoux, S., Eds.; Wiley-VCH Verlag GmbH & Co. KGaA: Weinheim, 2006.
- [3] Ahn, S.-k.; Kasi, R. M.; Kim, S.-C.; Sharma, N.; Zhou, Y. *Soft Matter* **2008**, *4*, 1151.
- [4] He, C.; Kim, S. W.; Lee, D. S. *J. Controlled Release* **2008**, *127*, 189.
- [5] Crowe, J. A.; Efimenko, K.; Genzer, J.; Schwark, D. W. Responsive siloxane-based polymeric surfaces. In *Responsive Polymer Materials: Design and Applications*; Minko, S., Ed.; Blackwell Publishing: Ames, Iowa, 2006; pp 184.
- [6] Roy, D.; Cambre, J. N.; Sumerlin, B. S. *Prog. Polym. Sci.* **35**, 278.
- [7] Pelton, R. H.; Chibante, P. *Colloids Surf.* **1986**, *20*, 247.
- [8] Fujishige, S.; Kubota, K.; Ando, I. *J. Phys. Chem.* **1989**, *93*, 3311.
- [9] Baltes, T.; Garret-Flaudy, F.; Freitag, R. *J. Polym. Sci., Part A: Polym. Chem.* **1999**, *37*, 2977.
- [10] Park, J.-S.; Kataoka, K. *Macromolecules* **2006**, *39*, 6622.
- [11] Hoogenboom, R. *Angew. Chem., Int. Ed.* **2009**, *48*, 7978.
- [12] Han, S.; Hagiwara, M.; Ishizone, T. *Macromolecules* **2003**, *36*, 8312.
- [13] Lutz, J. F.; Hoth, A. *Macromolecules* **2006**, *39*, 893.
- [14] Hoogenboom, R.; Lambermont-Thijs, H. M. L.; Jochems, M. J. H. C.; Hoepfener, S.; Guerlain, C.; Fustin, C.-A.; Gohy, J.-F.; Schubert, U. S. *Soft Matter* **2009**, *5*, 3590.
- [15] Koyama, M.; Hirano, T.; Ohno, K.; Katsumoto, Y. *J. Phys. Chem. B* **2008**, *112*, 10854.
- [16] Schulz, D. N.; Peiffer, D. G.; Agarwal, P. K.; Larabee, J.; Kaladas, J. J.; Soni, L.; Handwerker, B.; Garner, R. T. *Polymer* **1986**, *27*, 1734.
- [17] Virtanen, J.; Arotcarena, M.; Heise, B.; Ishaya, S.; Laschewsky, A.; Tenhu, H. *Langmuir* **2002**, *18*, 5360.
- [18] Yasushi, M.; Hiroki, M.; Isao, I. *Macromol. Rapid Commun.* **2004**, *25*, 1330.
- [19] Plamper, F. A.; Schmalz, A.; Müller, A. H. E. *J. Am. Chem. Soc.* **2007**, *129*, 14538.
- [20] Ma, R.; Wang, B.; Liu, X.; An, Y.; Li, Y.; He, Z.; Shi, L. *Langmuir* **2007**, *23*, 7498.

- [21] Pae, B. J.; Moon, T. J.; Lee, C. H.; Ko, M. B.; Park, M.; Lim, S.; Kim, J.; Choe, C. R. *Korean Polym. J.* **1997**, *5*, 126.
- [22] Dai, S.; Ravi, P.; Tam, K. C. *Soft Matter* **2008**, *4*, 435.
- [23] Plamper, F. A.; Ruppel, M.; Schmalz, A.; Borisov, O.; Ballauff, M.; Müller, A. H. E. *Macromolecules* **2007**, *40*, 8361.
- [24] Schmalz, A.; Hanisch, M.; Schmalz, H.; Müller, A. H. E. *Polymer* *51*, 1213.
- [25] Zhang, X.-Z.; Yang, Y.-Y.; Wang, F.-J.; Chung, T.-S. *Langmuir* **2002**, *18*, 2013.
- [26] Karg, M.; Pastoriza-Santos, I.; Rodriguez-González, B.; von Klitzing, R.; Wellert, S.; Hellweg, T. *Langmuir* **2008**, *24*, 6300.
- [27] Kratz, K.; Hellweg, T.; Eimer, W. *Colloids Surf. A* **2000**, *170*, 137.
- [28] Zhang, Y.; Furyk, S.; Bergbreiter, D. E.; Cremer, P. S. *J. Am. Chem. Soc.* **2005**, *127*, 14505.
- [29] Georgiev, G. S.; Mincheva, Z. P.; Georgieva, V. T. *Macromol. Symp.* **2001**, *164*, 301.
- [30] Ju, X. J.; Chu, L. Y.; Liu, L.; Mi, P.; Lee, Y. M. *J. Phys. Chem. B* **2008**.
- [31] Choi, H. S.; Yui, N. *Progress in Polymer Science* **2006**, *31*, 121.
- [32] Liu, F.; Urban, M. W. *Prog. Polym. Sci.* **2010**, *35*, 3.
- [33] Plamper, F. A.; Murtomäki, L.; Walther, A.; Kontturi, K. s.; Tenhu, H. *Macromolecules* **2009**, *42*, 7254.
- [34] Zong, Y.; Rühle, J.; Knoll, W. Azobenzene-containing photoswitchable polymeric Langmuir-Blodgett-Kuhn multilayer films. In *Responsive Polymer Materials: Design and Applications*; Minko, S., Ed.; Blackwell Publishing: Ames, Iowa 2006; pp 50.
- [35] Schumers, J.-M.; Fustin, C.-A.; Gohy, J.-F. *Macromol. Rapid Commun.* *9999*, NA.
- [36] Ichimura, K. *J. Mater. Chem.* **2007**, *17*, 632.
- [37] Bradley, M.; Vincent, B.; Warren, N.; Eastoe, J.; Vesperinas, A. *Langmuir* **2005**, *22*, 101.
- [38] Zrínyi, M. *Colloid. Polym. Sci.* **2000**, *278*, 98.
- [39] Zrínyi, M.; Barsi, L.; Büki, A. *Polym. Gels Netw.* **1997**, *5*, 415.
- [40] Kaiser, A.; Gelbrich, T.; Schmidt, A. M. *J. Phys.: Condens. Matter* **2006**, *18*, S2563.
- [41] Reinicke, S.; Döhler, S.; Tea, S.; Krekhova, M.; Messing, R.; Schmidt, A. M.; Schmalz, H. *Soft Matter* **2010**, *6*, 2760.
- [42] Schmidt, A. *Colloid Polym. Sci.* **2007**, *285*, 953.
- [43] Lu, A.-H.; Salabas, E. L.; Schüth, F. *Angew. Chem., Int. Ed.* **2007**, *46*, 1222.
- [44] Sorensen, C. M., *Magnetism in Nanoscale Materials in Chemistry*. Wiley-Interscience Publication: New York, 2001.

- [45] Batlle, X.; Labarta, A. *J. Phys. D: Appl. Phys.* **2002**, *35*, R15.
- [46] Leslie-Pelecky, D. L.; Rieke, R. D. *Chem. Mater.* **1996**, *8*, 1770.
- [47] Odenbach, S., *Magnetoviscous effects in ferrofluids* Springer: Berlin, 2002.
- [48] Berkovsky, B. M.; Bashtovoy, V., *Magnetic fluids and applications handbook*. Begell House: New York, 1996.
- [49] Blums, E.; Cebers, A.; Mairov, M. M., *Magnetic fluids*. Walter de Gruyter: Berlin, 1997.
- [50] Lloyd, D. J., *The problem of gel structure*. J. Alexander, The Chemical Catalog Co., New York 1926.
- [51] Gong, J. P., *Dictionary of Polymers*. Asakura Shoten, Tokyo: 2005; p 208.
- [52] Almdal, K.; Dyre, J.; Hvidt, S.; Kramer, O. *Polym. Gels Netw.* **1993**, *1*, 5.
- [53] Nishinari, K. *Prog. Colloid Polym. Sci.* **2009**, *136*, 87.
- [54] de Gennes, P. G., *Scaling concepts in polymer physics*. Cornell University Press, New York: 1979.
- [55] Stauffer, D., *Introduction to percolation theory*. Taylor and Francis, London: 1985.
- [56] Chambon, F.; Winter, H. H. *J. Rheol.* **1987**, *31*, 683.
- [57] Flory, P. J. *Faraday Discuss. Chem. Soc.* **1974**, *57*, 7.
- [58] Hadjichristidis, N.; Pispas, S.; Floudas, G. A. Block copolymer applications. In *Block Copolymers - Synthetic strategies, physical properties and applications*; John Wiley & Sons: Hoboken, New Jersey, 2003.
- [59] Klouda, L.; Mikos, A. G. *Eur. J. Pharm. Biopharm.* **2008**, *68*, 34.
- [60] Drury, J. L.; Mooney, D. J. *Biomaterials* **2003**, *24*, 4337.
- [61] Hoffmann, H.; Ulbricht, W. *Curr. Opin. Colloid Interface Sci.* **1996**, *1*, 726.
- [62] Lewis, R. N. A. H.; McElhaney, R. N. *Chem. Phys. Lipids* *96*, 9.
- [63] Ho, D. L.; Briber, R. M.; Glinka, C. J. *Chem. Mater.* **2001**, *13*, 1923.
- [64] Wanka, G.; Hoffmann, H.; Ulbricht, W. *Macromolecules* **1994**, *27*, 4145.
- [65] Livage, J. *Mater. Res. Soc. Symp. Proc.* **1984**, *32*, 125.
- [66] Nicolai, T.; Durand, D. *Curr. Opin. Colloid Interface Sci.* **2007**, *12*, 23.
- [67] Mohmeyer, N.; Schmidt, H. W. *Chem. Eur. J.* **2005**, *11*, 863.
- [68] Kopecek, J. *J. Polym. Sci., Part A: Polym. Chem.* **2009**, *47*, 5929.
- [69] Lee, K. Y.; Mooney, D. J. *Chem. Rev.* **2001**, *101*, 1869.
- [70] Reinicke, S.; Schmelz, J.; Lapp, A.; Karg, M.; Hellweg, T.; Schmalz, H. *Soft Matter* **2009**, *5*, 2648
- [71] Hart, D. S.; Gehrke, S. H. *J. Pharm. Sci.* **2007**, *96*, 484.

- [72] Dusek, K. *Adv. Polym. Sci.* **1993**, 109/110.
- [73] Shi, J.; Alves, N. M.; Mano, J. F. *Macromol. Biosci.* **2006**, 6, 358.
- [74] Oishi, M.; Nagasaki, Y. *Nanomedicine* **2010**, 5, 451.
- [75] Sugihara, S.; Kanaoka, S.; Aoshima, S. *J. Polym. Sci., Part A: Polym. Chem.* **2004**, 42, 2601.
- [76] Angelopoulos, S. A.; Tsitsilianis, C. *Macromol. Chem. Phys.* **2006**, 207, 2188.
- [77] Stavrouli, N.; Katsampas, I.; Angelopoulos, S.; Tsitsilianis, C. *Macromol. Rapid Commun.* **2008**, 29, 130.
- [78] Achilleos, M.; Krasia-Christoforou, T.; Patrickios, C. S. *Macromolecules* **2007**, 40, 5575.
- [79] Xu, F.-J.; Kang, E.-T.; Neoh, K.-G. *Biomaterials* **2006**, 27, 2787.
- [80] Xulu, P. M.; Filipcsei, G.; Zrínyi, M. *Macromolecules* **2000**, 33, 1716.
- [81] Varga, Z.; Filipcsei, G.; Zrínyi, M. *Polymer* **2006**, 47, 227.
- [82] Zhu, J. *Biomaterials* **2010**, 31, 4639.
- [83] Yu, L.; Ding, J. *Chem. Soc. Rev.* **2008**, 37, 1473.
- [84] Lao, L. L. R., R. V. . *J. Mater. Sci.: Mater. Med.* **2004**, 15, 1061.
- [85] Guenther, M.; Kuckling, D.; Corten, C.; Gerlach, G.; Sorber, J.; Suchaneck, G.; Arndt, K. F. *Sens. Actuators, B* **2007**, 126, 97.
- [86] Honda, M.; Kataoka, K.; Seki, T.; Takeoka, Y. *Langmuir* **2009**, 25, 8349.
- [87] Beebe, D. J.; Moore, J. S.; Bauer, J. M.; Yu, Q.; Liu, R. H.; Devadoss, C.; Jo, B.-H. *Nature* **2000**, 404, 588.
- [88] Nguyen, V. Q.; Ramanujan, R. V. *Macromolecular Chemistry and Physics* 211, 618.
- [89] Varga, Z.; Fehér, J.; Filipcsei, G.; Zrínyi, M. *Macromolecular Symposia* **2003**, 200, 93.
- [90] Hadjichristidis, N.; Pispas, S.; Floudas, G. A. Block copolymer synthesis. In *Block Copolymers - Synthetic strategies, physical properties and applications*; John Wiley & Sons: Hoboken, New Jersey, 2003.
- [91] Matyjaszewski, K.; Müller, A. H. E., *Controlled and Living Polymerizations - From Mechanisms to Applications*. Wiley-VCH: Weinheim, 2009.
- [92] Kamigaito, M.; Ando, T.; Sawamoto, M. *Chem. Rev.* **2001**, 101, 3689.
- [93] Matyjaszewski, K.; Xia, J. *Chem. Rev.* **2001**, 101, 2921.
- [94] Shipp, D. A.; Wang, J.-L.; Matyjaszewski, K. *Macromolecules* **1998**, 31, 8005.
- [95] Hsieh, H. L.; Quirk, R. P., *Anionic polymerization: principles and practice*. Marcel Dekker Inc.: New York, Basel, 1996.

- [96] Ogura, M.; Tokuda, H.; Imabayashi, S.-I.; Watanabe, M. *Langmuir* **2007**, *23*, 9429.
- [97] Price, C. C.; Akkapeddi, M. K.; DeBona, B. T.; Furie, B. C. *J. Am. Chem. Soc.* **1972**, *94*, 3964.
- [98] Taton, D.; Borgne, A. L.; Spassky, N.; Noël, C. *Macromol. Chem. Phys.* **1995**, *196*, 2941.
- [99] Ah Toy, A.; Reinicke, S.; Müller, A. H. E.; Schmalz, H. *Macromolecules* **2007**, *40*, 5241.
- [100] Esswein, B.; Möller, M. *Angew. Chem., Int. Ed.* **1996**, *35*, 623.
- [101] Stolarzewicz, A. *Makromol. Chem.* **1986**, *187*, 745.
- [102] Dondoni, A. *Angew. Chem., Int. Ed.* **2008**, *47*, 8995.
- [103] Huisgen, R. *Angew. Chem., Int. Ed.* **1963**, *2*, 565.
- [104] Huisgen, R. *Angew. Chem., Int. Ed.* **1963**, *2*, 633.
- [105] Binder, W. H.; Sachsenhofer, R. *Macromol. Rapid Commun.* **2007**, *28*, 15.
- [106] Hein, C. D.; Liu, X.-M.; Wang, D. *J. Pharm. Sci.* **2008**, *25*, 2216.
- [107] Sumerlin, B. S.; Vogt, A. P. *Macromolecules* **2009**, *43*, 1.
- [108] Vogt, A. P.; Sumerlin, B. S. *Macromolecules* **2006**, *39*, 5286.
- [109] Gao, H.; Louche, G.; Sumerlin, B. S.; Jahed, N.; Golas, P.; Matyjaszewski, K. *Macromolecules* **2005**, *38*, 8979.
- [110] Maxwell, J. C. *Phil. Trans.* **1867**, *157*, 49.
- [111] Gehm, L., http://www.rheologie.de/fileadmin/user_upload/pdfs/Messtechnik.pdf, 2010-08-09.
- [112] Macosko, C. W. Linear Viscoelasticity. In *Rheology: Principles, Measurements and Applications*; Macosko, C. W., Ed.; VCH Publishers, Inc.: New York, 1994; pp 109.
- [113] Clark, A.; Ross-Murphy, S. Structural and mechanical properties of biopolymer gels. In *Biopolymers*; 1987; pp 57.
- [114] Tobitani, A.; Ross-Murphy, S. B. *Macromolecules* **1997**, *30*, 4855.
- [115] Chambon, F.; Winter, H. H. *Polym. Bull.* **1985**, *13*, 499.
- [116] Winter, H.; Mours, M. Rheology of Polymers Near Liquid-Solid Transitions. In *Neutron Spin Echo Spectroscopy Viscoelasticity Rheology*; 1997; pp 165.
- [117] Richtering, H. W.; Gagnon, K. D.; Lenz, R. W.; Fuller, R. C.; Winter, H. H. *Macromolecules* **1992**, *25*, 2429.
- [118] Nyström, B.; Walderhaug, H.; Hansen, F. K. *Faraday Discuss.* **1995**, *101*, 335.
- [119] Nyström, B.; Walderhaug, H. *J. Phys. Chem.* **1996**, *100*, 5433.
- [120] Matsumoto, T.; Okubo, T. *J. Rheol.* **1991**, *35*, 135.

- [121] Hirashima, M.; Takaya, T.; Nishinari, K. *Thermochim. Acta* **1997**, *306*, 109.
- [122] ILL, <http://www.ill.eu/instruments-support/instruments-groups/instruments/d11>, 2010-08-09.
- [123] LLB, http://www-llb.cea.fr/en/Web/part_2_e.pdf, 2010-08-09.
- [124] Chen, S. H. *Annu. Rev. Phys. Chem.* **1986**, *37*, 351.
- [125] Pedersen, J. S. Modelling of small-angle scattering data from colloids and polymer systems. In *Neutrons, X-rays and Light: Scattering Methods Applied to Soft, Condensed Matter*; Lindner, P.; Zemb, T., Eds.; Elsevier Science B.V.: Amsterdam, 2002; pp 391.
- [126] Prud'homme, R. K.; Wu, G.; Schneider, D. K. *Langmuir* **1996**, *12*, 4651.
- [127] Huang, Y.-Y.; Chen, H.-L.; Hashimoto, T. *Macromolecules* **2003**, *36*, 764.
- [128] Föll, H., http://www.tf.uni-kiel.de/matwis/amat/mw1_ge/, 2010-08-09.
- [129] Lindner, P. Scattering experiments under external constraints: SANS and shear flow. In *Neutrons, X-rays and Light: Scattering Methods Applied to Soft, Condensed Matter*; Lindner, P.; Zemb, T., Eds.; Elsevier Science B.V.: Amsterdam, 2002; pp 423.
- [130] Perreur, C.; Habas, J.-P.; François, J.; Peyrelasse, J.; Lapp, A. *Phys. Rev. E* **2002**, *65*, 041802.
- [131] Berne, B. J.; Pecora, R., *Dynamic Light Scattering*. John Wiley & Sons: New York, 1976.
- [132] Schmitz, K. S., *An Introduction to Dynamic Light Scattering by Macromolecules*. Academic Press, Inc.: San Diego, 1990.
- [133] Brown, W., *Light Scattering - Principles and Development*. Calendron Press: Oxford, 1996.
- [134] Siegert, A. J. F. *MIT Rad Lab Rep No 465* **1943**.
- [135] <http://www.hydrogele.de/>.

2 Overview of the thesis

The research presented within this thesis, including five publications, focuses on the synthesis and the utilization of a novel, double stimuli-responsive ABC triblock terpolymer sequence for the construction of “smart” hydrogels being responsive to several stimuli, including pH, temperature and magnetic fields.

The synthesis of the desired triblock terpolymers first of all required the development of a new synthetic route based on sequential anionic polymerization. The success of this route was demonstrated by synthesizing exemplary triblock terpolymers, as shown in **Chapter 3**.

In a next step, a variety of P2VP-*b*-PEO-*b*-P(GME-*co*-EGE) triblock terpolymers for hydrogel formation was synthesized. Systematic investigations on the pH- and temperature-dependent solubility and gelation properties of these polymers, including DLS, rheology, and SANS, are presented in **Chapter 4**.

The initial SANS studies revealed, that gels formed at $\text{pH} > 5$ and room temperature are composed of a cubic packing of core-shell-corona (CSC) micelles. A determination of the exact crystal lattice of these gels was achieved by performing additional SANS measurements under steady shear. The different states of alignment correlated with rheological features and the exact type of crystal structure of the sample (body centered cubic) are discussed in **Chapter 5**.

After a successful proof of our “smart” hydrogel concept we further wanted to extend it to ABC triblock terpolymers with more versatile C blocks, in particular POEGMA und PDMAEMA. This purpose required the establishment of an alternative synthesis route combining anionic polymerization and ATRP via “click” chemistry. Challenges occurring during this procedure and rheological features of aqueous solutions of the finally obtained polymers are described in **Chapter 6**.

In a last part of the thesis, which is described in **Chapter 7**, the “smart” hydrogel concept was extended by introducing sensitivity to magnetic fields. Slightly modified P2VP-*b*-PEO-*b*-P(GME-*co*-EGE) triblock terpolymers were complexed with maghemite nanoparticles. The resulting hybrid micelles formed hydrogels under suitable conditions, which can be manipulated by remote heating via external AC magnetic fields.

In the following, a brief summary of all results is presented.

2.1 One-pot synthesis of polyglycidol-containing block copolymers with alkyl lithium initiators using the phosphazene base $t\text{-BuP}_4$

The one-pot synthesis of a variety of triblock terpolymers including a polystyrene-*block*-poly(ethylene oxide)-*block*-poly(ethoxyethyl glycidyl ether) (PS-*b*-PEO-*b*-PEEGE), a poly(2-vinylpyridine)-*block*-poly(ethylene oxide)-*block*-poly(ethoxyethyl glycidyl ether) (P2VP-*b*-PEO-*b*-PEEGE) and a poly(ethylene oxide)-*block*-poly(ethoxyethyl glycidyl ether) (PEO-*b*-PEEGE) diblock copolymer, according to Figure 2.1 is presented. The crucial step within this synthetic procedure is the addition of the phosphazene base $t\text{-BuP}_4$ right after ethylene oxide is added to the reaction mixture.

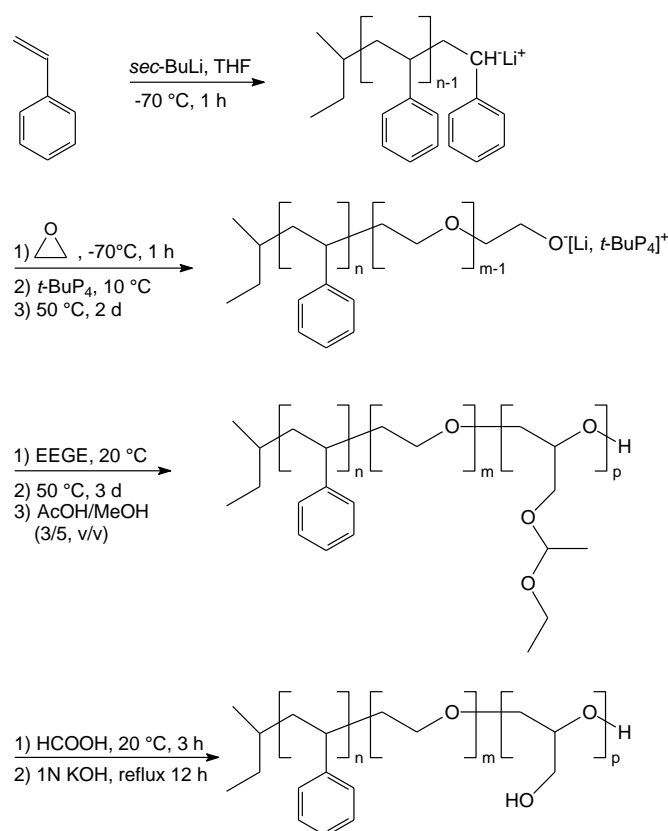


Figure 2.1. One-pot synthesis of polystyrene-*block*-poly(ethylene oxide)-*block*-poly(ethoxyethyl glycidylether) (PS-*b*-PEO-*b*-PEEGE) triblock terpolymers via sequential monomer addition using $sec\text{-BuLi}$ as initiator and subsequent deprotection of the PEEGE block to yield the corresponding polystyrene-*block*-poly(ethylene oxide)-*block*-polyglycidol (PS-*b*-PEO-*b*-PG) triblock terpolymer.

The initial polymerization of the vinyl monomers styrene and 2-vinylpyridine is initiated with commercially available $sec\text{-butyllithium}$, respectively. Consequently, the “living” carbanion

chain ends carry a Li^+ -counterion. After the addition of ethylene oxide, the chains are endcapped with an EO unit, i.e. the “living” carbanions are transferred into oxyanions. In combination with Li^+ , these anions form aggregates preventing further propagation. The phosphazene base $t\text{-BuP}_4$, however, acting as a complexing agent, helps to break up the aggregates by an effective complexation of Li^+ and thus promotes the polymerization of EO even in the presence of Li^+ .

In consequence, the block sequence could be built up in a one-pot procedure just by adding each monomer right after the previous block was finished. The SEC-traces in Figure 2.2 demonstrate the success of this procedure. The resulting product was free from precursor species and had a PDI of 1.02. In a final step, the resulting polymers were further treated with formic acid and KOH to deprotect the PEEGE block yielding polyglycidol (PG). The SEC-trace of the resulting polymer is shown in the inset of Figure 2.2.

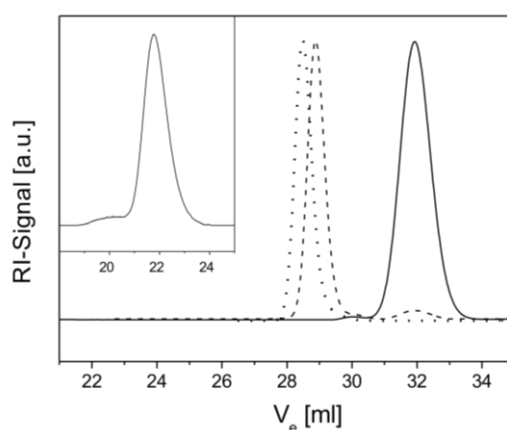


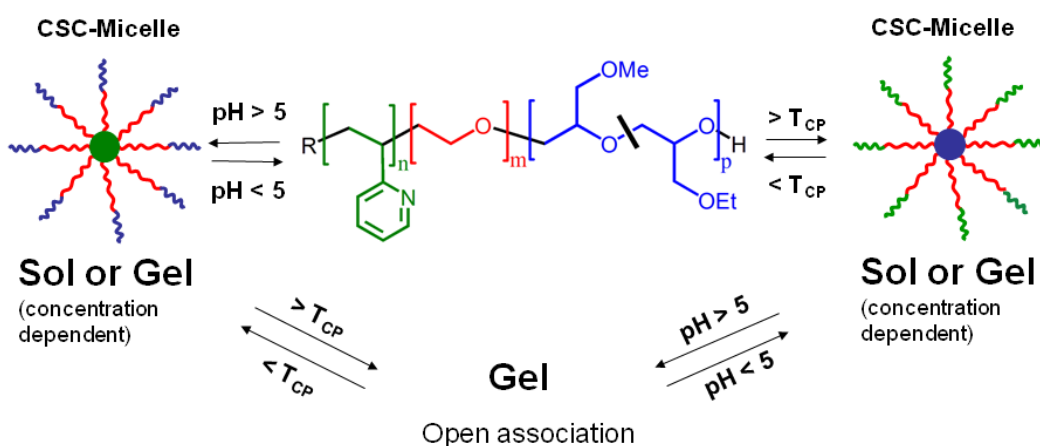
Figure 2.2. SEC (THF) traces of the synthesized $\text{PS}_{58}\text{-}b\text{-PEO}_{282}\text{-}b\text{-PEEGE}_{27}$ triblock terpolymer (dotted) including the PS (solid) and PS- b -PEO (dashed) precursors. The inset in shows the SEC trace of the $\text{PS}_{58}\text{-}b\text{-PEO}_{282}\text{-}b\text{-PG}_{27}$ triblock terpolymer obtained after deprotection of the PEEGE block, using NMP as eluent.

The polymerization of the last monomer, EEGE, was monitored by online FT-NIR spectroscopy. The first-order kinetic plot showed a slow initiation but appeared to be linear upon further progression, pointing to the absence of termination reactions.

It is emphasized, that the synthetic route presented here strongly simplifies the synthesis of block copolymers containing ethylene oxide and/ or glycidyl derivatives, since it avoids a change of counterions when switching from a vinyl to an epoxide monomer. Alternatively, potassium based initiators might be used throughout the whole synthesis, however, lithium based initiators are commercially available and provide for instance high 1,4-contents in polydienes.

2.2 Smart hydrogels based on double responsive triblock terpolymers

After the development of a suitable synthetic route (see section 2.1), a series of poly(2-vinyl pyridine)-*block*-poly(ethylene oxide)-*block*-poly(glycidyl methyl ether-*co*-ethyl glycidyl ether) (P2VP-*b*-PEO-*b*-P(GME-*co*-EGE)) triblock terpolymers was synthesized in order to realize our concept towards double stimuli-responsive hydrogels. The synthesized polymers contain a pH-sensitive P2VP and a thermo-sensitive P(GME-*co*-EGE) block. They are supposed to form core-shell-corona (CSC) micelles under conditions, where only one outer block is insoluble (Scheme 2.1), potentially leading to a gelation via a regular packing of the micelles. By switching the respective second block insoluble, too, these micelles will crosslink through their corona and form an open association, which will lead to gel formation as well, however with altered gel properties.



Scheme 2.1. Scheme of the formation of double responsive hydrogels based on P2VP-*b*-PEO-*b*-P(GME-*co*-EGE) triblock terpolymers.

Prior to the synthesis of the triblock terpolymers, a series of P(GME-*co*-EGE) copolymers with varying comonomer ratio was synthesized by anionic polymerization. The incorporation of GME was slightly preferred, yielding copolymers with a weak compositional gradient along the chain. It turned out, that the cloud point of P(GME-*co*-EGE) depends linearly on the GME/EGE molar ratio (Fig. 2.3). The coil-to-globule transition was very sharp in each case and showed almost no hysteresis. Within the P2VP-*b*-PEO-*b*-P(GME-*co*-EGE) triblock terpolymer, the respective coil-to-globule transition is shifted to higher temperatures by 5-10 °C at pH = 3, which marks the influence of the two hydrophilic blocks, PEO and P2VP.

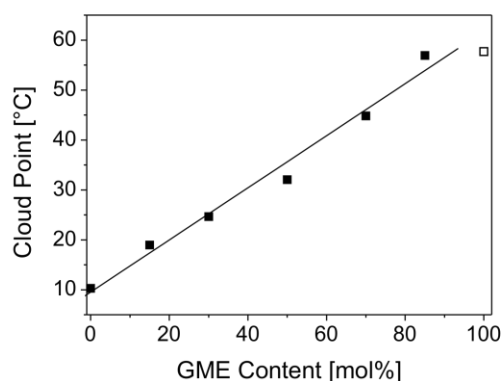


Figure 2.3. Cloud points of P(GME-*co*-EGE) copolymers and their dependence on the GME content (heating rate 1 K/min, 2.5 g/L in water, quality factor of the linear fit: 0.99); the open square corresponds to the cloud point of a homo-PGME taken from literature.

Concentrated aqueous solutions of P2VP₅₇-*b*-PEO₄₇₇-*b*-P(GME₂₂-*co*-EGE₂₂) and P2VP₆₂-*b*-PEO₄₅₂-*b*-P(GME₃₆-*co*-EGE₃₆) (subscripts denote the degree of polymerization of the corresponding block) at pH = 7 showed a gel-sol-gel transition upon temperature increase, which was accompanied with a unique gel strengthening (Fig. 2.4A).

It was further shown, that below certain threshold concentrations, only gel-sol transitions or no gelation at all were detectable in the case of both polymers. On the other hand, sol-gel transitions were observed at pH < 5. In this case, regular packings of CSC micelles with inverse structure, i.e. a P(GME-*co*-EGE) core and a P2VP corona were formed.

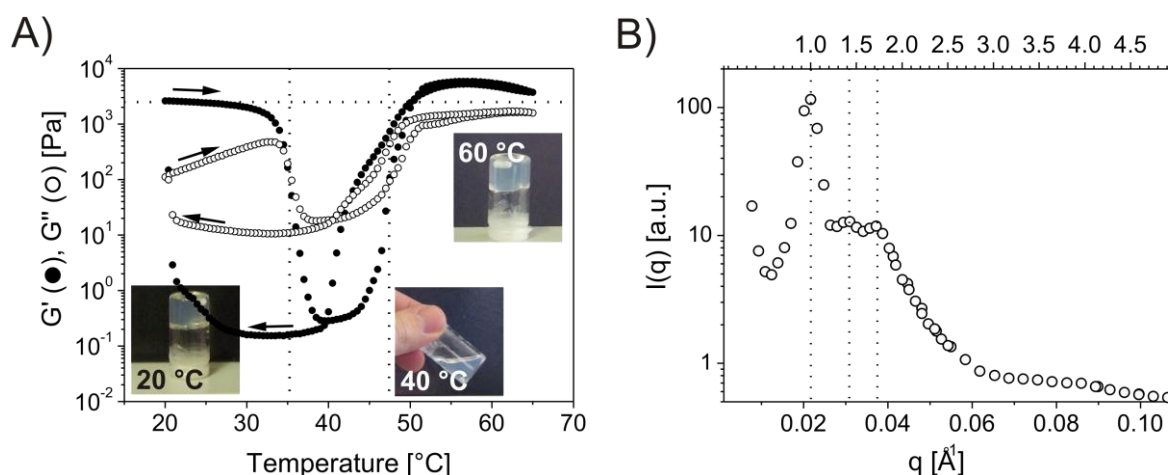


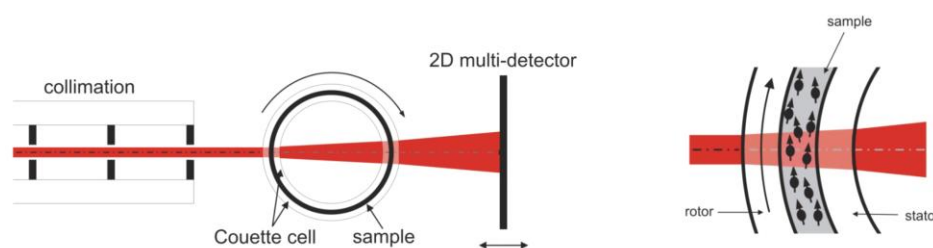
Figure 2.4. A) Temperature dependent G' and G'' of an 18 wt% aqueous solution of P2VP₅₇-*b*-PEO₄₇₇-*b*-P(GME₂₂-*co*-EGE₂₂) at pH = 7 solutions (1 Hz, 0.7 % strain, 0.1 K/min); B) SANS data for a 16.6 wt% solution of P2VP₆₂-*b*-PEO₄₅₂-*b*-P(GME₃₆-*co*-EGE₃₆) in D₂O at pH = 7, top x-axis normalized to 1st order reflection.

Small angle neutron scattering (SANS) experiments of diluted solutions at pH = 7 (not shown here) confirmed the presence of spherical micelles with the proposed core-shell-corona structure. The micellar dimensions were extracted from SANS and DLS experiments.

The low temperature gel (Fig. 2.4A) could be identified as a cubic packing of the CSC micelles. The relative peak positions of $1:2^{1/2}:3^{1/2}$ in the corresponding SANS profile (Fig. 2.4B) point to the presence of a simple cubic or a body centered cubic packing. It is noted, that it was not possible to make a decision about the exact type of the formed cubic lattice, due to the lack of higher order reflections. An improvement of the long-range order within the sample by applying steady shear should help to derive more information about the crystal structure.

2.3 Flow induced ordering in cubic gels formed by P2VP-*b*-PEO-*b*-P(GME-*co*-EGE) triblock terpolymer micelles: A rheo-SANS study

In this work, scattering patterns of a 19 wt% aqueous solution of P2VP₅₆-*b*-PEO₄₁₀-*b*-P(GME₄₈-*co*-EGE₄₈) at pH = 7 were recorded while the sample was subjected to steady shear. Previous SANS measurements of non-sheared samples of comparable polymers revealed the presence of a cubic lattice of CSC micelles, either of the simple cubic (sc) or the body centered cubic (bcc) type (see section 2.2). Now, steady shear was applied in order to enhance the long-range order in the cubic packing of the CSC micelles, giving the opportunity to determine the exact crystal structure but also to interpret structural transition phenomena of the system. For this purpose, a conventional SANS setup was coupled with a Couette-type shear cell according to Scheme 2.2.



Scheme 2.2. Schematic depiction of the rheo-SANS setup, using a Couette-type shear cell geometry.

Parallel to the SANS measurements, the shear stress and viscosity of the sample were recorded in dependence of the shear rate (Fig. 2.5). It turned out, that the sample shows a strong shear thinning behavior below shear rates of 80 s^{-1} .

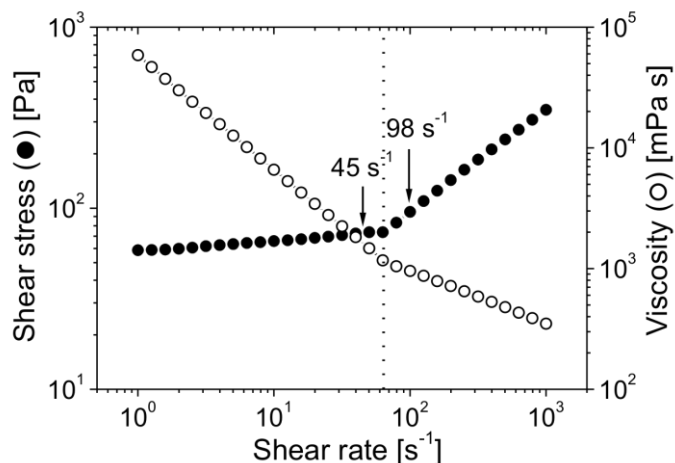


Figure 2.5. Shear stress and shear viscosity as a function of shear rate of a 19 wt% aqueous solutions of P2VP₅₆-*b*-PEO₄₁₀-*b*-P(GME₄₈-*co*-EGE₄₈) at pH = 7 and 20 °C.

Based on the SANS results we could conclude, that this strong shear thinning behavior is due to a structural reorganization process from a non-oriented polydomain structure to a polydomain structure with a weak preferential orientation and finally to a state of pronounced macroscopic alignment, as indicated by the development of a strong anisotropic pattern with sharp Bragg spots (Fig. 2.6B). The weak continuous Bragg ring originates from non-oriented polydomains, whereas the sharp Bragg spots represent the macroscopically aligned domains.

In Figure 2.6A, a theoretical diffraction pattern of bcc domains oriented with the [111] direction in shear direction is shown. The red spots represent a twinned structure with an exclusive orientation of the {110} planes parallel to the shear plane. The black spots originate from a set of non-twinned domains, which are oriented with their {110}, {211} or {321} planes parallel to the shear plane. From these theoretical predictions we could conclude that the pattern of Figure 2.6B originates from body centered cubic domains, which are oriented with their [111] direction in shear direction and either their {110} or, with a smaller fraction, their {211} planes parallel to the shear plane. Further measurements in tangential geometry supported the fact, that we deal with a twinned structure, although this feature could not be unambiguously verified.

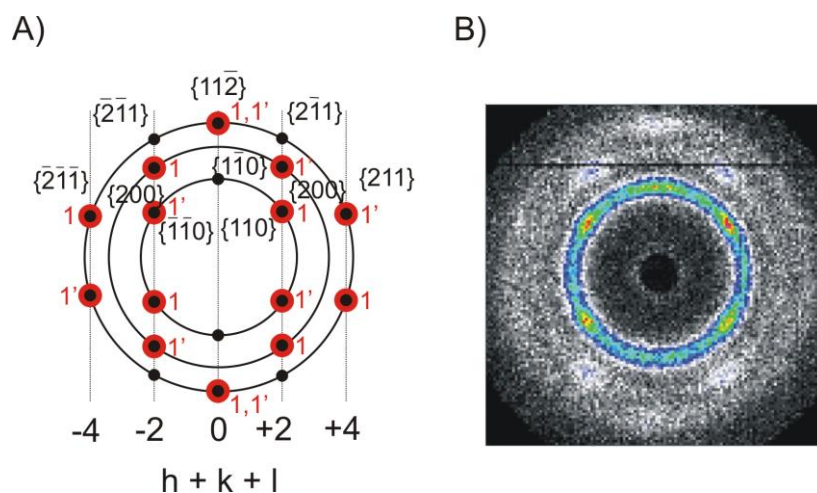


Figure 2.6. A) Theoretical diffraction pattern including indexation for a bcc structure oriented with the [111] direction in flow direction and the {110}, {211} and {321} planes parallel to the shear plane (black spots), and expected diffraction pattern for a homogeneously oriented twinned bcc structure with the [111] direction in flow direction and the {110} planes parallel to the shear plane (red spots); B) 2D SANS pattern of a 19 wt% solution of P2VP₅₆-*b*-PEO₄₁₀-*b*-P(GME₄₈-*co*-EGE₄₈) at pH = 7 and T = 20 °C for radial scattering geometry, obtained after cessation of shear at 98 s⁻¹ with a long period of pre-shearing.

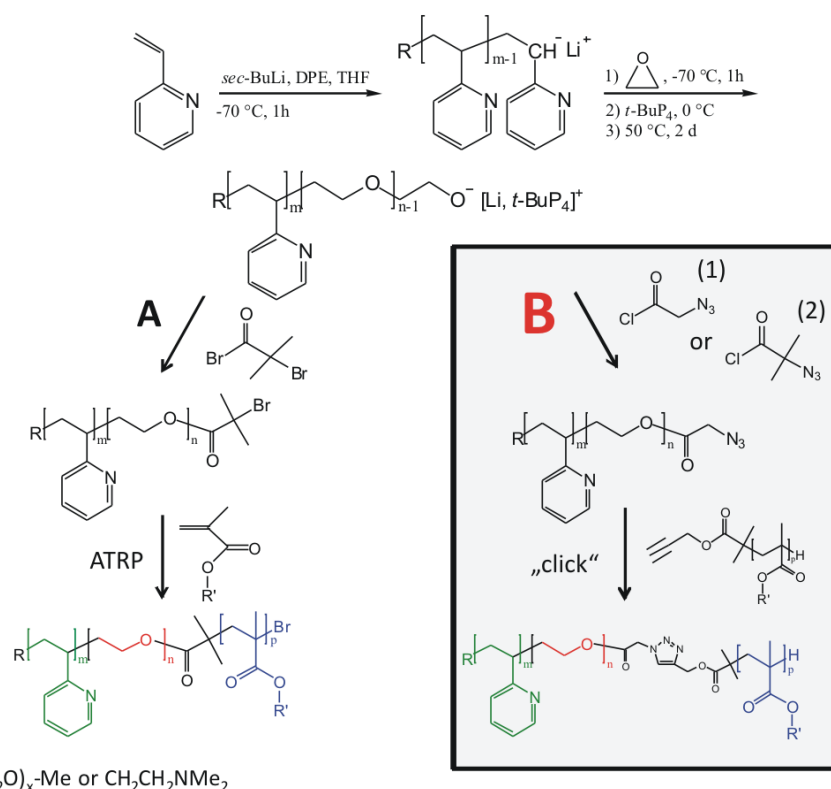
Finally, we could show that the gel-sol transition occurring upon temperature increase (as shown in section 2.2) is due to a shrinkage of the micellar corona. This was indicated by a decrease of the intermicellar distance, expressed by a shift of the structure factor maximum in the radially averaged data to higher q -values.

2.4 Combination of “living” anionic polymerization and ATRP via “click” chemistry as a versatile route to multiple responsive triblock terpolymers and corresponding hydrogels

The synthetic route towards ABC triblock terpolymers via sequential anionic polymerization presented in section 2.1 is limited to block sequences with epoxide based C blocks. The extension of our hydrogel concept towards more versatile multi-responsive systems, however, required the introduction of alternative C blocks. In this section, a new synthetic approach is presented combining anionic polymerization and ATRP via “click” chemistry (Scheme 2.3).

A “living” P2VP-*b*-PEO diblock copolymer was synthesized according to the procedure described in section 2.1 and subsequently terminated with an azide functionalized acid chloride in order to introduce an N₃ end group. Parallel to that, alkyne end-functionalized

poly(oligo(ethylene glycol) methacrylate) (POEGMA) and poly(dimethylaminoethyl methacrylate) (PDMAEMA) polymers were synthesized by ATRP using propargyl 2-bromoisobutyrate as initiator. The obtained polymer precursors were subsequently coupled together using the 1,3-dipolar Huisgen cycloaddition (“click” chemistry). A direct grafting of the C block from a P2VP-*b*-PEO diblock precursor via ATRP (route A, Scheme 2.3) was not successful, since P2VP strongly disturbs the polymerization process by complexing Cu(I).



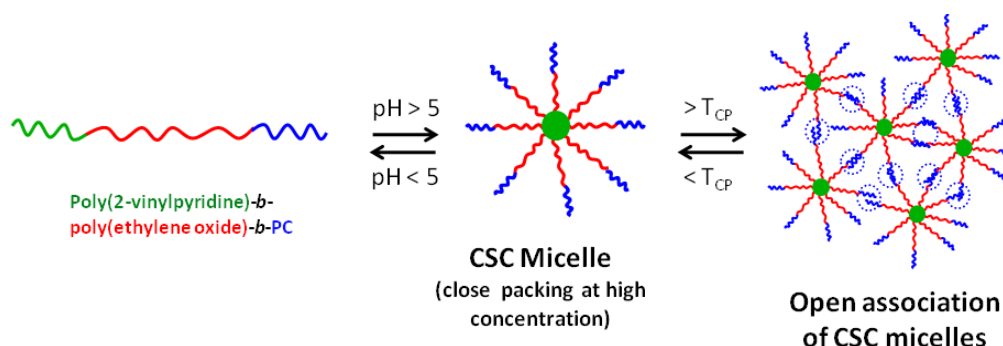
Scheme 2.3. Different approaches for a combined ATRP and anionic polymerization strategy towards ABC triblock terpolymers with a P2VP A block, a water soluble PEO B block and varying thermo-sensitive C blocks.

We recognized that POEGMA gets reactivated under “click” conditions (presence of CuBr and PMDETA), leading to the formation of polymerizable macromonomers. In consequence, the polymerization of OEGMA had to be terminated with Bu_3SnH , causing an exchange of the halogen end group by hydrogen and therefore avoiding the risk of reactivation during the “click” reaction.

The P2VP-*b*-PEO precursors were end-functionalized with either azidoacetyl chloride (1) or 2-azidoisobutyryl chloride (2) (Scheme 2.3). In the first case the subsequently performed “click” reaction proceeded quantitatively, whereas in the latter case no “click” product was observable. However, a model reaction in deuterated THF, which was directly monitored by

$^1\text{H-NMR}$, confirmed the formation and the stability of the triazol ring also in that case. The failure of the coupling reaction in fact arose from traces of the phosphazene base $t\text{-BuP}_4$, remaining in the P2VP- b -PEO precursor after polymerization. This base gets hydrolyzed by contact with moisture yielding hydroxide ions with $[t\text{-BuP}_4\text{-H}]^+$ counterion. A nucleophilic attack of these ions at the tertiary carbon atom to which the triazol ring is attached finally caused a cleavage of the C block. In consequence, a rigorous exclusion of moisture is required in order to provide a successful “click” reaction when using P2VP- b -PEO diblock precursors carrying end group (2).

For hydrogel formation, two triblock terpolymers, P2VP₅₆- b -PEO₃₇₀- b -P[(MEO₂MA)₈₉- co -(MEO_{8.5}MA)₇] and P2VP₅₆- b -PEO₃₇₀- b -PDMAEMA₇₀, were synthesized. Under neutral conditions, these polymers form core-shell-corona (CSC) micelles with a P2VP core, which can either pack in a cubic lattice or form an open association when reaching the cloud point of the respective C block (Scheme 2.4). A 20 wt% aqueous solution of P2VP₅₆- b -PEO₃₇₀- b -P[(MEO₂MA)₈₉- co -(MEO_{8.5}MA)₇] at pH = 7 showed a transition from a weak gel to a sol and finally to a strong gel upon temperature increase. The low temperature gel was assigned to a fractal network of micelles, whereas the high temperature gel was formed by the predicted open association of micelles.



Scheme 2.4. Schematic representation of the structure of the core-shell-corona micelles, formed by P2VP- b -PEO- b -PC triblock terpolymers in water at pH > 5, and the corresponding gelation mechanism at low and high temperature, respectively.

The temperature dependent behavior of concentrated solutions of the CSC micelles formed by P2VP₅₆- b -PEO₃₇₀- b -PDMAEMA₇₀ could be tuned by an additional pH-adjustment. At pH = 8, a 13.5 wt% solution of P2VP₅₆- b -PEO₃₇₀- b -PDMAEMA₇₀ showed a gel-sol transition, whereas at pH = 9, a transition from a weak to a strong gel was observed (Fig. 2.7). The altered behavior after the pH change could be explained by a different degree of protonation of the PDMAEMA corona of the CSC micelles at different pH, affecting the cloud point of the corona, the effective micellar volume and the intermicellar repulsion.

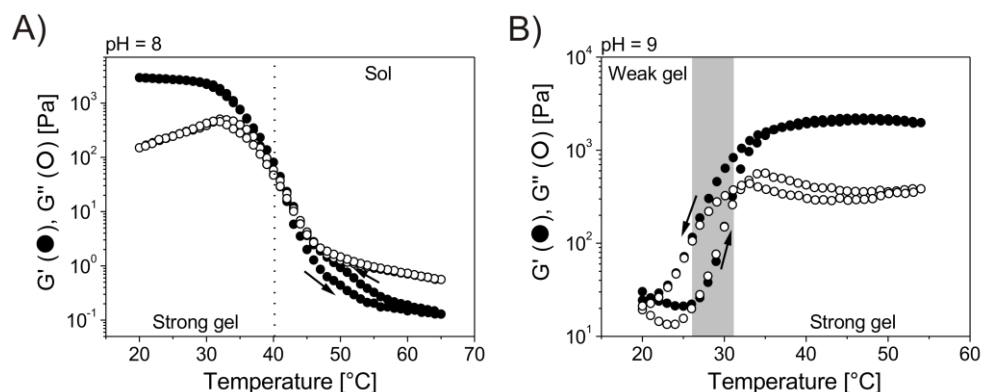


Figure 2.7. Temperature dependence of G' and G'' of a 13.5 wt% aqueous solution of P2VP₅₆-*b*-PEO₃₇₀-*b*-PDMAEMA₇₀ ($f = 1$ Hz, $\gamma = 0.7$ %, 0.1 K/min): A) at pH = 8, and B) at pH = 9.

At pH < 8 finally, no gelation at all was observed at room temperature at a comparable concentration, which was contradictory to what we expected, since the PDMAEMA corona should be expanded at low pH due to a higher degree of protonation. The micellar size, however, decreases upon decreasing pH, a feature, which we referred to a strong interaction with the PEO shell. Consequently, a 15.4 wt% sample at pH = 7.5 was fluid. Upon addition of trivalent hexacyanocobaltate(III) ($[\text{Co}(\text{CN})_6]^{3-}$) ions, however, an upper critical solution temperature (UCST) was induced, leading to gel formation below the UCST. This gel formation originated from a crosslinking effect based on electrostatic interactions. The gel-sol transition temperature strongly depends on the $[\text{Co}(\text{CN})_6]^{3-}$ concentration as shown in Figure 2.8. A gel-sol transition finally could also be triggered by UV-light within a certain temperature window (Fig. 2.8), since $[\text{Co}(\text{CN})_6]^{3-}$ ions exchange one CN⁻ ligand with H₂O upon UV-illumination (photo-aquation), causing a valency change from III to II.

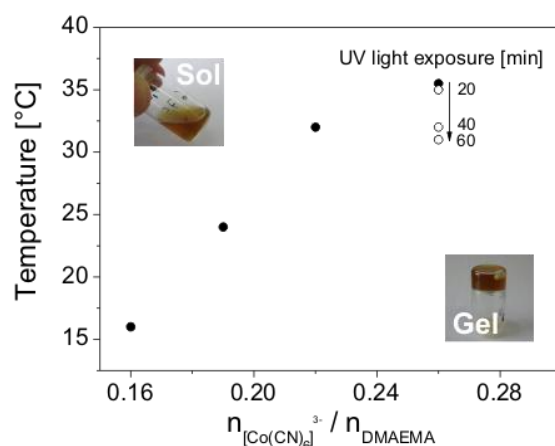


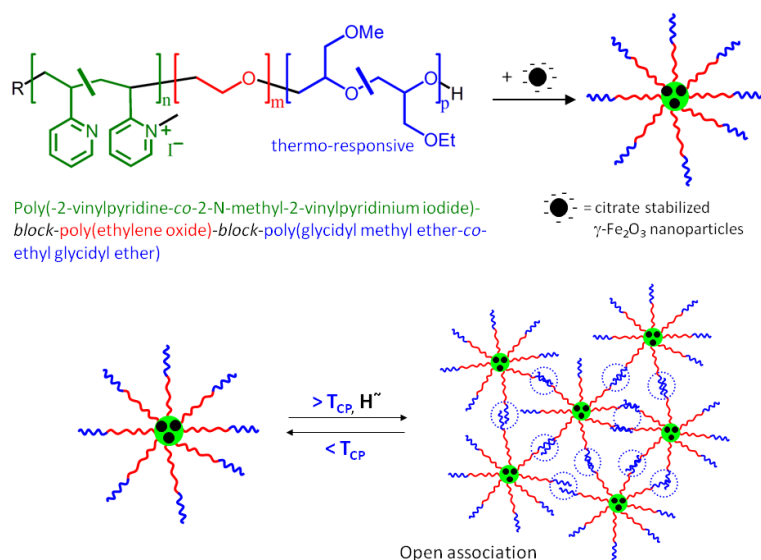
Figure 2.8. Gel-Sol transition temperatures of a 15.2 wt% aqueous solution of P2VP₅₆-*b*-PEO₃₇₀-*b*-DMAEMA₇₀ at pH = 7.5 in dependence of the molar ratio of hexacyanocobaltate(III) and DMAEMA units. The photographs show the sample in the gel and the sol state, respectively. The open symbols represent gel-sol transition temperatures after exposure to UV light with a wavelength band of 310 – 400 nm for different time intervals.

In conclusion, the combination of anionic polymerization and ATRP via “click” chemistry gave access to ABC triblock terpolymers which are suitable for the formation of hydrogels which respond to pH and temperature, multivalent anions and UV-light.

2.5 Magneto-responsive hydrogels based on maghemite/triblock terpolymer hybrid micelles

In this publication, the P2VP-*b*-PEO-*b*-P(GME-*co*-EGE) triblock terpolymers were utilized to form polymer/ magnetic nanoparticle hybrid structures in order to extend our “smart” hydrogel concept by introducing sensitivity to magnetic fields. The main goal was to create a hydrogel, which can be manipulated by a remote trigger.

We utilized the concept of hybrid structure formation via electrostatic interactions to create core-shell-corona hybrid micelles with a thermo-sensitive corona and a core, containing maghemite ($\gamma\text{-Fe}_2\text{O}_3$) nanoparticles. For that purpose, the P2VP block of a P2VP₆₀-*b*-PEO₃₉₈-*b*-P(GME₂₆-*co*-EGE₂₆) triblock terpolymer (TB1) was quaternized to a low extent in order to introduce positive charges. On the other hand, maghemite nanoparticles (R ≈ 4 nm) with a negatively charged citrate shell were synthesized. By a simple mixing of both components (Scheme 2.5), the desired hybrid micelles were formed.



Scheme 2.5. Formation of hybrid micelles via complexation of citrate stabilized $\gamma\text{-Fe}_2\text{O}_3$ nanoparticles with a quaternized Pq2VP-*b*-PEO-*b*-P(GME-*co*-EGE) triblock terpolymer, and subsequent reversible gelation via open association of hybrid micelles at temperatures above the cloud point (T_{CP}) of the P(GME-*co*-EGE) block.

DLS and TEM experiments revealed, that we deal with narrowly distributed hybrid micelles with a size independent of the polymer/ nanoparticle mixing ratio (Fig. 2.9). From TEM and TGA, we could further conclude, that each micelle consists of clusters of 3-4 nanoparticles, being stabilized by app. 30 polymer chains. Excess chains are present as unimers, as confirmed by field flow fractionation (AF4) and DLS.

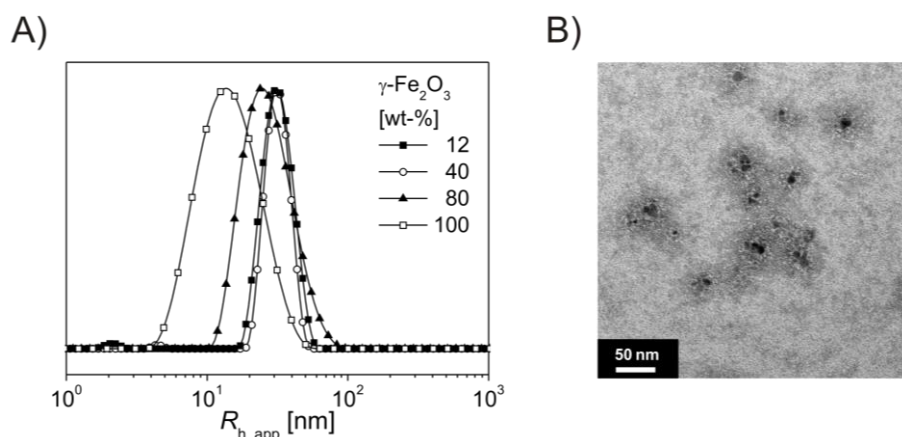


Figure 2.9. A) Intensity-weighted distribution of apparent hydrodynamic radii ($R_{h, app}$) of $\gamma\text{-Fe}_2\text{O}_3$ /TB1 hybrid micelles as a function of the $\gamma\text{-Fe}_2\text{O}_3$ fraction in the overall solids content (1 g/L; $\theta = 90^\circ$); B) TEM micrograph of hybrid micelles formed in a $\gamma\text{-Fe}_2\text{O}_3$ /TB1 mixture (0.2 g/L, $\gamma\text{-Fe}_2\text{O}_3$ /TB1 = 33/67 w/w), the sample was prepared by drop-coating onto a carbon-coated copper grid and subsequent staining with RuO_4 .

Temperature dependent DLS experiments revealed, that a minimum amount of nanoparticles, and thus hybrid micelles, is necessary in order to induce aggregation of micelles at elevated temperatures which is the crucial step in order to achieve gelation in concentrated samples. The temperature dependent dynamic moduli of a solution with 36 wt% solids content (maghemite/TB1 mixing ratio = 45/55 w/w) is shown in Figure 2.10A. The low temperature gel is assumed to be due to a regular packing of the hybrid micelles, whereas the high temperature gel originates from an open association of these micelles (Scheme 2.5).

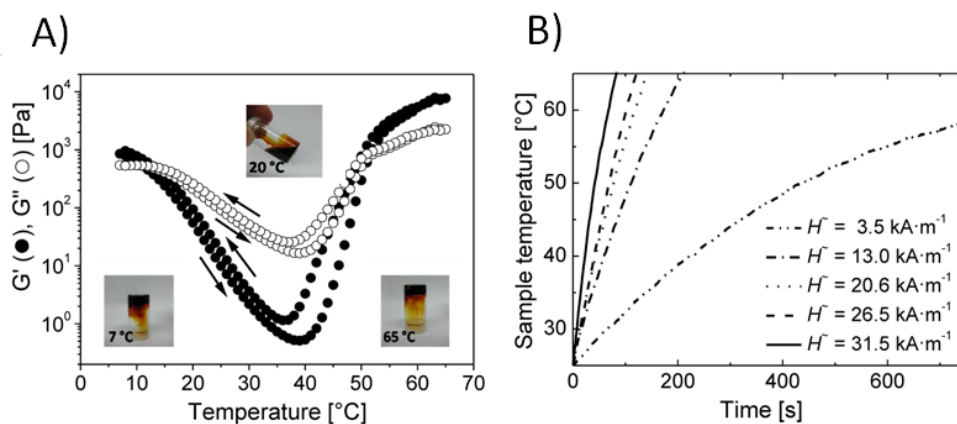


Figure 2.10. A) temperature dependent G' and G'' ($\gamma = 0.7\%$, $f = 1$ Hz, 0.1 K/min) including photographs at different temperatures and B) heating curves obtained in HF-MC experiments at different field strengths H for a 36 wt% solution with a $\gamma\text{-Fe}_2\text{O}_3$ /TB1 ratio of 45/55 w/w.

We also showed, that the superparamagnetic character of the maghemite nanoparticles is preserved upon micelle formation (not shown here). High frequency magnetocalorimetry (HF-MC) experiments finally demonstrated, that the hybrid solutions can be heated via AC magnetic fields (Fig. 2.10B). With a sufficiently high field strength ($H \sim > 13$ kA/m), the gelation temperature of around 50 °C can be reached within only 1-2 min. In consequence, we were able to establish a system with a magnetic field triggered gelation.

2.6 Individual contributions to joint publications

The results presented in this thesis were obtained in collaboration with others, and have been published or will be submitted to publication as indicated below. In the following, the contributions of all the coauthors to the different publications are specified. The asterisk denotes the corresponding author for each publication.

Chapter 3

This work is published in *Macromolecules* **2007**, *40*, 5241-5244 under the title:
“One-pot synthesis of polyglycidol-containing block copolymers with alkyllithium initiators using the phosphazene base *t*-BuP₄”

*by Andrew Ah Toy, Stefan Reinicke, Axel H. E. Müller, and Holger Schmalz**

I performed the synthesis of the P2VP-*b*-PEO-*b*-PEEGE triblock terpolymer and was involved in the molecular characterization of all synthesized polymers, including NMR and SEC measurements. The manuscript was written by me and Holger Schmalz. Andrew Ah Toy performed the remaining experiments. Axel H. E. Müller was involved in the discussions.

Chapter 4

This work is published in *Soft Matter* **2009**, *5*, 2648-2657 under the title:
“Smart hydrogels based on double responsive triblock terpolymers”

*by Stefan Reinicke, Joachim Schmelz, Alain Lapp, Matthias Karg, Thomas Hellweg, and Holger Schmalz**

I conducted most of the experiments including synthesis and characterization of all triblock terpolymers and wrote the publication. Joachim Schmelz was involved in the work on the P(GME-*co*-EGE) copolymers. Alain Lapp was the local contact at the LLB, CEA Saclay during the SANS experiments. Matthias Karg assisted the SANS experiments, performed SANS data treatment and wrote the experimental SANS part. Thomas Hellweg and Holger Schmalz were involved in the discussions and the correction of the manuscript.

Chapter 5

This work is published in *Macromolecules*, **2010**, *43*, 10045-10054 under the title:
“Flow induced ordering in cubic gels formed by P2VP-*b*-PEO-*b*-P(GME-*co*-EGE) triblock terpolymer micelles: A rheo-SANS study”

*by Stefan Reinicke, Matthias Karg, Alain Lapp, Lutz Heymann, Thomas Hellweg, and Holger Schmalz**

I performed most of the experiments and wrote the publication. Matthias Karg assisted the SANS experiments, performed data treatment and was involved in the discussions. Alain Lapp was the local contact at the LLB, CEA Saclay during the SANS experiments and was involved in the discussions. Lutz Heymann performed the rheology measurements. Thomas Hellweg and Holger Schmalz were involved in the discussions and the correction of the manuscript.

Chapter 6

This work is published in *Colloid and Polymer Science*, DOI: 10.1007/s00396-010-2359-7 under the title:
“Combination of living anionic polymerization and ATRP via click chemistry as a versatile route to multiple responsive triblock terpolymers and corresponding hydrogels”

*by Stefan Reinicke, and Holger Schmalz**

I performed all experiments and wrote the publication. Holger Schmalz was involved in the discussions and the correction of the manuscript.

Chapter 7

This work is published in *Soft Matter* **2010**, 6, 2760-2773 under the title:

“Magneto-responsive hydrogels based on maghemite/triblock terpolymer hybrid micelles”

*by Stefan Reinicke, Stefan Döhler, Sandrine Tea, Marina Krekhova, Renate Messing, Annette M. Schmidt and Holger Schmalz**

I performed the majority of the experiments and wrote the publication.

Stefan Döhler prepared a part of the hydrogel samples. Sandrine Tea performed the AF4 measurements. Marina Krekhova provided the maghemite nanoparticles. Renate Messing and Annette M. Schmidt performed the magnetization and magnetocalorimetry experiments and wrote the corresponding part of the manuscript. Holger Schmalz was involved in the discussions and the correction of the manuscript.

3 One-pot synthesis of polyglycidol containing block copolymers with alkyllithium initiators using the phosphazene base *t*-BuP₄

Andrew Ah Toy, Stefan Reinicke, Axel H. E. Müller, and Holger Schmalz*

Makromolekulare Chemie II, and Bayreuther Zentrum für Kolloide und Grenzflächen, Universität Bayreuth, D-95440 Bayreuth, Germany

ABSTRACT:

A novel and simple way of producing polyglycidol (PG) containing block copolymers via anionic ring-opening polymerization of the corresponding protected monomer, 1-ethoxyethyl glycidyl ether (EEGE), using alkyllithium initiators is presented. As an example, a polystyrene-*block*-poly(ethylene oxide)-*block*-poly(ethoxyethyl glycidyl ether) (PS-*b*-PEO-*b*-PEEGE) triblock terpolymer has been synthesized by sequential anionic polymerization in THF with *sec*-BuLi as initiator using the phosphazene base *t*-BuP₄, enabling the polymerization of EO and EEGE in the presence of Li⁺ counterions. All steps proceeded without side reactions, resulting in a narrowly distributed PS-*b*-PEO-*b*-PEEGE triblock terpolymer (PDI = 1.02). Deprotection of the PEEGE block yielded the corresponding PS-*b*-PEO-*b*-PG triblock terpolymer. First kinetic investigations on EEGE polymerization with a PEO[Li/*t*-BuP₄]⁺ macroinitiator are presented.

The advantage of this method is the possibility to produce PEEGE containing block copolymers with vinyl monomers in a one-pot synthesis, using commercially available alkyllithium initiators without the need of a time-consuming change of counterion to K⁺ or Cs⁺ in order to promote polymerization of EEGE.

3.1 Results and discussion

Polyglycidol and its derivatives have been of great interest during the last years due to its biocompatibility^{1,2} and to the fact that hyperbranched polyglycidols^{3,4} with a relatively narrow molecular weight distribution are accessible. In particular, the high functionality of linear and hyperbranched polyglycidols make them interesting for biomedical applications, such as drug carrier systems.

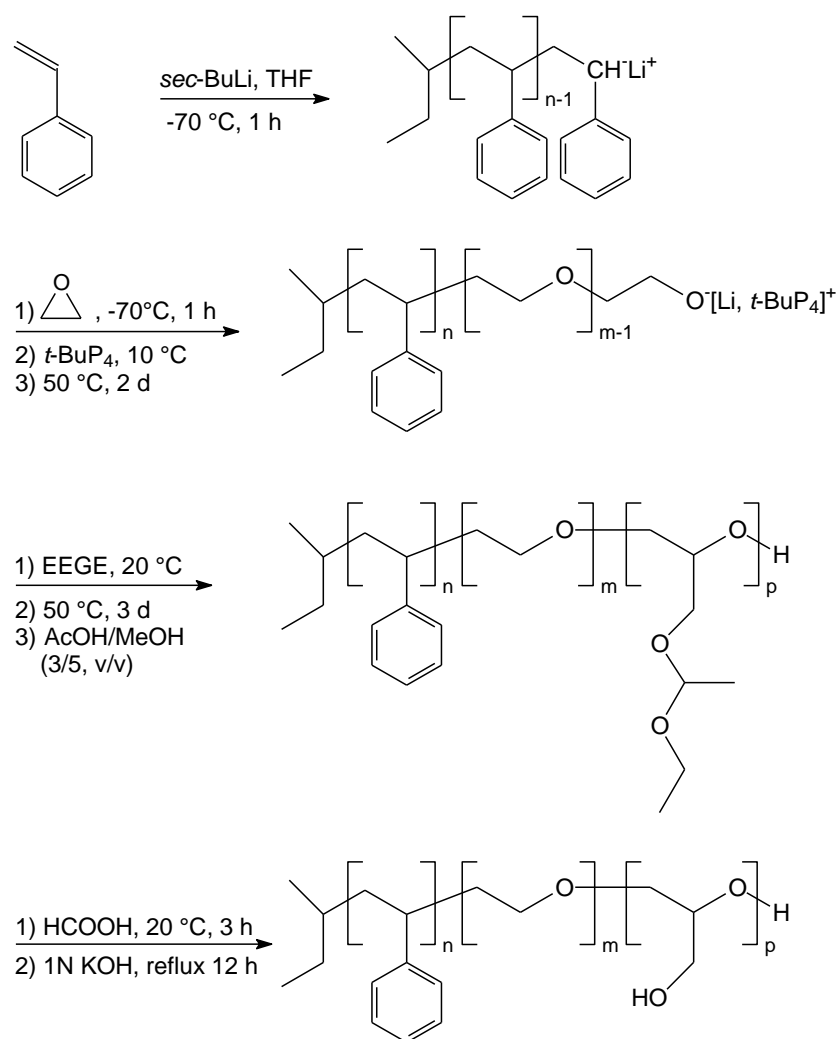
Linear polyglycidol can be synthesized via anionic ring-opening polymerization of the corresponding protected monomer, 1-ethoxyethyl glycidyl ether (EEGE) followed by deprotection in order to recover the pendant hydroxy groups.⁵⁻¹⁰ Various amphiphilic block copolymers based on polyglycidol as the water soluble component have been synthesized and their aggregation behavior studied in aqueous solutions, *e.g.* polystyrene-*b*-polyglycidol¹¹, poly(lactic acid)-*b*-poly(ethylene oxide)-*b*-polyglycidol^{12,13}, and polyglycidol-*b*-poly(propylene oxide)-*b*-polyglycidol^{5,14,15}. These block copolymers are able to form aggregates, such as micelles, in water at certain concentrations and/or temperatures, making them interesting for future applications in biomedical and other fields. Linear polyglycidol can be functionalized with acetic anhydride or ethyl isocyanate to obtain polymers which have easily adjustable lower critical solution temperatures.^{5,7,16} This opens a new application field for polyglycidol derivatives as thermosensitive polymers.

Up to now, most of the initiators used for the anionic ring-opening polymerization of EEGE are based on potassium or caesium alcoholates.^{5,6,8,17-19} However, block copolymers of EEGE and vinyl monomers, like styrene or dienes, cannot be synthesized in a one-pot procedure using commercially available alkyllithium initiators, as polymerization of epoxides does not proceed in the presence of Li⁺ counterions.^{20,21} Especially, in diene polymerization (butadiene, isoprene) to obtain a high content of 1,4-addition the use of Li⁺ counterions is indispensable. Thus, in order to promote polymerization of EEGE the counterion has to be changed to K⁺ or Cs⁺, resulting in additional functionalization and purification steps making the synthesis more time-consuming. It has been shown, that ethylene oxide (EO) can be polymerized in the presence of Li⁺ counterions using the phosphazene base *t*-BuP₄.^{22,23} This has been utilized in our group to synthesize block copolymers of vinyl monomers and EO, *e.g.* PS-*b*-PEO, in one-step using alkyllithium initiators without the need of changing the counterion to Na⁺ or K⁺ in order to facilitate EO polymerization.²⁴⁻²⁶ Here, this concept was applied to the anionic ring-opening polymerization of EEGE in the presence of Li⁺

counterions. In particular, we were interested in an extension of PEO based diblock copolymers by PEEGE in order to produce triblock terpolymers with a PEO middle block. The ability to produce well defined block copolymers is important in order to gain a deeper understanding of the self-assembly of block copolymers and justifies the use of expensive additives, like the phosphazene base *t*-BuP₄.

In this communication we describe the one-pot synthesis of poly(ethoxyethyl glycidyl ether) (PEEGE) containing block copolymers via sequential anionic polymerization using alkyllithium initiators in combination with the phosphazene base *t*-BuP₄. Deprotection of the PEEGE block resulted in the corresponding polyglycidol (PG) containing block copolymers.

A polystyrene-*block*-poly(ethylene oxide)-*block*-poly(ethoxyethyl glycidyl ether) (PS-*b*-PEO-*b*-PEEGE) triblock terpolymer was synthesized via sequential anionic polymerization of the corresponding monomers using *sec*-BuLi as initiator, as depicted in Scheme 3.1. First, styrene was polymerized at -70 °C in THF for 1 h. Subsequently, ethylene oxide (EO) was added. After stirring for 1 h the reaction mixture was slowly heated to 10 °C followed by addition of the phosphazene base *t*-BuP₄ in order to promote polymerization of EO, which was conducted at 50 °C for 2 days. A ratio of [*sec*-BuLi]/[*t*-BuP₄] = 1/0.95 was used in order to avoid an excess of phosphazene base, which might result in side reactions with 1-ethoxyethyl glycidyl ether (EEGE) due to its high basicity (^{MeCN}pK_{BH} = 42.7²⁷). After addition of EEGE at room temperature, it was allowed to polymerize at 50 °C for 3 days followed by termination with a mixture of acetic acid/methanol (3/5, v/v).



Scheme 3.1. One-pot synthesis of polystyrene-*block*-poly(ethylene oxide)-*block*-poly(ethoxyethyl glycidyl ether) (PS-*b*-PEO-*b*-PEEGE) triblock terpolymers via sequential monomer addition using *sec*-BuLi as initiator, and subsequent deprotection of the PEEGE block to yield the corresponding polystyrene-*block*-poly(ethylene oxide)-*block*-polyglycidol (PS-*b*-PEO-*b*-PG) triblock terpolymer.

Figure 3.1A shows the SEC traces of the synthesized $\text{S}_{58}\text{EO}_{282}\text{EEGE}_{27}$ triblock terpolymer (subscripts denote the degree of polymerization) including the corresponding precursors. All steps proceeded without termination and resulted in a narrowly distributed triblock terpolymer (PDI = 1.02, Table 3.1), revealing the successful polymerization of EEGE in the presence of $[\text{Li}/t\text{-BuP}_4]^+$ counterions.

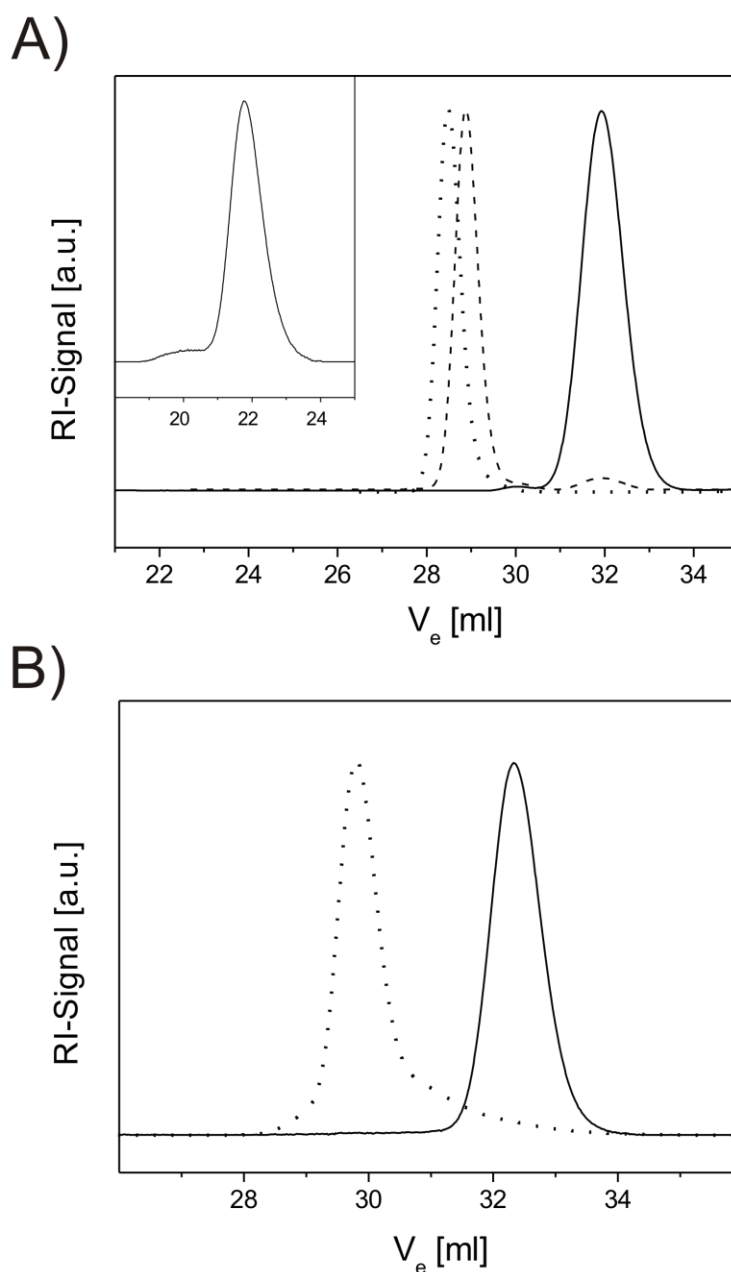


Figure 3.1. A) SEC (THF) traces of the synthesized $S_{58}EO_{282}EEGE_{27}$ triblock terpolymer (dotted) including the PS (solid) and PS-*b*-PEO (dashed) precursors; B) SEC (THF) traces of the EO₁₀₂EEGE₈₃ diblock copolymer (dotted) and the corresponding PEO (solid) precursor. The inset in A) shows the SEC trace of the $S_{58}EO_{282}G_{27}$ triblock terpolymer obtained after deprotection of the PEEGE block, using NMP as eluent.

Deprotection of the PEEGE block was achieved in a two-step procedure by reaction with formic acid and subsequent hydrolysis in alkaline media, according to the procedure given by Spassky et al.²⁸ Complete deprotection was verified via ¹H-NMR by the disappearance of specific EEGE signals at $\delta = 4.6$, 1.2, and 1.1 ppm (Figure 3.3). The deprotection proceeded

without significant side reactions, e.g. cleavage of the polymer chain, as a broadening of the corresponding SEC trace was not detected (Inset to Figure 3.1A). Furthermore, the number-average molecular weight, M_n , of the PS-*b*-PEO-*b*-PG triblock terpolymer determined via $^1\text{H-NMR}$ (Table 3.1) corresponds well with the theoretical M_n , calculated using the weight loss upon deprotection (72.11 g/mol per EEGE unit).

Table 3.1. Molecular weight characterization of synthesized block copolymers.

sample ^a	M_n (1 st block) [g/mol]	M_n (SEC) ^b [g/mol]	M_w/M_n ^b	M_n (NMR) ^c [g/mol]	M_n (deprotected) [g/mol]
S ₅₈ EO ₂₈₂ EEGE ₂₇	6 000 ^d	23 600	1.02	22 400	20 100 ^e / 20 500 ^f
2VP ₂₆ EO ₁₆₆ EEGE ₂₇	2 900 ^d	10 100	1.03	14 100	- / 12 200 ^f
EO ₁₀₂ EEGE ₈₃	4 500 ^e	12 100	1.10	16 600	- / 10 600 ^f

^a) The subscripts denote the degree of polymerization of the corresponding block;

^b) Determined by SEC in THF calibrated with PS standards;

^c) Calculated from $^1\text{H-NMR}$ spectra in CDCl_3 using the absolute M_n of the first block for calibration (for details see Supporting Information);

^d) Determined by MALDI-ToF (for details see Supporting Information);

^e) Determined by SEC in THF calibrated with PEO standards;

^f) Theoretical M_n calculated using the weight loss upon deprotection (72.11 g/mol per EEGE unit).

In addition, a poly(2-vinylpyridine)-*block*-poly(ethylene oxide)-*block*-poly(ethoxyethyl glycidyl ether) (P2VP-*b*-PEO-*b*-PEEGE) triblock terpolymer and a PEO-*b*-PEEGE diblock copolymer were synthesized (Table 3.1). 1,1-Diphenyl-3-methylpentyllithium (DPMPLi), prepared in situ by the reaction of *sec*-BuLi with 1,1-diphenylethylene (DPE) in THF at -70 °C, was used as initiator in order to suppress side reactions with 2VP and EO²⁶, respectively.

The synthesis of the P2VP-*b*-PEO-*b*-PEEGE triblock terpolymer was accomplished in analogy to Scheme 3.1 and proceeded without termination, as can be deduced from the SEC traces shown in Figure 3.4 and the low polydispersity index (Table 3.1). The PEO-*b*-PEEGE diblock copolymer was synthesized by addition of EO to DPMPLi at -70 °C. After stirring for 1 h, the temperature was slowly increased to 10 °C followed by the addition of *t*-BuP₄. EO and EEGE were polymerized according to Scheme 3.1. The SEC traces of the PEO precursor and the PEO-*b*-PEEGE diblock copolymer (Figure 3.1B) demonstrate that the block extension with EEGE proceeded without termination. The visible tailing at the lower molecular weight side might be attributed to a slow initiation of the EEGE polymerization (see discussion on

EEGE kinetics). SEC column adsorption phenomena due to partial hydrolysis of the EEGE might also contribute to the tailing, as a mixture of methanol/acetic acid was used for termination, and therefore a partial cleavage of the acetal protecting group cannot be excluded completely. The polydispersity index of 1.10 (Table 3.1) is comparable to that of PEEGE homopolymers and block copolymers synthesized by other groups using K^+ or Cs^+ counterions.^{5,6,9,10}

Homopolymerization of EEGE in THF at 50 °C using DPMPLi as initiator was accomplished in analogy to the reaction protocol used in the synthesis of the PEO-*b*-PEEGE diblock copolymer. The PEEGE homopolymers showed broad bimodal molecular weight distributions (PDI= 1.3 - 1.4, results not shown). Obviously, the nucleophilicity of DPMPLi, which is a model for DPE end-capped living anionic polymer chains, is still too high and results in side reactions, like transfer to EEGE by proton abstraction. This is a well known phenomena in propylene oxide polymerization.²¹ This demonstrates the need of end-capping with at least one EO unit in order to produce an alkoxide end group as an initiating site for EEGE polymerization, as side reactions were not observed in the synthesis of the block copolymers. The kinetics of EEGE polymerization was monitored during the synthesis of the PEO-*b*-PEEGE diblock copolymer using online FT-NIR spectroscopy in combination with a fiber optic equipment. This method has been already used in our group for monitoring EO kinetics.^{24,26} The FT-NIR spectrum of EEGE in THF was obtained by solvent subtraction in order to yield a pure component spectrum and to determine conversions since THF has strong absorptions close to the overtone vibrations of EEGE (Figure 3.2A). Specific monomer absorptions for EEGE were detected at 6062, and 4536 cm^{-1} . The strongest vibration is located at 4536 cm^{-1} and not separated from the solvent cutoff at ca. 4500 cm^{-1} . Thus, the first overtone C-H stretching of the epoxide ring in EEGE at 6062 cm^{-1} was chosen for conversion determination. In addition, peak heights were used instead of peak areas for evaluation, since they usually gave less noise.

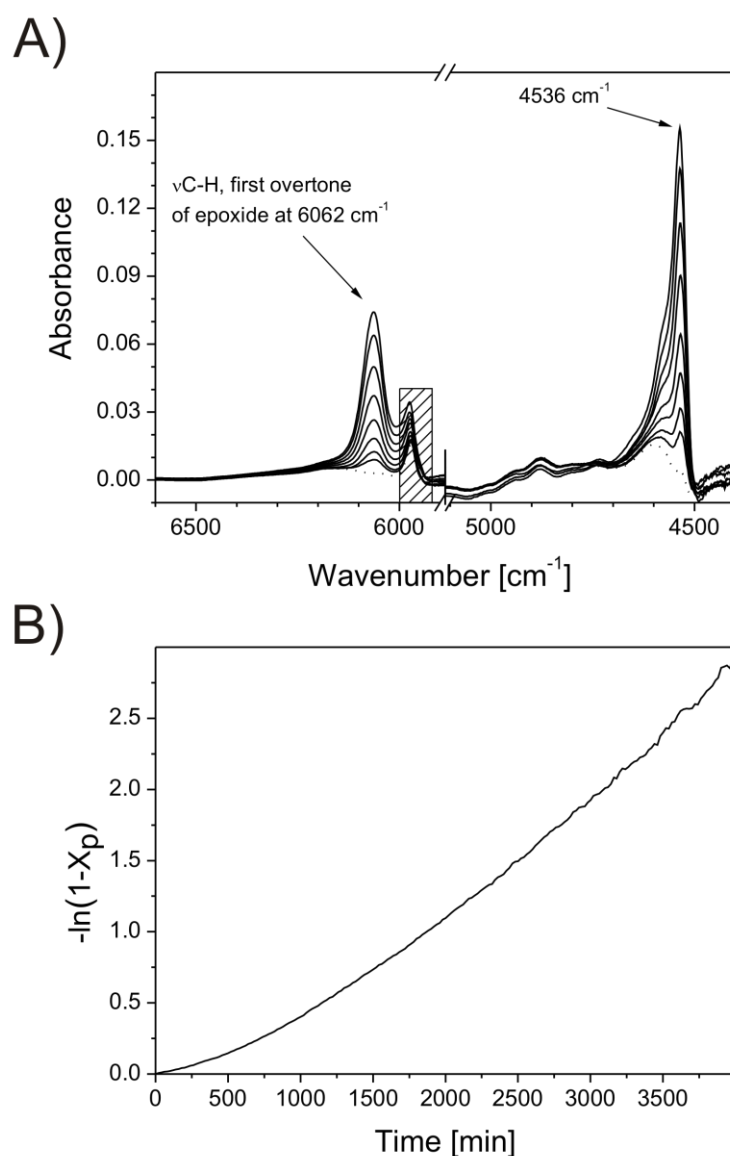


Figure 3.2. A) FT-NIR spectra of EEGE in THF at 50 °C obtained by solvent subtraction at reaction times of $t = 0, 500, 1000, 1500, 2000, 2500, 3000, 3500,$ and 5000 min monitored during synthesis of the $\text{EO}_{102}\text{EEGE}_{83}$ diblock copolymer (the band at ca. 5970 cm^{-1} is an artifact arising from solvent subtraction); B) Corresponding first-order time-conversion plot in EEGE polymerization at 50 °C ($[\text{PEOLi}]_0 = 1.46 \cdot 10^{-3}\text{ M}$, $[\text{EEGE}]_0 = 0.14\text{ M}$, $[\text{PEOLi}]/[t\text{-BuP}_4] = 1/0.95$).

Conversions, X_p , were calculated using the following equation:

$$X_p = \frac{A_0 - A_t}{A_0 - A_\infty}$$

where A_t is the absorbance at time t , $A_0 =$ initial absorbance, and $A_\infty =$ absorbance at full conversion.

The first-order time-conversion plot (Figure 3.2B) is not linear in the initial stage of the polymerization ($t < 1700$ min), but shows an increase in slope with increasing conversion. This might result from a slow initiation reaction of the $\text{PEO}^-[\text{Li}/t\text{-BuP}_4]^+$ macroinitiator, which is consistent with the observed tailing in the corresponding SEC trace (Figure 3.1B). On the other hand, during initiation a primary alkoxide is transferred into a secondary alkoxide which probably involves a change in aggregation number of the growing chain. This might contribute to the observed behavior, too. It has to be stressed that no induction period was found in EEGE polymerization. This is in agreement with the absence of an induction period in EO polymerization using $[\text{Li}/t\text{-BuP}_4]^+$ counterions when a 2nd batch of EO is added directly after full conversion of the 1st batch.²⁶ At higher conversions the first-order time-conversion plot is linear, i.e. termination does not occur during polymerization. From the slope in the linear regime ($t > 1700$ min) an apparent rate constant of propagation of $k_{\text{app}} = 8.36 \cdot 10^{-4}$ 1/min was derived. Using the initial initiator concentration of $[\text{I}]_0 = 1.46 \cdot 10^{-3}$ M (initiator efficiency $f = 1$) gives a rate constant of propagation of $k_p = 9.52 \cdot 10^{-3}$ L/mol·s. This value is comparable to that observed in EO polymerization at 50 °C in THF using a $\text{PEO}^-[\text{Li}/t\text{-BuP}_4]^+$ macroinitiator, $k_p = 12.0 \cdot 10^{-3}$ L/mol·s.²⁶

In conclusion, polymerization of EEGE with Li^+ counterions in the presence of the phosphazene base $t\text{-BuP}_4$ proceeds in a living and controlled way, and is comparable to the polymerization with K^+ and Cs^+ counterions with respect to the molecular weight distributions of the produced PEEGE (similar PDI). The advantage of our method is the possibility to use commercially available alkyllithium initiators, that are commonly used in anionic polymerization of styrene and dienes (butadiene and isoprene), without the need of changing the counterion to K^+ or Cs^+ . This new method reduces the need for time-consuming end-functionalization and purification steps, resulting in a novel and simple way of producing PEEGE containing block copolymers in a one-pot synthesis.

Acknowledgment

Financial support from BASF AG (Germany) and the German Science Foundation (priority program SPP 1259) is gratefully appreciated.

3.2 Supporting Information

3.2.1 Experimental

Materials

Tetrahydrofuran (Merck, p.a.) was purified by successive distillation over CaH_2 and potassium and kept under dry nitrogen before usage. Ethylene oxide (Linde, 3.0) was condensed onto CaH_2 and stirred at 0 °C for 3 h before being transferred into glass ampoules for storage. Prior to use ethylene oxide was additionally purified over *n*-BuLi and condensed into a sampling ampoule. Styrene (BASF, p.a.) was degassed three times via freeze pump thaw cycles using a high vacuum line (10^{-4} - 10^{-5} mbar). After degassing, styrene was stirred over Bu_2Mg and condensed under high vacuum into storage ampoules and kept frozen under N_2 until use. 2-Vinylpyridine (Acros, 97%) was distilled from CaH_2 under nitrogen, stirred over Et_3Al for 2 h and condensed into storage ampoules. 1,1-Diphenylethylene (Aldrich, 97%) was purified by stirring with *sec*-BuLi under N_2 followed by distillation. The phosphazene base *t*-BuP₄ (Fluka, 1 M in hexane), *sec*-BuLi (Acros, 1.3 M in cyclohexane/hexane: 92/8), *n*-BuLi (Acros, 1.6 M in hexane), Bu_2Mg (Aldrich, 1 M in heptane), Et_3Al (Aldrich, 1 M in hexanes) were used as received.

1-Ethoxyethyl glycidyl ether (EEGE) was synthesized following the method developed by Fitton et al.²⁹ Glycidol (Aldrich, 96%) and ethyl vinyl ether (Aldrich, 99%) were reacted using *p*-toluene sulfonic acid as the catalyst. EEGE was distilled twice over powdered CaH_2 immediately before use (bp. 47 °C, 5 mbar).

Polymerizations

Polymerizations were carried out in a thermostated laboratory autoclave (Büchi) under dry nitrogen atmosphere. The synthesis of the *polystyrene-block-poly(ethylene oxide)-block-poly(ethoxyethyl glycidyl ether)* (PS-*b*-PEO-*b*-PEEGE) triblock terpolymer was accomplished in THF (500 mL) by sequential anionic polymerization of the corresponding monomers using *sec*-BuLi as initiator. At -70 °C *sec*-BuLi (0.99 mL, 1.38 M) was added to THF followed by fast addition of styrene (7.35 g). After a reaction time of 1 h at -70 °C, EO (14.75 g) was added to the reaction mixture and stirred for 1 h. After slowly heating to 10 °C the phosphazene base *t*-BuP₄ (1.3 mL, [*sec*-BuLi]/[*t*-BuP₄] = 1/0.95) was injected via syringe to

promote polymerization of EO in the presence of Li^+ counterions. EO was polymerized at 50 °C for 2 d in order to ensure complete conversion (verified by online FT-NIR spectroscopy). After cooling to room temperature EEGE (7.3 g) was added and allowed to react at 50 °C for 3 d, followed by termination with a mixture of acetic acid/methanol (3/5, v/v). The polymer was isolated by precipitation in cold ethanol (-25 °C) and collected using a centrifuge.

The *poly(2-vinylpyridine)-block-poly(ethylene oxide)-block-poly(ethoxyethyl glycidyl ether)* (P2VP-*b*-PEO-*b*-PEEGE) triblock terpolymer was prepared in THF (1.2 L) using 1,1-diphenyl-3-methylpentyllithium (DPMPLi) as initiator. DPMPLi was prepared in-situ by the reaction of *sec*-BuLi (6.2 ml, 1.38 M) with 1,1-diphenylethylene (DPE; 1.67 ml, [*sec*-BuLi]/[DPE] = 1/1.1) in THF at -70 °C. After addition of 2VP (26 g) the reaction was kept at -70 °C for 1 h, followed by addition of EO (50.5 g). After stirring for 1 h at -70 °C, the temperature was increased stepwise (1 h at -30 °C, -10°C, and 30 min at 0 °C) to 10 °C in order to avoid side reactions resulting in termination of the P2VP block. Subsequently, the phosphazene base *t*-BuP₄ (8.2 mL, [DPMPLi]/[*t*-BuP₄] = 1/0.95) was added to start polymerization of EO. After complete conversion of EO at 50 °C 1/3 of the reaction mixture was taken out of the reactor in order to isolate a certain amount of the P2VP-*b*-PEO diblock copolymer. The polymerization of EEGE (8.8 g) in the remaining reaction mixture was accomplished as described for the PS-*b*-PEO-*b*-PEEGE triblock terpolymer. The polymer was isolated by precipitation in diethyl ether.

The *poly(ethylene oxide)-block-poly(ethoxyethyl glycidyl ether)* (PEO-*b*-PEEGE) diblock copolymer was synthesized in THF using 1,1-diphenyl-3-methylpentyllithium (DPMPLi) as initiator. DPMPLi was prepared in-situ by the reaction of *sec*-BuLi (0.53 ml, 1.38 M) with 1,1-diphenylethylene (0.19 ml, [*sec*-BuLi]/[DPE] = 1/1.5) in THF (500 mL) at -70 °C. Subsequently, EO (3.7 g) was added at -70 °C followed by stirring for 1 h. After slowly heating to 10 °C the phosphazene base *t*-BuP₄ (0.69 mL, [DPMPLi]/[*t*-BuP₄] = 1/0.95) was added and EO was polymerized at 50 °C for 3 d in order to ensure complete conversion (verified by online FT-NIR spectroscopy). Subsequently, EEGE (9.9 g) was polymerized according to the procedure used for the PS-*b*-PEO-*b*-PEEGE triblock terpolymer. The course of EEGE conversion was followed via online FT-NIR fiber optic spectroscopy.

Deprotection of PEEGE

Hydrolysis of the PEEGE blocks to the corresponding polyglycidol (PG) blocks was achieved following the method of Spassky et al.²⁸ The polymer was dissolved in formic acid and stirred for 3 h to yield the formate. The formic acid was then removed by rotary evaporation and the polymer redissolved in a methanol/dioxane mixture (1/1, v/v). Cleavage of the formate was achieved by addition of 1N KOH (2 times the molar concentration of EEGE monomer units) and heating to reflux for 12 h. The polymer solution was then dialyzed against a large excess of deionized water in order to neutralize the solution and remove excess salts, followed by freeze-drying.

Online FT-NIR Spectroscopy

NIR spectra were recorded with a Nicolet Magna 560 FT-IR optical bench equipped with a white light source and a PbS detector. Online monitoring was accomplished using a laboratory autoclave (Büchi) equipped with an all glass low-temperature immersion transmission probe (Hellma) with an optical path length of 10 mm and connected to the spectrometer via 2 m fiber-optical cables. The probe was fed through a port in the stainless steel top plate of the reactor and immersed into the reaction mixture. More detailed information about the setup can be found elsewhere.²⁴ Data processing was performed with Nicolet's OMNIC Series software. Each spectrum was accumulated from 32 scans with a resolution of 4 cm⁻¹. The total collection time per spectrum was about 22 s.

Matrix Assisted Laser Desorption Ionization Time of Flight Mass Spectrometry (MALDI-ToF MS)

MALDI-ToF MS was performed on a Bruker Reflex III with a UV laser operating at 337 nm and an accelerating voltage of 20 kV. 1,8,9-trihydroxyanthracene (dithranol) and silver triflate as cationizing agent were used for the PS and P2VP homopolymers. Samples were dissolved in THF (10 mg/mL) and mixed with matrix (20 mg/mL in THF) and salt (10 mg/mL in THF) at a mixing ratio of 20 : 5 : 1 (v/v, matrix : analyte : salt). 1 µL of this mixture was spotted onto the target and allowed to dry. 200 – 500 laser shots were accumulated for a spectrum.

Size Exclusion Chromatography (SEC)

SEC experiments were performed on a Waters instrument calibrated with narrowly distributed poly(ethylene oxide) standards for the PEO homopolymer, and polystyrene standards for the PEEGE containing block copolymers at 40 °C. Four PSS-SDV gel columns (5 μm) with a porosity range from 10² to 10⁵ Å (PSS, Mainz, Germany) were used together with a differential refractometer and a UV detector at 254 nm. Measurements were performed in THF with a flow rate of 1 mL/min using toluene as internal standard.

SEC of the PS-*b*-PEO-*b*-PG triblock terpolymer was performed using two PSS_GRAM (7 μm) columns with a porosity range from 10² to 10³ Å (PSS, Mainz, Germany) together with a differential refractometer and a UV detector at 270 nm. A 0.05 M solution of LiBr in 2-N-methylpyrrolidone (NMP) was used as eluent at a flow rate of 1 mL/min at 70 °C. PS standards were used for calibration.

The absolute number-average molecular weight (M_n) of the synthesized block copolymers was determined by ¹H-NMR in CDCl₃ (Bruker AC 250 spectrometer) using the absolute M_n of the first block, determined by MALDI-ToF or SEC, for calibration of the NMR signal intensities.

3.2.2 Characterization

Figure 3.3 shows the ¹H-NMR spectra of the synthesized PS-*b*-PEO-*b*-PEEGE triblock terpolymer and the corresponding PS-*b*-PEO-*b*-PG triblock terpolymer obtained after deprotection of the PEEGE block. Disappearance of specific PEEGE signals at δ = 4.6, 1.2, and 1.1 ppm in the hydrolyzed product (Figure 3.3B) verifies complete deprotection of the PEEGE block.

As an example, the M_n calculation for the S₅₈EO₂₈₂EEGE₂₇ triblock terpolymer via ¹H-NMR using the absolute M_n of the PS-precursor (determined by MALDI-ToF) for calibration of the ¹H-NMR signal intensities (Figure 3.3, A) is given by the following equation:

$$M_n(\text{triblock}) = M_n(\text{PS}) + \frac{M_n(\text{PS})}{104.15 \text{ g/mol}} \cdot \frac{5}{I(a)} \cdot \left(\frac{I(b-f,i) - 7I(g)}{4} \cdot 44.05 \text{ g/mol} + I(g) \cdot 146.19 \text{ g/mol} \right),$$

with I(x) = integral of the corresponding signal in the ¹H-NMR spectra.

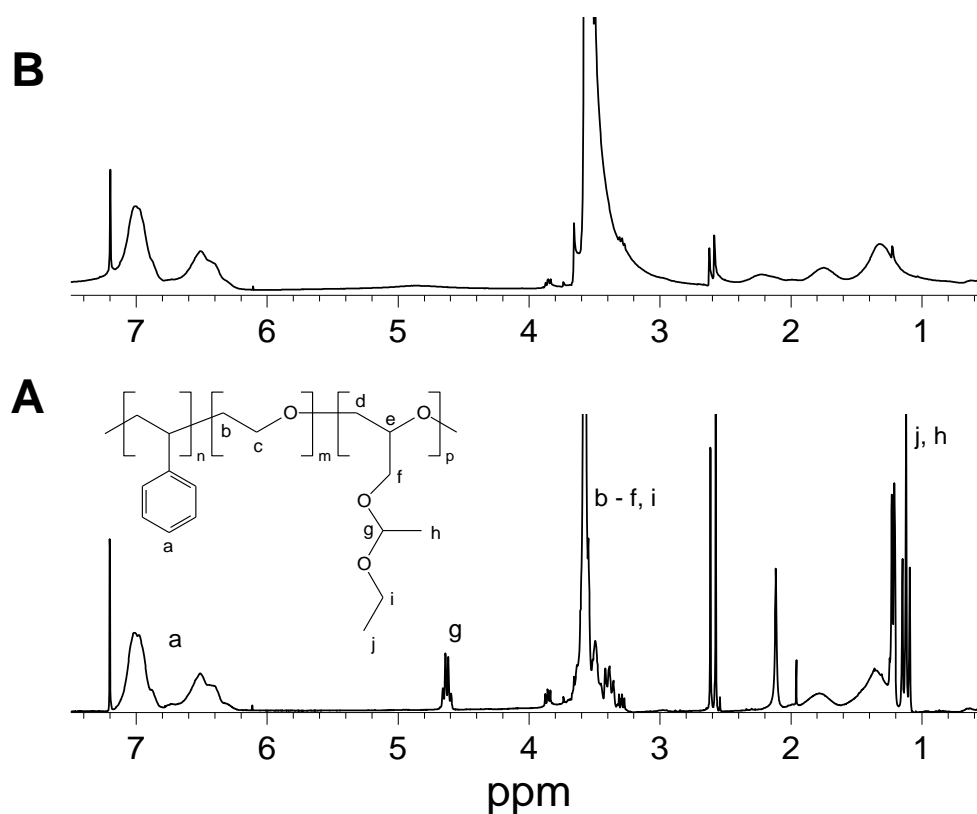


Figure 3.3. 1H -NMR spectra of the $S_{58}EO_{282}EEGE_{27}$ triblock copolymer (A) and the corresponding polymer after deprotection of the PEEGE block, $S_{58}EO_{282}G_{27}$ (B), in $CDCl_3$ at room temperature.

Figure 3.4 shows the SEC traces of the synthesized $P2VP$ -*b*- PEO -*b*- $PEEGE$ ($2VP_{26}EO_{166}EEGE_{27}$) triblock terpolymer, including the $P2VP$ and $P2VP$ -*b*- PEO precursors. The sequential anionic polymerization proceeded without termination or side reactions, resulting in a narrowly distributed triblock terpolymer ($PDI = 1.03$). The molecular weight distribution of the $P2VP$ precursor is broadened due to partial adsorption on the SEC columns.

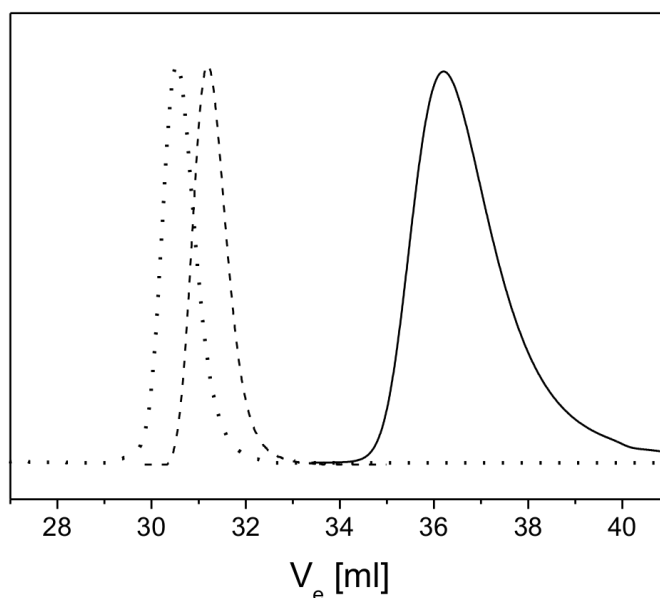


Figure 3.4. SEC (THF) traces of the synthesized $2VP_{26}EO_{166}EEGE_{27}$ triblock terpolymer (dotted) including the P2VP (solid) and P2VP-*b*-PEO (dashed) precursors.

3.3 References

- [1] Kainthan, R. K.; Janzen, J.; Levin, E.; Devine, D. V.; Brooks, D. E. *Biomacromolecules* **2006**, *7*, 703.
- [2] Kainthan, R. K.; Gnanamani, M.; Ganguli, M.; Ghosh, T.; Brooks, D. E.; Maiti, S.; Kizhakkedathu, J. N. *Biomaterials* **2006**, *27*, 5377.
- [3] Sunder, A.; Kramer, M.; Hanselmann, R.; Mülhaupt, R.; Frey, H. *Angew. Chem., Int. Ed.* **1999**, *38*, 3552.
- [4] Frey, H.; Haag, R. *Rev. Mol. Biotechnol.* **2002**, *90*, 257.
- [5] Dimitrov, P.; Rangelov, S.; Dworak, A.; Haraguchi, N.; Hirao, A.; Tsvetanov, C. B. *Macromol. Symp.* **2004**, *215*, 127.
- [6] Dworak, A.; Baran, G.; Trzebicka, B.; Walach, W. *React. Funct. Polym.* **1999**, *42*, 31.
- [7] Jamroz-Piegza, M.; Utrata-Wesolek, A.; Trzebicka, B.; Dworak, A. *Eur. Polym. J.* **2006**, *42*, 2497.
- [8] Lapienis, G.; Penczek, S. *Biomacromolecules* **2005**, *6*, 752.
- [9] Dworak, A.; Trzebicka, B.; Walach, W.; Utrata, A.; Tsvetanov, C. B. *Macromol. Symp.* **2004**, *210*, 419.
- [10] Dimitrov, P.; Utrata-Wesolek, A.; Rangelov, S.; Walach, W.; Trzebicka, B.; Dworak, A. *Polymer* **2006**, *47*, 4905.

- [11] Lopez-Villanueva, F.-J.; Barriau, E.; Schleuss, T. W.; Berger, R.; Kilbinger, A. F. M.; Frey, H. *Polym. Mater. Sci. Eng.* **2006**, *95*, 780.
- [12] Porjazoska, A.; Dimitrov, P.; Dimitrov, I.; Cvetkovska, M.; Tsvetanov, C. B. *Macromol. Symp.* **2004**, *210*, 427.
- [13] Slomkowski, S.; Gadzinowski, M.; Sosnowski, S.; Radomska-Galant, I.; Pucci, A.; De Vita, C.; Ciardelli, F. *J. Nanosci. Nanotech.* **2006**, *6*, 3242.
- [14] Dimitrov, P.; Rangelov, S.; Dworak, A.; Tsvetanov, C. B. *Macromolecules* **2004**, *37*, 1000.
- [15] Halacheva, S.; Rangelov, S.; Tsvetanov, C. B. *Macromolecules* **2006**, *39*, 6845.
- [16] Dworak, A.; Trzebicka, B.; Walach, W.; Utrata, A. *Polimery (Warsaw, Poland)* **2003**, *48*, 484.
- [17] Kaluzynski, K.; Pretula, J.; Lapienis, G.; Basko, M.; Bartczak, Z.; Dworak, A.; Penczek, S. *J. Polym. Sci., Polym. Chem.* **2001**, *39*, 955.
- [18] Mendrek, A.; Mendrek, S.; Trzebicka, B.; Kuckling, D.; Walach, W.; Adler, H.-J.; Dworak, A. *Macromol. Chem. Phys.* **2005**, *206*, 2018.
- [19] Walach, W.; Kowalczyk, A.; Trzebicka, B.; Dworak, A. *Macromol. Rapid Commun.* **2001**, *22*, 1272.
- [20] Hsieh, H. L., Quirk, R. P., *Anionic Polymerization - Principles and Practical Applications*. Marcel Dekker Inc.: New York, 1996; p 688.
- [21] Wesdemiotis, C.; Arnould, M. A.; Lee, Y.; Quirk, R. P. *Polym. Prep. (Am. Chem. Soc., Div. Polym. Chem.)* **2000**, *41*, 629.
- [22] Esswein, B.; Molenberg, A.; Möller, M. *Macromol. Symp.* **1996**, *107*, 331.
- [23] Esswein, B.; Möller, M. *Angew. Chem., Int. Ed.* **1996**, *35*, 623.
- [24] Lanzendörfer, M.; Schmalz, H.; Abetz, V.; Müller, A. H. E. Application of FT-NIR Spectroscopy for Monitoring the Kinetics of Living Polymerizations. In *In-Situ Spectroscopy of Monomer and Polymer Synthesis*; Puskas, J. E.; Storey, R., Eds.; Kluwer Academic/Plenum: New York/Dordrecht, 2002; p 67.
- [25] Schmalz, H.; Knoll, A.; Müller, A. J.; Abetz, V. *Macromolecules* **2002**, *35*, 10004.
- [26] Schmalz, H.; Lanzendörfer, M. G.; Abetz, V.; Müller, A. H. E. *Macromol. Chem. Phys.* **2003**, *204*, 1056.
- [27] Schwesinger, R.; Schlemper, H. *Angew. Chem.* **1987**, *99*, 1212.
- [28] Taton, D.; Le Borgne, A.; Sepulchre, M.; Spassky, N. *Macromol. Chem. Phys.* **1994**, *195*, 139.
- [29] Fitton, A.; Hill, J.; Jane, D.; Miller, R. *Synthesis* **1987**, 1140.

4 Smart Hydrogels Based on Double Responsive Triblock Terpolymers

Stefan Reinicke,^a Joachim Schmelz,^a Alain Lapp,^b Matthias Karg,^c Thomas Hellweg,^c and Holger Schmalz^{a,*}

a) Makromolekulare Chemie II, Universität Bayreuth, D-95440 Bayreuth, Germany

b) Laboratoire Léon Brillouin, CEA de Saclay, 99191 Gif sur Yvette, France

c) Physikalische Chemie I, Universität Bayreuth, D-95440 Bayreuth, Germany

ABSTRACT:

In this work a new kind of “smart” hydrogel is presented, which is composed of a poly(2-vinylpyridine)-*block*-poly(ethylene oxide)-*block*-poly(glycidyl methyl ether-*co*-ethyl glycidyl ether) (P2VP-*b*-PEO-*b*-P(GME-*co*-EGE)) triblock terpolymer. The thermo-sensitive poly(glycidyl methyl ether-*co*-ethyl glycidyl ether) block exhibits a cloud point which is easily adjustable by the comonomer ratio. Copolymerization of GME and EGE produces nearly statistical copolymers with a weak preferential incorporation of GME, exhibiting a sharp coil-to-globule transition with almost no hysteresis. The triblock terpolymers aggregate in aqueous solution triggered by both, pH and temperature. At sufficiently high concentration this stimuli-responsive behaviour leads to a reversible gel formation with gel strengths and transition points tuneable by pH, temperature, concentration, and block lengths. At pH = 7, an unique gel-sol-gel transition accompanied with a strengthening of the gel is observed upon heating using rheology. Moreover, the structure of the low temperature gel phase is investigated by means of small-angle neutron scattering (SANS).

4.1 Introduction

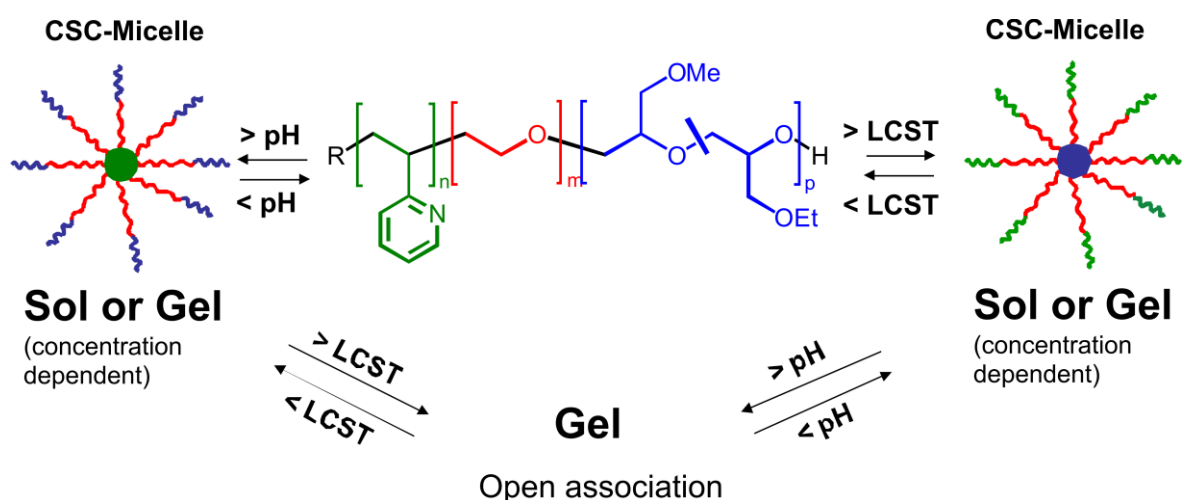
“Smart” hydrogels are networks of water soluble polymers which form/ disintegrate or swell/ contract upon changes of external stimuli like solution pH, temperature, or ionic strength. Such hydrogels can be utilized in drug delivery applications, since they can release trapped drug molecules upon shrinkage or disintegration.¹⁻³ Other applications can be found as storage media, in actuating systems, sensors, microfluidic switches, and many more.⁴⁻⁶

In general, one can distinguish between two classes of “smart” gels.⁷ Chemically crosslinked stimuli-responsive polymers constitute the first category.⁸ The most intensively studied example is chemically crosslinked poly(N-isopropylacrylamide) (PNIPAAm), a thermo-sensitive polymer becoming hydrophobic at around 32 °C, and very often used in hydrogel applications.⁹⁻¹² Other thermo-sensitive polymers used to construct such hydrogels are for instance poly(alkyl vinyl ethers),^{13,14} chemically modified polyglycidols,¹⁵ or copolymers of 2-(2-methoxyethoxy)ethyl methacrylate with oligo(ethylene glycol) methacrylate (P(MEO₂MA-*co*-OEGMA)).¹⁶ A typical monomer used for the synthesis of pH-sensitive hydrogels is methacrylic acid.¹⁷ The second class of hydrogels comprises physically crosslinked hydrogels, which disintegrate reversibly upon changes of a certain external parameter. Such systems are typically composed of linear or star-shaped block copolymers with an ABA and (BA)_x structure, respectively. The A-block is stimuli-responsive, i.e. becomes hydrophobic at a certain pH or temperature, and therefore forms the network junctions. Examples are poly(ethylene oxide)-*block*-poly(N-isopropylacrylamide) (PEO-*b*-PNIPAAm)¹⁸ and PEO-*b*-P(MEO₂MA-*co*-OEGMA)¹⁹ star block copolymers, poly(ε-caprolactone)-*block*-poly(ethylene oxide)-*block*-poly(ε-caprolactone) (PCL-*b*-PEO-*b*-PCL) triblock copolymers,²⁰ ABC triblock terpolymers composed of different poly(alkyl vinyl ether)s,²¹ or - as examples for pH-sensitive hydrogels - ABA and (BA)_x block copolymers where A is poly(diethyl aminoethyl methacrylate) (PDEAEMA) and B poly(glycerol monomethacrylate) (PGMA)²². Gels with permanent physical crosslinks, i.e. where the outer blocks are hydrophobic and not stimuli-responsive, are for instance based on ABCBA pentablock terpolymers with poly(methyl methacrylate) (PMMA) outer blocks, B is poly(acrylic acid) (PAA) and C is poly(2-vinyl pyridine) (P2VP).²³ In addition, ABA triblock or multiblock copolymers consisting of poly(*n*-butylacrylate) (PnBA), polystyrene (PS), poly(*n*-

butylmethacrylate) (P*n*BMA) and poly(dimethyl aminoethyl methacrylate) (PDMAEMA) blocks were described.^{24,25} Other systems, like the well known PluronicTM block copolymers, form gels by a regular packing of micelles, mostly in a cubic phase (bcc, or fcc).^{26,27} All examples discussed so far are hydrogels which respond to only one external stimuli, temperature or pH. However, some applications may require an independent response to several factors.²⁸ A suitable monomer for creating a pH- and temperature-responsive hydrogel is DMAEMA.²⁹⁻³¹ Since the number of dual responsive monomers is limited, a thermo-sensitive monomer is often copolymerized with a pH-sensitive monomer in order to obtain a double stimuli-responsive gel.³²⁻³⁴ Another approach utilizes interpenetrating networks or blends of two different stimuli-sensitive polymers.³⁵ One example for a double stimuli-responsive gel based on a crosslinked block copolymer with blocks responding to different stimuli is a P(DMAEMA-*co*-HEMA)-*b*-PNIPAAm-*b*-P(DMAEMA-*co*-HEMA) (HEMA = hydroxyethyl methacrylate) triblock copolymer.³⁶ However, all these systems belong to the class of chemically crosslinked gels. Examples for double responsive physical gels are still limited. They are formed for instance by a poly(N,N-diethylacrylamide)-*block*-poly(acrylic acid)-*block*-poly(N,N-diethylacrylamide) (PDEAAm-*b*-PAA-*b*-PDEAAm) ABA triblock copolymer,³⁷ or an ABCBA pentablock terpolymer, where A is a pH-sensitive poly(sulfamethazine methacrylate) block, B is PCL, and C is PEO.³⁸ With few exceptions, these polymers were synthesized by free radical polymerization or by atom transfer radical polymerization (ATRP) with limited control with respect to block length and polydispersity. An interesting approach towards temperature- and redox-responsive physical hydrogels is based on the incorporation of redox-cleavable disulfide linkages at the midpoint of ABA triblock copolymers with thermo-sensitive end blocks, e.g. PNIPAAm.^{39,40}

Our approach towards double stimuli-responsive (pH and temperature) hydrogels is based on an ABC triblock terpolymer (Scheme 4.1), where A is pH-sensitive poly(2-vinylpyridine) (P2VP), B water soluble poly(ethylene oxide) (PEO), and C a thermo-sensitive copolymer of glycidyl methyl ether and ethyl glycidyl ether (P(GME-*co*-EGE)). At a pH < 5, the 2VP units are protonated rendering the P2VP block hydrophilic,^{41,42} i.e. at low pH and room temperature, the polymer is molecularly dissolved. Increasing the pH above 5, the P2VP block becomes hydrophobic due to deprotonation. This should result in the formation of core-shell-corona (CSC) micelles with P2VP cores. An inverse micellar structure, with the thermo-sensitive P(GME-*co*-EGE) block forming the core, should be

obtained at low pH and for temperatures above the cloud point of P(GME-*co*-EGE). In both cases, a hydrogel might already be formed by close packing of CSC micelles for sufficiently high concentrations, i.e. analogous to the behaviour of PluronicsTM block copolymers.^{26,27} However, upon switching the responsive corona block of the CSC micelles insoluble, too, hydrogel formation should take place. This process is driven by the open association of CSC micelles, with physical crosslinks formed by the now insoluble corona blocks. Thus, depending on concentration, i.e. whether the CSC micelles already formed a gel or not, a hydrogel will be formed or the pre-formed hydrogel will transform into a stronger gel upon applying both stimuli. The produced hydrogel can be destroyed reversibly by adjusting either pH or temperature, resulting in a solubilisation of the A or C block, respectively.



Scheme 4.1 Scheme of the formation of double responsive hydrogels based on P2VP-*b*-PEO-*b*-P(GME-*co*-EGE) triblock terpolymers.

We use our recently developed synthetic route to produce P2VP-*b*-PEO-*b*-P(GME-*co*-EGE) triblock terpolymers in a one-pot reaction by sequential anionic polymerization of the corresponding monomers in THF.⁴³

The lower critical solution temperature (LCST) of alkyl glycidyl ethers is strongly affected by the length and structure of the alkyl chain.^{44,45} The copolymerization of GME and EGE promised a way of adjusting the LCST in a wide temperature range simply by changing the copolymer composition, similar to the copolymerization of 2-(2-methoxyethoxy)ethyl methacrylate with oligo(ethylene glycol) methacrylate,⁴⁶ and of 2-*n*-propyl-2-oxazoline with 2-ethyl-2-oxazoline or 2-isopropyl-2-oxazoline.⁴⁷ Thus, prior to

the triblock terpolymer synthesis the reactivity ratios for GME/EGE copolymerization were determined, and the LCST-type phase separation of the resulting copolymers in dependence of the composition and concentration was investigated.

The results and discussions part will be divided into two subsections. First, we present the results of the GME/EGE copolymerization and the dependence of P(GME-*co*-EGE) cloud points on composition. The second part will deal with the synthesis and characterization of P2VP-*b*-PEO-*b*-P(GME-*co*-EGE) triblock terpolymers. The ability to form micellar aggregates in aqueous solution triggered by pH and temperature is demonstrated using dynamic light scattering. The pH- and temperature dependent hydrogel formation and disintegration was monitored by the test tube inversion method as well as by rheology. At pH = 7, an unusual gel-sol-gel transition was observed upon heating, which goes along with a strengthening of the hydrogel. The influence of concentration and block lengths on the gel strength and the transition points was investigated, too. Finally, small-angle neutron scattering data are presented, which reveal the structure of the hydrogel in the low temperature regime.

4.2 Experimental

Materials

Tetrahydrofuran (Merck, p.a.) was purified by successive distillation over CaH₂ and potassium, and kept under dry nitrogen before use. Glycidyl methyl ether (TCI, > 85%) was distilled with a Vigreux column, first, at atmospheric pressure and then at 100 mbar from powdered CaH₂, followed by a purification over *t*-BuOK in order to remove residual epichlorohydrin. Finally, GME was condensed into a glass ampoule for storage. Prior to use, it was purified over *n*-BuLi and condensed into a sampling ampoule. Ethyl glycidyl ether (TCI, > 98%) was purified in the same way but without the distillation steps. Decane, used as internal standard for GC measurements, was purified over *n*-BuLi and condensed into a storage ampoule. The phosphazene base *t*-BuP₄ (Fluka, 1 M in hexane), *sec*-BuLi (Acros, 1.3 M in cyclohexane/hexane: 92/8), *n*-BuLi (Aldrich, 2 M in cyclohexane), *t*-BuOK (Aldrich, 1 M in THF), *t*-BuOLi (Aldrich, 1M in hexanes) were used as received. The *t*-BuOLi solution contained a small amount of *t*-BuOH, as detected by GC. 2-Vinylpyridine (Fluka, ≥ 97%) and ethylene oxide (Linde, 3.0) were purified as reported elsewhere.⁴³

Polymerizations

Polymerizations were carried out in a thermostated laboratory autoclave (Büchi) under dry nitrogen atmosphere. The synthesis of the GME/EGE copolymers was accomplished in THF by anionic ring-opening polymerization of the corresponding monomers using *t*-BuOK or *t*-BuOLi/*t*-BuP₄ as initiator. In a typical procedure, the monomer mixture (17.9 mL) and decane (4 mL) were added to THF (200 mL) at 50 °C, followed by fast addition of the initiator. Samples were taken for conversion determination via gas chromatography (GC). After 2 days the reaction was terminated by adding a few mL of MeOH containing 1-2 droplets of conc. HCl. The copolymers with a low GME content were purified by evaporation of the solvent, followed by repeated dispersion in water and centrifugation at 40 °C. Copolymers with higher GME content were purified via dialysis against Millipore water using a cellulose ester dialysis tube with a MWCO of 500 g/mol (Spectra/Por™). After drying for 2-3 days under vacuum at 40 °C, the copolymers were obtained as highly viscous colourless or pale yellow liquids. The synthesis of the P2VP-*b*-PEO-*b*-P(GME-*co*-EGE) triblock terpolymers via sequential anionic polymerization and the subsequent purification was performed analogously to the recently reported procedure.⁴³

Size exclusion chromatography (SEC)

SEC experiments were performed on an instrument equipped with four PSS SDV gel columns (porosities: 10², 10³, 10⁴ and 10⁵ Å, diameter: 5 µm), a pre-column (10² Å, 5 µm), a differential refractometer (Shodex), and a UV-detector at 254 nm (Waters). A calibration with narrowly distributed polystyrene standards was used. Measurements were performed in THF at 40 °C with a flow rate of 1 mL/min using toluene as internal standard.

Matrix assisted laser desorption ionization time of flight mass spectrometry (MALDI-ToF MS)

MALDI-ToF MS was performed on a Bruker Reflex III with a UV laser operating at 337 nm and an acceleration voltage of 20 kV. 1,8,9-Trihydroxyanthracene (dithranol) as matrix and silver triflate as cationizing agent were used for P2VP homopolymers. Samples were dissolved in THF (10 mg/mL) and mixed with matrix (20 mg/mL in THF) and salt (10 mg/mL in THF) at a mixing ratio of 20 : 5 : 1 (v/v, matrix : analyte : salt). 1 µL of this

mixture was spotted onto the target and allowed to dry. 200 – 500 laser shots were accumulated for a spectrum.

Nuclear magnetic resonance spectroscopy (NMR)

The absolute number averaged molecular weight (M_n) of the synthesized triblock terpolymers was determined by $^1\text{H-NMR}$ in CDCl_3 (Bruker AC 250 spectrometer) using the absolute M_n of the P2VP block, determined by MALDI-ToF, for calibration of the NMR signal intensities.

Cloud point determination

The P(GME-*co*-EGE) copolymers were dissolved in Millipore water and the concentration was fixed at 2.5 g/L. The cloud points were determined by turbidity measurements using a titrator (Titrand 809, Metrohm, Herisau, Switzerland) equipped with a turbidity probe ($\lambda_0 = 523$ nm, Spectrosense, Metrohm) and a temperature sensor (Pt 1000, Metrohm). The temperature program (1 K/min) was run by a thermostat (LAUDA RE 306 and Wintherm_Plus software), using a homemade thermostatable vessel. The cloud points were determined from the intersection of the two tangents applied to the two linear regimes of the transmission curve at the onset of turbidity.

Sample preparation for micellisation and gelation experiments

The triblock terpolymers were dissolved in Millipore water or deionised water containing 0.1M NaCl. The pH was fixed at a value of 3-4 using conc. HCl (Riedel-de-Haën). Samples to be characterized under neutral conditions were then titrated slowly to pH = 7 (titer 1M NaOH, Titrisol, Merck; 0.13-0.67 $\mu\text{L}/\text{min}$). The titrations and pH-measurements were performed using a titrator (Titrand 809, Metrohm, Herisau, Switzerland), equipped with a titration unit (Dosino 800, Metrohm, Herisau, Switzerland) and a common glass membrane pH-electrode (micro electrode, Metrohm, Herisau, Switzerland).

Dynamic light scattering (DLS)

DLS was performed on an ALV DLS/SLS-SP 5022F compact goniometer system with an ALV 5000/E cross-correlator and a He-Ne laser ($\lambda_0 = 632.8$ nm). The solutions were filtered prior to the measurement with 0.8 μm syringe filters (Cameo). For temperature

dependent measurements, the decaline bath of the instrument was thermostated using a LAUDA Proline RP 845 thermostat. The temperature was increased stepwise (2 K/step). After each step the sample was equilibrated for 10 min before data acquisition. pH dependent measurements were conducted using the DLS device in combination with a titrator (Titrande 809, Metrohm, Herisau, Switzerland). NaOH (titer 1M, Titrisol, Merck) was added in small portions of 2 μ L. The equilibration time after each titration step was 3 min. Presented scattering intensity data correspond to an average of five measurements, conducted for 1 min each.

Test tube inversion

The glass tubes (volume 5 mL) containing the samples were immersed into an oil bath, which was heated stepwise (1 K/min) using a heating plate (RCT basic, IKA) equipped with a contact thermometer (Ikatron, IKA). After each temperature step the test tubes were inverted in order to check whether the sample flows or not.

Rheology

For dynamic-mechanical measurements a Physica MCR 301 rheometer with a cone-plate shear cell geometry ($d = 50$ mm, cone angle = 1°) was used. Prior to the measurements the linear viscoelastic regime for each sample was determined performing a strain sweep test at a frequency of 1 Hz. For all temperature dependent measurements a frequency of 1 Hz, a strain of 0.7 %, and a heating rate of 0.1 K/min was applied. The temperature was controlled by a Peltier element. For frequency sweeps (10^{-1} to 10^2 Hz) at different temperatures the desired temperatures were adjusted by heating the sample slowly at a rate of 0.1 K/min.

Small-angle neutron scattering (SANS)

SANS experiments were performed using the PAXY instrument of the Laboratoire Léon Brillouin (CEA de Saclay). The scattered neutrons were collected employing a two-dimensional multi-detector. Three sample-to-detector distances of 1.05 m, 3.05 m, and 6.75 m were chosen to cover a rather large q -range. The sample temperature was controlled using a thermostat and a PT 100 temperature sensor leading to a stability of at least around ± 0.5 °C. The samples were prepared in pure D₂O in order to guarantee high

scattering contrasts and were measured in 1 mm standard quartz cells (Hellma, Germany). Due to the isotropic character of the scattering patterns, the collected data were circularly averaged. The resulting spectra were then corrected for electronic noise, detector efficiency, and the scattering of the empty cell and the solvent. Normalisation to achieve absolute intensity values was done using the method developed by Cotton. Further information on the data treatment procedure of the LLB can be found elsewhere.^{48,49} The data collected at the different sample-to-detector distances overlapped within the experimental precision after the treatment procedure. Hence, no further adjustment was necessary.

The normalised and merged scattering profiles were analyzed applying the SASfit program by J. Kohlbrecher.⁵⁰ The presented fits were done considering adjustable prefactors for the contrast of the different blocks. The model, which was chosen for the fitting process, comprises three different form factors: 1. The form factor for a spherical core:

$$K(q, R, \Delta\eta) = \frac{4}{3} \pi R^3 \Delta\eta^3 \frac{(\sin(qR) - qR \cos(qR))}{(qR)^3}$$

Here, R is the core radius and $\Delta\eta$ the scattering contrast.

2. The form factor for a spherical shell:

$$F(q, R, \nu R, \mu, \Delta\eta) = K(q, R, \Delta\eta) - K(q, \nu R, \Delta\eta(1 - \mu))$$

Here, R is the outer radius, the fraction νR accounts for the core radius, $\mu\Delta\eta$ defines the scattering contrast of the core and $\Delta\eta$ is the scattering contrast of the shell.

3. The form factor for Gaussian polymer chains:

$$F^2(q, R_g, I_0) = I_0 2 \left(\frac{(qR_g)^2 - 1 + \exp(-(qR_g)^2)}{(qR_g)^4} \right)$$

Here, R_g is the radius of gyration of the Gaussian polymer chains.

Further details on the SANS data analysis will be treated in the near future in a forthcoming work.

4.3 Results and discussion

4.3.1 Copolymerization of GME and EGE: reactivity ratios

The anionic ring-opening copolymerization of GME and EGE was carried out in THF at 50 °C using *t*-BuOK as initiator. The conversions as well as the copolymer compositions were determined by gas chromatography (see Supporting Information). Identical conditions were applied for the *t*-BuOLi/*t*-BuP₄ initiating system, which was used as a model for the active chain end in the triblock terpolymer synthesis with respect to the polymerization of the glycidyl ether block.⁴³ The obtained P(GME-*co*-EGE) copolymers had a molecular weight of about 5000 g/mol with polydispersity indices PDI \approx 1.07 (Table 4.2, Supporting Information).

The Skeist approach allows the determination of reactivity ratios from a single copolymerization experiment, as it considers the change in the feed composition when the reaction proceeds (integral copolymerization equation).⁵¹ Thus, reactivity ratios can be calculated from higher conversions, too, in contrast to the well known Fineman-Ross procedure.⁵² The solution of the integral copolymerization equation published by Meyer et al.^{53,54} was used to calculate the reactivity ratios numerically. In addition, the Fineman-Ross method was used for copolymerizations with *t*-BuOK. A detailed description concerning the determination of reactivity ratios is provided in the Supporting Information.

The reactivity ratios obtained from the Skeist approach for *t*-BuOK as initiator are $r(\text{GME}) = 1.42$ and $r(\text{EGE}) = 0.53$, respectively, i.e. there is only a weak preferential incorporation of GME into the propagating chain (Table 4.3, Supporting Information). Consequently, we obtained nearly statistical copolymers showing a very weak gradient in composition along the chain. The reactivity ratios determined by the Fineman-Ross method are $r(\text{GME}) = 1.31$ and $r(\text{EGE}) = 0.55$ (Figure 4.11, Supporting Information), which is in good agreement with the values obtained from the Skeist approach, showing its applicability. Finally, comparing these values with the ones obtained from the copolymerization with *t*-BuOLi/*t*-BuP₄, $r(\text{GME}) = 1.33$ and $r(\text{EGE}) = 0.72$, reveals that the initiating system does not influence the copolymerization behaviour significantly.

4.3.2. Synthesis of P2VP-*b*-PEO-*b*-P(GME-*co*-EGE)

The general strategy for the synthesis of the P2VP-*b*-PEO-*b*-P(GME-*co*-EGE) triblock terpolymers was already described in detail in a previous publication.⁴³ All three blocks were synthesized within one step by sequential monomer addition. First, 2-vinylpyridine was polymerized followed by ethylene oxide. Since the chain end of the “living” polymer carries a lithium counter ion, it is necessary to add the phosphazene base *t*-BuP₄ after the addition of ethylene oxide, which promotes ethylene oxide polymerization.⁵⁵⁻⁵⁷ Finally, an equimolar GME/EGE mixture was added. For molar ratios of GME/EGE to initiator higher than 80, we observed transfer reactions to the glycidyl ether monomers,⁵⁸ limiting the maximum achievable P(GME-*co*-EGE) block length. However, the produced P(GME-*co*-EGE) homopolymer can be easily removed from the triblock terpolymer by precipitation in diethyl ether. SEC analysis (Figure 4.1) shows, that P2VP-*b*-PEO-*b*-P(GME-*co*-EGE) triblock terpolymers with narrow molecular weight distributions were obtained (PDI \approx 1.02), and polymerization proceeds without significant side reactions when keeping the molar ratio of glycidyl ether monomers to initiator below 80.

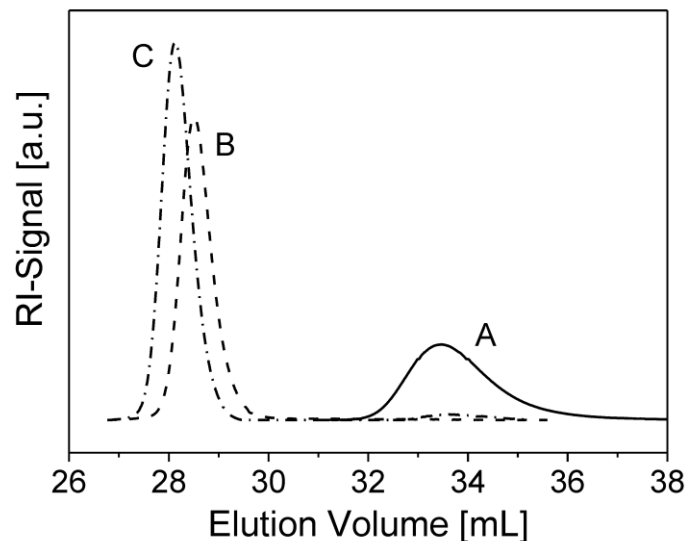


Figure 4.1. THF-SEC traces of a P2VP₅₇-*b*-PEO₄₇₇-*b*-P(GME₂₂-*co*-EGE₂₂) triblock terpolymer before purification (C) and its corresponding P2VP (A) and P2VP-*b*-PEO (B) precursors.

The molecular characteristics of the synthesized triblock terpolymers are summarized in Table 4.1.

Table 4.1. Molecular characteristics of P2VP-*b*-PEO-*b*-P(GME-*co*-EGE) triblock terpolymers.

sample	DP ^a (P2VP)	DP ^b (PEO)	DP ^b (GME- <i>co</i> -EGE)	M _n (10 ⁻³ g/mol) ^b / M _w /M _n ^c
1	57	477	22-22	31.2 / 1.02
2	62	452	36-36	33.2 / 1.02
3	33	236	11-12	16.0 / 1.02

a) determined via MALDI-ToF

b) determined from ¹H-NMR spectra using the absolute M_n(P2VP) for signal intensity calibration

c) determined via THF-SEC with polystyrene calibration

4.3.3 Thermoresponsiveness of GME/EGE copolymers

For the investigation of the temperature dependent solubility of the GME/EGE copolymers five different comonomer ratios were chosen (see Table 4.2, Supporting Information). Aqueous solutions with a concentration of 2.5 g/L were prepared, and the temperature dependent transmittance was measured at a heating rate of 1 K/min (Figure 4.12, Supporting Information).

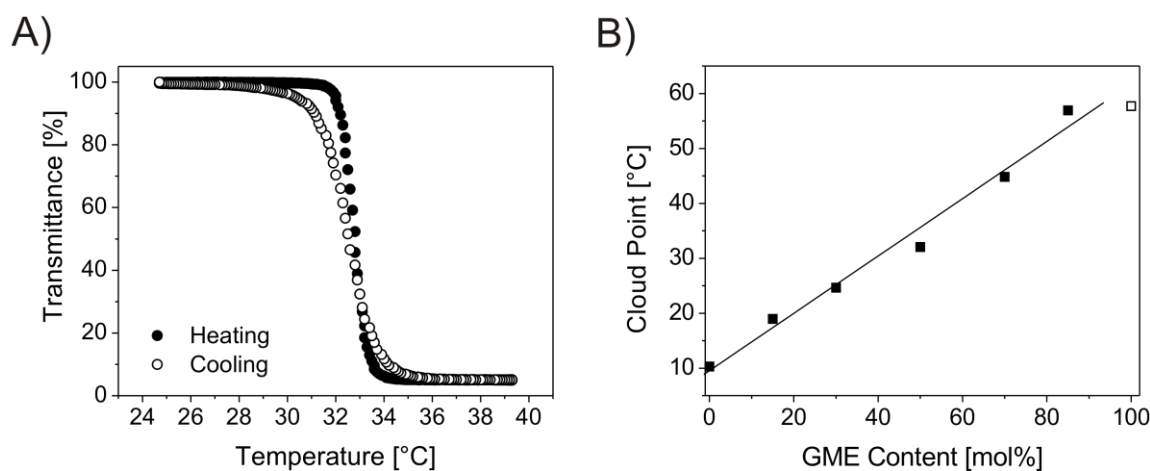


Figure 4.2. A) Transmittance curves (heating-cooling cycle) for an aqueous solution of P(GME-*co*-EGE) with 50 mol% GME (2.5 g/L, 1 K/min), and B) cloud points of P(GME-*co*-EGE) copolymers in dependence of the GME content (heating rate 1 K/min, 2.5 g/L in water, quality factor of the linear fit: 0.99); the open square corresponds to the cloud point of a homo-PGME taken from literature.⁴⁴

A representative heating-cooling cycle for a P(GME-*co*-EGE) with 50 mol% GME is shown in Figure 4.2A. The coil-to-globule transition is still very sharp, keeping in mind that the copolymers have a small gradient in composition along the chain. Similar observations were reported by Park et al. for gradient copolymers of 2-*n*-propyl-2-oxazoline and 2-isopropyl-2-oxazoline.⁴⁷ Furthermore, the cloud point of the P(GME-*co*-EGE) copolymers depends linearly on the copolymer composition (Figure 4.2B), which

was observed for 2-alkyl-2-oxazoline gradient copolymers, too. Most interestingly, the P(GME-*co*-EGE) copolymers show almost no hysteresis within one heating-cooling cycle (Figure 4.2A), similar to the poly(oligo(ethylene glycol) methacrylate) copolymers prepared by Lutz et al., but in contrast to the behaviour of the well known PNIPAAm.⁴⁶

4.3.4 Aggregation of P2VP-*b*-PEO-*b*-P(GME-*co*-EGE)

According to Scheme 4.1 we expect, that the P2VP-*b*-PEO-*b*-P(GME-*co*-EGE) triblock terpolymers form core-shell-corona micelles under conditions where only one of the two outer blocks is insoluble, i.e. at room temperature and a high pH, or at elevated temperatures and a low pH. This was verified by light scattering measurements, recording the scattering intensities of diluted aqueous solutions of P2VP₆₂-*b*-PEO₄₅₂-*b*-P(GME₃₆-*co*-EGE₃₆) as a function of pH and temperature.

Figure 4.3A shows the count rate of a 1 g/L aqueous solution of P2VP₆₂-*b*-PEO₄₅₂-*b*-P(GME₃₆-*co*-EGE₃₆) versus pH. At low pH a very small count rate is observed, which is due to the fact that only unimers are present under these conditions. Upon reaching a pH value of around 5, the count rate increases significantly and reaches a plateau for pH > 5.5. The transition is very sharp, and the corresponding pH value coincides very well with values already published.^{41,42} At this point the P2VP block becomes insoluble, resulting in the formation of core-shell-corona micelles with a P2VP core (Scheme 4.1). What is not shown here but nevertheless worth to be mentioned is that the micelle formation is fully reversible.

Figure 4.3B presents the count rate of the same solution in dependence of the temperature at pH = 3, i.e. the P2VP block is protonated and therefore soluble. To avoid interactions between the charged P2VP blocks the measurements were performed in the presence of salt (0.1M NaCl). At room temperature the count rate is very low and starts to increase strongly at 45 °C, i.e. the polymer chains start to aggregate at that point. The transition is not as sharp as in the case of the pH dependent measurement, the count rate continues to increase up to temperatures of 65 °C. Ogura et al. showed for PEO-*b*-PEGE diblock copolymers with a comparable temperature-sensitive PEGE block, that at temperatures above 40 °C PEO already starts to lose some of the bound water in its hydration shell, but still being well soluble. This results in a further increase in the hydrodynamic radius of the micelles despite the fact that the core forming PEGE block (cloud point of ca.

10 °C) is already strongly hydrophobic in this temperature range.⁵⁹ Partial dehydration of PEO at temperatures above 40 °C was observed for other PEO containing block copolymers, too.⁶⁰⁻⁶² Thus, the observed temperature induced aggregation over a broad temperature range is not only caused by the coil-to-globule transition of the P(GME-*co*-EGE) block, but is presumably combined with a beginning dehydration of the PEO, too.

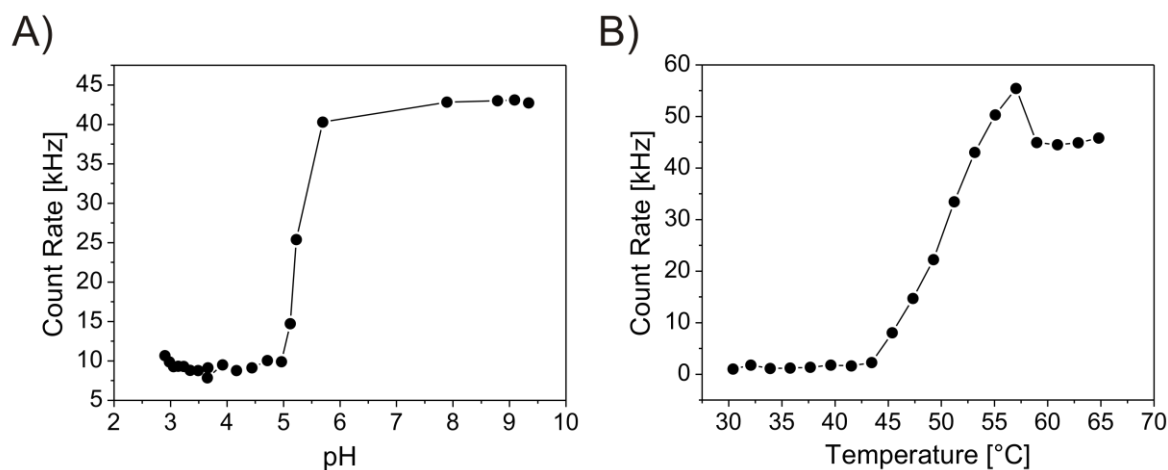


Figure 4.3. Scattering intensity at $\theta = 90^\circ$ of a 1 g/L solution of P2VP₆₂-*b*-PEO₄₅₂-*b*-P(GME₃₆-*co*-EGE₃₆) plotted vs. A) pH at room temperature (titer 1M NaOH, step-wise addition of 2 μ L, equilibration time 3 min), and B) temperature at pH = 3 (0.1M NaCl, 2 K/step, equilibration time 10 min).

Figure 4.4 shows the critical micellisation temperatures (cmt's), which correspond to the onset of the count rate increase upon heating (Figure 4.3B), of two triblock terpolymers in dependence of concentration. Compared to the cloud points of the P(GME-*co*-EGE) homopolymer (50 mol% GME) a significant shift of the cmt's to higher temperatures can be observed. For P2VP₅₇-*b*-PEO₄₇₇-*b*-P(GME₂₂-*co*-EGE₂₂) the difference is 10 °C and for P2VP₆₂-*b*-PEO₄₅₂-*b*-P(GME₃₆-*co*-EGE₃₆) 6.4 °C, respectively, for identical concentrations with regard to the thermo-sensitive P(GME-*co*-EGE) block (see open symbols in Figure 4.4). This result marks the influence of the attached hydrophilic PEO and P2VP (protonated at pH = 3) blocks, a common phenomenon already described in the literature.⁶³ As a conclusion, the P(GME-*co*-EGE) block should have a minimum block length in order to maintain its switchability at moderate temperatures, as the cmt increases with decreasing block length. Furthermore, the cmt's/ cloud points decrease with increasing concentration and level off at concentrations of about 8 - 10 g/L. This is in contrast to the results reported by Watanabe et al., revealing a less pronounced concentration dependence of the cloud point of a PEGE homopolymer.⁵⁹ A detailed investigation of the aggregation behaviour of the P2VP-*b*-PEO-*b*-P(GME-*co*-EGE)

triblock terpolymers is in progress and will be the topic of a forthcoming publication.

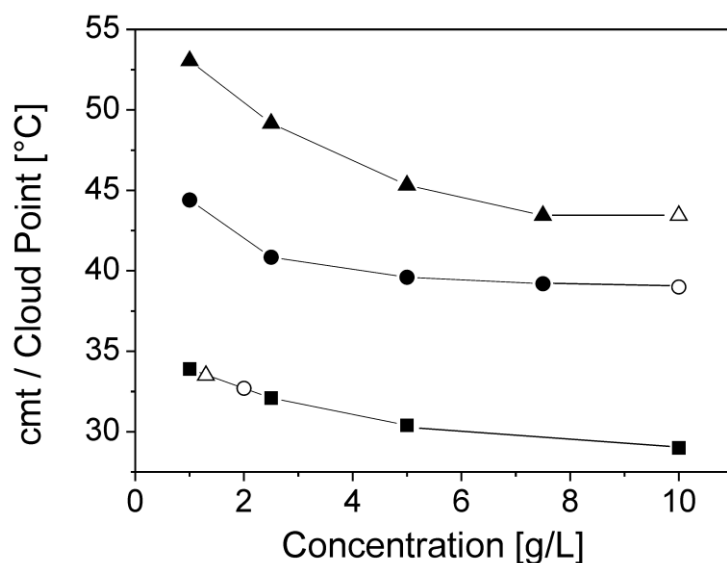


Figure 4.4. Critical micellisation temperatures (cmt)/ cloud points of different P2VP-*b*-PEO-*b*-P(GME-*co*-EGE) triblock terpolymers (at pH = 3, 0.1M NaCl) and a P(GME-*co*-EGE) homopolymer as a function of concentration: P2VP₅₇-*b*-PEO₄₇₇-*b*-P(GME₂₂-*co*-EGE₂₂) (▲); P2VP₆₂-*b*-PEO₄₅₂-*b*-P(GME₃₆-*co*-EGE₃₆) (●); P(GME-*co*-EGE), 50 mol% GME, M_n = 5,000 g/mol (■); the open symbols represent samples with an identical concentration of the P(GME-*co*-EGE) block, highlighting the shift to higher temperatures caused by the hydrophilic PEO and P2VP blocks.

4.3.5 Gel formation and rheology

As already discussed in the introduction, aqueous solutions of P2VP-*b*-PEO-*b*-P(GME-*co*-EGE) triblock terpolymers are supposed to form hydrogels under conditions where both end blocks are insoluble, i.e. at high pH and temperature (Scheme 4.1). Alternatively, hydrogels might be formed by close packing of core-shell-corona micelles, too. In this case, only one of the end blocks is insoluble, i.e. at high pH and low temperature (only P2VP insoluble), or at low pH and high temperature (only P(GME-*co*-EGE) insoluble). Hence, the ability of the synthesized P2VP-*b*-PEO-*b*-P(GME-*co*-EGE) triblock terpolymers to form hydrogels, and the respective response of the hydrogels to pH/temperature was studied in detail.

In order to investigate the gelation behaviour of our triblock terpolymers, we prepared aqueous solutions with concentrations between 10 and 18 wt% at pH = 3 followed by a slow titration to pH = 7 (titer 1M NaOH, 0.13-0.67 μL/min). At pH = 7 solutions of P2VP₅₇-*b*-PEO₄₇₇-*b*-P(GME₂₂-*co*-EGE₂₂) and P2VP₆₂-*b*-PEO₄₅₂-*b*-P(GME₃₆-*co*-EGE₃₆) form free standing gels already at room temperature at concentrations ≥ 14 wt% and

≥ 12 wt%, respectively, as revealed by the test tube inversion method (Figure 4.5A). The hydrogels are typically slightly turbid with a bluish colour, which might indicate a certain inhomogeneity of the samples.

In order to verify the thermoresponsiveness, the hydrogel based on P2VP₅₇-*b*-PEO₄₇₇-*b*-P(GME₂₂-*co*-EGE₂₂) (18 wt%, pH = 7) was heated from 20 °C to 65 °C, and the presence of a gel state was verified by the test tube inversion method (Figures 4.5A-C). The first observation is a “melting” of the hydrogel at temperatures between 25-35 °C, resulting in a viscous liquid. However, at temperatures between 40 and 45 °C, which coincides very well with the observed cmt (Figure 4.4), the gel state is restored due to the thermo-sensitive P(GME-*co*-EGE) block becoming hydrophobic at that point, and thus forming the network junctions. A similar behaviour was observed for P2VP₆₂-*b*-PEO₄₅₂-*b*-P(GME₃₆-*co*-EGE₃₆), with a slight shift of the corresponding transition temperatures to lower values, due to the increased P(GME-*co*-EGE) block length. This kind of gel-sol-gel transition upon heating is rather unusual, and is mostly accompanied with a softening of the gel at higher temperatures.^{62,64,65}

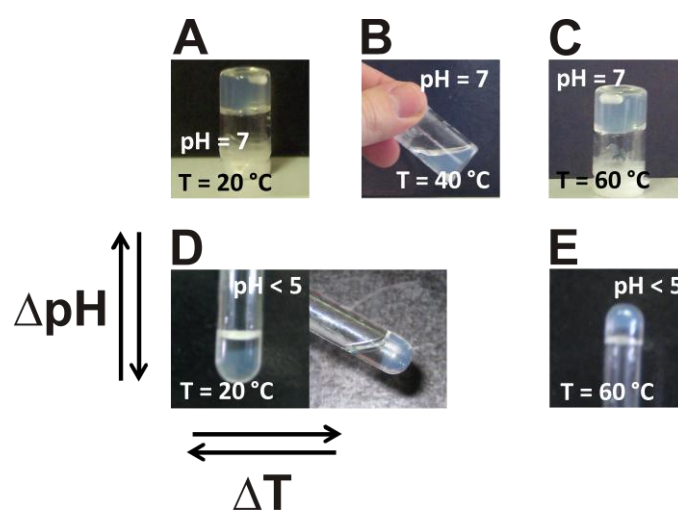


Figure 4.5. Photographs of an 18 wt% solution of P2VP₅₇-*b*-PEO₄₇₇-*b*-P(GME₂₂-*co*-EGE₂₂) at different pH and temperatures.

The hydrogel formed by P2VP₅₇-*b*-PEO₄₇₇-*b*-P(GME₂₂-*co*-EGE₂₂) at pH = 7 and room temperature can be disintegrated by the addition of HCl (solubilization of P2VP), which produces a clear solution being able to flow again. Most interestingly, the gel can be simply restored at elevated temperatures (Figures 4.5D,E). This is observed for P2VP₆₂-*b*-PEO₄₅₂-*b*-P(GME₃₆-*co*-EGE₃₆), too. It is noted, that a P2VP₃₃-*b*-PEO₂₃₆-*b*-P(GME₁₁-*co*-

EGE₁₂) triblock terpolymer, with identical composition compared to P2VP₅₇-*b*-PEO₄₇₇-*b*-P(GME₂₂-*co*-EGE₂₂) but only half the overall molar mass does not form a gel at any temperature or pH up to concentrations of 30 wt%. Thus, a minimum molar mass is required to obtain a gel at reasonable concentrations.

The thermo-responsive behaviour of our gels was investigated more systematically by rheology. We applied an oscillatory stress to the sample using a cone-plate shear cell geometry. Regimes with $G' > G''$ are referred to as gel state with respect to the common definitions.⁶⁶

In Figure 4.6A, the storage (G') and loss (G'') modulus are plotted vs. the temperature for an 18 wt% solution of P2VP₅₇-*b*-PEO₄₇₇-*b*-P(GME₂₂-*co*-EGE₂₂). Between 20 and 35 °C G' exceeds G'' significantly, i.e. the solution is in the gel state. At 35 °C G' crosses G'' , thus, at that point we reach the sol state with G' being significantly lower compared to G'' . Finally, G' exceeds G'' again at temperatures > 48 °C, i.e. the gel state is restored. These results agree well with the observations made by the test tube inversion method (Figures 4.5A-C). The value of G' at 60 °C is significantly higher compared to that at 20 °C. Hence, the gel-sol-gel transition upon heating is accompanied with a stiffening of the hydrogel. This behaviour is quite unique, as usually a softening of the gel is observed for comparable transitions.^{62,64,65} The whole process is fully reversible, however, the reformation of the low temperature gel phase is significantly shifted to lower temperatures. This might be due to the mechanical stress, which is applied to the solution during the measurement. Mechanical stress hinders the reformation of the micellar structures building the gel (see discussion SANS experiments).

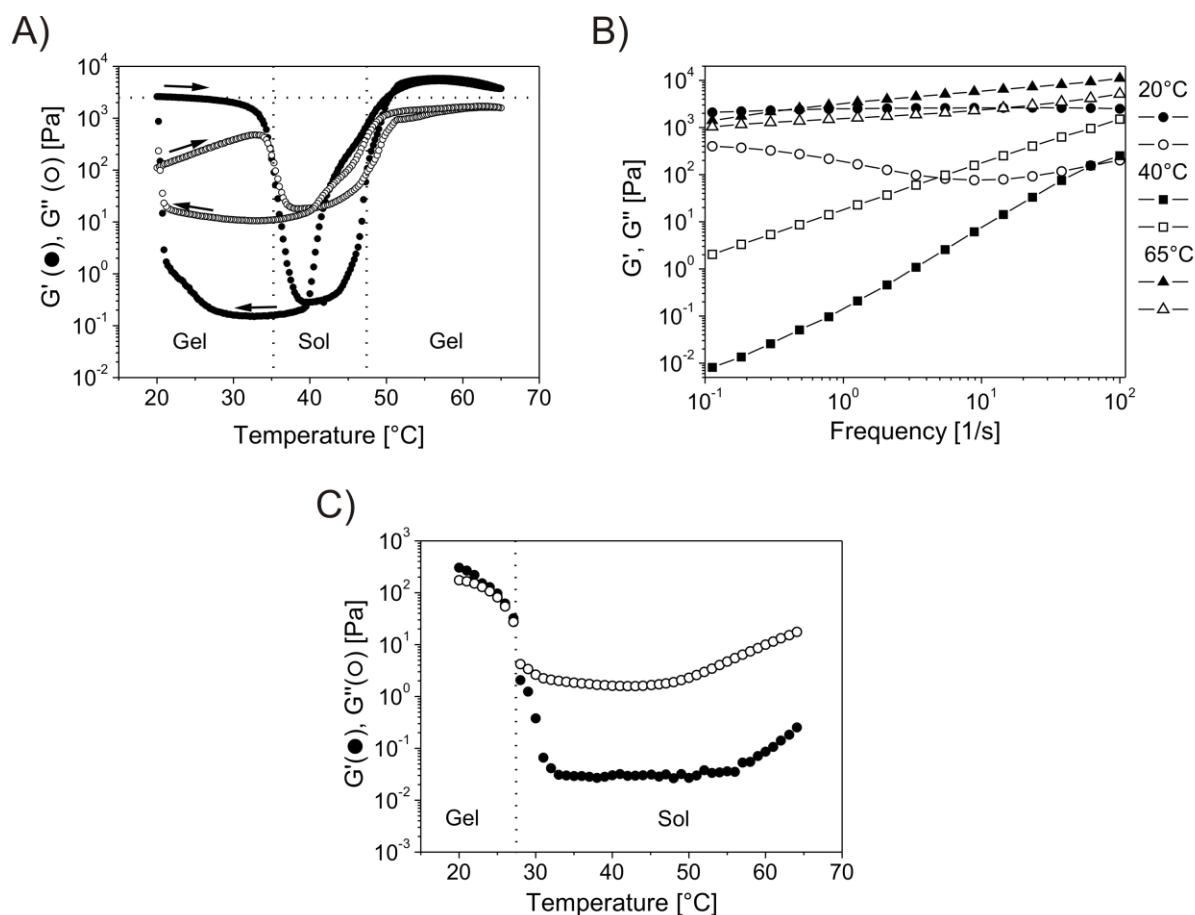


Figure 4.6. Rheological properties of aqueous P2VP₅₇-*b*-PEO₄₇₇-*b*-P(GME₂₂-*co*-EGE₂₂) solutions (0.7% strain): A) temperature dependent G' and G'' of an 18 wt% solution at pH = 7 (0.1 K/min), B) frequency dependent G' (filled symbols) and G'' (open symbols) of an 18 wt% solution at pH = 7 for different temperatures, and C) temperature dependent G' and G'' of a 13 wt% solution at pH = 7 (0.1 K/min).

Another proof for the presence of a gel is a weak linear dependence/independence of G' on frequency. For $G' \propto \omega^2$ and $G'' \propto \omega^1$ we deal with a viscoelastic fluid. In this case G' is always lower than G'' . Figure 4.6B shows the frequency dependence of G' and G'' at different temperatures. At 20 °C G' is nearly constant in the range of 10^{-1} - 10^2 Hz, and G'' shows a broad minimum. This is characteristic for gels formed by cubic micellar phases,⁶⁷⁻⁷⁰ and is supported by our SANS experiments, which will be discussed later, too. At 40 °C G' and G'' both increase with increasing frequency, with $G' \propto \omega^{1.7}$ and $G'' \propto \omega^1$, which is characteristic for the sol state. In the high temperature gel state at 65 °C, G' exceeds G'' again and both moduli run almost parallel with frequency, showing a weak linear dependence on frequency. The dynamic behaviour of crosslinked chemical and physical gels at the gel point is given by the relation $G' \propto G'' \propto \omega^n$, i.e. G' and G'' are parallel in a log-log plot.^{66,71,72} This supports the proposed crosslinking of CSC micelles with a P2VP core by the thermo-sensitive P(GME-*co*-EGE) corona block above the cmt, resulting in a

reformation of the gel via open association (Scheme 4.1).

A 13 wt% solution of P2VP₅₇-*b*-PEO₄₇₇-*b*-P(GME₂₂-*co*-EGE₂₂) undergoes only a gel-sol transition upon heating (Figure 4.6C). Although the viscosity starts to increase significantly at around 45 °C the gel state is not reached anymore. A further decrease in concentration leads to a solution which is in the sol state over the whole measured temperature range. After screening a series of concentrations we can conclude that a gel-sol transition occurs for P2VP₅₇-*b*-PEO₄₇₇-*b*-P(GME₂₂-*co*-EGE₂₂) only between 12 and 16 wt%. At slightly higher concentrations, i.e. 18 wt%, a gel-sol-gel transition is observed upon heating.

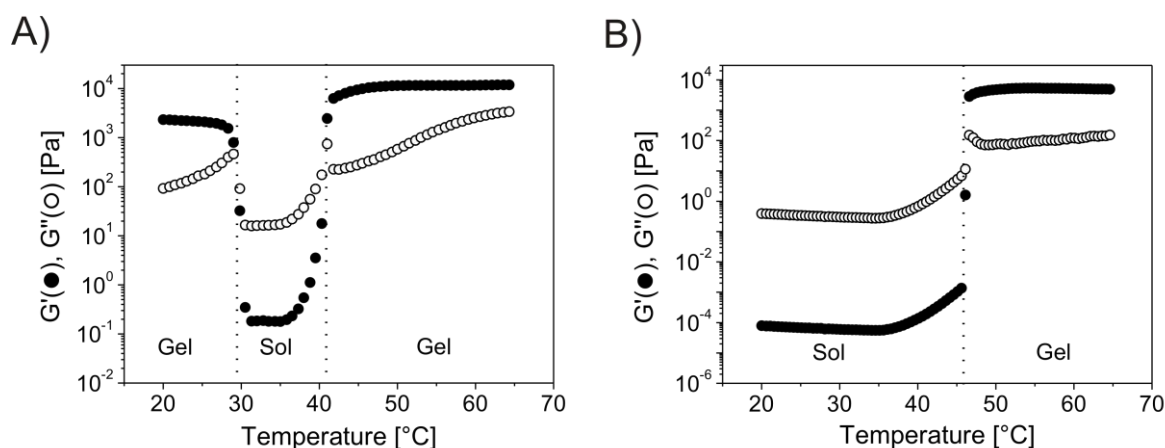


Figure 4.7. Temperature dependent G' and G'' for an 18 wt% solution of P2VP₆₂-*b*-PEO₄₅₂-*b*-P(GME₃₆-*co*-EGE₃₆): A) at pH = 7, and B) at pH = 3.5 (0.1 K/min, strain = 1%).

Switching to P2VP₆₂-*b*-PEO₄₅₂-*b*-P(GME₃₆-*co*-EGE₃₆), i.e. increasing only the block length of the thermo-sensitive block from 44 to 72 repeating units, while keeping the concentration at 18 wt%, the behaviour does not change qualitatively (Figure 4.7A). However, the high temperature gel state is restored at 10 °C lower compared to P2VP₅₇-*b*-PEO₄₇₇-*b*-P(GME₂₂-*co*-EGE₂₂), which is in line with the observed lowering of the cmt with increasing block length of the P(GME-*co*-EGE) block (Figure 4.4). In addition, the storage modulus increases from 5.4 kPa at 20 °C to 11.5 kPa at 60 °C, indicating a stiffening of the gel at higher temperatures. Finally, G' and G'' of an 18 wt% solution of P2VP₆₂-*b*-PEO₄₅₂-*b*-P(GME₃₆-*co*-EGE₃₆) were monitored at pH = 3.5 in dependence of temperature, too (Figure 4.7B). In that case, a sol-gel transition occurs at about 46 °C, which was also observed for P2VP₅₇-*b*-PEO₄₇₇-*b*-P(GME₂₂-*co*-EGE₂₂). These results are in good agreement with the observations made by the test tube inversion method (Figures 4.5D,E).

4.3.6 Small-angle neutron scattering

In order to gain a better understanding of the internal structure of the hydrogels at room temperature and $\text{pH} = 7$, we have performed SANS experiments on $\text{P2VP}_{62}\text{-}b\text{-PEO}_{452}\text{-}b\text{-P(GME}_{36}\text{-}co\text{-EGE}_{36})$ in D_2O for different concentrations.

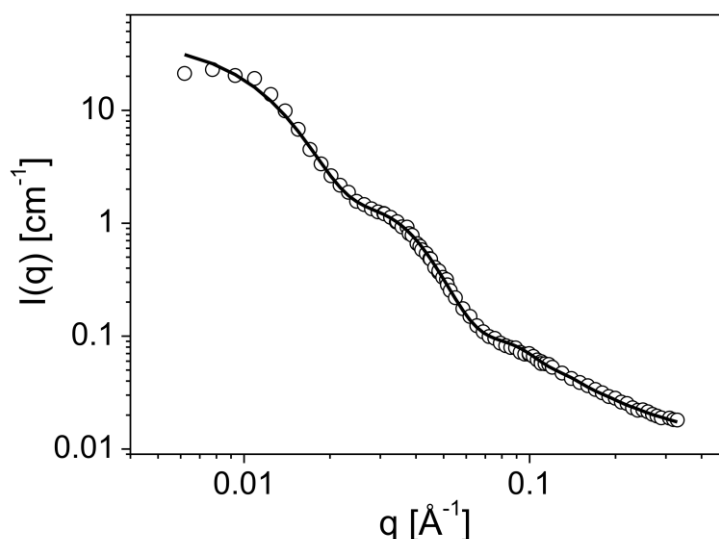


Figure 4.8. SANS data for a 1.2 wt% solution of $\text{P2VP}_{62}\text{-}b\text{-PEO}_{452}\text{-}b\text{-P(GME}_{36}\text{-}co\text{-EGE}_{36})$ in D_2O at $20\text{ }^\circ\text{C}$ and $\text{pH} = 7$. The solid line is a fit with a core-shell model plus Gaussian chains. The fit was done using the SASfit program by J. Kohlbrecher.⁵⁰

Scattering of the 1.2 wt% solution is mostly determined by the form factor of the triblock terpolymer micelles (Figure 4.8). The data can be well described with a core-shell model with additional Gaussian chains accounting for the soft corona. Figure 4.8 compares the measured SANS profile and the respective fit, which was done using the SASfit program by J. Kohlbrecher.⁵⁰ The insoluble P2VP forms the core, while the highly swollen shell and corona are formed by the soluble PEO and $\text{P(GME-}co\text{-EGE)}$ blocks, respectively. The fit gives a core radius of 6.5 nm for the block copolymer micelles. The total radius including the shell is found to be 12.6 nm. In addition, a Guinier radius of the coiled chains in the micellar corona of 2.0 nm is computed. These values are in rather good agreement with the block length of the investigated copolymer (Table 4.1). Using the hydrodynamic radius of the block copolymer micelles obtained by DLS, a ratio ρ of approximately 0.45 is obtained.⁷³ This is significantly below the hard sphere value and in good agreement with a strongly swollen corona.

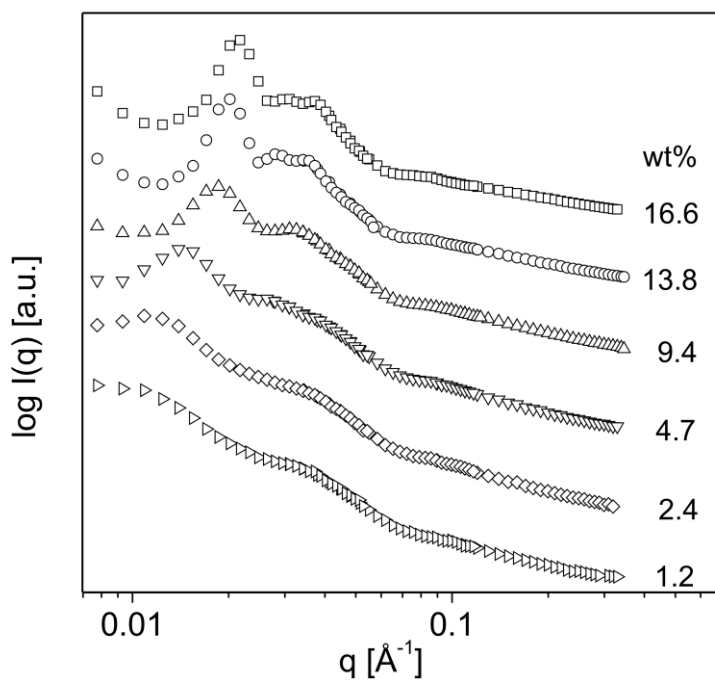


Figure 4.9. SANS data for P2VP₆₂-*b*-PEO₄₅₂-*b*-P(GME₃₆-*co*-EGE₃₆) solutions in D₂O at 20 °C and pH = 7. The curves were shifted vertically for clarity.

Scattering profiles for different concentrations are shown in Figure 4.9. Already at a concentration of 2.4 wt% interactions between micelles become important, which is reflected by the appearance of a structure factor maximum at $q \approx 0.012 \text{ \AA}^{-1}$. This maximum shifts to higher q -values with increasing concentration and gets more pronounced, i.e. the distance between micelles decreases and the micellar assembly exhibits increased order.

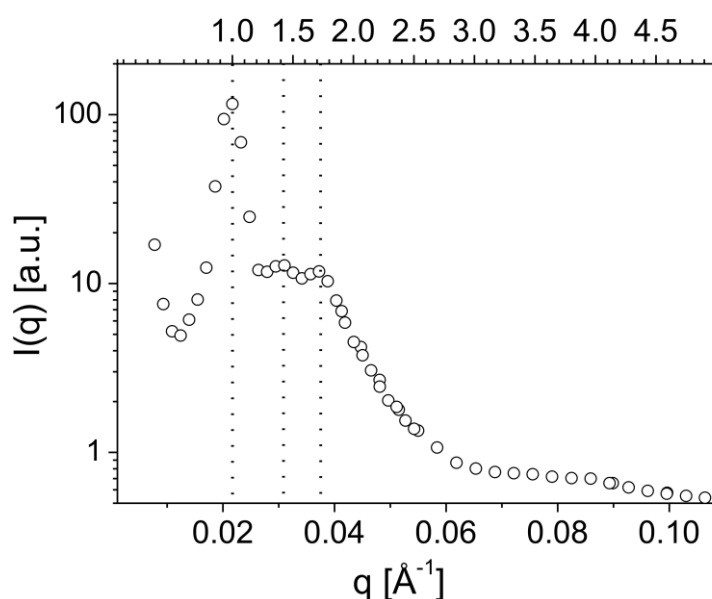


Figure 4.10. SANS data for a 16.6 wt% solution of P2VP₆₂-*b*-PEO₄₅₂-*b*-P(GME₃₆-*co*-EGE₃₆) in D₂O, top x-axis normalized to 1st order reflection.

In the SANS profile of the 16.6 wt% solution clearly 2 well-defined higher order reflections are visible, corresponding to relative peak positions of $1 : 2^{1/2} : 3^{1/2}$ (Figure 4.10). This is consistent with a simple cubic (sc) or body centred cubic (bcc) packing of the spherical CSC micelles. Due to a lack of higher order reflexes an assignment to sc or bcc is not possible. However, a bcc-type packing of spherical micelles is frequently observed for comparable diblock copolymer micelles having a star-like architecture, i.e. the soluble corona forming block is significantly larger compared to the insoluble core forming block, which supports a bcc-type structure for our system, too.⁷⁴⁻⁷⁶ We plan to perform SANS experiments under shear in order to differentiate between a sc- and bcc-type packing. This method was used to determine the exact structure of the micellar packing in aqueous solutions of star block copolymers composed of PEO and PPO, i.e. bcc-type packing, which was not possible by SANS under static conditions.⁷⁷

At this point we are not able to provide a detailed mechanism for the observed gel-sol-gel transition upon heating. In order to investigate the underlying structural changes, extensive SANS experiments are necessary and will be performed in the near future. However, based on our results a tentative mechanism might be given. At room temperature and $\text{pH} = 7$ the gel is formed by a cubic packing of spherical CSC micelles (probably bcc structure), as shown by SANS. Upon increasing temperature, but still below the cmt of the triblock terpolymers at low pH (Figure 4.4), the P(GME-*co*-EGE) blocks start to loose some bound water, similar to PEO but at significantly lower temperatures.^{41,59-62} This induces a shrinkage of the micelles, which will result in the observed transition into a sol phase if the volume fraction of micelles is below the critical value for a bcc phase ($\Phi = 0.68$). A further increase in temperature above the cmt of the triblock terpolymers will switch the outer P(GME-*co*-EGE) blocks insoluble, thus reforming the gel by additional physical cross linking of the CSC micelles. The presence of additional network points is supported by the higher storage modulus of the hydrogels in the gel phase at elevated temperatures compared to that at room temperature, and by the corresponding change in the frequency dependence of G' and G'' , too (Figures 4.6, 4.7).

4.4 Conclusions

We successfully synthesized well defined double stimuli-responsive P2VP-*b*-PEO-*b*-P(GME-*co*-EGE) triblock terpolymers by means of sequential anionic polymerization. The thermo-sensitive outer block consists of a glycidyl methyl ether (GME)/ ethyl glycidyl ether (EGE) copolymer. Even though the copolymers exhibit a small compositional gradient, the coil-to-globule transition remains sharp, and the cloud point is easily adjustable by the comonomer ratio. Since both outer blocks of the triblock terpolymer are stimuli-responsive, a micellisation of the triblock terpolymer in aqueous solution under conditions where at least one outer block is hydrophobic takes place, i.e. pH = 7 and room temperature, or pH = 3 and temperatures above 40 °C. At pH = 7 and sufficiently high concentrations a unique gel-sol-gel transition is observed upon heating, which is accompanied with a strengthening of the hydrogel. Depending on block lengths, concentration, and pH, one additionally observes gel-sol and sol-gel transitions, and the gel strength as well as the gel/sol and sol/gel transition temperatures vary. The low temperature gel at pH = 7 is based on a cubic arrangement of spherical CSC micelles with P2VP cores, as was shown using SANS experiments.

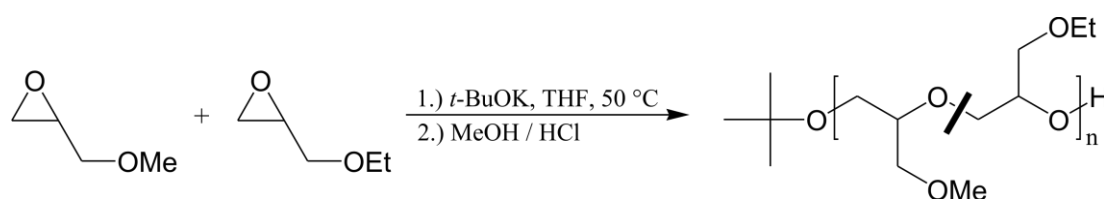
Acknowledgement

We would like to thank Jérôme Crassous (PC I, University of Bayreuth) for the introduction into rheological measurements, and Alejandro Müller (Universidad Simón Bolívar) for helpful discussions. Financial support from the German Science Foundation (priority program SPP 1259) is gratefully acknowledged.

4.5 Supporting Information

Determination of Reactivity Ratios for GME/EGE Copolymerization

The reaction scheme of the anionic ring-opening copolymerization of glycidyl methyl ether (GME) and ethyl glycidyl ether (EGE) is shown in Scheme 4.2. The molecular weights, polydispersity indices, and cloud points of all synthesized copolymers are summarized in Table 4.2. The commercially available lithium *tert*-butoxide initiator solution we used contains small amounts of the corresponding *tert*-butyl alcohol, as evidenced by gas chromatography. The alcohol can initiate the polymerization of epoxy monomers, too, since the proton exchange reaction between the alcohol and the alkoxide is much faster with respect to the propagation reaction. As a result, a lower molecular weight than theoretically expected is obtained. This has been observed in ethylene oxide polymerization, too, i.e. in this case no transfer reactions to the monomer occur, which might alternatively result in lower molecular weights.⁵⁷



Scheme 4.2. Anionic ring-opening copolymerization of GME and EGE in THF using *t*-BuOK as initiator.

Table 4.2. Molecular characteristics and cloud points of GME/EGE copolymers.

Initiator	[I] ₀ [mol/L]	X _{0, GME} [mol%] ^a	M _n (calc.) [g/mol]	M _n (SEC) ^b [g/mol]	M _w /M _n ^b	T _{cp} ^c [°C]
<i>t</i> -BuOK	1.67·10 ⁻²	0.15	4 900	5 200	1.07	19.1
<i>t</i> -BuOK	1.70·10 ⁻²	0.30	5 000	4 900	1.07	24.9
<i>t</i> -BuOK	1.70·10 ⁻²	0.50	5 000	5 400	1.06	32.1
<i>t</i> -BuOK	1.77·10 ⁻²	0.70	4 700	4 700	1.05	44.8
<i>t</i> -BuOK	1.73·10 ⁻²	0.85	4 900	4 500	1.09	57.1
<i>t</i> -BuOLi / <i>t</i> -BuP ₄	1.70·10 ⁻²	0.50	5 000	3 300	1.09	32.9

a) molar fraction of GME in the initial monomer mixture

b) determined by THF-SEC using PS-calibration

c) the cloud point T_{cp} is defined as the intercept of the tangents at the onset of turbidity (2.5 g/L, 1 K/min)

The copolymerization was followed by gas chromatography (GC) of samples taken during the course of reaction. The area of each monomer peak divided by the area of the decane peak (internal standard) is proportional to the corresponding monomer concentration:

$$\frac{A(\text{Monomer})}{A(\text{Decan})} = A_{\text{norm.}}(\text{Monomer}) \Rightarrow \sim[\text{Monomer}].$$

For the FINEMAN-ROSS approach⁵² samples were taken after approximately 10 % conversion ($[M] \approx [M]_0$) for each copolymerization and the molar fraction of GME (x_{GME}) in the copolymer was calculated using the equation:

$$x_{\text{gme}} = \frac{(1 - R(\text{GME})) \cdot X_{0,\text{GME}}}{(1 - R(\text{GME})) \cdot X_{0,\text{GME}} + (1 - R(\text{EGE})) \cdot X_{0,\text{EGE}}}$$

$$\text{with } R(\text{GME}) = \frac{A_{\text{norm.}}(\text{GME})}{A_{0,\text{norm.}}(\text{GME})} \quad R(\text{EGE}) = \frac{A_{\text{norm.}}(\text{EGE})}{A_{0,\text{norm.}}(\text{EGE})}$$

$X_{0,\text{GME}}$ and $X_{0,\text{EGE}}$ denote the molar fractions of GME and EGE in the initial monomer mixture, respectively.

According to the Fineman-Ross equation:

$$\frac{(f-1)F}{f} = r_1 \frac{F^2}{f} - r_2,$$

$$\text{with } F = \frac{X_{0,\text{GME}}}{X_{0,\text{EGE}}}, \quad \text{and } f = \frac{x_{\text{GME}}}{x_{\text{EGE}}},$$

the reactivity ratios $r_1 = r_{\text{GME}}$ and $r_2 = r_{\text{EGE}}$ were determined from the slope and the y-axis intercept, respectively, of the corresponding linear fit (Figure 4.11, Table 4.3). The quality factor of the linear fit is 0.997.

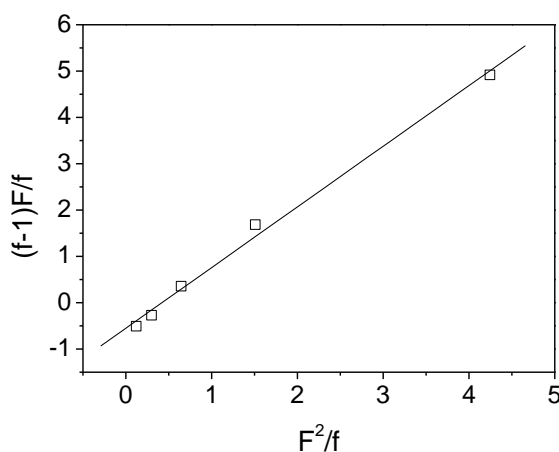


Figure 4.11. Fineman-Ross plot for GME/EGE copolymerization in THF with *t*-BuOK as initiator (50 °C).

The reactivity ratios were also calculated using the Skeist approach.⁵¹ The advantage of this procedure is that it considers the change in the comonomer ratio when the reaction proceeds, making it possible to determine the reactivity ratios also from higher conversions in contrast to the Fineman-Ross method. Consequently, only one copolymerization experiment is necessary to calculate r_{GME} and r_{EGE} . For calculating the reactivity ratios following the Skeist approach one needs also the fraction of each monomer in the monomer mixture X_{GME} and X_{EGE} after different reaction times and the corresponding overall monomer conversion $x_p = 1 - [M]/[M]_0$. These values were calculated using the following relations:

$$X_{GME} = \frac{R(GME) \cdot X_{0,GME}}{R(GME) \cdot X_{0,GME} + R(EGE) \cdot X_{0,EGE}}$$

$$1 - \frac{M}{M_0} = 1 - \left(R(GME) \cdot X_{0,GME} + R(EGE) \cdot X_{0,EGE} \right)$$

From the solution of the integrated copolymerization equation, derived by Meyer et al.^{53,54}, the reactivity ratios were calculated numerically using the software MathCad 5.0:

$$1 - \frac{M}{M_0} = 1 - \left[\frac{X_{GME}}{X_{0,GME}} \right]^{\frac{r_2}{1-r_1}} \left[\frac{X_{EGE}}{X_{0,EGE}} \right]^{\frac{r_1}{1-r_1}} \left[\frac{X_{0,GME} - \frac{1-r_2}{2-r_1-r_2}}{X_{GME} - \frac{1-r_2}{2-r_1-r_2}} \right]^{\frac{1-r_1 r_2}{(1-r_1)(1-r_2)}}$$

The reactivity ratios calculated via the Fineman-Ross- and Skeist-approach for both initiating systems, *t*-BuOK and *t*-BuOLi/*t*-BuP₄, are summarized in Table 4.3.

Table 4.3. Reactivity ratios for GME/EGE copolymerization with two different initiating systems.

Initiator	r_{GME} / r_{EGE} (Fineman-Ross)	r_{GME} / r_{EGE} (Skeist)
<i>t</i> -BuOK	1.31 / 0.55	1.42 / 0.53
<i>t</i> -BuOLi/ <i>t</i> -BuP ₄	-	1.33 / 0.72

Thermoresponsiveness of P(GME-*co*-EGE) Copolymers

Figure 4.12 shows the temperature dependent transmittance for aqueous solutions of P(GME-*co*-EGE) copolymers with varying composition.

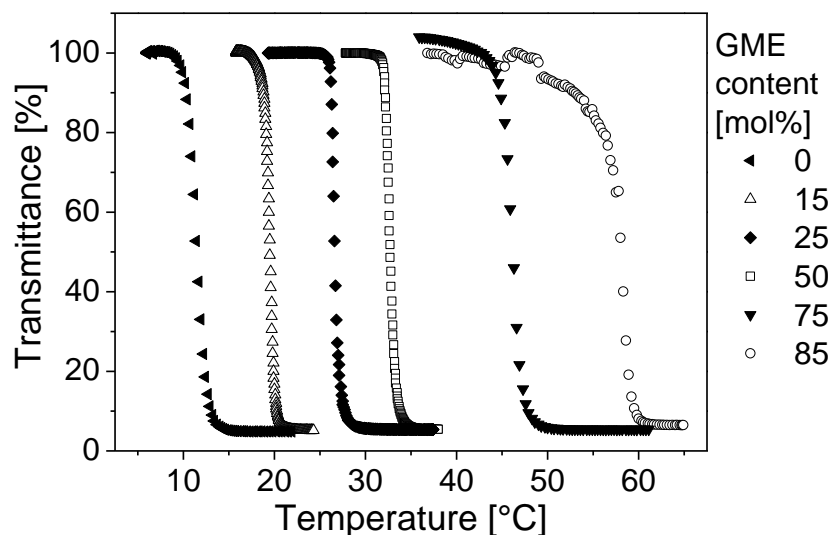


Figure 4.12. Transmittance vs. temperature for aqueous solutions of P(GME-*co*-EGE) in dependence of the GME content (2.5 g/L, 1 K/min).

4.6 References

- [1] Tachibana, Y.; Kurisawa, M.; Uyama, H.; Kakuchi, T.; Kobayashi, S. *Chem. Lett.* **2003**, *32*, 374.
- [2] Hart, D. S.; Gehrke, S. H. *J. Pharm. Sci.* **2007**, *96*, 484.
- [3] Yu, L.; Ding, J. *Chem. Soc. Rev.* **2008**, *37*, 1473.
- [4] Beebe, D. J.; Moore, J. S.; Bauer, J. M.; Yu, Q.; Liu, R. H.; Devadoss, C.; Jo, B.-H. *Nature* **2000**, *404*, 588.
- [5] Calvert, P.; Patra, P.; Duggal, D. *Proc. SPIE-Int. Soc. Opt. Eng.* **2007**, *6524*, 65240M/1.
- [6] Guenther, M.; Kuckling, D.; Corten, C.; Gerlach, G.; Sorber, J.; Suchaneck, G.; Arndt, K.-F. *Sens. Actuators B* **2007**, *126*, 97.
- [7] Ahn, S.-k.; Kasi, R. M.; Kim, S.-C.; Sharma, N.; Zhou, Y. *Soft Matter* **2008**, *4*, 1151.
- [8] Dušek ed., K. *Responsive Gels: Volume Transitions I/II in Adv. Polym. Sci* **1993**, *109/110*.
- [9] Zhang, X.-Z.; Zhuo, R.-X. *Eur. Polym. J.* **2000**, *36*, 643.

- [10] Kuckling, D.; Vo, C. D.; Adler, H.-J. P.; Völkel, A.; Cölfen, H. *Macromolecules* **2006**, *39*, 1585.
- [11] Park, T. G.; Hoffman, A. S. *J. Polym. Sci., Part A: Polym. Chem.* **1992**, *30*, 505.
- [12] Kratz, K.; Hellweg, T.; Eimer, W. *Ber. Bunsen Ges.* **1998**, *102*, 1603.
- [13] Theiss, D.; Schmidt, T.; Arndt, K.-F. *Macromol. Symp.* **2004**, *210*, 465.
- [14] Reichelt, R.; Schmidt, T.; Kuckling, D.; Arndt, K.-F. *Macromol. Symp.* **2004**, *210*, 501.
- [15] Utrata-Wesolek, A.; Trzebicka, B.; Dworak, A.; Ivanova, S.; Christova, D. *e-Polymers* **2007**, no. 19.
- [16] Lutz, J.-F.; Weichenhan, K.; Akdemir, Ö.; Hoth, A. *Macromolecules* **2007**, *40*, 2503.
- [17] He, H.; Li, L.; Lee, L. J. *Polymer* **2006**, *47*, 1612.
- [18] Lin, H. H.; Cheng, Y. L. *Macromolecules* **2001**, *34*, 3710.
- [19] Fechler, N.; Badi, N.; Schade, K.; Pfeifer, S.; Lutz, J.-F. *Macromolecules* **2009**, *42*, 33.
- [20] Bae, S. J.; Joo, M. K.; Jeong, Y.; Kim, S. W.; Lee, W. K.; Sohn, Y. S.; Jeong, B. *Macromolecules* **2006**, *39*, 4873.
- [21] Sugihara, S.; Kanaoka, S.; Aoshima, S. *J. Polym. Sci., Part A: Polym. Chem.* **2004**, *42*, 2601.
- [22] Iddon, P. D.; Armes, S. P. *Eur. Polym. J.* **2007**, *43*, 1234.
- [23] Stavrouli, N.; Katsampas, I.; Angelopoulos, S.; Tsitsilianis, C. *Macromol. Rapid Commun.* **2008**, *29*, 130.
- [24] Achilleos, M.; Krasia-Christoforou, T.; Patrickios, C. S. *Macromolecules* **2007**, *40*, 5575.
- [25] Hadjiantoniou, N. A.; Patrickios, C. S. *Polymer* **2007**, *48*, 7041.
- [26] Alexandridis, P.; Hatton, T. A. *Colloids Surf. A: Physicochem. Eng. Aspects* **1995**, *96*, 1.
- [27] Wanka, G.; Hoffmann, H.; Ulbricht, W. *Macromolecules* **1994**, *27*, 4145.
- [28] Dong, L.-C.; Hoffman, A. S. *J. Controlled Release* **1991**, *15*, 141.
- [29] Han, M.-H.; Kim, J.-W.; Kim, J.; Ko, J. Y.; Magda, J. J.; Han, I. S. *Polymer* **2003**, *44*, 4541.
- [30] Plamper, F. A.; Ruppel, M.; Schmalz, A.; Borisov, O.; Ballauff, M.; Müller, A. H. E. *Macromolecules* **2007**, *40*, 8361.
- [31] Yildiz, B.; Isik, B.; Kis, M.; Birgül, O. *J. Appl. Polym. Sci.* **2003**, *88*, 2028.
- [32] Karg, M.; Pastoriza-Santos, I.; Rodriguez-González, B.; von Klitzing, R.; Wellert, S.; Hellweg, T. *Langmuir* **2008**, *24*, 6300.

- [33] Kratz, K.; Hellweg, T.; Eimer, W. *Colloids Surf. A: Physicochem. Eng. Aspects* **2000**, *170*, 137.
- [34] Zhang, X.-Z.; Yang, Y.-Y.; Wang, F.-J.; Chung, T.-S. *Langmuir* **2002**, *18*, 2013.
- [35] Shi, J.; Alves, N. M.; Mano, J. F. *Macromol. Biosci.* **2006**, *6*, 358.
- [36] Xu, F.-J.; Kang, E.-T.; Neoh, K.-G. *Biomaterials* **2006**, *27*, 2787.
- [37] Angelopoulos, S. A.; Tsitsilianis, C. *Macromol. Chem. Phys.* **2006**, *207*, 2188.
- [38] Dayananda, K.; Pi, B. S.; Kim, B. S.; Park, T. G.; Lee, D. S. *Polymer* **2007**, *48*, 758.
- [39] Li, C.; Madsen, J.; Armes, S. P.; Lewis, A. L. *Angew. Chem. Int. Ed.* **2006**, *45*, 3510.
- [40] Vogt, A. P.; Sumerlin, B. S. *Soft Matter* **2009**, Advance Article (doi: 10.1039/b817586a).
- [41] Vamvakaki, M.; Papoutsakis, L.; Katsamanis, V.; Afchoudia, T.; Fragouli, P. G.; Iatrou, H.; Hadjichristidis, N.; Armes, S. P.; Sidorov, S.; Zhurov, D.; Zhurov, V.; Kostylev, M.; Bronstein, L. M.; Anastasiadis, S. H. *Faraday Discuss.* **2005**, *128*, 129.
- [42] Yin, J.; Dupin, D.; Li, J.; Armes, S. P.; Liu, S. *Langmuir* **2008**, *24*, 9334.
- [43] Ah Toy, A.; Reinicke, S.; Müller, A. H. E.; Schmalz, H. *Macromolecules* **2007**, *40*, 5241.
- [44] Aoki, S.; Koide, A.; Imabayashi, S.-I.; Watanabe, M. *Chem. Lett.* **2002**, 1128.
- [45] Labbe, A.; Carlotti, S.; Deffieux, A.; Hirao, A. *Macromol. Symp.* **2007**, *249/250*, 392.
- [46] Lutz, J. F.; Akdemir, Ö.; Hoth, A. *J. Am. Chem. Soc.* **2006**, *128*, 13046.
- [47] Park, J. S.; Kataoka, K. *Macromolecules* **2007**, *40*, 3599.
- [48] Brulet, A.; Lairez, D.; Lapp, A.; Cotton, J.-P. *J. Appl. Crystallogr.* **2007**, *40*, 165.
- [49] Cotton, J. P. Initial Data Treatment. In *Neutron, X-Ray and Light Scattering*; Lindner, P.; Zemb, T., Eds.; Elsevier Science Publishers B. V.: 1991.
- [50] Kohlbrecher, J. *SASfit: A Program for Fitting Simple Structural Models to Small Angle Scattering Data*, Paul Scherrer Institut, Laboratory for Neutron Scattering: CH-5232, Villigen Switzerland, 2008.
- [51] Skeist, I. *J. Am. Chem. Soc.* **1946**, *68*, 1781.
- [52] Fineman, M.; Ross, S. D. *J. Polym. Sci.* **1950**, *5*, 259.
- [53] Chan, R. K. S.; Meyer, V. E. *J. Polym. Sci. Polym. Symp.* **1968**, *25*, 11.
- [54] Meyer, V. E.; Lowry, G. G. *J. Polym. Sci., Part A: Polym. Chem.* **1965**, *3*, 2843.
- [55] Esswein, B.; Molenberg, A.; Möller, M. *Macromol. Symp.* **1996**, *107*, 331.
- [56] Esswein, B.; Möller, M. *Angew. Chem. Int. Ed.* **1996**, *35*, 623.
- [57] Schmalz, H.; Lanzendörfer, M. G.; Abetz, V.; Müller, A. H. E. *Macromol. Chem. Phys.* **2003**, *204*, 1056.

- [58] Stolarzewicz, A. *Makromol. Chem.* **1986**, *187*, 745.
- [59] Ogura, M.; Tokuda, H.; Imabayashi, S.-I.; Watanabe, M. *Langmuir* **2007**, *23*, 9429.
- [60] Li, H.; Yu, G.-E.; Price, C.; Booth, C.; Hecht, E.; Hoffmann, H. *Macromolecules* **1997**, *30*, 1347.
- [61] Prud'homme, R. K.; Wu, G.; Schneider, D. K. *Langmuir* **1996**, *12*, 4651.
- [62] Castelletto, V.; Hamley, I. W.; English, R. J.; Mingvanish, W. *Langmuir* **2003**, *19*, 3229.
- [63] Schilli, C. M.; Zhang, M.; Rizzardo, E.; Thang, S. H.; Chong, Y. K.; Edwards, K.; Karlsson, G.; Müller, A. H. E. *Macromolecules* **2004**, *37*, 7861.
- [64] Almgren, M.; Brown, W.; Hvidt, S. *Colloid Polym. Sci.* **1995**, *273*, 2.
- [65] Kellarakis, A.; Castelletto, V.; Chaibundit, C.; Fundin, J.; Havredaki, V.; Hamley, I. W.; Booth, C. *Langmuir* **2001**, *17*, 4232.
- [66] Winter, H. H.; Mours, M. *Adv. Polym. Sci.* **1997**, *134*, 165.
- [67] Barbosa, S.; Cheema, M. A.; Taboada, P.; Mosquera, V. *J. Phys. Chem. B* **2007**, *111*, 10920.
- [68] Hamley, I. W. *Phil. Trans. R. Soc. Lond. A* **2001**, *359*, 1017.
- [69] Jones, J. L.; McLeish, T. C. B. *Langmuir* **1995**, *11*, 785.
- [70] Kossuth, M. B.; Morse, D. C.; Bates, F. S. *J. Rheol.* **1999**, *43*, 167.
- [71] Chambon, F.; Winter, H. H. *J. Rheol.* **1987**, *31*, 683.
- [72] Richtering, H. W.; Gagnon, K. D.; Lenz, R. W.; Fuller, R. C.; Winter, H. H. *Macromolecules* **1992**, *25*, 2429.
- [73] Burchard, W.; Richtering, W. *Prog. Colloid Polym. Sci.* **1989**, *80*, 151.
- [74] Gast, A. P. *Langmuir* **1996**, *12*, 4060.
- [75] Hamley, I. W.; Daniel, C.; Mingvanish, W.; Mai, S.-M.; Booth, C.; Messe, L.; Ryan, A. J. *Langmuir* **2000**, *16*, 2508.
- [76] McConnell, G. A.; Gast, A. P.; Huang, J. S.; Smith, S. D. *Phys. Rev. Lett.* **1993**, *71*, 2102.
- [77] Perreur, C.; Habas, J.-P.; Francois, J.; Peyrelasse, J.; Lapp, A. *Phys. Rev. E* **2002**, *65*, 041802/1.

5 Flow induced ordering in cubic gels formed by P2VP-*b*-PEO-*b*-P(GME-*co*-EGE) triblock terpolymer micelles: A rheo-SANS study

Stefan Reinicke^a, Matthias Karg^b, Alain Lapp^c, Lutz Heymann^d, Thomas Hellweg^{e,f},
Holger Schmalz^{a,*}

a) Makromolekulare Chemie II, Universität Bayreuth, D-95440 Bayreuth, Germany

b) Bio21 Institute & School of Chemistry, University of Melbourne, 3010 Victoria, Australia

c) Laboratoire Léon Brillouin, CEA de Saclay, 99191 Gif sur Yvette, France

d) Technische Mechanik und Strömungsmechanik, Universität Bayreuth, D-95440 Bayreuth, Germany

e) Physikalische Chemie I, Universität Bayreuth, D-95440 Bayreuth, Germany

f) Physikalische und Biophysikalische Chemie, Fakultät für Chemie, Universität Bielefeld, D-33615 Bielefeld, Germany

ABSTRACT:

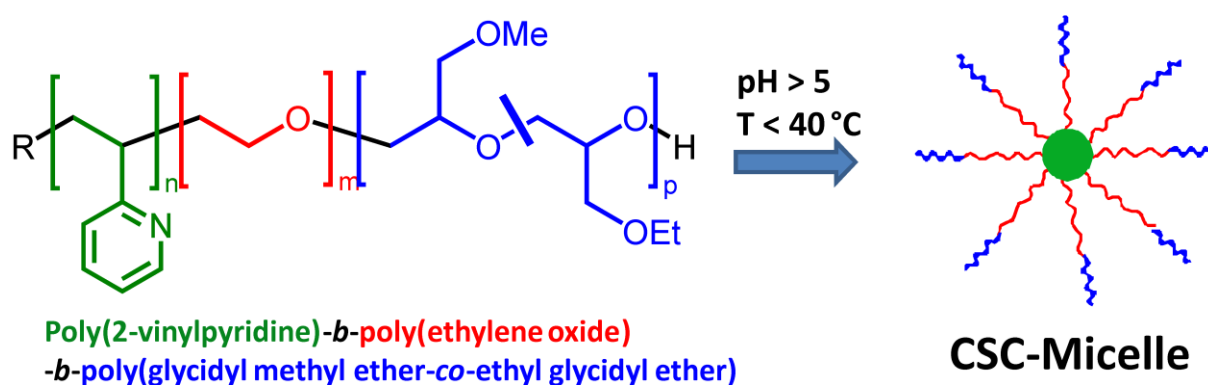
Small-angle neutron scattering (SANS) measurements under steady shear were performed to determine the exact nature and degree of structural order within a hydrogel based on poly(2-vinylpyridine)-*block*-poly(ethylene oxide)-*block*-poly(glycidyl methyl ether-*co*-ethyl glycidyl ether) (P2VP₅₆-*b*-PEO₄₁₀-*b*-P(GME₄₈-*co*-EGE₄₈)) triblock terpolymer micelles. Previous static SANS measurements indicated the presence of a simple cubic (sc) or body centered cubic (bcc) packing. By exposing the sample to steady shear, different macroscopic structural transitions were induced, indicated by a stress plateau and a significant change of the 2D SANS patterns. A comparison of these 2D patterns with patterns from analogous systems reported in literature and theoretical predictions revealed the presence of a bcc structure. Furthermore, with increasing shear rate the structural alignment changes from a non-oriented state to an intermediate state consisting of polycrystalline bcc domains with weak preferential orientation, and finally to a highly aligned state in which twinned bcc domains exist. The

[111] axis of the twinned bcc crystals is aligned in the direction of the shear flow, and the {110} slipping planes are preferentially aligned parallel to the shear plane (walls of the Couette cell). A minor fraction of twinned bcc domains, probably located in regions of lower shear velocity, i.e. close to the inner wall of the Couette cell (stator), is tilted by an angle of 90° with respect to the shear plane.

5.1 Introduction

“Smart” hydrogels, i.e. networks of water soluble polymers being sensitive to external stimuli like pH, temperature, light, or ionic strength, constitute a very active research field due to their versatility with respect to potential applications. “Smart” hydrogels can be utilized in biomedical applications like drug delivery and tissue engineering¹⁻⁶, but also in sensors, storage media, actuating systems, or microfluidic devices.⁷⁻¹¹ In recent years, new concepts of “smart” hydrogels were established, mostly dealing with ABA, ABC, (AB)_x, and ABCBA type block copolymers. Here, the different blocks combine water solubility with stimuli-responsive behavior, and as a result physical network junctions can be reversibly formed and destroyed upon changes of an external stimulus.¹²⁻¹⁸ Alternatively, chemically crosslinked hydrogels can swell or shrink, when different external parameters like temperature or pH are changed.¹⁹⁻²²

Recently, we developed a new approach towards double stimuli-sensitive hydrogels, i.e. responding to both pH and temperature.^{23,24} The physical hydrogels are based on ABC triblock terpolymers, which are composed of a water soluble poly(ethylene oxide) (PEO) middle block, a pH-sensitive poly(2-vinylpyridine) (P2VP) A block, and a thermo-sensitive poly(glycidyl methyl ether-*co*-ethyl glycidyl ether) P(GME-*co*-EGE) C block. At pH = 7, core-shell-corona (CSC) micelles with a P2VP core, a PEO shell, and a thermo-sensitive corona composed of the P(GME-*co*-EGE) block are formed (Scheme 5.1).



Scheme 5.1. Structure of the studied P2VP₅₆-*b*-PEO₄₁₀-*b*-P(GME₄₈-*co*-EGE₄₈) triblock terpolymer (subscripts denote the number average degree of polymerization of the corresponding block), and formation of core-shell-corona (CSC) micelles in water at pH = 7 and room temperature.

As an example, a P2VP₆₂-*b*-PEO₄₅₂-*b*-P(GME₃₆-*co*-EGE₃₆) triblock terpolymer (subscripts denote the number average degree of polymerization of the corresponding block) undergoes a gel-sol-gel transition upon heating at concentrations higher than 12 wt%.²³ The high temperature gel state is formed via an open association of the CSC micelles, since the thermo-sensitive micellar corona collapses above the cloud point of the P(GME-*co*-EGE) block and forms the network junctions. The low temperature gel phase on the other hand is based on a close packing of CSC micelles. The form factor of the CSC micelles was extracted from small-angle neutron scattering (SANS) on dilute solutions at pH = 7, and could be fitted with a spherical core-shell model including additional Gaussian chains accounting for the soft corona. In concentrated solutions, a pronounced structure factor with higher order reflections at the relative peak positions of 1 : 2^{1/2} : 3^{1/2} was observed, indicating an ordered cubic packing of the CSC micelles. Due to the absence of additional higher order reflections, a differentiation between a simple cubic (sc) or a body centered cubic (bcc) packing was not possible. However, the P2VP-*b*-PEO-*b*-P(GME-*co*-EGE) micelles have a relatively small P2VP core and a large, highly swollen PEO shell and P(GME-*co*-EGE) corona. Consequently, these micelles can be considered as “soft” spheres. In contrast to micelles with thin coronas (acting more or less like “hard” spheres), favoring a face centered cubic (fcc) structure,^{25,26} “soft” spheres preferentially form a body centered cubic (bcc) structure. A bcc packing was reported for micelles based on different PluronicsTM type copolymers,²⁷⁻²⁹ PEO endcapped with octadecyl groups at high concentration,³⁰ and polystyrene-*block*-polyisoprene/-polybutadiene (PS-*b*-PI/PS-*b*-PB) diblock copolymers³¹⁻³⁴. However, micelles acting as “soft” spheres often pack in a sc structure, too, as observed for poly(ethylene-*co*-

propylene)-*block*-polydimethylsiloxane (PEP-*b*-PDMS),³⁵ poly(ethylene-*co*-propylene)-*block*-polystyrene (PEP-*b*-PS),³⁶ and PS-*b*-PB diblock copolymers in selective solvents³⁷. Besides, systems were reported which can pack both in a fcc and a bcc structure, just depending on concentration and/or temperature. Such a behavior can be found for instance for a poly(ethylene oxide)-*block*-poly(butylene oxide) (PEO-*b*-PBO) diblock copolymer.³⁸ Additionally, Perreur et al. claimed that many differences in published interpretations of experimental data could be due to such fcc-bcc transitions.²⁷ Nevertheless, in most cases only one type of lattice is observed.

This work aims at the determination of the exact structure, i.e. sc or bcc, of a cubic gel formed by P2VP₅₆-*b*-PEO₄₁₀-*b*-P(GME₄₈-*co*-EGE₄₈) CSC micelles utilizing SANS measurements under steady shear, a frequently applied technique for studying block copolymer micellar gels.^{27,28,34,38-43} The analysis of diffraction patterns of a sample under flow allows for the assignment of the exact sample structure due to a macroscopic alignment of the polycrystalline domains. For this purpose, we prepared a sample with a concentration of 19 wt% (pH = 7) and performed SANS measurements at 20 °C during shear at various shear rates, as well as directly after cessation of the shear. The use of a Couette type shear cell geometry allowed us to record scattering patterns both in radial and tangential scattering geometry.

5.2 Experimental

Materials

The P2VP₅₆-*b*-PEO₄₁₀-*b*-P(GME₄₈-*co*-EGE₄₈) triblock terpolymer was synthesized via sequential anionic polymerization according to the procedure described elsewhere.^{23,24} The triblock terpolymer exhibits a very narrow molecular weight distribution (PDI = 1.02), as determined by size exclusion chromatography using THF as eluent (PS calibration). D₂O (99.9%, Deutero GmbH), DCl conc. (36 - 38% in D₂O, Deutero GmbH), and NaOD (40% in D₂O, Deutero GmbH) were used as received.

Sample preparation

8 g of triblock terpolymer were dissolved in 40 mL D₂O. The apparent pH was adjusted to a value of 3 - 4 using conc. DCl in order to protonate the P2VP block, rendering it hydrophilic. This ensures molecular dissolution of the polymer. The solution was then titrated slowly to pH_{app} = 7 (titer 1M NaOD, dosing rate 1.3 μL min⁻¹), causing the deprotonation of the P2VP block, and consequently the formation of CSC micelles with a hydrophobic P2VP core. The apparent hydrodynamic radius of the CSC micelles is 23 nm with a polydispersity index of 0.14, as revealed by dynamic light scattering (ALV DLS/SLS-SP 5022F compact goniometer system with an ALV 5000/E cross-correlator and a He-Ne laser at λ₀ = 632.8 nm, 1 g L⁻¹, θ = 90°). The titrations and pH-measurements were performed using a titrator (Titrand 809, Metrohm, Herisau, Switzerland), equipped with a titration unit (Dosino 800, Metrohm, Herisau, Switzerland) and a common glass membrane pH-electrode (micro electrode, Metrohm, Herisau, Switzerland).

Rheology

Rheological experiments were performed using a Modular Compact Rheometer MCR500 (Anton Paar GmbH, Germany). For the temperature sweep under oscillatory shear, a truncated coaxial cone-and-plate geometry with a diameter D = 25 mm, a cone angle β = 1 °, and a minimum truncation gap κ = 51 μm was employed. For the steady shear experiment, a coaxial cylinder system (Searle cell) having an outer radius R_a = 5.4235 mm, an inner radius R_i = 5.00 mm, and a gap length L = 15 mm was used. The lower end of the inner cylinder had a conical shape with an aperture of 120° in order to reduce end effects such as end face vortices at the end plane. Due to the small relative gap width (R_a - R_i)/R_i = 0.0847, the variation of the shear rate and shear stress in the gap can be assumed to be linearly dependent on the radial position, and independent of the material investigated. Hence, arithmetic mean values of shear rate and shear stress, calculated from the values at the inner and outer cylinder surface, could be used as representative values. The temperature was controlled with a precision of ± 0.1 °C using a TEZ150P-C Peltier thermal unit for the coaxial cylinder geometry, and a TEK150P-C Peltier thermal unit for the cone-and-plate geometry in combination with a fluid bath thermostat VT2 (Julabo, Germany) for cooling. To avoid evaporation effects and axial temperature gradients, the Peltier thermal units were equipped

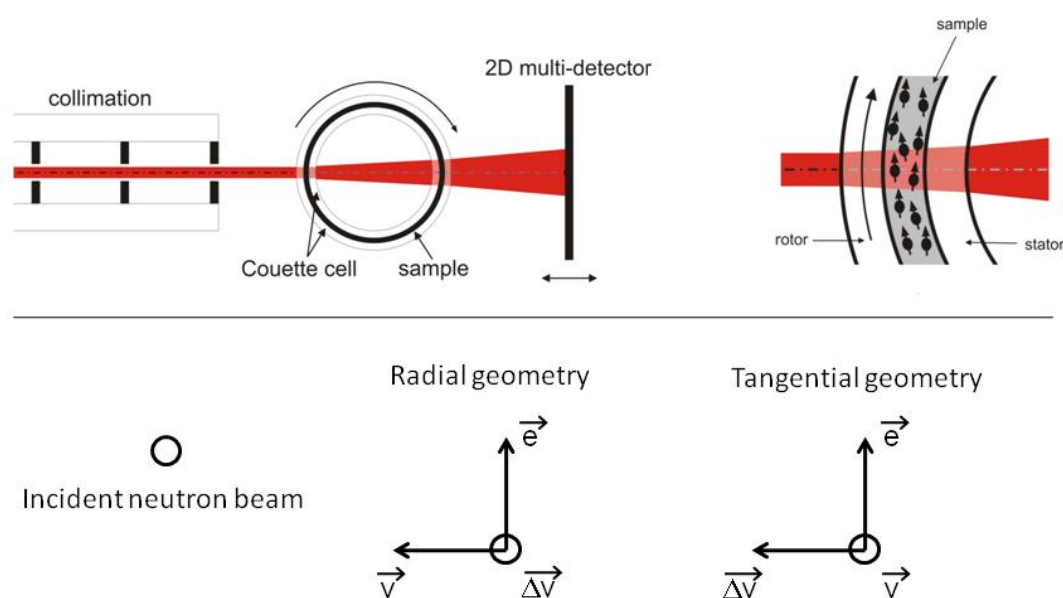
with an insulating heated hood. Prior to all measurements, a four-step test and calibration procedure for the rheometer were performed, including measurement of the torque of the air bearing, detection of the inertia of the rheometer motor and the rotating part of the measurement systems, a careful calibration of the Peltier thermal units using calibrated thermal sensors (Ahlborn, Germany), and finally an accurate calibration with two certified Newtonian calibration liquids having viscosities of approx. 10^2 mPa·s and 10^4 mPa·s, respectively, at 20 °C.

In order to be able to load the sample (about 1.02 mL for the coaxial cylinder and 0.1 mL for the cone-and-plate geometry) easily into the corresponding measuring cell, both the cell and the sample were preheated to 40 °C. At this temperature, the sample is in the fluid state with a rather low viscosity. The cone-and-plate geometry was filled by means of a graduated pipette (Eppendorf, Germany). After equilibration at 20 °C for approx. half an hour, respectively, the measurement was started.

For the temperature-dependent screening of the dynamic moduli, a frequency of 1 Hz, a strain of 1%, and a heating rate of 0.1 K s^{-1} were applied. Data points were recorded every 2 seconds. The steady shear sweep experiment was performed at a constant temperature of 20 °C. The flow curves were measured in CSR mode (shear rate controlled measurement) with shear rates $\dot{\gamma}$ given logarithmically in the range between 1 s^{-1} and 10^3 s^{-1} with 10 data points per decade. The measuring time per data point was set automatically by the rheometer software based on the accuracy of the raw data. The measurement time of one flow curve was about 480 s. All measurements were repeated twice using the same sample.

Small-angle neutron scattering (SANS)

The presented SANS investigations were performed using the PAXY instrument of the Laboratoire Léon Brillouin (LLB, Saclay, France). A neutron wavelength of $\lambda = 6 \text{ \AA}$ with a spread of $\Delta\lambda/\lambda = 10\%$ and a sample-to-detector distance of 6.798 m was selected, covering the q -range of interest. Spherical sample apertures of 5 mm (radial) and 3 mm (tangential) were used. All samples were prepared in pure D₂O providing a good scattering contrast. The temperature of the sample was controlled by a thermostat to $20 \pm 1 \text{ °C}$.



Scheme 5.2. Schematic depiction of the setup used for the rheo-SANS measurements, applying a Couette shear cell geometry: \vec{v} = velocity vector, $\overline{\Delta v}$ = shear gradient vector, and \vec{e} = vorticity vector.

The cell for rheological measurements as well as the scattering geometry is presented in Scheme 5.2. The custom made shear cell is built from quartz glass and consists of two cylindrical vessels (Couette cell type), an inner stator ($D = 45$ mm) and an outer rotator ($D = 47$ mm). The gap between the stator and rotator is ca. 1 mm. The shear cell could be moved along the direction perpendicular to the incident neutron beam. Hence, we were able to measure in radial (neutron beam perpendicular to the velocity vector \vec{v} , the shear direction) as well as in tangential scattering geometry (neutron beam parallel to the velocity vector). The outer rotator of the cell could be rotated at variable speed, inducing a changeable shear force. As a result, the slowest flow appears close to the inner wall, and the fastest close to the outer wall of the Couette cell.

Special care was taken while filling the shear cell. First, the inner stator was removed, and the sample was filled slowly in the rotator avoiding the formation of air bubbles. Then, the stator was slowly placed in its final position. First scattering profiles were taken without applying any shear. In case of anisotropic scattering patterns due to pre-shearing from the sample filling, the sample cell was heated to about 35 °C to reach the sol state²³, and subsequently

cooled down to room temperature again. After equilibration for approx. 1 hour, recorded scattering patterns were isotropic, revealing the absence of any long-range order. Intensity profiles were calculated by circularly averaging the corresponding 2D scattering patterns, including corrections accounting for electronic noise, detector efficiency, and empty cell scattering. Normalization of the data to an absolute scale has not been performed, since the data analysis did not require absolute intensity values. All performed treatments were done using software provided by the LLB. Further information on the data treatment procedure of the LLB can be found elsewhere.^{44,45} Analysis of the anisotropic scattering data was basically carried out using the 2D detector images. A self-written program was used to evaluate the azimuthal intensities at specific q-regions.

5.3 Results and Discussion

5.3.1 Rheological behavior under steady shear

Before discussing the results obtained from SANS measurements, we first address the rheological properties of a 19 wt% solution of P2VP₅₆-*b*-PEO₄₁₀-*b*-P(GME₄₈-*co*-EGE₄₈) at pH = 7. At this pH, the polymer chains are aggregated into core-shell-corona (CSC) micelles with a hydrophobic P2VP core (Scheme 5.1). As mentioned in the Introduction, these micelles can either pack regularly in a cubic lattice, or form an open association via reversible physical crosslinking at elevated temperatures caused by the thermo-sensitive corona. This behavior is demonstrated in Fig. 5.1A, showing the temperature-dependent dynamic moduli of the sample exposed to oscillatory shear. Regions, where G' exceeds G'' are defined as gel state, whereas regions with $G'' > G'$ are consistent with a fluid like behavior. Consequently, we observe a gel-sol-gel transition upon temperature increase. First, a cubic packing exists, which “melts” at about 30 °C. Upon a further increase in temperature, the thermo-sensitive P(GME-*co*-EGE) corona blocks become insoluble at ca. 40 °C and a micellar network is formed. The aim of this work is to clarify the structure of the low temperature gel phase by recording 2D SANS patterns under steady shear. Consequently, we studied the shear rate dependence of the steady shear stress and viscosity within the low temperature gel phase. This will give us the opportunity to discuss structural features and transitions observed by SANS in context with the rheological behavior of the gel. The results of the shear rate sweep are shown

in Fig. 5.1B. Basically, two different regimes can be identified with increasing shear rate. Both exhibit a power law behavior with different exponents. For shear rates $\leq 60 \text{ s}^{-1}$ we detect $\sigma \propto \dot{\gamma}^{0.06}$, i.e. the shear stress is almost independent of the shear rate, or in other words the shear stress reaches a plateau value. Consequently, the viscosity decreases strongly with increasing shear rate following a power law of $\eta \propto \dot{\gamma}^{-0.94}$. This behavior is typical for physical gels consisting of regularly packed micelles. As an example, for a 20 wt% solution of PEO₁₁₀ endcapped with octadecyl groups, viscosity follows a power law with an exponent of -0.83, which is even increasing at higher shear rates.³⁰ This strong shear thinning behavior, resembling qualitatively the behavior of strong shear thinning solids rather than the behavior of normal fluids,^{46,47} originates from a structural reorganization process.^{28,30,47,48} We will discuss this phenomenon in more detail within the following sections. For shear rates $> 60 \text{ s}^{-1}$ the stress plateau is left and the shear stress becomes shear rate dependent following a power law with an exponent of 0.56. In this regime structural reorganization is complete, and stress dissipation takes place through crystal layers slipping past each other.³⁹

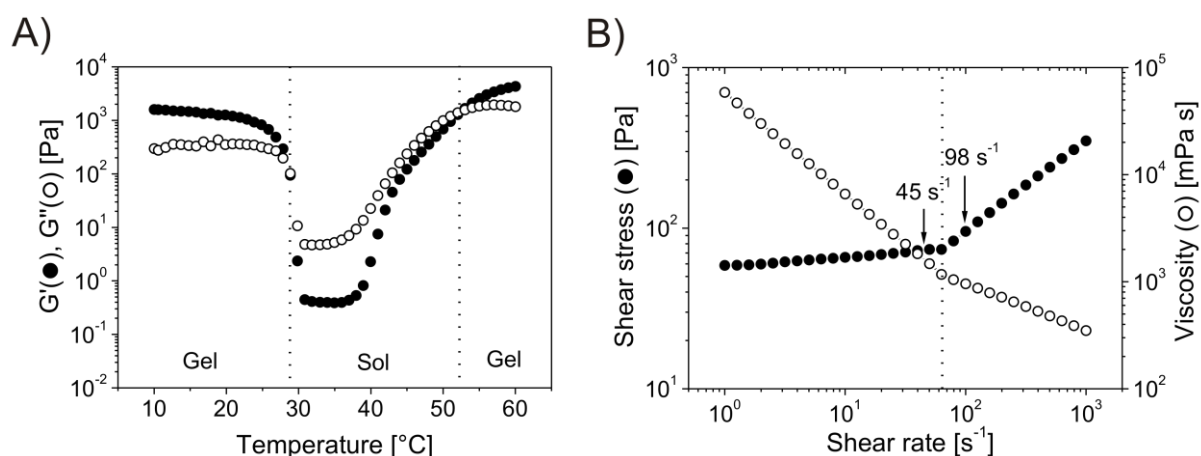


Figure 5.1. Rheological properties of a 19 wt% aqueous solution of P2VP₅₆-*b*-PEO₄₁₀-*b*-P(GME₄₈-*co*-EGE₄₈) at pH = 7: A) temperature-dependent G' and G'' (0.1 K s^{-1} , 1 Hz, 1% strain), B) Shear stress and shear viscosity as a function of shear rate at $20 \text{ }^\circ\text{C}$.

Unfortunately, we were not able to detect the onset of the observed stress plateau, due to limitations with respect to the minimum accessible shear rate for the used cylindrical shear cell geometry. Thus, the existence of a yield stress, which is expected for close packed micellar mesophases,^{29,39,47-49} could not be verified with this set-up. To address the question whether a yield stress exists for our system, we have switched to a cone-and-plate shear cell geometry, extending the measurement range to lower shear rates. The corresponding flow

curve is shown in Fig. 5.9 (Supporting Information), indicating a yield stress of about 10 Pa, and an onset of the stress plateau at a shear rate of 0.1 s^{-1} . However, in order to keep the comparability with the SANS experiments, which were performed using a Couette-type shear cell, the results obtained with the cylindrical shear cell geometry will be used for further discussion.

5.3.2 Small-angle neutron scattering of a non-sheared sample

A crucial aspect of SANS experiments on concentrated micellar solutions is the effect of pre-shearing due to the filling of the sample cell. In our case, the 2D SANS image recorded right after filling the Couette cell at $20 \text{ }^\circ\text{C}$ shows a strong anisotropic character (Fig. 5.2A). In the corresponding radially averaged intensity profile (Fig. 5.2B), two well-defined higher order reflections can be detected, indicating a highly ordered state. The features of this SANS profile will be discussed later on in more detail. As shown in the rheology section, the investigated sample undergoes a gel-sol transition at approximately $30 \text{ }^\circ\text{C}$. As a result, the higher order reflections, found right after filling the Couette cell, vanish if the sample is heated to $35 \text{ }^\circ\text{C}$ (Fig. 5.2B). Additionally, the position of the structure factor maximum (q_{max}) shifts towards higher values of q , and a broadening of the structure peak is observed. The shift of q_{max} to higher q values indicates a smaller center-to-center distance of the micelles. Thus, we can conclude that the temperature induced disintegration of the close micellar packing is caused by a shrinkage of the micelles, in accordance to our previous assumption.²³ This is consistent with the macroscopically observed gel-sol transition. If the sample is again cooled down to $20 \text{ }^\circ\text{C}$ and equilibrated for 1 hour, q_{max} is shifted towards smaller values of q almost reaching its initial value directly after filling the cell. However, the structure peak at q_{max} is still broadened and no higher order reflections are visible. Only a plateau remains, originating from the form factor of the micelles.²³ Furthermore, the 2D scattering pattern has a purely isotropic character (not shown here). Consequently, the long-range order induced by the sample filling procedure is lost throughout the heating-cooling cycle. Therefore, every sample being under investigation in the following was subjected to a heating-cooling cycle prior to the measurements in order to eliminate any pre-shearing effects.

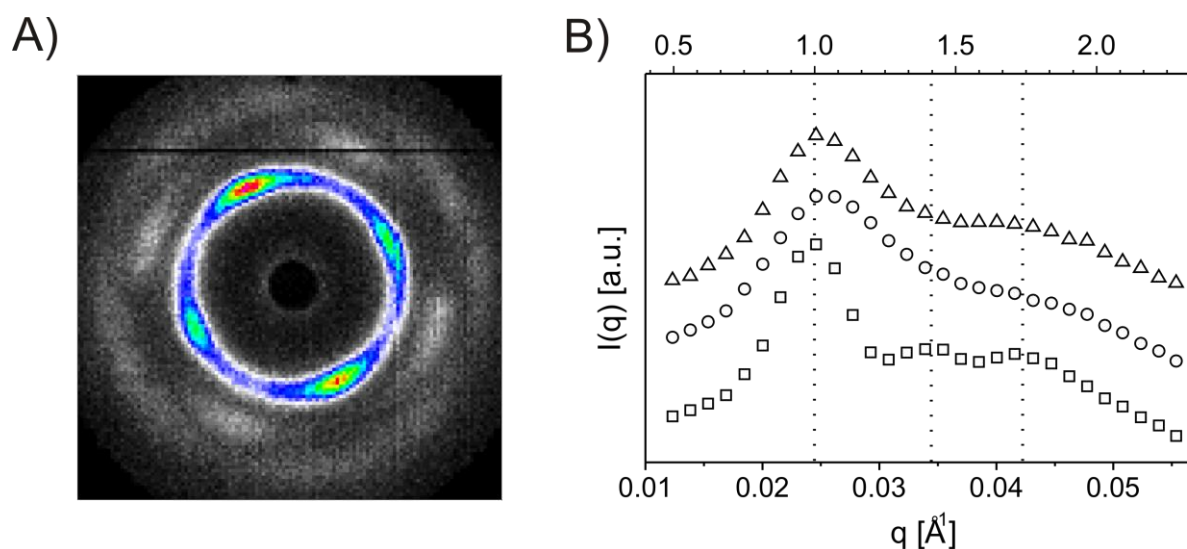


Figure 5.2. A) 2D SANS pattern of a 19 wt% solution of P2VP₅₆-*b*-PEO₄₁₀-*b*-P(GME₄₈-*co*-EGE₄₈) at pH = 7 and T = 20 °C for radial scattering geometry, directly after filling the Couette cell. B) Radially averaged static SANS profiles ($\dot{\gamma} = 0$), immediately after loading the Couette cell (squares), at 35 °C (circles), and after cooling from 35 °C to 20 °C (triangles). The dashed vertical lines indicate the peak positions, which are in agreement with sc or bcc lattices.

Nevertheless, the SANS pattern obtained at 20 °C right after filling the Couette cell provides first information on the structure of the gel, and can also be used for a comparison to our SANS results obtained for a P2VP-*b*-PEO-*b*-P(GME-*co*-EGE) triblock terpolymer exhibiting slightly different block lengths.²³ Compared to our previous findings, the position of the first order structure peak (q_{\max}) is almost preserved and the same higher order reflections are visible, indicating that the type of crystal lattice is not altered and the lattice spacing is not considerably changed. The relative peak positions of the higher order reflections of $1 : 2^{1/2} : 3^{1/2}$ are consistent with a body centered cubic (bcc) or a simple cubic (sc) packing, but not with a fcc structure, where reflections should be located at relative peak positions of $1 : 4/3^{1/2} : 8/3^{1/2} : 11/3^{1/2}$.⁵⁰ Our results are consistent with the general prediction, that fcc lattices are unfavorable for micelles acting as “soft” spheres. For these systems the formation of bcc structures is frequently observed,²⁵⁻³⁴ however, from our data the presence of a sc lattice cannot be excluded so far.

5.3.3 Small-angle neutron scattering under steady shear

Fig. 5.3A shows 2D scattering patterns recorded at different shear rates for radial scattering geometry (Scheme 5.2). Starting with the lowest shear rate of 2 s^{-1} , a continuous Bragg ring with strong reinforcements in the meridional position and weaker ones on the equatorial axis, as well as four relative diffuse, ellipsoidal reflexes at higher q values are visible. This indicates a polycrystalline structure with a weak preferential orientation of the crystal domains. Upon increasing the shear rate, the described pattern first becomes more defined but then more diffuse again. Finally, at a rate of 98 s^{-1} the pattern is fully isotropic. Therefore, at a first glance it seems, that a weak order is induced upon exposing the sample to low shear rates. This order subsequently disappears again, when the shear rate exceeds a certain value. The same trend is observed following the azimuthal evolution of the scattering intensity along the first Bragg ring, i.e. at a fixed value of $q = 0.24 \text{ \AA}^{-1}$ (Fig. 5.3B).

In contrast, a completely different picture evolves, when scattering patterns are recorded right after the shear was stopped. At low shear rates ($< 18 \text{ s}^{-1}$), the low degree of ordering vanishes after cessation of the shear (not shown here). At higher shear rates ($\geq 18 \text{ s}^{-1}$), the anisotropy is preserved and becomes even more pronounced (Fig. 5.4). This is consistent with the common observation that the alignment process becomes irreversible upon exceeding a critical shear rate.^{27,28,41} Finally, the fully isotropic pattern, obtained during shear at high rates (98 s^{-1}), develops into a strong anisotropic pattern with sharp Bragg spots after cessation of the shear (Figs. 5.4C,D). However, the Bragg spots in Figs. 5.4B and 5.4C are rather grainy with weakly defined positions, indicating a rather ill-defined alignment. This is due to the fact, that the shearing process during the shear rate screening was interrupted several times in order to record scattering patterns from the quiescent state for each applied shear rate. A really defined pattern, represented in Fig. 5.4D, is only obtained when the sample is sheared continuously without any interruption for several hours.

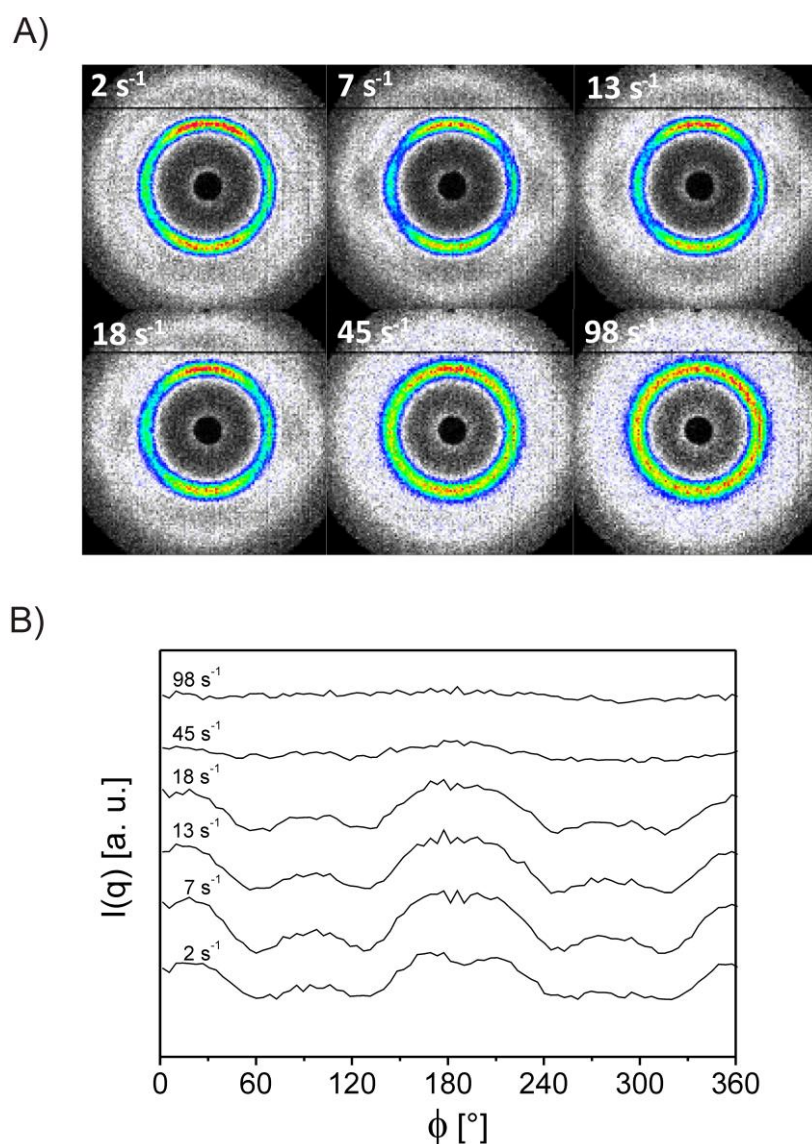


Figure 5.3. A) 2D SANS patterns of a 19 wt% solution of P2VP₅₆-*b*-PEO₄₁₀-*b*-P(GME₄₈-*co*-EGE₄₈) at pH = 7 and T = 20 °C for radial scattering geometry, obtained during shear at different shear rates. B) Azimuthal scattering intensities along the first Bragg ring (clockwise, starting from the southern meridian) calculated from the 2D SANS patterns shown in A).

The fact, that the structural order is generally less pronounced during shearing, is most probably related to the soft character of the studied CSC micelles.²³ The relatively large, soft shell might be easily deformed by mechanical stress. As a consequence, the number of defects in the crystal domains increases, which affects the degree of long-range structural order under shear. Watanabe et al. observed a similar behavior for a 15 wt% solution of a PS₁₀₆-*b*-PB₄₂₆ diblock copolymer in *n*-tetradecane. When shear was switched off, the obtained patterns became more defined as well.⁴⁹ However, regarding hydrogels based on a close cubic packing

of micelles, scattering patterns presented in literature are mostly obtained under steady shear, and a shear-induced disordering at moderate shear rates has not been reported so far. In one particular contribution, dealing with a PEO₇₆-*b*-PPO₂₉-*b*-PEO₇₆ (PluronicTM F68) solution, the authors note that small-angle X-ray scattering (SAXS) patterns at any given shear rate and after cessation of shear are identical.²⁸ Despite, there are reports on shear-induced disordering in block copolymer melts or highly concentrated block copolymer solutions at temperatures close to the order-disorder transition (ODT).⁵¹⁻⁵⁴ Interestingly, after cessation of shear the shear-induced disorder vanished again. For a highly oriented twinned bcc structure a complete destruction of the ordered melt phase was observed at intermediate shear rates, however, after cessation of shear the initial twinned bcc structure was recovered completely.⁵³ This is quite similar to our observations. The apparent disordering during steady shear was explained by an increasing number of defects being introduced above a certain shear rate. When the defects are generated faster than they can move or be annihilated by slipping, the translational order between crystal layers is lost resulting in the observed isotropic scattering pattern. However, the orientational order is retained, i.e. after cessation of shear the layers can easily restack and reestablish the crystalline order.

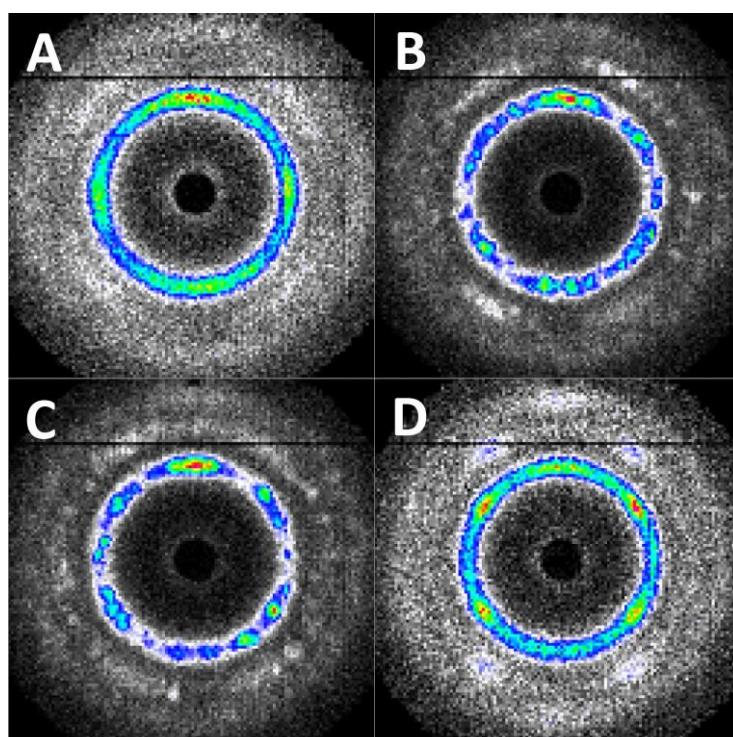


Figure 5.4. 2D SANS patterns of a 19 wt% solution of P2VP₅₆-*b*-PEO₄₁₀-*b*-P(GME₄₈-*co*-EGE₄₈) at pH = 7 and T = 20 °C for radial scattering geometry, obtained after cessation of shear at A) 18 s⁻¹, B) 45 s⁻¹, C) 98 s⁻¹, and D) 98 s⁻¹ with a long period of pre-shearing (several hours).

The deformability of a micelle should strongly depend on the absolute size of the micellar shell, expressed by the overall average degree of polymerization (DP_{shell}), and its relative size with respect to that of the core forming block, expressed by the $DP_{\text{shell}}:DP_{\text{core}}$ ratio. The higher both values, the easier the shear-induced deformation of the micelles should take place. It appears, that in most reports on micellar hydrogels either the relative shell size or the absolute size is lower compared to our system ($DP_{\text{PEO-}b\text{-P(GME-co-EGE)}}:DP_{\text{P2VP}} = 9:1$; $DP_{\text{PEO-}b\text{-P(GME-co-EGE)}} = 506$). Consequently, the shear-induced disordering observed for P2VP-*b*-PEO-*b*-P(GME-*co*-EGE) based hydrogels for shear rates $> 18 \text{ s}^{-1}$ is most probably attributed to defects induced by a significant deformation of the micellar shell, which results in a decrease of the translational order between the crystal layers.

The deformation of the CSC micelles can be verified by comparing the positions of the structure factor maximum in the radially averaged intensity profiles obtained under shear and after cessation of shear, respectively (Fig. 5.5). Under shear, the peak maximum is located at slightly lower q values compared to the sample, which was not subjected to shear before. This phenomenon can only be explained by a deformation of the spherical micelles, causing a change in the average center-to-center distance, as expressed by the shift of the peak maximum. Additionally, the structure factor peak is slightly broadened, which is consistent with an overall less defined arrangement of the micelles. An analogous behavior was described by Stellbrink et al. for a poly(ethylene-*co*-propylene)-*block*-poly(ethylene oxide) (PEP₁₅-*b*-PEO₄₉₇) diblock copolymer.⁴⁶ After cessation of shear, q_{max} is shifted back to the initial position, indicating that this process is reversible, i.e. the original spherical shape of the micelles is recovered (Fig. 5.5). The reversibility can be understood, if we keep in mind that the core of the micelles is composed of fully collapsed, glassy poly(2-vinylpyridine), which is more or less unaffected by moderate mechanical stress, and therefore forces the micellar shell back to its original shape after cessation of shear.

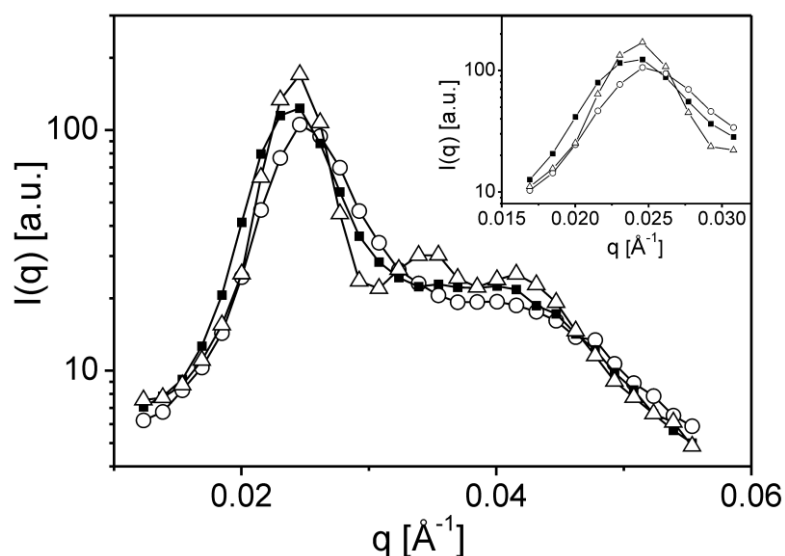


Figure 5.5. Radially averaged SANS profiles for a 19 wt% solution of P2VP₅₆-*b*-PEO₄₁₀-*b*-P(GME₄₈-*co*-EGE₄₈) at pH = 7 and T = 20 °C before (circles), during (squares), and after (triangles) exposure to a shear rate of 98 s⁻¹. The inset shows an enlargement of the *q*-range corresponding to the first order structure peak.

Some first conclusions can be drawn from the results obtained so far. Upon increasing the shear rate, a structural reorganization from a fully polycrystalline to a polycrystalline structure with a weak preferential orientation takes place, becoming irreversible at shear rates ≥ 18 s⁻¹. At even higher shear rates (> 45 s⁻¹), a second transition to a more defined structural alignment occurs. When patterns are recorded under steady shear, structural reorganization is overlapped by a reversible deformation of the micelles, decreasing the degree of long-range structural order. It is noted, that the initial SANS results can nicely be related to the findings from rheological measurements. All shear rates at which 2D patterns were recorded, except the highest one, are located in the region where the stress plateau was observed (Fig. 5.1B). Therefore, this stress plateau is clearly correlated with structural reorganization processes. The highest shear rate applied (98 s⁻¹) is already located outside the stress plateau, which indicates that the reorganization process is more or less completed at that point. In the corresponding scattering pattern (Fig. 5.4D), relatively sharp Bragg spots are observed, which is typical for a defined long-range structural alignment. However, a full alignment of the whole sample is not achieved even at 98 s⁻¹, as evidenced by the superposition of the Bragg spots with a continuous Bragg ring. This might indicate the existence of some remaining non-oriented polycrystalline domains. In radial scattering geometry, the incident neutron beam is parallel to the shear gradient vector $\vec{\Delta v}$, and therefore passes all different states of orientation (Scheme 5.2). It is obvious, that different states of alignment might occur along this shear

gradient axis, due to the fact that the flow next to the outer wall of the cell (rotator) is relatively fast, whereas the crystal domains next to the inner wall (stator) are almost at rest. Nevertheless, the abrupt change of the power law exponents for the shear rate dependent shear stress and viscosity at around 60 s^{-1} indicates, that stress dissipation is not longer dominated by structural reorganization but rather by slipping of crystal layers, i.e. the sample is almost fully aligned.

In the last section, the 2D SANS patterns are analyzed in more detail in order to derive information about the exact crystal lattice and macroscopic alignment of the hydrogel. The main feature of the pattern observed after shearing at a shear rate of 18 s^{-1} (Fig. 5.4A) is the existence of a continuous inner Bragg ring with significantly reinforced scattering at the meridional positions, and weaker scattering at the equatorial positions. As already mentioned, the continuous Bragg ring points to the presence of a non-oriented, polycrystalline texture. However, the higher scattering intensity at the meridional positions of the inner Bragg ring indicates a weak preferential orientation of the domains. In agreement with the results of Hamley et al.,^{40,41} the observed pattern corresponds to a bcc structure, with the pair of meridional reflections originating from $\{110\}$ planes oriented perpendicular to the \vec{v} , \vec{e} -shear plane. The polydomain nature of the structure is further verified by the fact, that weak equatorial $\{110\}$ reflections exist as well. Since no monodomain bcc structure leading to such a pattern exists, it must represent differently oriented domains. The diffuse Bragg spots on the second ring, i.e. corresponding to the $\{200\}$ reflections, enclose an angle of 45° with the meridional $\{110\}$ reflections. Hence, they originate from the same oriented bcc domain.

We now turn to the scattering pattern obtained after shearing at a rate of 98 s^{-1} . Easiest stress dissipation in the case of fully aligned domains is accomplished by layer-by-layer slipping of specific planes, oriented parallel to the shear plane, and with the most closely packed direction being aligned along the shear direction.⁵⁵ In bcc crystal lattices the $[111]$ direction is the most densely packed one, and the energetically most favored slipping plane is the $\{110\}$ plane. Alternative slipping planes are the $\{211\}$ and $\{321\}$ planes, although they are energetically less favored. Eiser et al. investigated a 46 wt% solution of PEO₇₆-*b*-PPO₂₉-*b*-PEO₇₆ (SynperonicTM F68),²⁸ observing a scattering pattern strongly resembling the pattern obtained in our study after cessation of shear at 98 s^{-1} (Fig. 5.6A). By increasing the shear rate to a very high value of 365 s^{-1} , however, the meridional reflections on the first Bragg ring

vanished. This phenomenon went along with a second stress plateau, indicating a second structural reorganization process. The remaining spots, marked in red in the theoretical scattering pattern (Fig. 5.6B), were assigned to a fully oriented twinned bcc monodomain, with the [111] direction being oriented parallel to the flow direction and the energetically most favored {110} planes being exclusively stacked parallel to the shear plane, as predicted. It is noted, that we do not observe the reflections on the third ring located around the equator. This is probably due to a poor contrast as a consequence of the relatively low neutron flux in the present experiments. By recording scattering patterns in tangential scattering geometry, Eiser et al. could conclude that the additional meridional spots on the first Bragg ring observed at intermediate shear rates (which we also observe) originated from twinned bcc monodomains as well, but tilted by an angle of 90° around the velocity axis. In consequence, these domains were oriented with their {211} planes parallel and their {110} planes perpendicular to the shear plane. It was shown, that the differently oriented domains were separated from each other along the shear gradient axis $\overline{\Delta v}$. Close to the outer cell wall (rotator), where the shear velocity was the highest, domains with the densely packed {110} slipping planes oriented parallel to the Couette walls were formed, since these planes provide easiest stress dissipation. On the other hand, domains with the {211} slipping planes being oriented parallel to the Couette walls, which is energetically less favored, consequently were located more or less in the middle of the cell gap where the shear velocity was lower. A similar dependence of the orientation of twinned bcc crystals on the applied shear was found by Mortensen for organogels based on polystyrene-*block*-poly(ethylene-*co*-butylene)-*block*-polystyrene (PS-*b*-PEB-*b*-PS) triblock copolymers.⁵⁶ Since the neutron beam we used was wider than the gap of the measuring cell, we were not able to verify the separation of the different orientations along the shear gradient axis by performing measurements in tangential geometry in our case. However, we should at least observe a superposition of the patterns of the two different orientations analogous to the measurements in radial geometry.

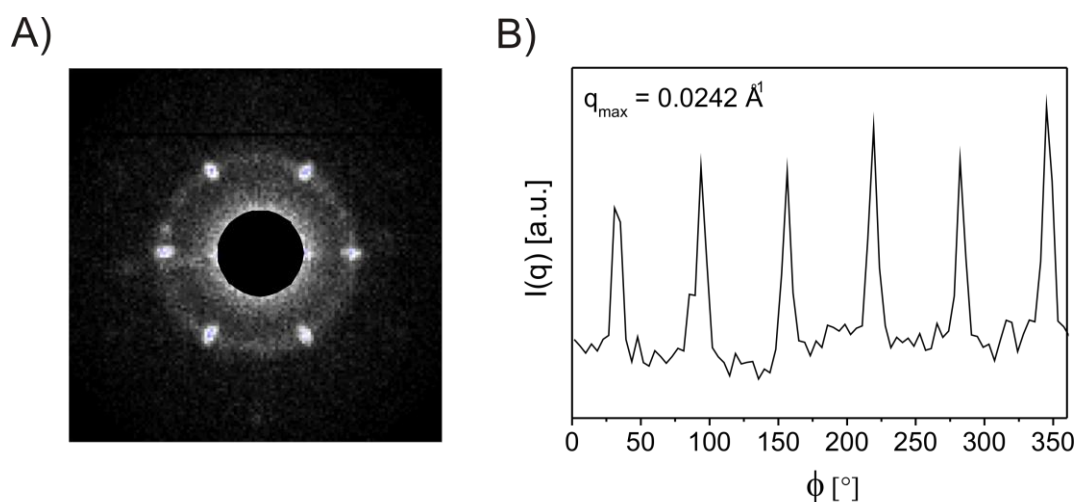


Figure 5.7. A) 2D SANS pattern of a 19 wt% solution of P2VP₅₆-*b*-PEO₄₁₀-*b*-P(GME₄₈-*co*-EGE₄₈) at pH = 7 and T = 20 °C for tangential scattering geometry, obtained after cessation of shear at 98 s⁻¹ with a long period of pre-shearing. B) Corresponding plot of the scattering intensity of the Bragg spots on the first Bragg ring as a function of the azimuthal angle (clockwise, starting from the southern meridian).

Consequently, the scattering pattern in Fig. 5.6A can be explained in a satisfying way by considering the presence of twinned bcc monodomains with two different preferred orientations. Nevertheless, the scattering pattern might also be explained without considering the presence of a twinned structure. In order to orient the favored {110} slipping planes parallel to the shear plane, the domains can be rotated around the [111] direction by two different angles. The resulting pattern, which consequently is a superposition of two single patterns, is identical with the one observed for the corresponding twinned structure (red spots in Fig. 5.6B).^{41,57} The black spots in Fig. 5.6B represent the theoretical pattern, which arises when the domains are rotated around the [111] direction by all eight possible angles, i.e. any angle for which one of the three energetically favored slipping planes ({110}, {211}, {321}) are oriented parallel to the shear plane.^{27,41,57} The pattern in Fig. 5.6A does not match exactly with this theoretical pattern, since the {211} reflections next to the meridian are missing. However, neither Perreux et al. nor Eiser et al. were able to detect the {211} reflection near the meridian, which indicates that it is rather unfavorable for the domains to orient with the {321} planes parallel to the shear plane.^{27,28} This is reasonable, since the {321} planes are the energetically least favored slipping planes.

What we can conclude so far is that the position of the Bragg spots in Fig. 5.6A at least fully corresponds to a bcc structure with the [111] direction oriented parallel to the flow direction.

An additional procedure of proving the nature of the network and its preferred orientation direction is also given by Perreur et al.²⁷ The indices $\{hkl\}$ of the spots on the pattern all follow the relation $uh + vk + wl = n$. Spots with the same order n lie on the same vertical axis in the 2D pattern. All axes are equidistant to each other, separated by a gap Δ . If we deal with bcc crystals oriented around the $[111]$ direction, the radius of the first Bragg ring in the SANS pattern (r_1), divided by Δ should give a value of 1.22. In our case, we determine a value of 1.21, which is in good agreement with the theoretical prediction.

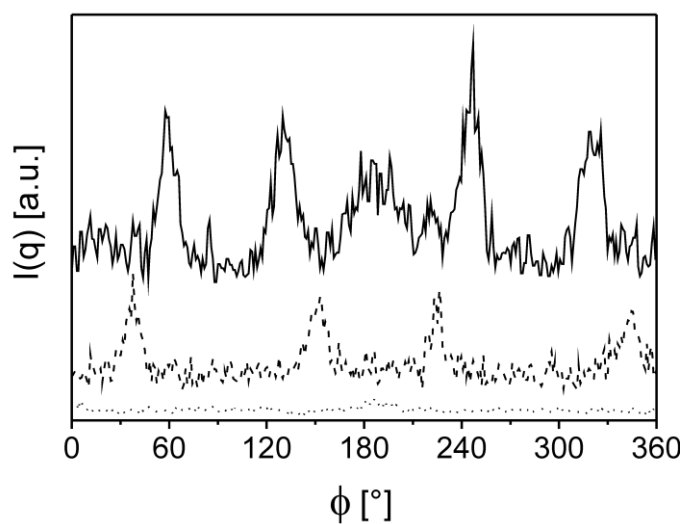


Figure 5.8. Intensity of reflections located on different rings of constant q values as a function of the azimuthal angle (clockwise, starting from the southern meridian) calculated from Fig 6A: $q_{\max,1} = 0.0244 \text{ \AA}^{-1}$ (solid), $q_{\max,2} = 0.0348 \text{ \AA}^{-1}$ (dashed), and $q_{\max,3} = 0.0416 \text{ \AA}^{-1}$ (dotted).

We now still have to address the question whether we deal with a twinned bcc structure or not. The distribution of the Bragg spots in the radial scattering pattern of the shear oriented sample (Fig. 5.6A) can be fully explained by both scenarios (see discussion above). However, a twinned structure would require equal intensities of all Bragg spots appearing on the first ring in the pattern, except for the meridional ones. When having a look at the scattering intensity of the Bragg spots on the first ring as a function of the azimuthal angle Φ , this requirement seems to be fulfilled for radial geometry in good approximation, though the general signal-to-noise ratio is relatively low (Fig. 5.8). A similar behavior is observed for the tangential scattering geometry. A closer look to the intensity of the Bragg spots (Fig. 5.7B) implies the existence of two sets of intensities, as only spots separated by an angle of 120° exhibit the same intensity. This in turn would be contradictory to a twinned bcc structure. However, within the accuracy of the experiment, the intensities of the different Bragg spots

are identical. In conclusion, the shear oriented sample (shear rate 98 s^{-1}) most likely exhibits an almost fully aligned twinned bcc structure with the $\{110\}$ planes oriented parallel to the shear plane. Nevertheless, the presence of non-twinned bcc domains exhibiting different orientations with respect to the $[111]$ axis cannot completely be ruled out.

Finally, we still need to discuss the patterns obtained at shear rates of 45 and 98 s^{-1} after a stepwise increase of the shear rate, i.e. in this case the sample was not continuously pre-sheared at a given shear rate prior to the measurement (Figs. 5.4B,C). Both patterns exhibit an irregular distribution of the Bragg spots. It is obvious, that the $[111]$ axis of the bcc domains in these cases is not fully aligned in direction of the shear. A small tilt of the $[111]$ axis of some of the domains causes a shift of the angle for which the Bragg relation is fulfilled. However, we observe irregularly distributed Bragg spots and not continuous banana-like patterns of high intensity, as observed in Fig. 5.4A. This indicates, that in contrast to a polydomain structure, the fraction of domains exhibiting a defined orientation of the $[111]$ axis with respect to the shear direction is comparatively large.

5.4 Conclusion

A 19 wt% aqueous solution of P2VP₅₆-*b*-PEO₄₁₀-*b*-P(GME₄₈-*co*-EGE₄₈), forming a free-standing gel at pH = 7 and room temperature, was exposed to steady shear in order to induce a macroscopic alignment of the crystal domains, enabling the assignment of the exact structure of the micellar packing by SANS. Higher order reflections at relative peak positions of $1 : 2^{1/2} : 3^{1/2}$ in the radially averaged SANS intensity profile of a pre-sheared sample indicated the presence of either a simple cubic (sc), or body centered cubic (bcc) lattice.

Upon exposure to steady shear, the sample exhibited a stress plateau at shear rates below 60 s^{-1} , i.e. a strong shear thinning behavior was found. Small-angle neutron scattering experiments at different shear rates revealed, that the existence of this plateau is due to two different structural transitions. First, a transition from a fully non-oriented polydomain to a polydomain with weak preferential orientation occurred at intermediate shear rates. Subsequently, at the end of the stress plateau a macroscopic alignment was observed, where flow is provided by different crystal layers slipping past each other. The latter highly aligned structure was identified as a twinned bcc lattice, with a major fraction of the crystal domains

oriented with the [111] direction in shear direction, and the {110} slipping planes parallel to the shear plane. A small fraction, most probably located close to the inner wall (stator) of the Couette cell, was oriented with the {211} planes parallel to the shear plane. This is consistent with literature data, showing that the perpendicular alignment is preferentially formed for moderate shear rates. It is noted, that at the highest applied shear rate of 98 s^{-1} still non-oriented polydomains are detectable, indicating that the alignment is incomplete. This is due to the velocity gradient along the gap of the used Couette shear cell. A fully oriented sample might be achievable at very high shear rates, which were not accessible in our case.

Finally, we observed that the structural transitions induced by shear are irreversible for shear rates higher than 18 s^{-1} . Furthermore, the shape of the micelles is distorted during shear due to their relatively large and soft shell, which lowers the degree of structural order. This results in an apparent shear-induced disordering at moderate shear rates, as the corresponding 2D scattering pattern became isotropic under shear. However, upon cessation of shear a highly anisotropic pattern evolved, indicating that the shear-induced distortion of the micellar shell is fully reversible.

Acknowledgements

The authors acknowledge the German Science Foundation (priority program SPP 1259) for financial support. M. K. is grateful to the Alexander von Humboldt foundation for a Feodor-Lynen research fellowship. The SANS experiments were partially supported by the European Union within the framework of the NMI3 program.

5.5 Supporting Information

The flow curve (Fig. 5.9) was obtained using an ARES-G2 (TA Instruments, USA) equipped with an Advanced Peltier System (APS). For the measurements a cone-and-plate shear cell geometry (diameter $D = 40$ mm, cone angle $\beta = 1^\circ$) was used to assure a homogeneous shear field. The flow curve was measured in the stress controlled mode, i.e. a logarithmically increasing shear stress σ was applied to the sample, and the corresponding shear rate was measured. The measuring time per data point was set to 30 s. The sample filling procedure was identical to that described in the *Experimental Part* of the manuscript. Repeated measurements showed the reproducibility of the results.

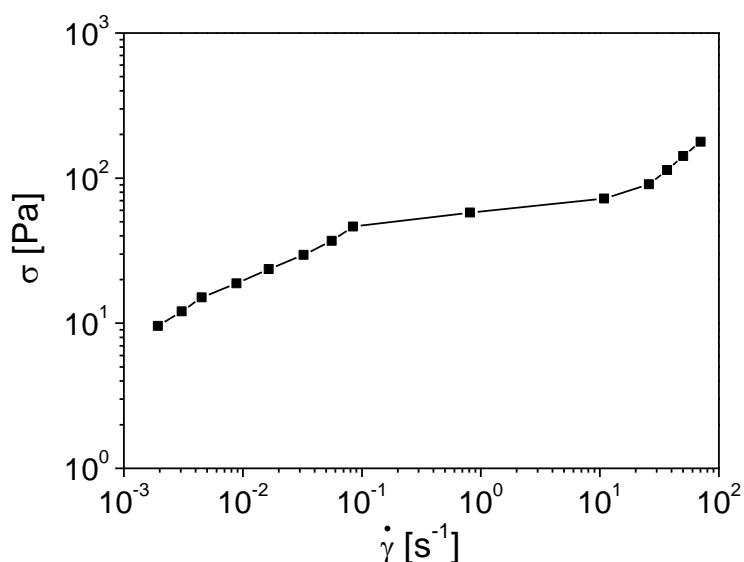


Figure 5.9. Flow curve of a 19 wt% aqueous solution of P2VP₅₆-*b*-PEO₄₁₀-*b*-P(GME₄₈-*co*-EGE₄₈) at pH = 7 and $T = 20$ °C, obtained by using a cone-and-plate shear cell geometry.

From the flow curve a yield stress of about 10 Pa can be deduced within the limit of accuracy of the measurement. For low shear rates, the shear stress follows a power-law dependence with an exponent of 0.40, until a stress plateau develops at about 0.1 s^{-1} . This is consistent with the observed stress plateau, using a cylindrical shear cell geometry (Fig. 5.1, manuscript). For increasing shear rate, the stress plateau is left at about 25 s^{-1} , i.e. at a slightly lower shear rate compared to the measurements with a cylindrical shear cell geometry (60 s^{-1}). This can be attributed to the different geometries of the used shear cells, and thus different characteristics of the acting shear fields.

5.6 References

- [1] Tachibana, Y.; Kurisawa, M.; Uyama, H.; Kakuchi, T.; Kobayashi, S. *Chem. Lett.* **2003**, 32, 374.
- [2] Hart, D. S.; Gehrke, S. H. *J. Pharm. Sci.* **2007**, 96, 484.
- [3] Yu, L.; Ding, J. *Chem. Soc. Rev.* **2008**, 37, 1473.
- [4] Ahn, S.-k.; Kasi, R. M.; Kim, S.-C.; Sharma, N.; Zhou, Y. *Soft Matter* **2008**, 4, 1151.
- [5] He, C.; Kim, S. W.; Lee, D. S. *J. Controlled Release* **2008**, 127, 189.
- [6] Klouda, L.; Mikos, A. G. *Eur. J. Pharm. Biopharm.* **2008**, 68, 34.
- [7] Beebe, D. J.; Moore, J. S.; Bauer, J. M.; Yu, Q.; Liu, R. H.; Devadoss, C.; Jo, B.-H. *Nature* **2000**, 404, 588.
- [8] Calvert, P.; Patra, P.; Duggal, D. *Proc. SPIE-Int. Soc. Opt. Eng.* **2007**, 6524, 65240M/1–65240M/6.
- [9] Guenther, M.; Kuckling, D.; Corten, C.; Gerlach, G.; Sorber, J.; Suchaneck, G.; Arndt, K. F. *Sens. Actuators, B* **2007**, 126, 97.
- [10] Dai, S.; Ravi, P.; Tam, K. C. *Soft Matter* **2008**, 4, 435.
- [11] Jindrich, K. *J. Polym. Sci., Part A: Polym. Chem.* **2009**, 47, 5929.
- [12] Lin, H.-H.; Cheng, Y.-L. *Macromolecules* **2001**, 34, 3710.
- [13] Fechler, N.; Badi, N.; Schade, K.; Pfeifer, S.; Lutz, J.-F. *Macromolecules* **2008**, 42, 33.
- [14] Bae, S. J.; Joo, M. K.; Jeong, Y.; Kim, S. W.; Lee, W.-K.; Sohn, Y. S.; Jeong, B. *Macromolecules* **2006**, 39, 4873.
- [15] Shinji, S.; Shokyoku, K.; Sadahito, A. *J. Polym. Sci., Part A: Polym. Chem.* **2004**, 42, 2601.
- [16] Iddon, P. D.; Armes, S. P. *Eur. Polym. J.* **2007**, 43, 1234.
- [17] Sotirios, A. A.; Constantinos, T. *Macromol. Chem. Phys.* **2006**, 207, 2188.
- [18] Dayananda, K.; Pi, B. S.; Kim, B. S.; Park, T. G.; Lee, D. S. *Polymer* **2007**, 48, 758.
- [19] Nikoletta, S.; Ilias, K.; Sotirios, A.; Constantinos, T. *Macromol. Rapid Commun.* **2008**, 29, 130.
- [20] Hadjiantoniou, N. A.; Patrickios, C. S. *Polymer* **2007**, 48, 7041.
- [21] Achilleos, M.; Krasia-Christoforou, T.; Patrickios, C. S. *Macromolecules* **2007**, 40, 5575.

- [22] Xu, F.-J.; Kang, E.-T.; Neoh, K.-G. *Biomaterials* **2006**, *27*, 2787.
- [23] Reinicke, S.; Schmelz, J.; Lapp, A.; Karg, M.; Hellweg, T.; Schmalz, H. *Soft Matter* **2009**, *5*, 2648.
- [24] Ah Toy, A.; Reinicke, S.; Müller, A. H. E.; Schmalz, H. *Macromolecules* **2007**, *40*, 5241.
- [25] Hamley, I. W.; Daniel, C.; Mingvanish, W.; Mai, S.-M.; Booth, C.; Messe, L.; Ryan, A. J. *Langmuir* **2000**, *16*, 2508.
- [26] McConnell, G. A.; Gast, A. P.; Huang, J. S.; Smith, S. D. *Phys. Rev. Lett.* **1993**, *71*, 2102.
- [27] Perreur, C.; Habas, J.-P.; François, J.; Peyrelasse, J.; Lapp, A. *Phys. Rev. E* **2002**, *65*, 041802/1.
- [28] Eiser, E.; Molino, F.; Porte, G.; Diat, O. *Phys. Rev. E* **2000**, *61*, 6759.
- [29] Eiser, E.; Molino, F.; Porte, G.; Pithon, X. *Rheol. Acta* **2000**, *39*, 201.
- [30] Nicolai, T.; Benyahia, L. *Macromolecules* **2005**, *38*, 9794.
- [31] Tan, H.; Watanabe, H. *Polym. J.* **2004**, *36*, 430.
- [32] Sebastian, J. M.; Lai, C.; Graessley, W. W.; Register, R. A. *Macromolecules* **2002**, *35*, 2707.
- [33] Park, M. J.; Char, K.; Bang, J.; Lodge, T. P. *Macromolecules* **2005**, *38*, 2449.
- [34] Gast, A. P. *Langmuir* **1996**, *12*, 4060.
- [35] Fleischer, G.; Rittig, F.; Kärger, J.; Papadakis, C. M.; Mortensen, K.; Almdal, K.; Stepanek, P. *J. Chem. Phys.* **1999**, *111*, 2789.
- [36] Higgins, J. S.; Dawkins, J. V.; Maghami, G. G.; Shakir, S. A. *Polymer* **1986**, *27*, 931.
- [37] Watanabe, H.; Kotaka, T.; Hashimoto, T.; Shibayama, M.; Kawai, H. *J. Rheol.* **1982**, *26*, 153.
- [38] Hamley, I. W.; Pople, J. A.; Fairclough, J. P. A.; Terrill, N. J.; Ryan, A. J.; Booth, C.; Yu, G. E.; Diat, O.; Almdal, K.; Mortensen, K.; Vigild, M. *J. Chem. Phys.* **1998**, *108*, 6929.
- [39] McConnell, G. A.; Lin, M. Y.; Gast, A. P. *Macromolecules* **1995**, *28*, 6754.
- [40] Hamley, I. W.; Pople, J. A.; Booth, C.; Derici, L.; Impéror-Clerc, M.; Davidson, P. *Phys. Rev. E* **1998**, *58*, 7620.
- [41] Hamley, I. W.; Pople, J. A.; Booth, C.; Yang, Y. W.; King, S. M. *Langmuir* **1998**, *14*, 3182.

-
- [42] Jiang, J.; Burger, C.; Li, C.; Li, J.; Lin, M. Y.; Colby, R. H.; Rafailovich, M. H.; Sokolov, J. C. *Macromolecules* **2007**, *40*, 4016.
- [43] Schmidt, G.; Richtering, W.; Lindner, P.; Alexandridis, P. *Macromolecules* **1998**, *31*, 2293.
- [44] Brulet, A.; Lairez, D.; Lapp, A.; Cotton, J.-P. *J. Appl. Crystallogr.* **2007**, *40*, 165.
- [45] Cotton, J. P. Initial Data Treatment. In *Neutron X-Ray and Light Scattering*; Lindner, P.; Zemb, T., Eds.; Elsevier Science Publishers B. V.: Amsterdam, 1991.
- [46] Stellbrink, J.; Lonetti, B.; Rother, G.; Willner, L.; Richter, D. *J. Phys.: Condens. Matter* **2008**, 404206.
- [47] Prud'homme, R. K.; Wu, G.; Schneider, D. K. *Langmuir* **1996**, *12*, 4651.
- [48] Singh, M.; Agarwal, V.; De Kee, D.; McPherson, G.; John, V.; Bose, A. *Langmuir* **2004**, *20*, 5693.
- [49] Watanabe, H.; Kanaya, T.; Takahashi, Y. *Macromolecules* **2001**, *34*, 662.
- [50] Huang, Y.-Y.; Chen, H.-L.; Hashimoto, T. *Macromolecules* **2003**, *36*, 764.
- [51] Balsara, N. P.; Dai, H. J. *J. Chem. Phys.* **1996**, *105*, 2942.
- [52] Di Cola, E.; Fleury, C.; Panine, P.; Cloitre, M. *Macromolecules* **2008**, *41*, 3627.
- [53] Koppi, K. A.; Tirell, M.; Bates, F. S. *J. Rheol.* **1994**, *38*, 999.
- [54] Wang, H.; Kesani, P. K.; Balsara, N. P.; Hammouda, B. *Macromolecules* **1997**, *30*, 982.
- [55] Ackerson, B. J.; Clark, N. A. *Phys. Rev. A* **1984**, *30*, 906.
- [56] Mortensen, K. *J. Polym. Sci., Part B: Polym. Phys.* **2004**, *42*, 3095.
- [57] Hamley, I. W.; Pople, J. A.; Fairclough, J. P. A.; Ryan, A. J.; Booth, C.; Yang, Y. W. *Macromolecules* **1998**, *31*, 3906.

6 Combination of living anionic polymerization and ATRP via “click” chemistry as a versatile route to multiple responsive triblock terpolymers and corresponding hydrogels

Stefan Reinicke and Holger Schmalz*

Makromolekulare Chemie II, Universität Bayreuth, D-95440 Bayreuth, Germany

ABSTRACT:

A combination of anionic polymerization, ATRP and “click” chemistry was used to construct trishydrophilic ABC triblock terpolymers composed of a pH-sensitive A block, a water soluble B block, and two different thermo-sensitive C blocks, without any block sequence limitation problems. First, an azido end-functionalized poly(2-vinylpyridine)-*block*-poly(ethylene oxide) (P2VP-*b*-PEO-N₃) diblock copolymer was synthesized by anionic polymerization. In a second step, poly(N,N-dimethylaminoethyl methacrylate) (PDMAEMA) and poly(oligo(ethylene glycol) methacrylate) (POEGMA) were synthesized via ATRP, using an alkyne functionalized initiator. The resulting polymers were attached to the P2VP-*b*-PEO-N₃ diblock copolymer using the 1,3-dipolar Huisgen cycloaddition (“click” chemistry). For the “click” step, P2VP-*b*-PEO-N₃ diblock copolymers with either an azidoacetyl or a 2-azidoisobutyryl group were tested. In the latter case, however, a side reaction involving the cleavage of the formed “click” product via nucleophilic substitution occurred, preventing a permanent attachment of PDMAEMA or POEGMA to the P2VP-*b*-PEO-N₃ diblock copolymer. Finally, P2VP-*b*-PEO-*b*-POEGMA (with POEGMA = P(MEO₂MA-*co*-MEO_{8,5}MA)) and P2VP-*b*-PEO-*b*-PDMAEMA triblock terpolymers were successfully synthesized and used to construct stimuli-responsive hydrogels. A concentrated solution of P2VP₅₆-*b*-PEO₃₇₀-*b*-P(MEO₂MA₈₉-*co*-OEGMA₇) showed a gel-sol-gel transition at pH = 7 upon temperature increase, whereas in the case of P2VP₅₆-*b*-PEO₃₇₀-*b*-PDMAEMA₇₀, a gel-

sol or a weak gel-strong gel transition was observed, depending on the applied pH. Finally, the addition of trivalent hexacyanocobaltate(III) ions to the P2VP₅₆-*b*-PEO₃₇₀-*b*-PDMAEMA₇₀ solution induced an upper critical solution temperature (UCST) for the PDMAEMA block, which led to gel formation. This allows for the construction of light-sensitive hydrogels, utilizing the photo-aquation of hexacyanocobaltate(III) ions.

6.1 Introduction

The discovery of ionic polymerization in the 1950's and controlled radical polymerization later in the mid 1990's, were milestones in polymer synthesis, since they provided access to well-defined block copolymer architectures.^{1,2} Block copolymers have become an important class of polymers since they find application as compatibilizers in polymer blends, as thermoplastic elastomers, in nanopatterning, and as macrosurfactants.³ In recent years, block copolymers were utilized further to construct stimuli-responsive ("smart") physical hydrogels.⁴⁻⁶ Such gels are used for biomedical applications like drug delivery, or in sensors, storage media, actuating systems, and microfluidic switches.^{4,5,7,8}

We reported recently on "smart" hydrogels based on double responsive poly(2-vinylpyridine)-*block*-poly(ethylene oxide)-*block*-poly(glycidyl methyl ether-*co*-ethyl glycidyl ether) (P2VP-*b*-PEO-*b*-P(GME-*co*-EGE)) triblock terpolymers, with P2VP constituting the pH-sensitive block and P(GME-*co*-EGE) the thermo-sensitive block.^{9,10} Under conditions, where one of the end blocks is insoluble, this polymer formed micelles with a core-shell-corona structure, and hydrogels were formed via a body centered cubic packing of micelles at sufficiently high concentrations.¹¹ Upon switching the respective second outer block insoluble, too, a micellar network was obtained by formation of crosslinks via the micellar corona. This behaviour led to an unusual gel-sol-gel transition at pH = 7 upon temperature increase. All transitions were rather sharp and the obtainable gel strengths were reasonably high. In conclusion, our concept of using double stimuli-responsive ABC triblock terpolymers for the construction of "smart" hydrogels appeared to be successful.

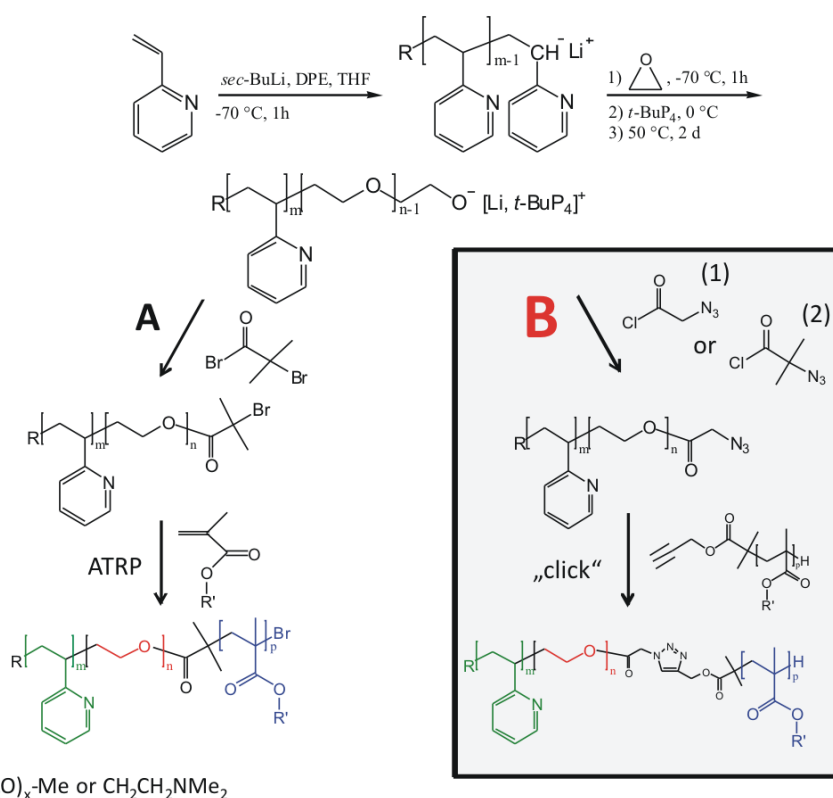
The combination of P2VP, PEO and P(GME-*co*-EGE) was not only chosen because of the good performance of each block with respect to its solubility and responsive behaviour, but also because of the feasibility to synthesize the triblock terpolymer in a one-pot reaction using sequential anionic polymerization. Unfortunately, one general problem occurs in the anionic

polymerization of glycidyl ethers. The active chain ends of such monomers undergo transfer reactions to the monomer, leading to a limitation in the maximum achievable block lengths and the formation of poly(glycidyl ether) homopolymers as side products.^{9,12-16} In consequence, there is a need for an alternative monomer supposed to form the thermo-sensitive block. Oligo(ethylene glycol) methacrylates (OEGMA) might be a suitable substitute, due to the tunable lower critical solution temperature (LCST), which depends on the length of the oligo(ethylene glycol) side chain.¹⁷ The copolymerization of methoxyethoxyethyl methacrylate (MEO₂MA; LCST of the homopolymer: 24 °C) with an OEGMA monomer with 8-9 ethylene glycol units in the side chain (MEO_{8.5}MA; LCST of the homopolymer: 90 °C) was shown to result in statistical copolymers with a sharp coil-to-globule transition, and the transition temperature can be easily tuned by the comonomer ratio.^{18,19}

The main motivation to utilize an alternative thermo-sensitive C block, however, was to introduce a block which is more versatile in terms that it responds to more than just one stimulus. The transition temperature of poly(N,N-dimethylaminoethyl methacrylate) (PDMAEMA) depends strongly on the pH, and can therefore be tuned even in the final product after polymerization. This was demonstrated by Plamper et al. for linear and star-shaped PDMAEMA homopolymers.^{20,21} For PDMAEMA stars, the cloud points shifted from around 80 °C at pH = 7 to around 30 °C at pH = 10, depending on the molecular weight and arm number. It was further demonstrated, that the addition of trivalent hexacyanocobaltate(III) ([Co(CN)₆]³⁻) counterions, at conditions where the PDMAEMA chains are still slightly charged (pH = 8), induces an upper critical solution temperature (UCST).²² In this case, the trivalent [Co(CN)₆]³⁻ ions act as crosslinker between the PDMAEMA chains. UV light can be applied to trigger the exchange of a cyanide ligand with a neutral water molecule (photo-aquation), leading to a divalent aquapentacyanocobaltate(III) ([Co(CN)₅H₂O]²⁻) ion. Consequently, the UCST vanishes when the PDMAEMA solution is exposed to UV light. Therefore, PDMAEMA, forming the C block in the corresponding P2VP-*b*-PEO-*b*-PC triblock terpolymers, is a promising candidate for constructing multi responsive hydrogels, in terms of being sensitive to pH, temperature, and UV light.

Unfortunately, the choice of the monomer sequence within an anionic polymerization goes along with one crucial limitation. The active chain end of a living polymer can only be blocked by another monomer, if the resulting chain end is of equal or lower nucleophilicity than the initial one. In consequence, the living P2VP-*b*-PEO precursor, exhibiting a relatively

stable oxyanion chain end, can only be extended by another epoxide monomer but not by a vinyl based one. There are some exceptions, however, commonly leading to relatively broad molecular weight distributions.²³ The use of silacyclobutanes, being able to transfer oxyanions back into carbanions (“carbanion pump”), could help to overcome this problem.²⁴⁻²⁶ Nevertheless, we decided to develop an alternative route.



Scheme 6.1 Different approaches for the combination of anionic polymerization and ATRP to construct ABC triblock terpolymers with a P2VP A block, a water soluble PEO B block, and varying stimuli-responsive C blocks.

Monomers like DMAEMA and OEGMA can be polymerized in an easy and controlled fashion via atom transfer radical polymerization (ATRP).^{27,28} The synthesis of triblock terpolymers exclusively by ATRP, however, is not trivial. In the particular case of P2VP-*b*-PEO-*b*-PC triblock terpolymers it is even impossible, because control in the ATRP of 2VP is hard to achieve and PEO is not accessible at all through radical polymerization. In order to obtain P2VP-*b*-PEO-*b*-PC triblock terpolymers without any sequence limitation problems, we consequently need to combine both anionic polymerization and ATRP. Scheme 6.1 summarizes two different possible strategies, both based on the initial synthesis of a living P2VP-*b*-PEO diblock copolymer by anionic polymerization and differing only in the last step, through which the third block is introduced. It is noted, that with this strategy a systematic

investigation of the influence of the C block on the gel properties can be carried out, since the different polymers to be synthesized are based on one single P2VP-*b*-PEO diblock copolymer precursor. This ensures, that only the nature and/or length of the C block is altered.

Within route A (Scheme 6.1) the living diblock is terminated with 2-bromoisobutyryl bromide. Subsequently, the thermo-sensitive block can be grown from the diblock precursor via ATRP. However, initial experiments revealed that the P2VP block strongly disturbs the polymerization of the C block, since it can act as chelating agent for Cu(I). The second approach (route B) is based on the end-functionalization of the P2VP-*b*-PEO precursor with an azide group, being suitable for “click” chemistry. The C block is synthesized separately by ATRP, and subsequently attached to the diblock copolymer in that case. The alkyne function, needed in order to “click” the C block to the P2VP-*b*-PEO-N₃ diblock copolymer, is introduced by using an alkyne functionalized ATRP initiator (propargyl 2-bromoisobutyrate). By synthesizing the C block separately, we have a very good control over block lengths and polydispersities, and are able to characterize the resulting polymer before its attachment to the diblock copolymer precursor. In addition, the Cu(I) catalyzed “click” reaction (1,3-dipolar Huisgen cycloaddition),²⁹⁻³¹ is known to take place under ambient conditions and is quantitative. Many groups were using the “click” approach to build up a huge variety of polymeric architectures, and to functionalize chain ends, surfaces, and particles.³²⁻³⁴ Therefore, simply by using an excess of the C block during the “click” reaction, we can ensure a full conversion of the P2VP-*b*-PEO-N₃ diblock copolymer precursor to the respective P2VP-*b*-PEO-*b*-PC triblock terpolymer.

In this work, we want to demonstrate the versatility of route B by synthesizing ABC triblock terpolymers with two different C blocks, in particular PDMAEMA and P(MEO₂MA-*co*-MEO_{8.5}MA). The synthesis of the P2VP-*b*-PEO diblock precursor and of the C blocks will be shortly discussed followed by a more detailed discussion of the “click” reaction. Finally, we present first results on the formation of “smart” hydrogels composed of P2VP-*b*-PEO-*b*-P(MEO₂MA-*co*-MEO_{8.5}MA) and P2VP-*b*-PEO-*b*-PDMAEMA.

6.2 Experimental

Materials

CuBr (Aldrich, 98%) and CuCl (Aldrich, > 99%) were treated with glacial acetic acid and filtered to remove traces of Cu(II) compounds. N,N-dimethylaminoethyl methacrylate (DMAEMA) (Aldrich, 98%), and both oligo(ethylene glycol) methacrylates (MEO₂MA: Aldrich, 95%; and MEO_{8.5}MA: Aldrich) were passed through a basic alumina column to remove the stabilizer. K₃[Co(CN)₆] solutions (0.9 M) were freshly prepared by dissolving K₃[Co(CN)₆] (Aldrich, > 95%) in Millipore water. Bromoacetic acid (Aldrich, 98%), sodium azide (Merck, > 99%), diethyl ether (Aldrich, p.a.), sulfuric acid (Fisher, > 95%), ethanol (VWR, anhydrous), anisole (Aldrich, 99%), THF (Aldrich, p.a.), CuBr₂ (Aldrich, 99%), N,N,N',N'',N'''-pentamethyl diethylenetriamine (PMDETA; Aldrich, 99%), N,N,N',N'',N''',N''''-hexamethyl triethylenetetramine (HMTETA; Aldrich, 97%), propargyl alcohol (Aldrich, 99%), 2-bromoisobutyryl bromide (Aldrich, 98%), ethyl 2-bromoisobutyrate (EBiB; Aldrich, 98%), propargyl acetate (Aldrich, 98%), triethylamine (TEA; Merck, 99%), dichloromethane (Aldrich, p.a.), tributyltin hydride (Aldrich, 97%), NaOH (Merck, 99%), KOH (VWR, 85%), Na₂SO₄ (Merck, 95%), and CaCl₂ (Fluka, > 97%) were used as received.

Synthesis

2-Azidoisobutyryl chloride was prepared in a three-step procedure starting from ethyl 2-bromoisobutyrate (EBiB) and sodium azide.^{35,36} Azidoacetyl chloride was synthesized in a two-step procedure from bromoacetic acid and sodium azide.³⁷ Propargyl 2-bromoisobutyrate was obtained by esterification of 2-bromoisobutyryl bromide with propargyl alcohol.³⁸ Ethyl 2-(4-acetylmethyl)triazolyl isobutyrate was synthesized via “click” chemistry. The detailed procedures are given in the Supporting Information.

Azido end-functionalized poly(2-vinylpyridine)-block-poly(ethylene oxide) (P2VP-b-PEO-N₃)

First, 2-vinylpyridine was polymerized in THF at -70 °C using diphenylhexyllithium, formed in situ from *sec*-butyllithium and diphenylethylene, as initiator. After complete consumption of 2VP, ethylene oxide (EO) was added to the reaction mixture, followed by addition of the phosphazene base *t*-BuP₄, which enables the polymerization of EO in the presence of lithium counterions. The polymerization was completed after two 2 days at 50 °C. Subsequently, the

degassed azido functionalized acid chloride (azidoacetyl chloride or 2-azidoisobutyryl chloride) was added to the solution in a 5-fold excess with respect to the number of living chain ends. Finally, the product was isolated by precipitation in diethyl ether followed by drying in a vacuum oven. A detailed description of the P2VP-*b*-PEO diblock copolymer synthesis can be found elsewhere.¹⁰

Alkyne end-functionalized PDMAEMA

In a typical polymerization procedure, DMAEMA (20 g, 127 mmol), anisole (95 mL), CuBr₂ (17 mg, 0.08 mmol), and propargyl 2-bromoisobutyrate as initiator (0.2 g, 1 mmol) were mixed in a reaction vessel, equipped with a screw cap containing a septum. A second vessel contained anisole (5 mL) and CuBr (63 mg, 0.44 mmol), and a third one a solution of HMTETA (0.2 mL, 0.9 mmol) in anisole (7 mL). After each vessel was degassed by purging with nitrogen for 30 min, respectively, 5 mL of the HMTETA/anisole mixture were added to the second vessel via syringe. After the CuBr was dissolved, the content of the second vessel was transferred into the first one, which was already preheated to 60 °C ([I]:[CuBr]:[CuBr₂]:[L]:[M] = 1:0.44:0.08:0.64:127). After a few seconds, the reaction mixture turned green. Samples were taken in appropriate time intervals and diluted with deuterated chloroform for conversion determination by ¹H-NMR spectroscopy. Signals corresponding to the methyl group at the polymeric backbone (0.6 – 1.3 ppm) were compared with signals originating from the vinyl protons of the monomer (close to 5.6 and 6.2 ppm). After the desired conversion was reached ($x_P \sim 40\%$), the reaction mixture was exposed to air, diluted with 100 mL THF, and passed through a silica column. The solution was concentrated using a rotary evaporator, transferred into a dialysis tube (SpectraPorTM, regenerated cellulose, MWCO 1000), and dialysed against dioxane. The dry polymer was obtained by freeze drying.

Alkyne end-functionalized P(MEO₂MA-co-MEO_{8.5}MA)

In a typical polymerization procedure MEO₂MA (M₁) (17 g, 92 mmol), MEO_{8.5}MA (M₂) (3.2 g, 6.8 mmol), anisole (140 mL), CuCl (25 mg, 0.25 mmol), and the initiator propargyl 2-bromoisobutyrate (0.2 g, 1 mmol) were mixed in a reaction vessel equipped with a screw cap containing a septum. After degassing the mixture by purging with nitrogen for 30 min and preheating to 85 °C, degassed PMDETA (65 μL, 0.5 mmol) was added ([I]:[CuCl]:[L]:[M₁]:[M₂] = 1:0.25:0.5:92:6.8). After a few seconds, the reaction mixture

turned pale brown. Conversion determination was achieved according to the procedure applied for the polymerization of DMAEMA. After the desired conversion was reached, the mixture was either exposed to air, or tributyltin hydride (0.8 mL, 4 mmol) was added via syringe followed by stirring for 3 h at 85 °C, in order to exchange the halogen atom at the chain end by hydrogen. Subsequently, the solution was passed through a basic alumina column and concentrated using a rotary evaporator. The polymer was isolated by precipitation into *n*-hexane and subsequently dried in a vacuum oven.

Model “click” reaction

CuBr (28 mg, 0.2 mmol), THF- d_8 (Deutero GmbH, 2 mL), propargyl 2-bromoisobutyrate (20 mg, 0.1 mmol), and ethyl 2-azidoisobutyrate (20 mg, 0.13 mmol) were mixed in a flask equipped with a Teflon valve, and degassed by several freeze-pump-thaw cycles. Afterwards, degassed PMDETA (70 mg, 0.42 mmol) was added and the reaction mixture was transferred into an NMR-tube under nitrogen flow. $^1\text{H-NMR}$ spectra were recorded at appropriate time intervals.

*Decomposition of ethyl 2-(4-acetylmethyl)triazolyl isobutyrate in the presence of the phosphazene base *t*-BuP₄ and air*

3 droplets of a *t*-BuP₄ solution in *n*-hexane (Fluka, 1 M) were added to 2 mL of THF- d_8 . After a short waiting period of approximately 10 min, one droplet of ethyl 2-(4-acetylmethyl)triazolyl isobutyrate was added. After another 15 min, the solution was transferred to an NMR tube and a $^1\text{H-NMR}$ spectrum was recorded. Signal assignment was carried by comparison with the $^1\text{H-NMR}$ spectra of the pure substances, or by simulating spectra with ACD/Chem Sketch 11.01 (ACD/Labs).

*P2VP-*b*-PEO-*b*-P(MEO₂MA-*co*-MEO_{8.5}MA), P2VP-*b*-PEO-*b*-PDMAEMA (“click” reaction)*

In a typical procedure, the azidoacetyl end-functionalized P2VP-*b*-PEO- N_3 diblock copolymer (DB1, Table 6.1; 1.4 g, 0.07 mmol) was dissolved in THF (80 mL) and transferred into a reaction vessel, equipped with a screw cap containing a septum. In a second vessel, CuBr (120 mg, 0.8 mmol), propargyl end-functionalized P(MEO₂MA-*co*-MEO_{8.5}MA) (2.7 g, ca. 0.27 mmol), and THF (80 mL) were mixed. After degassing both vessels by purging with nitrogen for 30 min, the content of the second vessel was transferred completely into the first

one, and degassed PMDETA (0.4 mL, 3 mmol) was added via a syringe. Samples were taken with a syringe, passed through a basic alumina column, and used directly for SEC analysis. In case of PDMAEMA, both polymeric precursors were dissolved in the first vessel, the second vessel only contained CuBr and THF (PDMAEMA is able to complex Cu(I)). For reactions with the 2-azidoisobutyryl end-functionalized P2VP-*b*-PEO-N₃ diblock copolymer (DB-2, Table 6.1), the reaction vessels were exchanged by flasks equipped with Teflon valves, THF was dried before over potassium, and the reaction mixtures were carefully degassed by several freeze-pump-thaw cycles.

Hydrogel preparation

0.8 g of the triblock terpolymer were dissolved in THF (ca. 20 mL). The solution was filtered using a syringe filter (Roth, PTFE, 0.45 μm), transferred into a dialysis tube (SpectraPor, regenerated cellulose, MWCO 1000) and dialyzed against Millipore water for 4 days. Afterwards, the aqueous solutions were concentrated under mild conditions using a vacuum oven (30 °C, 75 mbar) until the desired concentration was reached.

In case of P2VP-*b*-PEO-*b*-PDMAEMA, buffer solution (VWR) was added (final ionic strength in the concentrated samples in the order of 0.05 mol/L), and the pH was adjusted to the required value using a titrator (Titrand 809, Metrohm, Herisau, Switzerland) before concentrating the solution. [Co(CN)₆]³⁻ ions were introduced by adding a defined amount of aqueous K₃[Co(CN)₆] solution (0.9 M) to the triblock terpolymer solution, followed by stirring for approximately 15 min. In order to study the impact of UV light, the [Co(CN)₆]³⁻ containing sample was irradiated using a Honle UVAHAND 250_{H1/BL} lamp (310 W) operated with black light filter, which transmits light in the wavelength range 310 - 400 nm. IR radiation was diminished with a water flow filter. The sample was placed 10 cm away from the lamps surface. The experiment was performed using a snap cap vial (*D* = 1.7 cm) as well as a glass cuvette (*D* = 3 mm) in order to determine the influence of the sample thickness. No special care was taken for the transmittance of the glass used.

Characterization

Nuclear magnetic resonance (NMR) spectroscopy

Conversions of the ATRP and the model “click” reaction were determined by ^1H -NMR using a Bruker Avance 300 spectrometer. CDCl_3 or THF-d_8 (both Deutero GmbH) were used as solvents.

Size exclusion chromatography (SEC)

SEC experiments using THF as eluent were performed on an instrument equipped with four PSS SDV gel columns (porosities: 10^2 , 10^3 , 10^4 and 10^5 Å, diameter: 5 μm), a pre-column (10^2 Å, 5 μm), a differential refractometer (Shodex), and a UV-detector at 254 nm (Waters). Measurements were conducted at 40 °C with a flow rate of 1 mL/min using toluene as the internal standard. For experiments with dimethyl acetamide (DMAc) as eluent another instrument, equipped with two PSS GRAM columns (porosities: 10^2 and 10^3 Å, diameter: 8 μm), a pre-column (10^2 Å), a differential refractometer and a UV-detector at 260 nm (both Agilent Technologies), was used. Measurements were performed at 60 °C with a flow rate of 0.7 mL/min. A calibration with narrowly distributed polystyrene standards was applied.

Matrix assisted laser desorption ionization - time of flight mass spectrometry (MALDI-ToF MS)

MALDI-ToF MS was performed on a Bruker Reflex III with a UV laser operating at 337 nm and an acceleration voltage of 20 kV. For P2VP, 1,8,9-trihydroxyanthracene (dithranol) as matrix and silver triflate as cationizing agent were used. For POEGMA, 2,5-dihydroxy benzoic acid (DHB) was used as matrix without adding an additional cationizing agent. In all cases, samples were dissolved in THF (10 mg/mL) and mixed with the matrix (20 mg/mL in THF) and the salt (10 mg/mL in THF) at a mixing ratio of 20:5:1 (v/v, matrix: analyte: salt). 1 μL of this mixture was spotted onto the target and allowed to dry. 200–500 laser shots were accumulated for each spectrum.

Rheology

Rheology measurements were conducted using a Physica MCR 301 rheometer (Anton Paar GmbH) with a cone-and-plate shear cell geometry ($D = 50$ mm, cone angle = 1°). The linear

viscoelastic regime was determined prior to the measurements by performing a strain sweep at a frequency of 1 Hz for each sample. For all temperature-dependent measurements a frequency of 1 Hz, a strain of 0.7%, and a heating rate of 0.1 K/min were applied. The temperature was controlled by a Peltier element. For frequency sweeps (10^{-2} to 10^2 Hz) at a given temperature the desired temperature was adjusted by heating the sample slowly at a rate of 0.1 K/min.

Test tube inversion

The snap cap vials (volume 5 mL) containing the samples were immersed in an oil bath, which was heated stepwise (1 K per step) using a heating plate (RCT basic, IKA) equipped with a contact thermometer (Ikatron, IKA). After each temperature step, the test tubes were inverted in order to check whether the sample flows or not.

6.3 Results and Discussion

6.3.1 Azido end-functionalized P2VP-*b*-PEO-N₃ diblock copolymers

The first part of the triblock terpolymer synthesis includes the fabrication of an azido end-functionalized P2VP-*b*-PEO-N₃ diblock copolymer (Scheme 6.1). The synthesis of the P2VP-*b*-PEO precursor was carried out by sequential anionic polymerization (see Experimental Part). A detailed description of the whole procedure is given elsewhere.^{9,10} Table 6.1 summarizes the molecular characteristics of the synthesized diblock copolymers.

Table 6.1. Molecular characteristics of azido end-functionalized P2VP-*b*-PEO-N₃ diblock copolymers obtained from anionic polymerization and subsequent end-capping

	DP(P2VP) ^{a)}	DP(PEO) ^{b)}	M _n [kg/mol] ^{b)} / PDI ^{c)}	End group
DB-1	56	370	22.2 / 1.02	azidoacetyl (1)
DB-2	28	217	12.5 / 1.02	2-azidoisobutyryl (2)

a) Degree of polymerization (DP), determined via MALDI-ToF

b) Determined from ¹H-NMR spectra using the absolute M_n(P2VP) for signal intensity calibration

c) Determined via THF-SEC with polystyrene calibration

One great advantage of anionic polymerization is that the chain end stays active even after full consumption of the monomer, and thus can be easily functionalized. The chain end of the

living P2VP-*b*-PEO diblock copolymer precursor is an oxyanion. Therefore, an azido group, which is needed for the “click” reaction, can be easily introduced via esterification with an azido functionalized acid chloride. This reaction proceeds quickly and quantitatively. In our case, we used two different acid chlorides (Scheme 6.1), namely azidoacetyl chloride (1) and 2-azidoisobutyryl chloride (2). It cannot be excluded, that a small part of the acid chloride forms a complex with the 2VP units, since the latter act as weak base. Furthermore, it might also interact with the phosphazene base *t*-BuP₄, although the bulky structure of *t*-BuP₄ should prevent a strong binding to the acid chloride. Considering these potential side reactions we added the acid chloride in excess in order to ensure the full functionalization of the P2VP-*b*-PEO diblock copolymer.

The crude product was precipitated into cold diethyl ether, which removes most of the impurities originating from polymerization and functionalization. It is noted, that the precipitate still contains traces of *t*-BuP₄, as revealed by ¹H-NMR (results not shown), which has a certain impact on the success of the coupling reaction in the case of the diblock copolymers carrying end group (2). This aspect will be addressed later on in detail.

6.3.2 Alkynyl end-functionalized POEGMA und PDMAEMA

Table 6.2 summarizes the molecular characteristics of all synthesized stimuli-responsive polymers to be used later on for the “click” reaction. Details concerning the synthesis via ATRP using propargyl 2-bromoisobutyrate as initiator can be found in the Experimental Part.

In the case of POEGMA, the monomer feed was composed of 84 wt% MEO₂MA and 16 wt% MEO_{8.5}MA, respectively, in order to establish a cloud point in the range of physiological temperatures for the resulting copolymer. All synthesized polymers exhibit a monomodal and narrow molecular weight distribution.

Table 6.2. Specifications of alkynyl end-functionalized POEGMA and PDMAEMA

	POEGMA			PDMAEMA	
	P(MEO ₂ MA) MA	P(MEO ₂ MA- <i>co</i> - MEO _{8.5} MA)-1 ^{a)}	P(MEO ₂ MA- <i>co</i> - MEO _{8.5} MA)-2 ^{a)}	PDMAEMA- 1	PDMAEMA- 2
M _n [kg/mol] / DP ^{b)}	10.2 / 54	10.6 / 47 - 3.5	19.9 / 89 - 7	11.0 / 70	6.0 / 38
PDI ^{b)}	1.14	1.09	1.08	1.05	1.10
ATRP end group modi- fication ^{c)}	no	yes	yes	no	no

a) MEO₂MA/MEO_{8.5}MA = 84/16 w/w

b) POEGMA was characterized via MALDI-ToF MS; PDMAEMA was characterized in an indirect manner from ¹H-NMR spectra of the corresponding P2VP-*b*-PEO-*b*-PDMAEMA triblock terpolymers, using the absolute M_n of the P2VP block for signal intensity calibration (DP = degree of polymerization)

c) Exchange of the halogen atom with hydrogen by treatment with Bu₃SnH (see Experimental Part for details)

6.3.3 Synthesis of P2VP-*b*-PEO-*b*-POEGMA and P2VP-*b*-PEO-*b*-PDMAEMA via “click” coupling

The last step in the synthesis of P2VP-*b*-PEO-*b*-PC triblock terpolymers is the attachment of the C block to the P2VP-*b*-PEO-N₃ diblock copolymer precursor utilizing “click” chemistry (Scheme 6.1). As already mentioned, the “click” reaction itself works quantitatively without any side reactions under ambient conditions. However, there are still two crucial points we have to consider if we want to utilize the “click” approach for our purpose. First of all, it is necessary to use the C block in excess in order to ensure a full conversion of the P2VP-*b*-PEO-N₃ precursor. POEGMA and PDMAEMA are soluble in diethyl ether in contrast to P2VP and PEO, and can therefore easily be removed by precipitating the “click” product in diethyl ether. A second point which has to be considered, is the fact that the “click” reaction, expressed by the formation of a triazol ring from the azide group at the diblock copolymer precursor and the alkyne group at the C block (1,3-dipolar Huisgen cycloaddition), is copper(I) catalyzed and therefore resembles ATRP conditions. The reaction can alternatively be performed in a metal free environment, however, this would require special activated “click” components.^{39,40} In consequence, POEGMA as well as PDMAEMA, could get reactivated throughout the “click” reaction, and subsequently undergo disproportionation reactions, as long as they still carry their halogen end group. This in turn would result in the

formation of polymerizable macromonomers, which can add to the activated chain end. Hence, we first investigated the extent of coupling, when POEGMA and PDMAEMA are exposed to “click” conditions, respectively. Consequently, PMEO₂MA and PDMAEMA-2, both still carrying the activatable halogen end group (Table 6.2), were dissolved in THF in the presence of CuBr and PMDETA ([CuBr]:[end group] \approx 7:1) under inert atmosphere. Figure 6.1 shows the corresponding SEC traces of the polymers after being kept under the aforementioned conditions for different time periods.

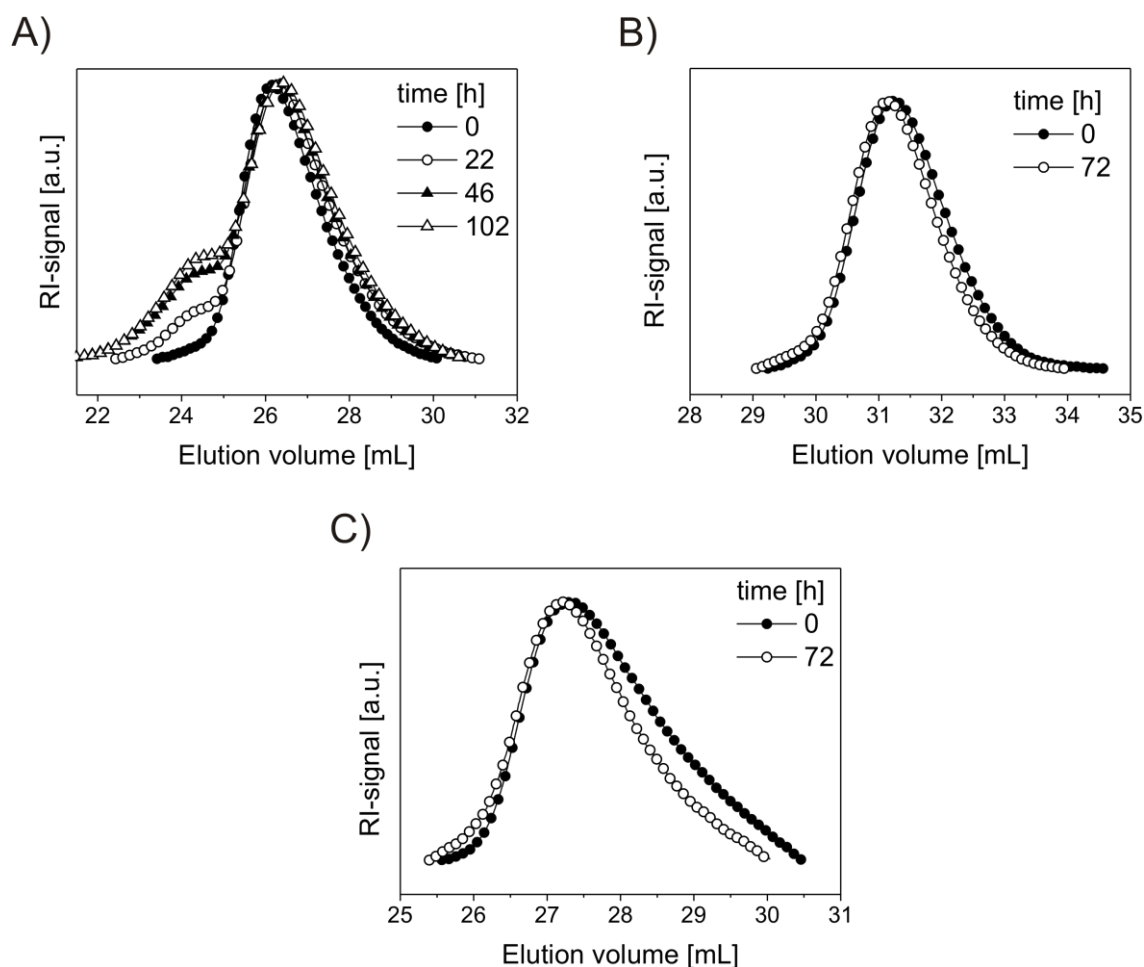


Figure 6.1. SEC traces of POEGMA and PDMAEMA before and after exposure to “click” conditions (CuBr, PMDETA, THF, room temperature) for different time periods: A) PMEO₂MA (DMAC-SEC), B) P(MEO₂MA-co-MEO_{8.5}MA)-1 (THF-SEC), and C) PDMAEMA-2 (DMAC-SEC)

A coupling shoulder only develops in the case of PMEO₂MA. This indicates that PDMAEMA-2 has lost the halogen end group during the course of polymerization, which was shown to be most pronounced for bromine end groups,⁴¹ and is further supported by the significant tailing frequently observed in the SEC traces of PDMAEMA synthesized by ATRP. In the case of POEGMA, reactivation during the “click” reaction can be avoided by terminating the polymerization of OEGMA with Bu₃SnH, which exchanges the halogen end

group by a hydrogen.⁴² Figure 6.1B shows the SEC trace of the modified POEGMA (P(MEO₂MA-*co*-MEO_{8.5}MA)-1) after exposure to “click” conditions for 24 h, verifying the absence of coupling.

P2VP-*b*-PEO-N₃ diblock copolymers with two different azido containing end groups were tested for the “click” coupling (Scheme 6.1, Table 6.1). End group (1) is known to be an efficient “click” component.³²⁻³⁴ Our motivation to use also end group (2) as an alternative is based on the easy transformation of ATRP initiating sites into “click” components by a simple nucleophilic substitution of the halogen atom by an azide. There are numerous reports presenting a combined ATRP/“click” approach for the synthesis of block copolymer structures,⁴³⁻⁴⁶ however, the functionalized isobutyryl group has so far rarely been used. Additionally, the few examples reported in literature showed “click” efficiencies far below 100%.^{47,48} This might be explained by the sterically demanding structure of the isobutyryl group. In order to get a better insight in the performance of the 2-azidoisobutyryl group as “click” agent, we included it in our investigations. A comparison of both azide containing end groups was made by performing “click” reactions using P(MEO₂MA-*co*-MEO_{8.5}MA)-1 as the C block. Figure 6.2 shows the SEC traces of the crude “click” products after 1 day reaction time together with the corresponding precursors. The “click” reaction was successful when the diblock copolymer carrying end group (1) (DB-1) was used, whereas no “click” product was formed when end group (2) (DB-2) was involved, as indicated by the absence of a peak shift to lower elution volumes. At a first glance, this observation seems to support the assumption of steric repulsion preventing the formation of the triazol ring. However, if air and moisture are excluded more rigorously, i.e., by drying THF over potassium prior to use and performing several freeze-pump-thaw cycles instead of just purging with nitrogen, a “click” product is also formed in the case of DB-2 (Figure 6.3). A decomposition of this “click” product, however, takes place after approximately 1h, most likely due to the introduction of small traces of air upon sample withdrawal.

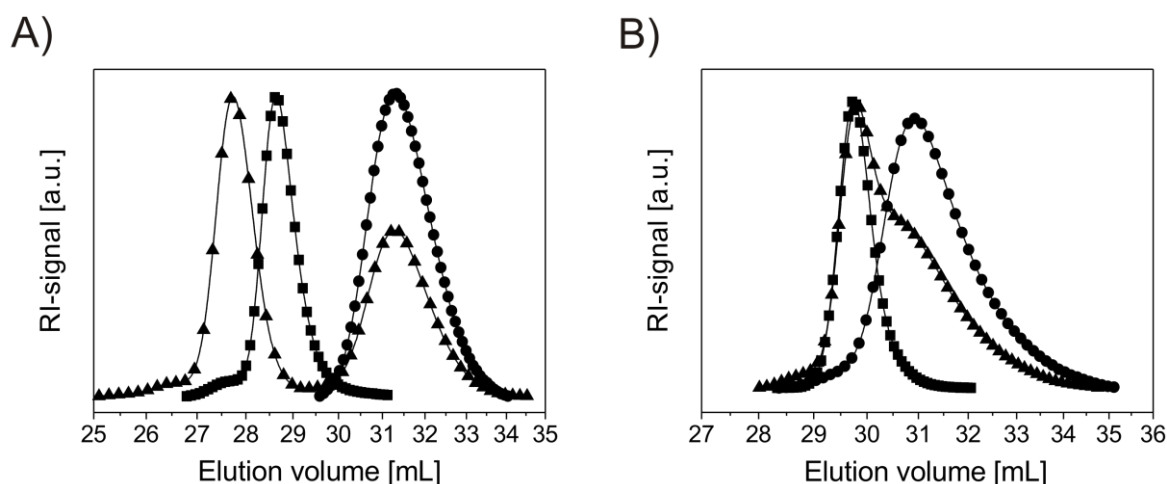


Figure 6.2. THF-SEC traces of crude “click” products (triangles) together with the corresponding precursors: A) DB-1 (squares), and P(MEO₂MA-*co*-MEO_{8.5}MA)-1 (circles); B) DB-2 (squares), and P(MEO₂MA-*co*-MEO_{8.5}MA)-1 (circles). The reaction mixtures were degassed by purging with nitrogen for 15 min.

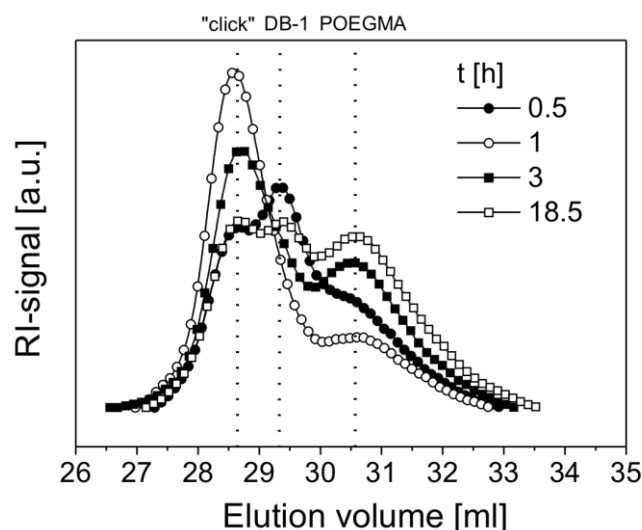


Figure 6.3. THF-SEC traces of crude “click” products obtained from P(MEO₂MA-*co*-MEO_{8.5}MA)-1 and DB-2 after different reaction times. The reaction mixture was degassed by freeze-pump-thaw cycles.

In order to get a better insight into the “click” reaction mechanism when DB-2 is involved, we performed a model reaction using ethyl 2-azidoisobutyrate and propargyl 2-bromoisobutyrate as reactants. The reaction was carried out in deuterated THF in order to be able to follow the reaction by ¹H-NMR. It is noted, that the deuterated THF was not additionally dried before use. This means, that the reaction conditions resemble the conditions which led to the failure of the initially performed “click” reaction with DB-2 (Figure 6.2B).

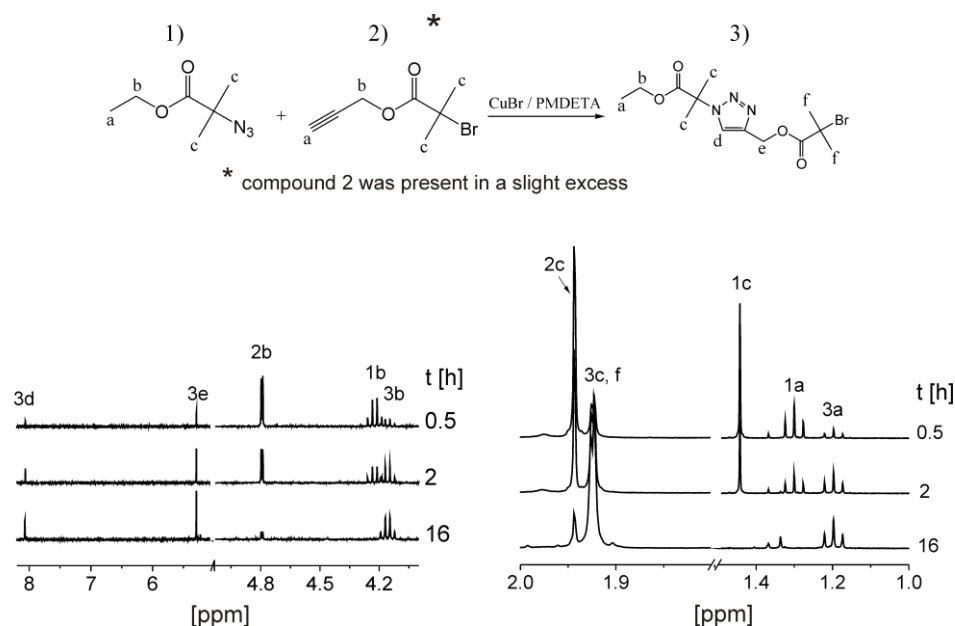


Figure 6.4. Sections of $^1\text{H-NMR}$ spectra, obtained in situ from a model “click” reaction in THF-d_8 involving ethyl 2-azidoisobutyrate (1) and propargyl 2-bromoisobutyrate (2), recorded at different reaction times.

Surprisingly, it can be observed that signals being assigned to the formation of the triazol ring were not only developing but also remaining for elevated times (Figure 6.4). This indicates, that the “click” reaction took place and that the formed triazol ring is long-term stable, regardless of the degassing and workup procedure. This contradiction can be understood if we keep in mind, that the $\text{P2VP-}b\text{-PEO-N}_3$ precursors still contain traces of the phosphazene base $t\text{-BuP}_4$ (Figure 6.5A), which of course is not present in the model “click” reaction. This base easily reacts with moisture, resulting in the formation of hydroxide ions with bulky $[t\text{-BuP}_4\text{-H}]^+$ counterions. Such a hydroxide ion is expected to be much more active towards nucleophilic substitution and elimination reactions compared to common hydroxides like KOH due to an increased solubility in THF . Consequently, the hydroxide ion should be able to either attack the tertiary carbon atom to which the triazol ring is attached or abstract a proton from one of the methyl groups in the vicinity, causing a cleavage of the “click” product via nucleophilic substitution or elimination, respectively (Figure 6.5B).

In order to verify this assumption, $t\text{-BuP}_4$ (ca. 0.03 mmol) was added to untreated deuterated THF , followed by the addition of a small amount of the “click” product ethyl 2-(4-acetylmethyl)triazolyl isobutyrate (ca. 0.04 mmol). The $^1\text{H-NMR}$ spectrum of this mixture, which was recorded approximately 15 min after the addition of the “click” compound, clearly indicates a decomposition of the latter, as the characteristic signals at 8, 5.2, and 4.2 ppm have disappeared (Figure 6.5C). The question now arises, what kind of decomposition mechanism

takes place. It is obvious that saponification of the ester groups takes place, indicated by the presence of ethanol (compound 5, Figure 6.5B). If the decomposition of ethyl 2-(4-acetylmethyl)triazolyl isobutyrate occurred exclusively via this mechanism, we should detect only one triazol containing species, provided the saponification was complete. This is obviously not the case, as indicated by the signals between 8.1 and 8.4 ppm, and 4.5 and 5.2 ppm, respectively (Figure 6.5C). Partial saponification on the other hand should lead to a mixture of 4 different triazol compounds which, however, is also not observable. A satisfying explanation can be given by considering a simultaneous cleavage of the “click” product by the proposed nucleophilic substitution or elimination reaction. Evidence for a significant contribution of elimination was not found, i.e., cleavage occurs predominantly via nucleophilic substitution. We assume this substitution to be quantitative, and the simultaneous saponification to take place only partially. The particular set of detected signals strongly supports this mechanism.

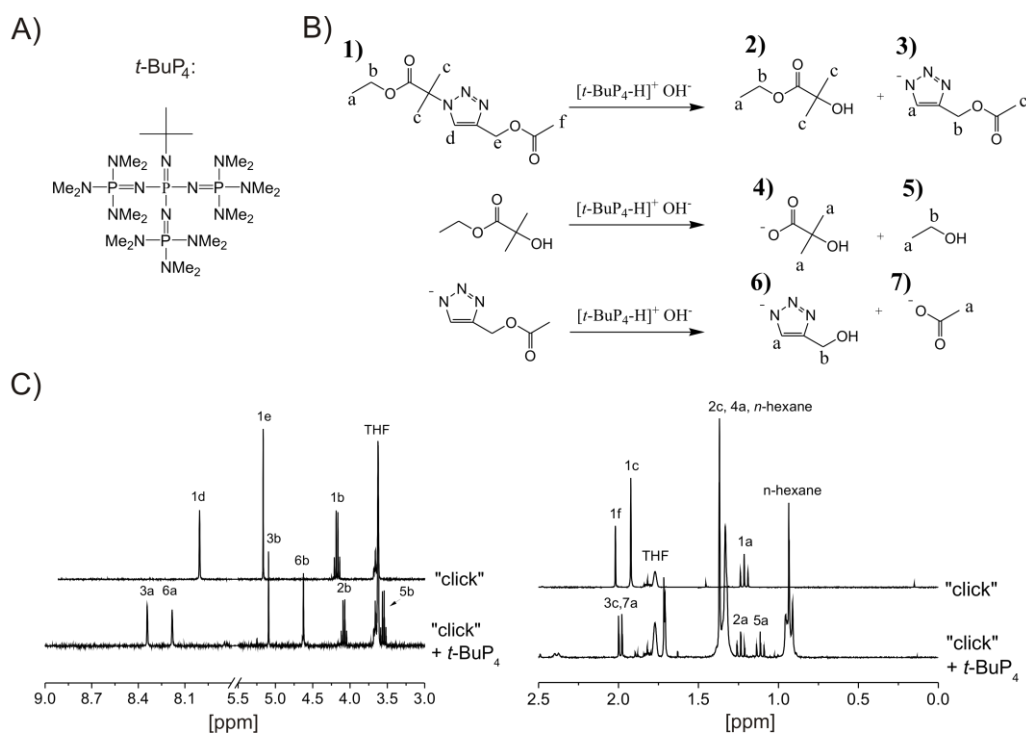


Figure 6.5. A) Structure of the phosphazene base $t\text{-BuP}_4$; B) proposed mechanism of the decomposition of ethyl 2-(4-acetylmethyl)triazolyl isobutyrate in the presence of the phosphazene base $t\text{-BuP}_4$ and moisture; C) sections of $^1\text{H-NMR}$ spectra (THF-d_8) of ethyl 2-(4-acetylmethyl)triazolyl isobutyrate before and after mixing with a 1 M $t\text{-BuP}_4$ solution in $n\text{-hexane}$.

In conclusion, the 2-azidoisobutyryl group works in principle for the “click” reaction but is unsuitable in our particular case, as long as phosphazene base traces remain in the P2VP- b -PEO- N_3 precursor. Recrystallization from ethanol or dialysis against water should help to get

rid of the base prior to the “click” reaction. However, stirring in ethanol might cause a cleavage of the azido function due to transesterification, catalyzed by the P2VP units. Consequently, we decided to continue with the azidoacetyl functionalized diblock copolymer (DB-1) to synthesize the P2VP-*b*-PEO-*b*-PC triblock terpolymers, using P(MEO₂MA-*co*-MEO_{8.5}MA)-2 and PDMAEMA-1 (Table 6.2) as corresponding stimuli-sensitive C blocks. Accordingly two triblock terpolymers were obtained, P2VP₅₆-*b*-PEO₃₇₀-*b*-PDMAEMA₇₀, and P2VP₅₆-*b*-PEO₃₇₀-*b*-P[(MEO₂MA)₈₉-*co*-(MEO_{8.5}MA)₇].

Figure 6.6 shows the SEC traces of both products after being purified by precipitation into cold diethyl ether. The SEC trace of the P2VP₅₆-*b*-PEO₃₇₀-*b*-PDMAEMA₇₀ triblock terpolymer still significantly overlaps with the SEC trace of the corresponding diblock copolymer precursor (Figure 6.6B). However, one should keep in mind that the PDMAEMA block is relatively short, and that a significant tailing is frequently observed for PDMAEMA in DMAc-SEC. The small peak at lower elution volumes in the SEC traces of the diblock copolymer precursor originates from coupled diblock copolymer, which is formed by traces of SOCl₂ present in the azidoacetyl chloride used for end-functionalization.

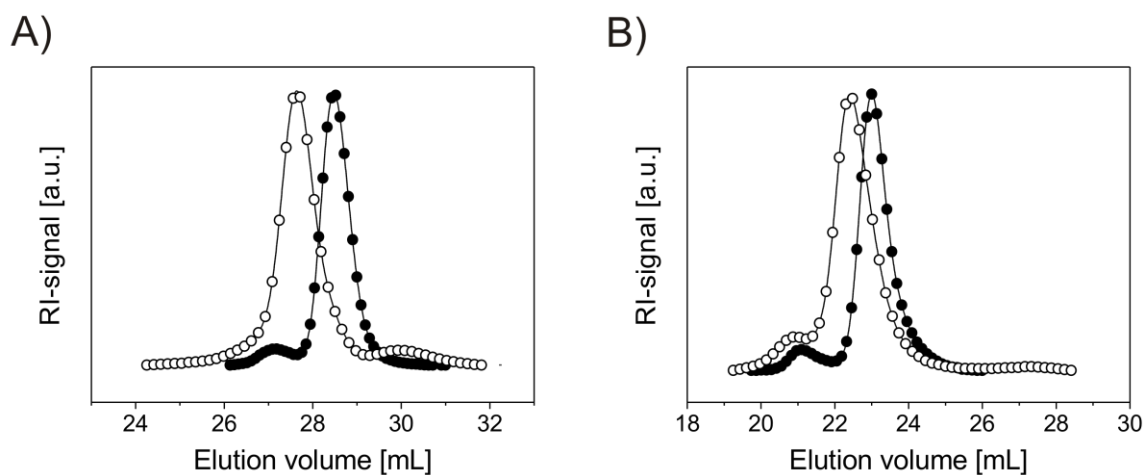
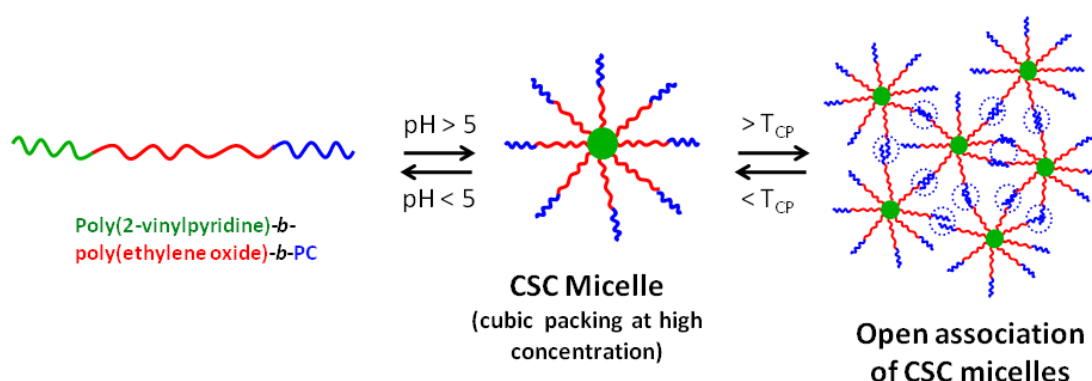


Figure 6.6. SEC traces of purified “click” products (open circles) and the corresponding P2VP-*b*-PEO-N₃ precursor (filled circles): a) P2VP₅₆-*b*-PEO₃₇₀-*b*-P[(MEO₂MA)₈₉-*co*-(MEO_{8.5}MA)₇] (THF-SEC), b) P2VP₅₆-PEO₃₇₀-PDMAEMA₇₀ (DMAc-SEC).

6.3.4 Hydrogels

In order to prepare the hydrogel samples, the synthesized triblock terpolymers were dissolved in THF and subsequently dialyzed against Millipore water. Millipore water exhibits a pH of approximately 6.5. Under these conditions the P2VP block is deprotonated and therefore hydrophobic.⁹ Consequently, the P2VP block collapses as the water fraction increases during dialysis. As a result, core-shell-corona (CSC) micelles with a P2VP core, a PEO shell, and a C block corona are formed (Scheme 6.2). Two different gelation mechanisms can take place if the volume fraction of micelles is high enough. First, these micelles can arrange on a regular lattice. Second, the corona forming block can be switched insoluble, too, resulting in an open association of the CSC micelles via physical crosslinking through the coronal chains. This was recently demonstrated for a concentrated solution of a P2VP₆₀-*b*-PEO₄₅₂-*b*-P(GME₃₆-*co*-EGE₃₆) triblock terpolymer, which showed a gel-sol-gel transition upon heating at pH = 7.⁹ The low temperature gel phase was based on a body centered cubic packing of CSC micelles,¹¹ whereas the high temperature gel phase was formed by a micellar network, as predicted.



Scheme 6.2. Schematic depiction of the structure of the core-shell-corona (CSC) micelles, formed by P2VP-*b*-PEO-*b*-PC triblock terpolymers in water at pH > 5, and the corresponding gelation mechanism at low and high temperatures, respectively (PC = PDMAEMA; P(MEO₂MA-*co*-MEO_{8.5}MA)).

The gelation behaviour of concentrated solutions of the triblock terpolymers P2VP₅₆-*b*-PEO₃₇₀-*b*-P[(MEO₂MA)₈₉-*co*-(MEO_{8.5}MA)₇] and P2VP₅₆-*b*-PEO₃₇₀-*b*-PDMAEMA₇₀ was studied by rheology, applying an oscillatory stress to the samples using a cone-and-plate shear cell geometry. The storage modulus G' and the loss modulus G'' were recorded in dependence on temperature and frequency. Regimes with $G' > G''$ are referred to as gel state with respect to common definitions.⁴⁹ A weak or no frequency dependence of G' , and $G' > 1$ kPa is characteristic for strong, free-standing gels.⁵⁰ Sol states on the other hand are characterized by

$G'' > G'$, and a strong frequency dependence of both moduli. A viscoelastic fluid in particular shows $G' \propto \omega^2$ and $G'' \propto \omega$.

6.3.4.1 P2VP₅₆-*b*-PEO₃₇₀-*b*-P[(MEO₂MA)₈₉-*co*-(MEO_{8.5}MA)₇]

Figure 6.7A shows the temperature-dependent dynamic moduli for a 20 wt% solution of P2VP₅₆-*b*-PEO₃₇₀-*b*-P[(MEO₂MA)₈₉-*co*-(MEO_{8.5}MA)₇] at pH = 7. At 20 °C, the solution behaves as a weak gel, indicated by G' being slightly higher than G'' and exhibiting only a value of 72 Pa. Upon temperature increase, G' decreases smoothly leading to $G' < G''$ (gel-sol transition). Finally at 45 °C, G' starts to exceed G'' again indicating a sol-gel transition. At 55 °C, G' shows only a weak dependence on frequency, and exceeds G'' over the whole measured frequency range with values > 1 kPa (Figure 6.7B). These features verify the presence of a strong, physically crosslinked gel at elevated temperatures, originating from an open association of the CSC micelles as depicted in Scheme 6.2. The formation of a weak gel at 20 °C most likely originates from a jammed micellar solution with a fractal arrangement of the micelles (percolation network).^{8,51,52} The low order of the gel state also explains the rather smooth change of the dynamic moduli upon the initial temperature increase. In contrast, for an abrupt disintegration of a highly regular lattice a distinct gel-sol transition would be expected, as observed for P2VP-*b*-PEO-*b*-P(GME-*co*-EGE) triblock terpolymers.⁹ The observed gel-sol transition is most probably caused by a shrinkage of the micellar corona.^{9,11} It is noted, that the sample remains in the sol state after one heating-cooling cycle (Figure 6.7A). This observation coincides with the behaviour of the P2VP-*b*-PEO-*b*-P(GME-*co*-EGE) triblock terpolymers. The rearrangement of the micelles into a fractal network, and in consequence the reformation of the gel, is significantly retarded under the particular experimental conditions.

The sol-gel transition temperature ($T_{SG} = 45$ °C) determined by rheology is significantly higher compared to the cloud point of the corresponding P[(MEO₂MA)₈₉-*co*-(MEO_{8.5}MA)₇] homopolymer ($T_{CP} = 32.8$ °C; Figure 6.10, Supporting Information). This is consistent with the results obtained for the P2VP-*b*-PEO-*b*-P(GME-*co*-EGE) triblock terpolymers, showing a sol-gel transition temperature which is 5-10 °C higher compared to the cloud point of the glycidyl ether block.⁹ This shift is caused by the influence of the hydrophilic PEO block.

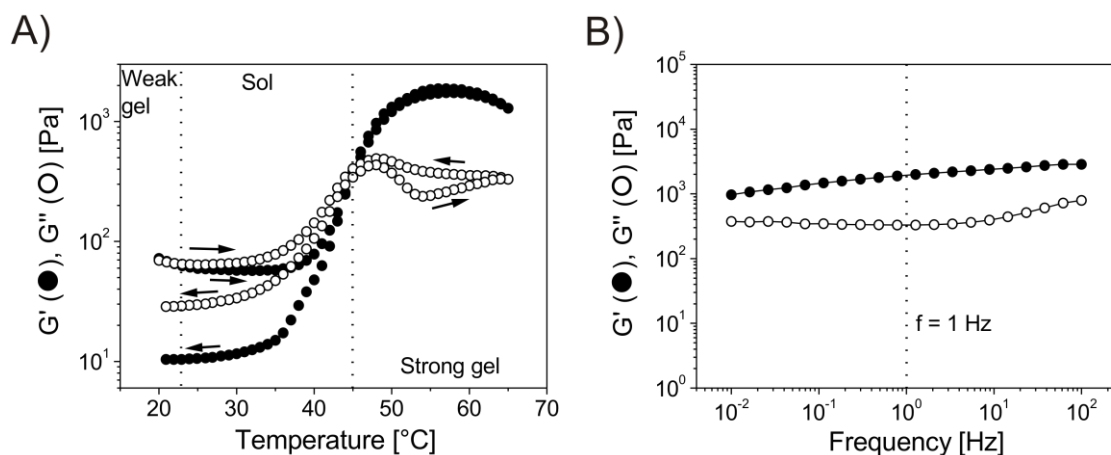


Figure 6.7. Rheological properties of a 20 wt% aqueous solution of P2VP₅₆-*b*-PEO₃₇₀-*b*-P[(MEO₂MA)₈₉-*co*-(MEO_{8.5}MA)₇] at pH = 7: A) temperature dependence of G' and G'' (0.1 K/min, $f = 1$ Hz, $\gamma = 1\%$), B) frequency dependence of G' and G'' at 55 °C ($\gamma = 0.7\%$).

6.3.4.2 P2VP₅₆-*b*-PEO₃₇₀-*b*-PDMAEMA₇₀

As already pointed out, PDMAEMA is of special interest since it is responsive to both pH and temperature. At pH < 7, PDMAEMA ($pK_a \approx 6.2$)²¹ is significantly charged due to protonation, and therefore water soluble even at very high temperatures. With increasing pH, PDMAEMA gets continuously deprotonated and therefore becomes more and more hydrophobic. As a result, PDMAEMA exhibits a lower critical solution temperature (LCST) for pH ≥ 7 , being strongly pH dependent.²¹ Consequently, the thermo-responsiveness of the PDMAEMA corona of the CSC micelles formed by P2VP₅₆-*b*-PEO₃₇₀-*b*-PDMAEMA₇₀ at pH > 5 (Scheme 6.2), and in turn the temperature at which the CSC micelles form an open association, can be easily tuned by pH adjustment. Furthermore, an increasing number of charges located in the micellar corona upon decreasing the pH should result in a stronger intermicellar repulsion, i.e., an increased effective volume fraction of the CSC micelles. This in turn provides the possibility to additionally tune the mechanical properties of the low temperature gel phase, which is based on a close packing of micelles, by adjusting the pH.

This is demonstrated in Figure 6.8. The pH of a 13.5 wt% solution of P2VP₅₆-*b*-PEO₃₇₀-*b*-PDMAEMA₇₀ was adjusted to a value of 8 and 9, respectively, by using appropriate buffer solutions for the hydrogel preparation, and the temperature-dependent dynamic moduli were measured. The sample held at pH = 8 appears as a strong, free-standing gel at room temperature, formed by a close packing of CSC micelles. Upon heating, a gel-sol transition occurs at 40 °C, which is most probably caused by a shrinkage of the micellar corona (Figure 6.8A).^{9,11} Although we were able to detect a cloud point at 53.8 °C for the corresponding

PDMAEMA-1 homopolymer (Figure 6.10, Supporting Information), we did not observe a sol-gel transition at pH = 8 and elevated temperatures. This phenomenon cannot be attributed to the influence of the hydrophilic PEO block, since a dilute solution of P2VP₅₆-*b*-PEO₃₇₀-*b*-PDMAEMA₇₀ at pH = 8 shows clouding at an even lower temperature (ca. 49 °C, results not shown). A satisfying explanation can be given, taking into account that the slightly charged PDMAEMA promotes electrostatic repulsion between the micelles, which in turn might prevent an effective intermicellar crosslinking. As a result, the sample does not form a gel via open association of CSC micelles above the cloud point of the PDMAEMA block.

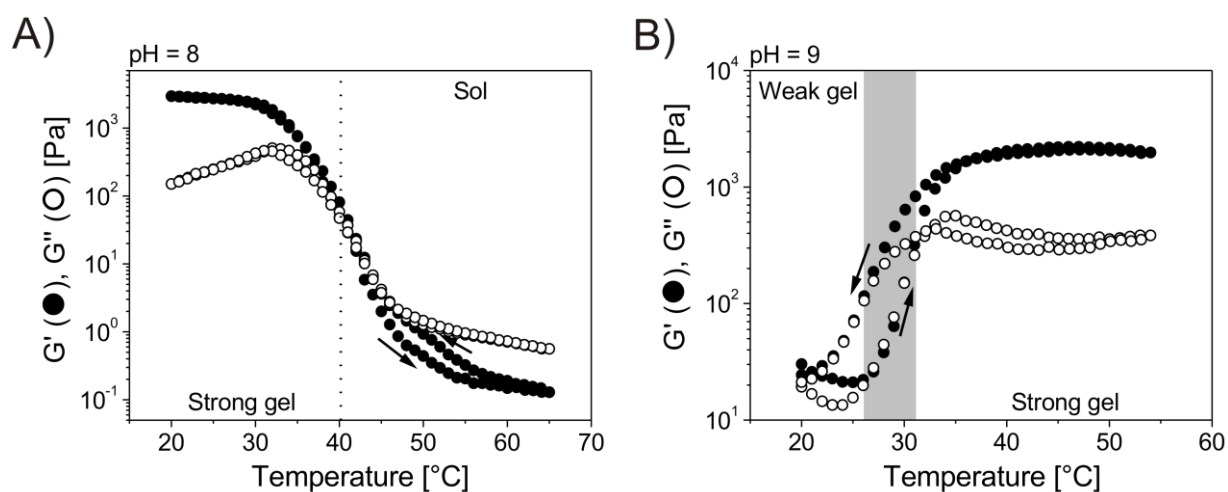


Figure 6.8. Temperature dependence of G' and G'' for a 13.5 wt% aqueous solution of P2VP₅₆-*b*-PEO₃₇₀-*b*-PDMAEMA₇₀ ($f = 1$ Hz, $\gamma = 0.7\%$, 0.1 K/min): A) at pH = 8, and B) at pH = 9.

The sample at pH = 9, where the PDMAEMA corona should be almost uncharged and therefore less expanded in comparison to pH = 8, exhibits much lower moduli at room temperature (Figure 6.8B). G' still exceeds G'' , but the sample flows under gravitational forces, as revealed by test tube inversion, and the loss factor is rather high ($\tan\delta = G''/G' = 0.65$), which points to the presence of a weak gel. Analogous to the behaviour of the P2VP₅₆-*b*-PEO₃₇₀-*b*-P[(MEO₂MA)₈₉-*co*-(MEO_{8.5}MA)₇] based hydrogel, G'' starts to exceed G' upon increasing temperature, indicating the break-up of a weakly ordered micellar packing. The transition is not very pronounced and further overlapped with an increase of both moduli with temperature. At temperatures above 32 °C a strong gel is formed, evidenced by a rather low loss factor ($\tan\delta(45^\circ\text{C}) = 0.17$) and a high storage modulus ($G'(45^\circ\text{C}) = 2.2$ kPa). In this case, the hydrogel is formed by an open association of the CSC micelles (Scheme 2). It is noted, that the sol-gel transition temperature at pH = 9 ($T_{\text{SG}} = 32$ °C) is significantly decreased with respect to the cloud point of the corresponding PDMAEMA-1 homopolymer ($T_{\text{CP}} = 42.4$ °C; Figure 6.10, Supporting Information). As reported by Plamper et al., the change from a linear

to a star-shaped architecture decreases the cloud point of PDMAEMA to a significant extent at high pH.²¹ This shift gets more pronounced with increasing arm number, and in turn increasing molecular weight. The CSC micelles formed by P2VP₅₆-*b*-PEO₃₇₀-*b*-PDMAEMA₇₀ can be considered as star-shaped aggregates with high arm numbers, explaining the observed strong shift of the cloud point to lower temperatures.

It is noted, that gel formation does not occur at room temperature and pH < 8, keeping the concentration constant (results not shown). In order to understand this phenomenon, we performed pH-dependent dynamic light scattering (DLS) on a dilute P2VP₅₆-*b*-PEO₃₇₀-*b*-PDMAEMA₇₀ solution (Figure 6.11, Supporting Information). We observed that the hydrodynamic radius of the micelles decreases with decreasing pH. This is contrary to the expected behaviour, since the charge density within the PDMAEMA corona should be increased, resulting in a stretching of the chains. Furthermore, the fraction of larger aggregates, being present in the solution, too, increases with decreasing pH. From these findings it can be deduced, that an interaction between PDMAEMA and PEO takes place at low pH, which is most likely attributed to hydrogen bonding between the protonated PDMAEMA units and PEO. In general, the effective volume fraction of the micelles, which influences the ability to form a gel at room temperature, is affected by two antagonistic processes. On the one hand, the micellar corona shrinks if the pH is decreased, because of the aforementioned interactions with the PEO shell. At the same time, however, the electrostatic repulsion between the PDMAEMA chains is increased, which in turn increases the effective volume occupied by the micelles. At pH = 8, the contribution from the electrostatic repulsion obviously dominates, as we obtain a strong gel under these conditions (Figure 6.8A). At lower pH, however, the shrinkage of the micellar corona becomes more and more important until finally gel formation does not take place anymore.

In conclusion, it is possible to completely alter the temperature-dependent behaviour of P2VP-*b*-PEO-*b*-PDMAEMA based hydrogels just by small variations in the pH value. At pH = 9 a weak gel-strong gel transition is observed upon heating, whereas at pH = 8 a strong gel-sol transition occurs. Upon a further decrease in pH gel formation is completely prevented.

As a last step, we wanted to introduce UV sensitivity to the hydrogel. As shown by Plamper et al., PDMAEMA exhibits an upper critical solution temperature (UCST) in the presence of trivalent hexacyanocobaltate(III) ions at a suitable pH.²² This is due to electrostatic

interactions, inducing a crosslinking effect. We utilized this effect to trigger an open association of the CSC micelles at low temperatures, too. $[\text{Co}(\text{CN})_6]^{3-}$ ions are sensitive to UV light, which is expressed by an exchange of one cyanide ligand with H_2O (photo-aquation). The resulting $[\text{Co}(\text{CN})_5\text{H}_2\text{O}]^{2-}$ ions are only divalent, and thus the induced UCST vanishes upon exposure to UV light.²² With respect to our system, this should result in a gel disintegration upon illumination.

The pH of a 15.2 wt% solution of $\text{P2VP}_{56}\text{-}b\text{-PEO}_{370}\text{-}b\text{-PDMAEMA}_{70}$ was adjusted to 7.5 in order to have a sufficient amount of positive charges in the micellar corona, ensuring a strong interaction between the partially protonated PDMAEMA chains and trivalent $[\text{Co}(\text{CN})_6]^{3-}$ ions. As mentioned before, the sample is a free-flowing liquid at $\text{pH} = 7.5$. The $\text{K}_3[\text{Co}(\text{CN})_6]$ solution was added dropwise to the sample under rigorous stirring. After each addition and a short waiting period the sample tube was inverted in order to check whether the sample flows or not. If gel formation occurred, the gel-sol transition point was determined by a stepwise heating. A corresponding phase diagram in dependence on the $[\text{Co}(\text{CN})_6]^{3-}$ concentration is shown in Figure 6.9. Gel formation is observed for the first time at a $[\text{Co}(\text{CN})_6]^{3-}/\text{DMAEMA}$ molar ratio of 0.16. In comparison, for star-shaped PDMAEMA ($M_n = 480 \text{ kg/mol}$) at $\text{pH} = 8$, a minimum molar ratio of about 0.39 was necessary to induce a UCST.²² This difference might be explained taking into account that Plamper et al. considered the precipitation of the PDMAEMA stars as the transition point, i.e., the point at which the polymer completely collapses. In our case, however, the UCST is monitored via the gelation of the micellar solution, which presumably requires much less $[\text{Co}(\text{CN})_6]^{3-}$ ions. Moreover, the significantly higher polymer concentration applied in the gelation studies might contribute to the observed reduction of the critical $[\text{Co}(\text{CN})_6]^{3-}/\text{DMAEMA}$ ratio necessary to induce a UCST, too. Analogous to the behaviour of the PDMAEMA stars,²² the UCST is shifted to higher temperatures with increasing $[\text{Co}(\text{CN})_6]^{3-}/\text{DMAEMA}$ ratio (Figure 6.9). Finally, at a ratio of 0.26 phase separation occurs, though only with a very slow rate (within hours).

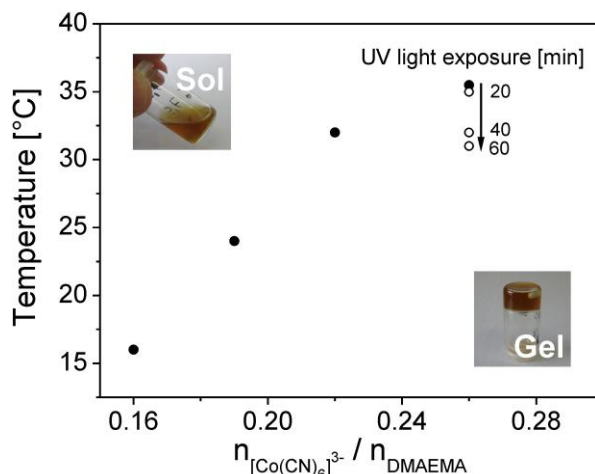


Figure 6.9. Gel-sol transition temperatures of a 15.2 wt% aqueous solution of P2VP₅₆-*b*-PEO₃₇₀-*b*-PDMAEMA₇₀ at pH = 7.5 in dependence on the molar ratio of hexacyanocobaltate(III) to DMAEMA units. The photographs show the sample in the gel and the sol state, respectively. The open symbols represent gel-sol transition temperatures after exposure to UV light with a wavelength band of 310 – 400 nm for the indicated time intervals.

In order to demonstrate the UV switchability of the gel, the sample was placed under a UV lamp emitting light of wavelengths between 310 and 400 nm. For a $[Co(CN)_6]^{3-}/DMAEMA$ molar ratio of 0.26, the gel-sol transition temperature ($T_{GS} = 35.5$ °C) shifts only slightly to lower temperatures upon illumination and finally settles at 31 °C. The relatively long illumination times can be lowered to a significant extent (from 60 to 15 min) by decreasing the sample tube diameter (from 1.5 cm to 3 mm). However, a further shift of the gel-sol transition temperature below 31 °C with continuing illumination does not occur. This might result from the fact, that the UV sensitivity is expressed by a change in valency of the cobaltate counterions from III to II upon illumination. Thus, it is reasonable to assume that divalent counterions can still act as crosslinking agents between the micelles, but with a lower efficiency.

In consequence, a gel disintegration can be induced within a certain temperature window by illumination with UV light. Further studies including adjustment of block lengths, pH, concentration, and ionic strength have to be carried out in order to optimize the system.

6.4 Conclusion

P2VP-*b*-PEO-*b*-P(MEO₂MA-*co*-MEO_{8.5}MA) and P2VP-*b*-PEO-*b*-PDMAEMA triblock terpolymers were successfully synthesized by a combination of anionic polymerization and ATRP utilizing the 1,3-dipolar Huisgen cycloaddition (“click” reaction). The key step was the

coupling of PDMAEMA or POEGMA with a P2VP-*b*-PEO diblock copolymer via the “click” reaction. For that purpose, azido end-functionalized P2VP-*b*-PEO-N₃ precursors were synthesized by sequential anionic polymerization followed by termination with azide containing acid chlorides. Alkyne end-functionalized PDMAEMA and POEGMA homopolymers, on the other hand, were obtained by ATRP using an initiator with an alkyne function. Two different azide containing moieties were tested. “Click” reactions in which an azidoacetyl group was involved proceeded straightforward, yielding well-defined triblock terpolymers. In contrast, a cleavage of the initially formed triblock terpolymer via nucleophilic substitution of the triazol ring occurred when the 2-azidoisobutyryl moiety was used. This was attributed to traces of the strongly hygroscopic phosphazene base *t*-BuP₄, remaining in the diblock copolymer precursor.

A 20 wt% aqueous solution of P2VP₅₆-*b*-PEO₃₇₀-*b*-P[(MEO₂MA)₈₉-*co*-(MEO_{8.5}MA)₇] was shown to form a strong gel based on an open association of CSC micelles at pH = 7 and temperatures above the cloud point of the P[(MEO₂MA)₈₉-*co*-(MEO_{8.5}MA)₇] block. At room temperature, on the other hand, a weak gel was obtained due to a fractal arrangement of the micelles (percolation network).

The temperature-dependent phase behaviour of P2VP-*b*-PEO-*b*-PDMAEMA based hydrogels can be easily varied by small variations in the pH value. A 13.5 wt% solution of P2VP₅₆-*b*-PEO₃₇₀-*b*-PDMAEMA₇₀ at pH = 8 formed a strong gel at room temperature but not at elevated temperatures. This was attributed to electrostatic repulsion between the CSC micelles originating from their slightly charged PDMAEMA corona, hindering the open association of micelles above the cloud point of PDMAEMA. At pH = 9, only a weak gel was formed at room temperature, with a transition to a strong gel at $T > 32$ °C, since the PDMAEMA corona is almost uncharged under these conditions but exhibits a cloud point in this temperature range. At pH < 8, gel formation was prevented by a significant decrease of the effective micellar size, most probably originating from hydrogen bonding between protonated PDMAEMA and PEO units. Gelation, however, could be easily induced under these conditions by the addition of trivalent hexacyanocobaltate(III) ions, interacting with the charged PDMAEMA chains, and therefore inducing an intermicellar crosslinking below a certain temperature (UCST). Exposure of the cobaltate containing gel to UV light caused a disintegration of the gel within a narrow temperature window, due to a reduction of the valency of the cobaltate ions from three to two (photo-aquation).

Acknowledgement

We would like to thank Ingo Rehberg and Reinhard Richter (Experimental Physics V, University of Bayreuth) for providing us with the rheology equipment, Marietta Böhm (MCII, University of Bayreuth) for conducting the SEC measurements, and Felix Plamper (RWTH Aachen) for helpful discussion. Financial support from the German Science Foundation (priority program SPP 1259) is gratefully acknowledged.

6.5 Supporting Information

Synthesis of the azido acid chlorides, propargyl 2-bromoisobutyrate and ethyl 2-(4-acetylmethyl)triazolyl isobutyrate

2-Azidoisobutyryl chloride^{35,36}

37 mL of ethyl 2-bromoisobutyrate (EBiB) and 31 mL ethanol were mixed in a one necked 250 mL flask equipped with a reflux condenser. After addition of 23 g NaN₃, dissolved in 60 mL H₂O, the mixture was refluxed for 20 h at 98 °C. Afterwards, the organic phase was separated and the remaining ethanol was removed using a rotary evaporator. The organic phase was then extracted twice with H₂O and dried with CaCl₂. The first intermediate product, ethyl 2-azidoisobutyrate, was finally obtained by vacuum distillation (10 mbar, 51-53 °C). 18 mL of the ester were then mixed with 8.14 g KOH, dissolved in 28 mL H₂O containing 10 vol% ethanol, and subsequently heated to 80-100 °C until the organic phase disappeared. After additional stirring for half an hour at 80-100 °C, the solution was poured over ice, acidified with conc. sulfuric acid, and extracted three times with diethyl ether. The combined organic fractions were washed with water and dried over Na₂SO₄. The second intermediate product, 2-azidoisobutyric acid, was obtained by vacuum distillation (1.9 mbar, 70 °C). In a last step, 9 mL of the acid were transferred to a flask equipped with a dropping funnel and a reflux condenser. The whole apparatus was held under nitrogen atmosphere. 7.5 mL of thionyl chloride were added dropwise to the preheated acid (50 °C), and subsequently the temperature was raised to 85 °C. After the release of HCl had ceased, the mixture was refluxed for 1 h. Afterwards, the reflux condenser was removed and a distillation apparatus was attached to the flask. The final product was obtained by vacuum distillation.

*Azidoacetyl chloride*³⁷

46 g of bromo acetic acid were dissolved in 100 mL NaOH solution (3.3 M) under cooling. Subsequently, 25 g of NaN₃ and 10 mL of diethyl ether were added. The whole mixture was refluxed for approximately 60 h at 40 °C. Afterwards, 175 mL of an ice/H₂SO₄ (2 M) mixture were added and the solution was extracted three times with diethyl ether. The combined organic fractions were dried over Na₂SO₄, and diethyl ether was removed using a rotary evaporator. The obtained crude product was transferred into the corresponding acid chloride according to the procedure described for the synthesis of 2-azidoisobutryl chloride.

*Propargyl 2-bromoisobutyrate*³⁸

29 mL of propargyl alcohol were mixed with 69 mL triethylamine and 150 mL dichloromethane. After cooling down to 0 °C, 115 g of 2-bromoisobutryl bromide were added dropwise and the reaction mixture was stirred for 24 h at room temperature. Subsequently, the mixture was filtrated, washed with saturated sodium chloride solution, and dried over Na₂SO₄. After the solvent was removed, the final product was obtained by vacuum distillation.

Ethyl 2-(4-acetylmethyl)triazolyl isobutyrate

10 g propargyl acetate (Aldrich, 98%), 16 g ethyl 2-azidoisobutyrate (synthesized according to the procedure described above), 8 mg CuBr, and 50 mL THF were mixed in a reaction vessel equipped with a septum. After degassing by purging with N₂ for 30 min, 40 μL of degassed PMDETA were added. After one day, the mixture was passed through a basic alumina column, and the THF was removed using a rotary evaporator. The remaining product was used without further purification.

Cloud point measurements

P(MEO₂MA-*co*-MEO_{8.5}MA)-2 was dissolved in Millipore water. PDMAEMA-1 was dissolved in pH = 8 and pH = 9 buffer (AVS Titrimorm), respectively. In each case, the concentration was fixed to 2.5 g/L. The cloud points were determined by turbidity measurements using a titrator (Titrand 809, Metrohm, Herisau, Switzerland) equipped with a turbidity probe ($\lambda_0 = 523$ nm, Metrohm) and a temperature sensor (Pt 1000, Metrohm). The temperature program (heating rate: 1 K/min) was run by a thermostat (LAUDA RE 306 and

Wintherm_Plus software), using a homemade thermostatable vessel. The cloud points were determined from the intersection of the two tangents applied to the two linear regimes of the transmittance curves at the onset of turbidity. The cloud point of P(MEO₂MA-co-MEO_{8.5}MA)-2 is located at 32.8 °C (Fig. 6.10A), whereas the cloud point of PDMAEMA-1 was found to be 53.8 °C at pH = 8, and 42.4 °C at pH = 9 (Fig. 6.10B), respectively.

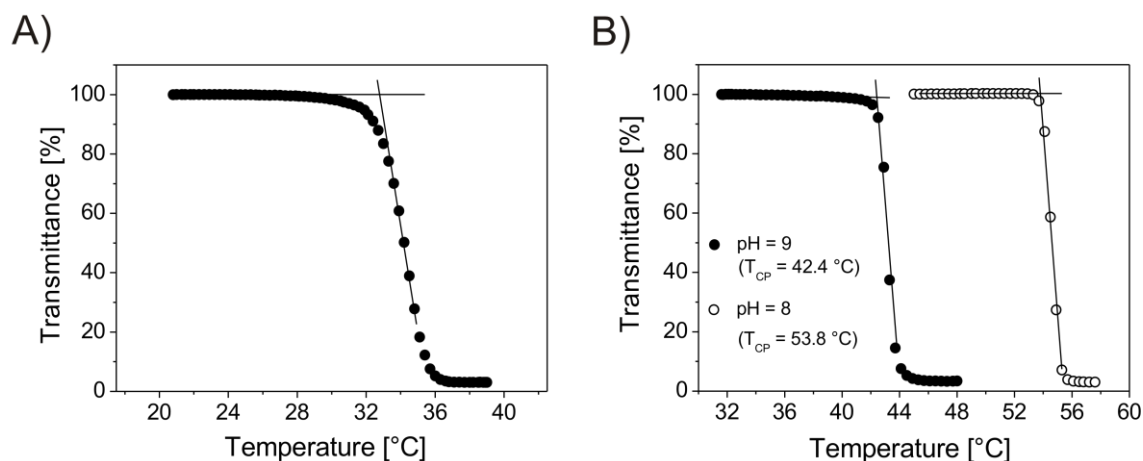


Figure 6.10. Temperature-dependent transmittance (2.5 g/L, 1 K/min) for aqueous solutions of: a) P(MEO₂MA-co-MEO_{8.5}MA)-2, and b) PDMAEMA-1 at pH = 8 and pH = 9, respectively.

pH-dependent dynamic light scattering (DLS)

DLS was performed on an ALV DLS/SLS-SP 5022F compact goniometer system with an ALV 5000/E cross-correlator and a He-Ne laser ($\lambda_0 = 632.8$ nm). The solutions (1g/L) were filtered with 0.8 μm syringe filters (Cameo) prior to the measurement. The decaline bath of the instrument was kept at 20 °C using a LAUDA Proline RP 845 thermostat. The pH sweep was conducted using the DLS device in combination with a titrator (Titrand 809, Metrohm, Herisau, Switzerland). NaOH (titer 1M, Titrisol, Merck) was added in small portions of 2 μL , applying an equilibration time of 3 min after each titration step. All scattering data presented correspond to an average of five measurements, conducted for 1 min each. Figure 6.11 shows the distribution of apparent hydrodynamic radii of P2VP₅₆-*b*-PEO₃₇₀-*b*-PDMAEMA₇₀ CSC micelles (P2VP core, PEO shell and PDMAEMA corona) at different pH. Two distributions are visible for each pH, indicating the presence of a major fraction of single CSC micelles ($R_{h,app} = 17\text{-}20$ nm) and some bigger micellar aggregates ($R_{h,app} \approx 100$ nm). The radius of the micelles decreases and the fraction of the bigger aggregates increases with decreasing pH ($pK_b(\text{PDMAEMA}) \approx 7.7^{21}$). These findings point to intra- and intermicellar interactions between protonated DMAEMA and PEO chains most likely due to hydrogen bonding.

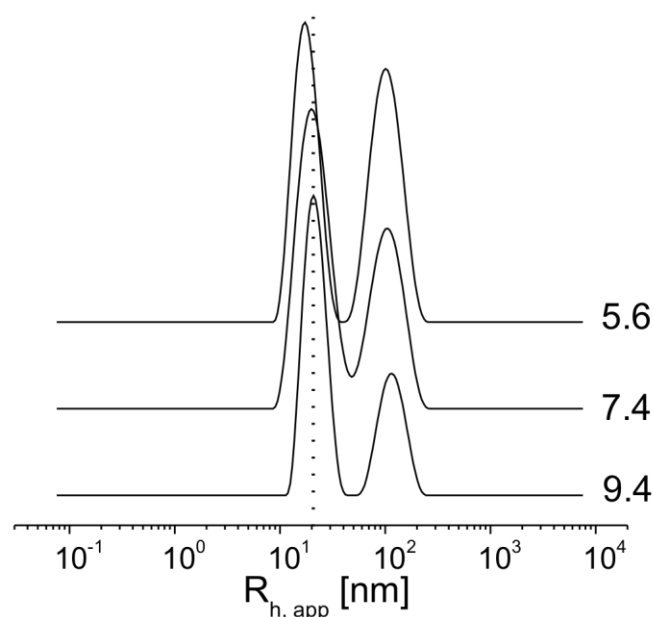


Figure 6.11. Intensity-weighted distribution of apparent hydrodynamic radii ($R_{h,app}$) of an aqueous solution of P2VP₅₆-*b*-PEO₃₇₀-*b*-PDMAEMA₇₀ at different pH (1 g/L; $\theta = 90^\circ$). The distributions of hydrodynamic radii were obtained using the CONTIN algorithm.

6.6 References

- [1] Baskaran, D.; Müller, A. H. E. *Prog. Polym. Sci.* **2007**, *32*, 173.
- [2] Matyjaszewski, K.; Müller, A. H. E., *Controlled and Living Polymerizations - From Mechanisms to Applications*. Wiley-VCH: Weinheim, 2009.
- [3] Hadjichristidis, N.; Pispas, S.; Floudas, G. A., *Block Copolymers - Synthetic Strategies, Physical Properties and Applications*. John Wiley & Sons: Hoboken, New Jersey, 2003.
- [4] Ahn, S.-k.; Kasi, R. M.; Kim, S.-C.; Sharma, N.; Zhou, Y. *Soft Matter* **2008**, *4*, 1151.
- [5] He, C.; Kim, S. W.; Lee, D. S. *J. Controlled Release* **2008**, *127*, 189.
- [6] Tsitsilianis, C. *Soft Matter* **2010**, *6*, 2372.
- [7] Guenther, M.; Kuckling, D.; Corten, C.; Gerlach, G.; Sorber, J.; Suchaneck, G.; Arndt, K. F. *Sens. Actuators, B* **2007**, *126*, 97.
- [8] Yu, L.; Ding, J. *Chem. Soc. Rev.* **2008**, *37*, 1473.
- [9] Reinicke, S.; Schmelz, J.; Lapp, A.; Karg, M.; Hellweg, T.; Schmalz, H. *Soft Matter* **2009**, *5*, 2648
- [10] Ah Toy, A.; Reinicke, S.; Müller, A. H. E.; Schmalz, H. *Macromolecules* **2007**, *40*, 5241.
- [11] Reinicke, S.; Karg, M.; Lapp, A.; Heymann, L.; Hellweg, T.; Schmalz, H. *Macromolecules* **2010**, *submitted*.

- [12] Banks, P.; Peters, R. H. *J. Polym. Sci., Part A: Polym. Chem.* **1970**, *8*, 2595.
- [13] Stolarzewicz, A. *Makromol. Chem.* **1986**, *187*, 745.
- [14] Stolarzewicz, A.; Grobelny, Z. *Makromol. Chem.* **1992**, *193*, 531.
- [15] Dworak, A.; Panchev, I.; Trzebicka, B.; Walach, W. *Macromol. Symp.* **2000**, *153*, 233.
- [16] Hans, M.; Keul, H.; Möller, M. *Polymer* **2009**, *50*, 1103.
- [17] Han, S.; Hagiwara, M.; Ishizone, T. *Macromolecules* **2003**, *36*, 8312.
- [18] Lutz, J.-F.; Hoth, A. *Macromolecules* **2005**, *39*, 893.
- [19] Mertoglu, M.; Garnier, S.; Laschewsky, A.; Skrabania, K.; Storsberg, J. *Polymer* **2005**, *46*, 7726.
- [20] Plamper, F. A.; Schmalz, A.; Penott-Chang, E.; Drechsler, M.; Jusufi, A.; Ballauff, M.; Müller, A. H. E. *Macromolecules* **2007**, *40*, 5689.
- [21] Plamper, F. A.; Ruppel, M.; Schmalz, A.; Borisov, O.; Ballauff, M.; Müller, A. H. E. *Macromolecules* **2007**, *40*, 8361.
- [22] Plamper, F. A.; Schmalz, A.; Müller, A. H. E. *J. Am. Chem. Soc.* **2007**, *129*, 14538.
- [23] Schacher, F.; Müllner, M.; Schmalz, H.; Müller, A. H. E. *Macromol. Chem. Phys.* **2009**, *210*, 256.
- [24] Kloninger, C.; Rehahn, M. *Macromolecules* **2004**, *37*, 1720.
- [25] Sheikh, M. R. K.; Tharanikkarasu, K.; Imae, I.; Kawakami, Y. *Macromolecules* **2001**, *34*, 4384.
- [26] Sheikh, M. R. K.; Imae, I.; Tharanikkarasu, K.; Lestrat, V. M.-J.; Kawakami, Y. *Polym. J.* **2000**, *32*, 527.
- [27] Kamigaito, M.; Ando, T.; Sawamoto, M. *Chem. Rev.* **2001**, *101*, 3689.
- [28] Matyjaszewski, K.; Xia, J. *Chem. Rev.* **2001**, *101*, 2921.
- [29] Kolb, H. C.; Finn, M. G.; Sharpless, K. B. *Angew. Chem., Int. Ed.* **2001**, *40*, 2004.
- [30] Huisgen, R. *Angew. Chem., Int. Ed.* **1963**, *2*, 633.
- [31] Huisgen, R. *Angew. Chem., Int. Ed.* **1963**, *2*, 565.
- [32] Binder, W. H.; Sachsenhofer, R. *Macromol. Rapid Commun.* **2007**, *28*, 15.
- [33] Hein, C. D.; Liu, X.-M.; Wang, D. *J. Pharm. Sci.* **2008**, *25*, 2216.
- [34] Sumerlin, B. S.; Vogt, A. P. *Macromolecules* **2009**, *43*, 1.
- [35] Forster, M. O.; Fierz, H. E. *J. Chem. Soc., Trans.* **1908**, *93*, 669.
- [36] Huber, W. F. *J. Am. Chem. Soc.* **1955**, *77*, 112.
- [37] Wieland, T. H.; Hennig, H. J. *Chem. Ber.* **1960**, *93*, 1236.

- [38] Gang-Yin, S.; Xue-Zhi, T.; Cai-Yuan, P. *J. Polym. Sci., Part A: Polym. Chem.* **2008**, *46*, 2390.
- [39] Lutz, J.-F. *Angew. Chem., Int. Ed.* **2008**, *47*, 2182.
- [40] Becer, C. R.; Hoogenboom, R.; Schubert, U. S. *Angew. Chem., Int. Ed.* **2009**, *48*, 4900.
- [41] Zeng, F.; Shen, Y.; Zhu, S. *Macromol. Rapid Commun.* **2002**, *23*, 1113.
- [42] Coessens, V.; Matyjaszewski, K. *Macromol. Rapid Commun.* **1999**, *20*, 66.
- [43] Gao, H.; Louche, G.; Sumerlin, B. S.; Jahed, N.; Golas, P.; Matyjaszewski, K. *Macromolecules* **2005**, *38*, 8979.
- [44] Whittaker, M. R.; Urbani, C. N.; Monteiro, M. J. *J. Am. Chem. Soc.* **2006**, *128*, 11360.
- [45] Vogt, A. P.; Sumerlin, B. S. *Macromolecules* **2006**, *39*, 5286.
- [46] Mustafa, D.; Nasrettin, G. *Macromol. Chem. Phys.* **2009**, *210*, 1617.
- [47] Xiaohua, H.; Liyuan, L.; Kai, W.; Shaoliang, L.; Deyue, Y.; Yiqun, Z. *J. Appl. Polym. Sci.* **2009**, *111*, 560.
- [48] Ozcan, A.; Gurkan, H.; Umit, T. *J. Polym. Sci., Part A: Polym. Chem.* **2006**, *44*, 5699.
- [49] Winter, H. H.; Mours, M. *Adv. Polym. Sci.* **1997**, *134*, 165.
- [50] Nishinari, K. *Prog. Colloid. Polym. Sci.* **2009**, *136*, 87.
- [51] Chaibundit, C.; Ricardo, N. M. P. S.; Costa, F. d. M. L. L.; Yeates, S. G.; Booth, C. *Langmuir* **2007**, *23*, 9229.
- [52] Stokes, J. R.; Frith, W. J. *Soft Matter* **2008**, *4*, 1133.

7 Magneto-responsive hydrogels based on maghemite/triblock terpolymer hybrid micelles

Stefan Reinicke^a, Stefan Döhler^a, Sandrine Tea^a, Marina Krekhova^a, Renate Messing^b,
Annette M. Schmidt^b, and Holger Schmalz^{a,*}

a) Makromolekulare Chemie II, Universität Bayreuth, D-95440 Bayreuth, Germany

b) Institut für Organische Chemie und Makromolekulare Chemie, Heinrich-Heine-Universität Düsseldorf, D-40225 Düsseldorf, Germany

ABSTRACT:

We report on a new approach towards magneto-responsive hydrogels, showing a reversible gelation upon inductive heating via AC magnetic fields. An aqueous solution of a triblock terpolymer with a partially quaternized poly(2-vinylpyridine) (Pq2VP) outer block, a water soluble poly(ethylene oxide) (PEO) middle block and a thermo-sensitive poly(glycidyl methyl ether-*co*-ethyl glycidyl ether) (P(GME-*co*-EGE)) end block (Pq2VP-*b*-PEO-*b*-P(GME-*co*-EGE)) was mixed with a solution of sodium citrate stabilized superparamagnetic maghemite nanoparticles. Due to electrostatic interactions between the oppositely charged particles surface and the Pq2VP block of the triblock terpolymer, well-defined hybrid micelles with a superparamagnetic core were formed. The number of triblock terpolymer chains stabilizing the nanoparticles was found to be constant above a critical triblock terpolymer/maghemite ratio, i.e. for higher polymer contents hybrid micelles and free (non-bound) triblock terpolymers are present in solution. Thermo-reversible hydrogels are formed via an open association of hybrid micelles at temperatures above the cloud point of the P(GME-*co*-EGE) corona blocks, which form the network junctions. The superparamagnetic character of the maghemite nanoparticles enables contactless heating, and thus gelation, by applying AC magnetic fields, as demonstrated by high frequency magnetocalorimetry. The thermo-reversible

gelation and the dynamic-mechanical properties of the hydrogels were studied by rheology.

7.1 Introduction

The field of “smart” hydrogels includes gels which respond to pH, ionic strength, temperature, light, electric fields, or redox processes.¹⁻⁷ Recently, magnetic fields achieve growing interest as highly selective stimulus. Magneto-responsive hydrogels, also called ferrohydrogels, usually consist of a crosslinked polymer forming the gel matrix, and magnetic nanoparticles being dispersed in the matrix.⁸ The magnetic nanoparticles provide the sensitivity to magnetic fields by transferring the forces acting on the nanoparticle to the surrounding polymer network. The application of a nonuniform magnetic field causes an attraction of the nanoparticles to regions of higher field strengths, and thus can lead to a contraction or deformation of the gel. This can be utilized in actuating systems, e.g. for robots, or other devices like switches, seals, or damping controls.⁸⁻¹¹ In contrast, uniform magnetic fields result in an alignment of the nanoparticles parallel to the field direction. This can be used to influence the strength/rigidity of the gel matrix in order to tune the release properties of hydrogels for drug delivery purposes.¹²⁻¹⁵ In addition, hydrogels with anisotropic swelling or mechanical properties can be produced by crosslinking the polymeric matrix while it is exposed to an uniform magnetic field, causing the alignment of the incorporated magnetic nanoparticles.¹⁶⁻¹⁸

The property of superparamagnetic particles to dissipate local heat upon the application of AC magnetic fields is very attractive for several fields of application.^{19,20} Inductive heating so far finds a widespread use in hyperthermia applications, i.e. for cancer therapy.^{21,22} The combination of magnetic heatability with a polymeric matrix, which is sensitive to temperature changes, leads to systems which can be used for drug delivery,^{23,24} and shape transition applications.²⁵ Moreover, flocculation of magnetic core-shell nanoparticles grafted with a thermo-responsive polymer shell can be remotely controlled via AC magnetic fields.^{23,26,27}

Currently, most ferrohydrogels described in literature are based on covalent networks, with the magnetic nanoparticles being dispersed, or prepared, within a solution of the polymer, followed by a subsequent chemical crosslinking to form the network. Frequently used water soluble polymers are poly(vinyl alcohol),^{9,10,12,16} poly(acryl amide) and

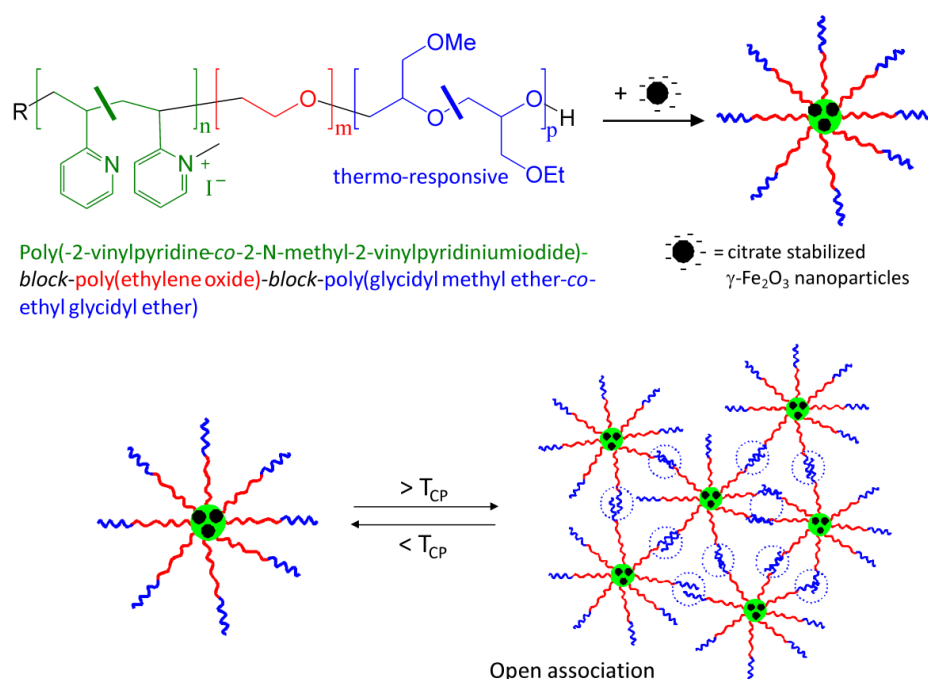
derivatives,^{28,29} hydroxypropyl cellulose,³⁰ and gelatine¹⁴. A disadvantage of these chemical gels is the irreversibility of the gelation, i.e. once the gel is formed, the shape and mechanical properties of the gels are fixed. This drawback can be overcome by using physically crosslinked gels, showing for example a reversible temperature-induced gelation. However, only a few examples of physically crosslinked magnetic hydrogels are reported. Thermo-reversible poly(vinyl alcohol) (PVA) hydrogels were prepared via consecutive freeze-thaw cycles, with physical crosslinks based on hydrogen bonding or PVA crystallites.¹³ Magneto-responsive hydrogels based on polysaccharides,³¹ showing a temperature-induced coil-helix transition, and PluronicTM-type block copolymers,³² forming gels via a regular packing of micelles, were reported, too.

However, in the described thermo-responsive hydrogels the magnetic nanoparticles are only dispersed in the hydrogel matrix but not chemically or physically bound to the polymer network, which might result in a release of magnetic nanoparticles from the hydrogel over time. To prevent particle leaching, it is desirable to fix them permanently to the gel network. Although preparation techniques are available to chemically or physically bind polymer chains onto magnetic nanoparticles, these techniques have not been applied to the construction of magneto-responsive physical hydrogels yet. One example for the covalent coupling of polymers and magnetic particles is the grafting of polymer chains directly from the particle surface, like poly(2-methoxyethyl methacrylate),³³ polystyrene,^{26,34-36} and poly(ϵ -caprolactone),^{23,37} using controlled radical and anionic ring-opening polymerization, respectively. Alternatively, a grafting-onto approach using end-functionalized polymers with suitable anchor-groups can be applied.³⁸⁻⁴⁰ Another elegant way is to physically trap magnetic nanoparticles or nanoparticle clusters inside the core of block copolymers micelles via hydrophobic or electrostatic interactions.⁴¹⁻⁴⁸ Functional polymers or diblock copolymers, acting as ligands during the nanoparticle synthesis, have been used for the preparation of magnetic core-shell nanoparticles, too.⁴⁹⁻⁵¹

These techniques can be applied for the construction of magneto-responsive hydrogels. The strategy is to prepare magnetic nanoparticle/triblock terpolymer hybrid micelles with a thermo-responsive corona, that are able to reversibly form an open association at elevated temperatures in order to build up the network structure (Scheme 7.1). Such a micellar hydrogel has two main advantages compared to the common systems. First of all, the nanoparticles are physically trapped in the cores of the micelles, and thus strongly bound to the hydrogel network. This provides a stronger sensitivity to magnetic fields, as

the transfer of the forces, that act on the nanoparticles, to the surrounding polymer network is improved. Second, the gelation process is thermo-reversible, and the dissipative heat loss of the incorporated magnetic particles in AC magnetic fields can be utilized to externally trigger the gel formation by magnetic heating.

For the synthesis of the magneto-responsive hydrogels we follow an electrostatic interaction approach. We utilize poly(2-vinyl pyridine)-*block*-poly(ethylene oxide)-*block*-poly(glycidyl methyl ether-*co*-ethyl glycidyl ether) (P2VP-*b*-PEO-*b*-P(GME-*co*-EGE)) triblock terpolymers, which were originally designed to form pH- and temperature-responsive hydrogels.⁵² By partially quaternizing the P2VP-block, i.e. introducing positive charges, the triblock terpolymer can complex with the negatively charged surface of the nanoparticles due to electrostatic interactions. This is expected to result in the formation of hybrid micelles with a nanoparticle containing complex coacervate core (Scheme 7.1). Here, superparamagnetic γ -Fe₂O₃ (maghemite) nanoparticles, stabilized with a sodium citrate shell, were used.



Scheme 7.1. Formation of hybrid micelles via complexation of citrate stabilized γ -Fe₂O₃ nanoparticles with a quaternized Pq2VP-*b*-PEO-*b*-P(GME-*co*-EGE) triblock terpolymer, and subsequent reversible gelation via open association of hybrid micelles at temperatures above the cloud point (T_{CP}) of the P(GME-*co*-EGE) block.

The formation of well-defined hybrid micelles was studied by dynamic light scattering (DLS), transmission electron microscopy (TEM), thermogravimetric analysis (TGA), and asymmetric flow field-flow fractionation (AF4). Characterization of the magnetic

properties of the micellar solutions by vibrating sample magnetometry (VSM) showed, that the superparamagnetic behaviour of the maghemite nanoparticles was not altered by the incorporation into the hybrid micelles. Furthermore, the temperature-induced gelation was followed by test-tube inversion as well as rheology, revealing that the process is fully reversible. High-frequency magnetocalorimetry was utilized to investigate inductive heating as a remote trigger for gelation.

7.2 Experimental

Materials

Iron(III)-chloride hexahydrate (Fluka, p.a.), iron(II)-chloride tetrahydrate (Fluka > 99 %), ammonium hydroxide solution (Fluka, 25 %), nitric acid (Merck, 65 %), iron(III)-nitrate (Sigma-Aldrich, p.a.), tetrahydrofuran (Sigma-Aldrich, p.a.), methyl iodide (Fluka, > 99.5 %), dimethyl sulfate (Fluka, > 99 %), *n*-hexane (Sigma-Aldrich, p.a.), silver nitrate solution (Grüssing, 0.1 mol/L) and potassium chromate (Grüssing, > 99 %) were used as received. Millipore (Milli-Q, deionized water) water was freshly taken from the Millipore⁺ apparatus, equipped with filtration packs QPAK2E (0.5 µm prefilter, macroreticular activated carbon, high purity mixed bed ion-exchange resin, Organex polisher). The resistance of the Millipore water was always around 18.2 µΩ, ensuring that ions were sufficiently removed.

Synthesis

Maghemite ferrofluid

Maghemite (γ -Fe₂O₃) nanoparticles were synthesized via co-precipitation of ferrous and ferric chloride to produce magnetite (Fe₃O₄) nanoparticles, followed by oxidation to maghemite.^{53,54} Solutions of iron(III)-chloride hexahydrate and iron(II)-chloride tetrahydrate in H₂O (dest.) were mixed under strong stirring, and subsequently poured into a 1.6 M ammonium hydroxide solution. A fast addition was necessary in order to achieve a narrow size distribution of the particles. The black coloured suspension was heated to 60 °C for 10 min under stirring, in order to remove excess ammonium hydroxide. The batch was then cooled down on a neodymium magnet (Fehrenkemper; r = 3 cm, h = 1 cm). After the magnetite particles had settled down, the supernatant solution was removed, and the black precipitate was washed three times with H₂O (dest.) to decrease the pH from 10 to

8. Subsequently, the precipitate was treated with 2 M nitric acid, preheated to 80 °C, in order to oxidize the magnetite particles to maghemite. After 5 min, the nanoparticles were stabilized in the strongly acidic medium by addition of a 0.35 M iron(III)-nitrate solution. The reaction vessel was again placed on the neodymium magnet to separate the maghemite nanoparticles. After the reddish brown suspension settled down, the supernatant clear red solution was removed, and the remaining precipitate was suspended immediately in as less H₂O (dest.) as possible and transferred into a dialysis tube (Spectrum[®] SpectraPor 1, MWCO: 6000-8000). Subsequently, the suspension was dialysed against a 0.005 M sodium citrate solution to exchange the nitrate ions by citrate, resulting in an increase in pH from 2 to 7. Finally, the solution was concentrated using a rotary evaporator until the desired concentration was reached. To remove bigger aggregates, the ferrofluid was filtered several times using a steel wool filled column, being surrounded by a neodymium-iron-boron magnet. The final solids content was determined by gravimetric analysis, and the magnetic component was quantified by VSM.

*P2VP-*b*-PEO-*b*-P(GME-*co*-EGE) triblock terpolymers*

The P2VP-*b*-PEO-*b*-P(GME-*co*-EGE) triblock terpolymers were synthesized by sequential anionic polymerization. A detailed description of the procedure is given elsewhere.^{52,55}

*Quaternized Pq2VP-*b*-PEO-*b*-P(GME-*co*-EGE) triblock terpolymers*

2 g of the P2VP-*b*-PEO-*b*-P(GME-*co*-EGE) triblock terpolymer were dissolved in 200 mL THF, and 2.4 mL methyl iodide were added (10-fold excess of MeI with respect to the number of 2VP units). After stirring for 24 h at room temperature, the reaction was terminated by transferring the solution into a dialysis tube (SpectraPor[™], regenerated cellulose, MWCO ~ 6000-8000 g/mol), followed by dialysis against Millipore water. The molar fraction of quaternized 2VP units was calculated from the iodine content, which was determined by titration with silver nitrate (0.1 mol/L) using potassium chromate as indicator, revealing a degree of quaternization of 20 mol%. In case dimethyl sulfate was used as quaternization agent, 2 g of the P2VP-*b*-PEO-*b*-P(GME-*co*-EGE) triblock terpolymer were dissolved in 200 mL THF, and 7.2 mL dimethyl sulfate were added (18-fold excess of Me₂SO₄ with respect to the number of 2VP units). The solution was stirred at room temperature for 1 week, and the reaction was terminated by repeated precipitation of the solution into *n*-hexane. Here, the degree of quaternization was estimated from the

FT-IR spectrum to ca. 60 mol% (Fig. 7.10, Supporting Information).

Preparation of hybrid micelles

Aqueous solutions of the quaternized Pq2VP-*b*-PEO-*b*-P(GME-*co*-EGE) triblock terpolymer were prepared by direct dissolution in Millipore water (pH ~ 6.5). To obtain the nanoparticle/triblock terpolymer hybrid micelles, a defined amount of the maghemite stock solution (0.27 wt%, pH = 7) was added dropwise to the rigorously stirred solution of the quaternized triblock terpolymer (typically 0.5 to 1 g/L, pH = 7.4). Higher concentrated samples for rheological investigations were prepared in a diluted state (polymer concentration < 10 g/L), first. Subsequently, the solvent was slowly evaporated under mild conditions (room temperature, 70 mbar) until the desired concentration was reached.

Dynamic light scattering (DLS)

DLS was performed on an ALV DLS/SLS-SP 5022F compact goniometer system with an ALV 5000/E cross-correlator and a He-Ne laser ($\lambda = 632.8$ nm). The solutions were filtered prior to the measurement with 0.45 μm syringe filters (Cameo). The overall solids content in each sample, i.e. amount of triblock terpolymer and maghemite, was fixed at 1 g/L. Presented scattering data for standard DLS measurements at room temperature correspond to an average of three measurements, conducted for 1 min each. For the temperature dependent measurements, the decaline bath of the instrument was thermostated using a LAUDA Proline RP 845 thermostat. The temperature was increased stepwise (2 K/step), and after each step the sample was equilibrated for 10 min before data acquisition. Here, single measurements with an acquisition time of 1 min were conducted. For calculation of the presented distribution functions of apparent hydrodynamic radii ($R_{h,\text{app}}$) the CONTIN algorithm⁵⁶ was applied, which yields an intensity-weighted distribution of relaxation times (τ) after an inverse Laplace transformation of the intensity autocorrelation function. The intensity-weighted distribution of the apparent hydrodynamic radius ($R_{h,\text{app}}$) was calculated using the Stokes-Einstein relation: $R_{h,\text{app}} = kT/6\pi\eta D$, where k is the Boltzmann constant, T the absolute temperature, and η the viscosity of the solvent. The apparent diffusion coefficients D were calculated according to $D = (q^2\tau)^{-1}$, where q is the scattering vector defined as $q = (4\pi n/\lambda_0 \sin(\theta/2))$, with n the refractive index of the solvent.

Zeta potential measurements

The ζ potential was determined on a Malvern Zetasizer Nano ZS. Prior to the measurements, the measuring cells (folded capillary cells, Malvern) were rinsed subsequently with ethanol p.a. and Millipore water. The electrophoretic mobilities (u) were converted into ζ potentials *via* the Smoluchowski equation $\zeta = u\eta/\epsilon_0\epsilon$, where η denotes the viscosity and $\epsilon_0\epsilon$ the permittivity of the solution. Each sample was measured three times and the obtained values were averaged.

Transmission electron microscopy (TEM)

TEM images were taken using a Zeiss 922OMEGA EFTEM (Zeiss NTS GmbH, Oberkochen, Germany) operated at 200 kV. Samples were prepared by placing a drop of a dilute solution of the nanoparticle/triblock terpolymer hybrid micelles (0.3 g/L) onto a carbon-coated copper grid (Electron Microscopy Sciences, 200 mesh). After 20 s, excess solution was removed by blotting with a filter paper. Prior to the measurement, the sample was stained with RuO₄ vapor for 1h.

Cryogenic transmission electron microscopy (cryo-TEM)

For cryo-TEM studies, a 2 μ L droplet of the 15 g/L solution of the nanoparticle/triblock terpolymer hybrid micelles was placed on a lacey carbon-coated copper grid (Electron Microscopy Sciences) where most of the liquid was removed with blotting paper, leaving a thin film stretched over the lace. The specimens were instantly vitrified by rapid immersion into liquid nitrogen and cooled to about 77 K using a temperature-controlled freezing unit (Zeiss Cryobox, Zeiss NTS GmbH, Oberkochen, Germany). The temperature was monitored and kept constant in the chamber during all sample preparation steps. After freezing, the specimen was inserted into a cryo-transfer holder (CT3500, Gatan, München, Germany) and transferred to a Zeiss 922OMEGA EFTEM (Zeiss NTS GmbH, Oberkochen, Germany). Examinations were carried out at temperatures around 95 K. The TEM was operated at an acceleration voltage of 200 kV. Zero-loss filtered micrographs ($\Delta E = 0$ eV) were recorded under reduced dose conditions (100–1000 e/nm²). All images were registered digitally by a bottom-mounted CCD camera (Ultrascan 1000, Gatan) combined and processed with a digital image processing system (Gatan Digital Micrograph 3.9 for GMS 1.4).

Thermogravimetric analysis

Measurements were performed using a Mettler Toledo TGA/SDTA851^e, applying a temperature ramp from 30 – 1000 °C at a heating rate of 10 K/min in the presence of air (flow rate 60 mL/min). For TGA measurements the hybrid micelles were isolated from solution by centrifugation (15000 rpm), followed by drying under vacuum at 40 °C for at least 24 h. Due to the hygroscopic nature of the PEO block, traces of water remained in the dried sample. Thus, the weight of the sample at 150 °C, i.e. after evaporation of remaining water during the TGA scan, was normalized to 100 %.

Asymmetric flow field-flow fractionation (AF4)

AF4 measurements were performed on an Eclipse 2 separation system (Wyatt Technology, USA) equipped with an autosampler, a degasser, and a programmable pump (Isocratic 1200, Agilent Technologies). The flow channel was equipped with a 10 kDa regenerated cellulose membrane and a 350 μm thickness spacer (Wyatt Technology, USA). For online detection a multi-angle laser light scattering detector (Dawn EOS, Wyatt Technology, $\lambda = 690$ nm), and a refractive index detector (Shodex RI-101) were used. Astra Software version 4.90.08 (Wyatt Technology, USA) was used to collect the MALLS, and RI detector signals. The absolute scattering intensity was calculated based on Rayleigh scattering from toluene, and the MALLS detectors sensitivities at various angles were calibrated using pure HPLC grade toluene (Merck), and normalized using an aqueous solution of dextran (MW = 65 000, $R_g = 7$ nm). Degassed and filtered Millipore water containing NaNO₃ (25 mM) and NaN₃ (200 ppm) was used as the carrier solvent. The flow profile was 1 min of an initial focusing step, 50 μL sample injection into the flow channel over 2 min, followed by a sample focusing step of 2 min. The volumetric channel flow rate was set at 1 mL/min and a constant cross-flow rate of 0.60 mL/min was applied for 60 minutes. The sample concentration was typically 1 g/L.

Rheology

Rheology measurements were performed using a Physica MCR 301 rheometer with a cone-plate shear cell geometry ($d = 50$ mm, cone angle = 1°). Prior to the measurements the linear viscoelastic regime was determined performing a strain sweep test at a frequency of 1 Hz for each sample. For the temperature dependent measurements a

frequency of 1 Hz, a strain of 0.7 %, and a heating rate of 0.1 K/min was applied. The temperature was controlled by a Peltier element. For frequency sweeps (10^{-2} to 10^2 Hz) at different temperatures the desired temperature was adjusted by heating the sample slowly at a rate of 0.1 K/min.

Quasi-static vibrating sample magnetometry (VSM)

Magnetization curves were monitored at room temperature with an ADE Magnetics Vibrating Sample Magnetometer EV7 up to a maximum field strength of 2.2 T. A typical experiment consisted of a virgin curve, followed by a full hysteresis loop. Samples were measured in sealed Teflon vessels, placed on a glass sample holder between two poles of an electromagnet, and vibrated at a frequency of 70 Hz.

In order to get information on the maghemite content v_M and the volume-average particle diameter d_v of the superparamagnetic particles, we apply Chantrells method⁵⁷ of using high and low fields expressions of the Langevin equation (eq. 1).

$$M = M_s \left(\coth \alpha - \frac{1}{\alpha} \right) \quad \text{with} \quad \alpha = \frac{\mu_0 m H}{k_B T} \quad (\text{eq. 1})$$

(M sample magnetization, H applied field strength, M_s saturation magnetization of the sample, μ_0 permeability of space, m magnetic moment of a single particle, $k_B T$ thermal energy).

$$v_M = \frac{M_s}{M_{s, Fe_2O_3}} \quad \text{with} \quad M_s = M(H)_{H \rightarrow \infty} \quad (\text{eq. 2})$$

$$d_v = \sqrt[3]{\frac{6m}{\mu_0 \pi}} \quad \text{with} \quad m = \frac{3}{M_s} \frac{k_B T}{\mu_0} \cdot \left(\frac{M}{H} \right)_{H \rightarrow 0} \quad (\text{eq. 3})$$

Here, M_{s, Fe_2O_3} is the saturation magnetization of maghemite nanoparticles in the present size range (325 kA/m).⁵⁸ Using the density of maghemite, $\rho = 4.907 \text{ g/cm}^3$,⁵⁹ we access the mass fraction μ_M of maghemite particles.

HF-Magnetocalorimetry (HF-MC)

The magnetic heating behaviour of ferrofluids and gels was investigated using a Hüttinger HF generator AXIO T5 equipped with a water-cooled copper induction coil. The system was operated between 246 and 385 kHz, depending on the magnetic field strength H between 31.5 kA/m and 3.5 kA/m. The sample volume of 2.0 ml was filled in a glass tube,

sealed and isolated with polyurethane foam, and placed inside the induction coil. The sample temperature was detected with an Opsens fiber optic temperature sensor OTG-A-62 mounted inside the experimental container.

7.3 Results and discussion

7.3.1 Synthesis of aqueous maghemite (γ -Fe₂O₃) ferrofluid

The maghemite nanoparticles, that are used in this study, were obtained by oxidation of initially formed magnetite nanoparticles, prepared via co-precipitation of FeCl₂·4H₂O and FeCl₃·6H₂O under basic conditions.^{53,54} The γ -Fe₂O₃ nanoparticles were stabilized with trisodium citrate, resulting in a ferrofluid with a pH of about 7, i.e. the nanoparticles are negatively charged. This was confirmed by ζ potential measurements, revealing a value of -40 mV for the diluted (1 g/L) ferrofluid.

Complementary information on the particle size and content can be gained from TGA, TEM and magnetization experiments (VSM). The number-average radius of the particles was 4.1 ± 1.2 nm, as determined by TEM analysis (Fig. 7.11, Supporting Information). From TGA, we calculated an iron oxide content in the used ferrofluid of 27 wt%. The magnetization curves of the particle dispersion as well as of the dried powder (see Fig. 7.8) are characterized by a lack of hysteresis (low coercitivity and remanence), confirming the superparamagnetic behaviour that is expected in this particle size range.⁵⁸ We calculated a volume-average particle radius of 5.7 nm from the magnetization behaviour of the ferrofluid. Taking into account the experimental error of the employed methods, this is in accordance with the TEM findings. With 23.5 wt%, the maghemite content in the ferrofluid was slightly lower compared to the value determined by TGA. The minor discrepancy can be explained by the marginal presence of non-magnetic iron oxide phases, probably on the particle surface.

7.3.2 Synthesis of Pq2VP-*b*-PEO-*b*-P(GME-*co*-EGE)

The poly(2-vinyl pyridine)-*block*-poly(ethylene oxide)-*block*-poly(glycidyl methyl ether-*co*-ethyl glycidyl ether) (P2VP-*b*-PEO-*b*-P(GME-*co*-EGE)) triblock terpolymers were synthesized by sequential anionic polymerization in THF. A detailed description of the synthetic procedure is given elsewhere.^{52,55} The molecular characteristics of the used triblock terpolymers are summarized in Table 7.1.

Table 7.1 Molecular characteristics of the used Pq2VP-*b*-PEO-*b*-P(GME-*co*-EGE) triblock terpolymers.

	DP (P2VP) ^{a)}	DP (PEO) ^{b)}	DP P(GME- <i>co</i> -EGE) ^{b)}	M _n [Kg/mol] ^{b)}	q2VP [mol%] ^{c)}
TB1	60	398	26-26	30.5	20
TB2	62	452	36-36	35.0	20

a) Determined via MALDI-ToF measurements, using dithranol as matrix and silver triflate as cationizing agent

b) Determined from ¹H-NMR spectra, using the absolute M_n(P2VP) for signal calibration

c) Degree of quaternization of the P2VP block, determined via titration with silver nitrate using potassium chromate as indicator

The P2VP blocks of the triblock terpolymers were quaternized with methyl iodide (MeI) in THF in order to introduce positive charges at the P2VP block, necessary for the later complexation with the negatively charged γ -Fe₂O₃ nanoparticles. The obtained degree of quaternization was about 20 mol%, as determined by titration with silver nitrate using potassium chromate as indicator, and verified by FT-IR spectroscopy (Fig. 7.10, Supporting Information). Due to the presence of 20 mol% quaternized 2VP units, the Pq2VP-*b*-PEO-*b*-P(GME-*co*-EGE) triblock terpolymers are molecularly dissolved over the entire pH range, i.e. no micellization was observed in pH-dependent light scattering experiments (Fig. 7.13, Supporting Information). In contrast, our previous investigations on non-quaternized P2VP-*b*-PEO-*b*-P(GME-*co*-EGE) triblock terpolymers revealed a strong increase in scattering intensity at pH = 5. This was attributed to the P2VP block getting deprotonated and thus insoluble, resulting in the formation of core-shell-corona micelles with a P2VP core.⁵² Consequently, a similar behaviour would be expected for the corresponding quaternized triblock terpolymers, if aggregation would take place. However, no change in scattering intensity with increasing pH, i.e. no micellization, was observed. This information is important later on for the discussion of the temperature-induced aggregation and gelation of γ -Fe₂O₃/Pq2VP-*b*-PEO-*b*-P(GME-*co*-EGE) hybrid

micelles.

7.3.3 Preparation and characterization of hybrid micelles

The $\gamma\text{-Fe}_2\text{O}_3/\text{Pq2VP-}b\text{-PEO-}b\text{-P(GME-co-EGE)}$ hybrid micelles were prepared by mixing aqueous solutions of the quaternized triblock terpolymer with the citrate stabilized maghemite ferrofluid. A detailed description of the sample preparation can be found in the Experimental Part. It turned out that it makes no difference whether the triblock terpolymer solution is added to the ferrofluid, or vice versa, which indicates that the obtained aggregates (hybrid micelles) represent an equilibrium structure rather than a kinetically frozen structure.

For the following structural investigations in this section the triblock terpolymer $\text{Pq2VP}_{60}\text{-}b\text{-PEO}_{398}\text{-}b\text{-P(GME}_{26}\text{-co-EGE}_{26})$ (TB1, Table 7.1) was used. The subscripts denote the degree of polymerization of the corresponding block. The maghemite nanoparticles and the triblock terpolymer were mixed at different ratios, always keeping the overall concentration of solid material (triblock terpolymer + nanoparticle) constant at 1 g/L. The size and size distribution of the formed aggregates were monitored by dynamic light scattering (DLS).

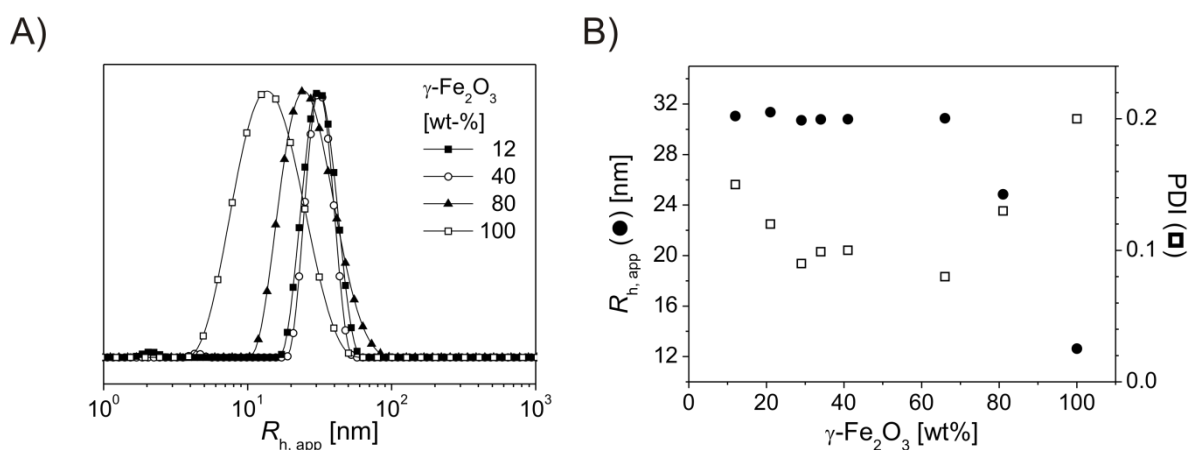


Figure 7.1. A) Intensity-weighted distribution of apparent hydrodynamic radii ($R_{h,app}$), and B) $R_{h,app}$ and polydispersity index (PDI) of $\gamma\text{-Fe}_2\text{O}_3/\text{TB1}$ hybrid micelles as a function of the $\gamma\text{-Fe}_2\text{O}_3$ fraction in the overall solids content (1 g/L; $\theta = 90^\circ$). The distributions of hydrodynamic radii were obtained using the CONTIN algorithm, and the $R_{h,app}$ and PDI values given in B) were obtained by cumulant analysis of the autocorrelation functions.

The hydrodynamic radius of the pure maghemite nanoparticles from DLS is about 12 nm (Fig. 7.1B), which is higher compared to the average particle radius of 4.1 nm obtained by TEM analysis (Fig. 7.11, Supporting Information). This can be attributed to the presence of loosely aggregated maghemite nanoparticles in solution, which is supported by the observed broad size distribution (Fig. 7.1A). The pure quaternized Pq2VP₆₀-*b*-PEO₃₉₈-*b*-P(GME₂₆-*co*-EGE₂₆) triblock terpolymer does not form micelles irrespective of the pH, as discussed above.

However, upon addition of a small amount of negatively charged maghemite nanoparticles, the formation of well-defined micellar aggregates ($R_{h, app} = 31$ nm) can be clearly observed, as obvious from the sample with a γ -Fe₂O₃/TB1 fraction of 12/88 w/w (Fig. 7.1A). ζ potential measurements confirmed, that electrostatic interactions between the positively charged Pq2VP blocks of the triblock terpolymers and the negatively charged γ -Fe₂O₃ nanoparticles are responsible for the formation of hybrid micelles with a γ -Fe₂O₃/Pq2VP complex coacervate core (Scheme 7.1). Upon mixing, the ζ potential changed from the value of the pure ferrofluid (-40 mV) to about 0 mV for the mixture with a γ -Fe₂O₃/TB1 ratio of 75/25 w/w. This ratio turned out to be the optimum ratio for the formation of hybrid micelles, i.e. the triblock terpolymer chains are almost completely bound to the maghemite nanoparticles, as will be discussed in the following section.

A closer look to the sample with a γ -Fe₂O₃/TB1 ratio of 12/88 w/w reveals the presence of a second very weak distribution at low radii ($R_{h, app}$ ca. 2 nm), which might be attributed to excess non-bound triblock terpolymer unimers (Fig. 7.1A). It has to be taken into account, that due to the intensity-weighted representation of the data the scattering of the larger hybrid micelles is strongly overrepresented. Thus, the actual amount of “free” triblock terpolymer can not directly be calculated from the data, and is expected to be significantly higher compared to that estimated from the peak area ratios. This aspect will be addressed in detail later on in the discussion.

Variation of the γ -Fe₂O₃ fraction indicated, that the hydrodynamic radius is independent from the γ -Fe₂O₃/TB1 ratio up to 70 % maghemite, at a constant narrow size distribution (Fig. 7.1B). The second distribution at low $R_{h, app}$ values is not detected at higher γ -Fe₂O₃ fractions, indicating a decrease of the concentration of non-bound triblock terpolymer unimers (Fig. 7.1A). However, upon further increasing the γ -Fe₂O₃/TB1 ratio to 80/20 w/w a significantly broadened size distribution and a shift to lower hydrodynamic radii is

observed. This indicates, that a minimum amount of triblock terpolymer is necessary to form well-defined hybrid micelles. For lower triblock terpolymer fractions, hybrid micelles and non-complexed maghemite nanoparticles are present in solution, resulting in the observed broadening of the size distribution. As a conclusion, the optimum maghemite fraction, i.e. resulting in well-defined hybrid micelles with a narrow size distribution, is about 30 to 70 wt%.

The formation of well-defined hybrid micelles, as deduced from the DLS data, is supported by transmission electron microscopy (TEM) investigations. Fig. 7.2A shows a cryogenic-TEM (cryo-TEM) micrograph of a sample with a $\gamma\text{-Fe}_2\text{O}_3$ /TB1 ratio of 41/59 w/w, revealing the presence of well-defined nanoparticle clusters in solution. The average number of $\gamma\text{-Fe}_2\text{O}_3$ nanoparticles within a cluster is 3.5 ± 1.5 (average over 130 hybrid micelles), and the clusters are regularly arranged. Such a defined arrangement is in agreement with the presence of a triblock terpolymer shell stabilizing the clusters, i.e. the formation of hybrid micelles with a $\gamma\text{-Fe}_2\text{O}_3$ /Pq2VP complex coacervate core (Scheme 7.1). However, due to the low scattering contrast between the soluble PEO and P(GME-*co*-EGE) blocks and the surrounding frozen water film, it is not possible to detect the corona of the hybrid micelles.

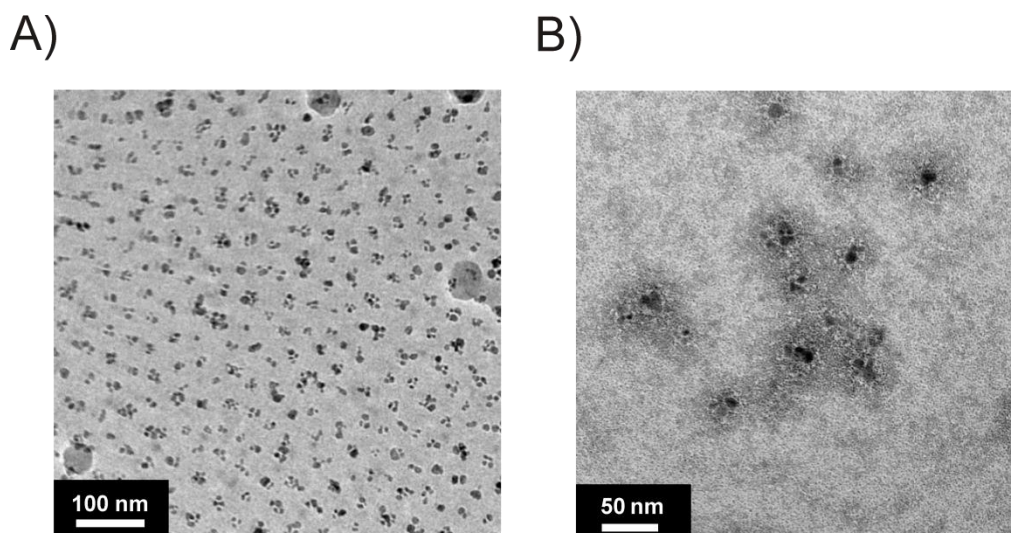


Figure 7.2. A) Cryo-TEM micrograph of a $\gamma\text{-Fe}_2\text{O}_3$ /TB1 mixture (15 g/L, $\gamma\text{-Fe}_2\text{O}_3$ /TB1 = 41/59 w/w); and B) TEM micrograph of hybrid micelles formed in a $\gamma\text{-Fe}_2\text{O}_3$ /TB1 mixture (0.2 g/L, $\gamma\text{-Fe}_2\text{O}_3$ /TB1 = 33/67 w/w), the sample was prepared by drop-coating onto a carbon-coated copper grid and subsequent staining with RuO_4 .

In order to visualize the stabilizing triblock terpolymer shell, we analyzed a sample prepared by drop-coating and subsequent staining with ruthenium tetroxide (Fig. 7.2B). Here, the corona formed by the water soluble PEO and P(GME-*co*-EGE) blocks can be clearly distinguished from the maghemite nanoparticle containing complex coacervate core and the grid surface, respectively. The average radius of the hybrid micelles extracted from the TEM micrograph is about 30 ± 5.5 nm, which corresponds well to the hydrodynamic radius obtained by DLS ($R_{h, app} = 31$ nm). The fuzzy background in Fig. 7.2B points to the presence of unimers in the solution, being deposited on the grid upon drying of the sample. This supports the conclusion drawn from the DLS data, that - depending on the γ -Fe₂O₃/TB1 ratio - a certain fraction of non-bound triblock terpolymer unimers is present in the solution.

For a quantitative analysis of the triblock terpolymer fraction bound to the maghemite nanoparticles, the γ -Fe₂O₃/TB1 hybrid micelles were isolated from the solution via centrifugation and subsequent drying. The content of bound polymer was determined by thermogravimetric analysis (TGA). Interestingly, the TGA traces show an almost constant weight loss of about 26-27 wt% for nanoparticle contents below 80 wt%, irrespective of the γ -Fe₂O₃/TB1 ratio applied in the preparation of the solution (Fig. 7.3A). Thermogravimetric analysis of the pure maghemite nanoparticles revealed a citrate content of 4 wt% (results not shown). Consequently, the citrate shell of the maghemite nanoparticles contributes with about 3 wt% to the overall weight loss of the hybrid micelles, i.e. the weight loss attributable to bound triblock terpolymer is 23-24 wt%. This indicates, that a constant number of triblock terpolymer chains are bound to the maghemite nanoparticles for sufficiently high polymer fractions, i.e. excess non-bound triblock terpolymer unimers are present in solution. Using the molecular weight of the TB1 triblock terpolymer (Table 7.1) together with the density ($\rho = 4.907$ g/cm³)⁵⁹ and average size of the maghemite nanoparticles ($r = 4.1$ nm) it can be calculated, that on average 30 triblock terpolymer chains stabilize a nanoparticle cluster. For polymer fractions close to the optimum value of 23-24 wt%, e.g. for the sample with γ -Fe₂O₃/TB1 = 80/20 w/w, most of the triblock terpolymer chains are used to stabilize the nanoparticle clusters. As a result, the observed weight loss for the isolated hybrid micelles is close to the fraction of triblock terpolymer in the corresponding γ -Fe₂O₃/polymer mixture.

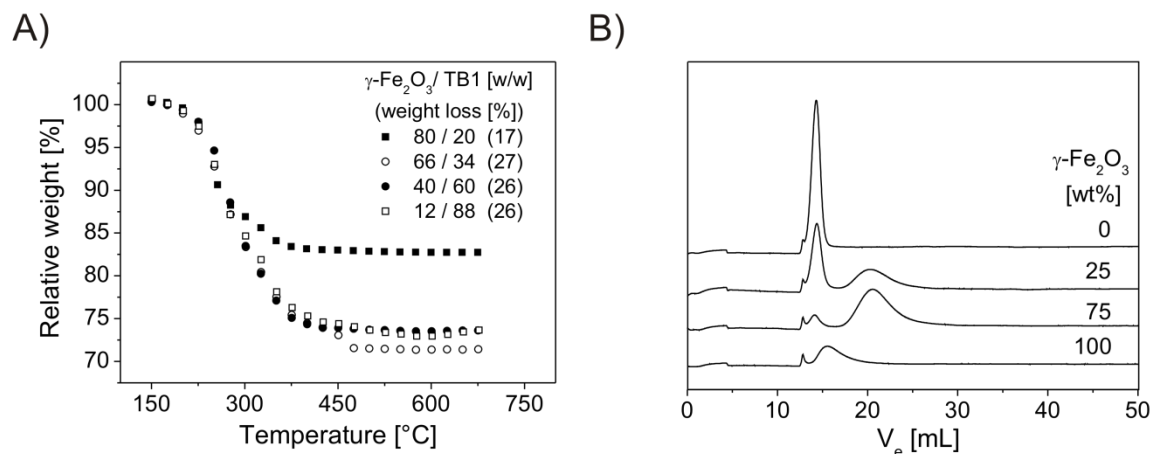


Figure 7.3. A) TGA traces of $\gamma\text{-Fe}_2\text{O}_3/\text{TB1}$ hybrid micelles isolated by centrifugation of solutions with varying $\gamma\text{-Fe}_2\text{O}_3/\text{TB1}$ ratio and subsequent drying, B) AF4 RI-traces of samples with varying $\gamma\text{-Fe}_2\text{O}_3/\text{TB1}$ ratio in comparison to the pure TB1 triblock terpolymer and the maghemite ferrofluid, respectively (1 g/L, peak at 12.7 mL is inherent to the system).

The presence of free (non-bound) triblock terpolymer unimers in $\gamma\text{-Fe}_2\text{O}_3/\text{TB1}$ mixtures was verified by directly analyzing the solutions via asymmetric flow field-flow fractionation (AF4). Fig. 7.3B shows AF4 eluograms of the pure triblock terpolymer (TB1), the pure ferrofluid, and two mixtures with different $\gamma\text{-Fe}_2\text{O}_3/\text{TB1}$ ratio. Besides the fact that the addition of triblock terpolymer to the ferrofluid causes a shift to higher elution volume, revealing the formation of hybrid micelles, a second peak at lower elution volume is present in both $\gamma\text{-Fe}_2\text{O}_3/\text{TB1}$ mixtures. This second peak corresponds to free triblock terpolymer present in solution, as deduced by comparison with the AF4 eluogram of the pure triblock terpolymer. The amount of non-bound unimers decreases with increasing $\gamma\text{-Fe}_2\text{O}_3$ fraction, and is lowest for the sample with $\gamma\text{-Fe}_2\text{O}_3/\text{TB1} = 75/25$ w/w, which is consistent with the TGA data (Fig. 7.3A). Using the online MALLS detector coupled to the AF4 device, a radius of gyration (R_g) of 20 nm was determined for the hybrid micelles. Together with the hydrodynamic radius of the hybrid micelles obtained by DLS, a shape factor $\rho = R_g/R_h$ of approximately 0.65 is calculated, which is significantly below the hard sphere value ($\rho = 0.775$)⁶⁰. This can be attributed to the strongly swollen corona of the hybrid micelles.

In conclusion, well-defined hybrid micelles are formed upon addition of quaternized Pq2VP-*b*-PEO-*b*-P(GME-*co*-EGE) triblock terpolymers to citrate stabilized maghemite nanoparticles, due to electrostatic interactions between the positively charged Pq2VP blocks and the negatively charged $\gamma\text{-Fe}_2\text{O}_3$ nanoparticles. The hybrid micelles consist of a $\gamma\text{-Fe}_2\text{O}_3/\text{Pq2VP}$ complex coacervate core, containing clusters of maghemite nanoparticles

(on average 3.5 nanoparticles), a water soluble PEO shell, and a thermo-responsive P(GME-*co*-EGE) corona (Scheme 7.1, and Fig. 7.2). The number of triblock terpolymer chains stabilizing the nanoparticle clusters, i.e. the aggregation number of the hybrid micelles, is constant for sufficiently high triblock terpolymer fractions (> 30 wt-%). As a result, free (non-bound) triblock terpolymer unimers are present in solution, and the amount of unimers decreases with increasing nanoparticle fraction. The optimum γ -Fe₂O₃/polymer ratio is about 75/25 w/w, as deduced from the constant weight loss observed by TGA and the AF4 data (Fig. 7.3), i.e. in this case the triblock terpolymers are almost completely bound to the maghemite nanoparticles. For lower polymer fractions, there are not enough triblock terpolymer chains available to stabilize all maghemite nanoparticles. This results in a broadening of the size distribution of the hybrid micelles due to the presence of non-complexed γ -Fe₂O₃ nanoparticles (Fig. 7.1).

It is important to note, that the γ -Fe₂O₃/Pq2VP-*b*-PEO-*b*-P(GME-*co*-EGE) hybrid micelles are long term stable. The solutions remained clear without any visible precipitation for several months, and the size and size distribution of the micelles was not altered upon storage as proven by DLS (Fig. 7.4).

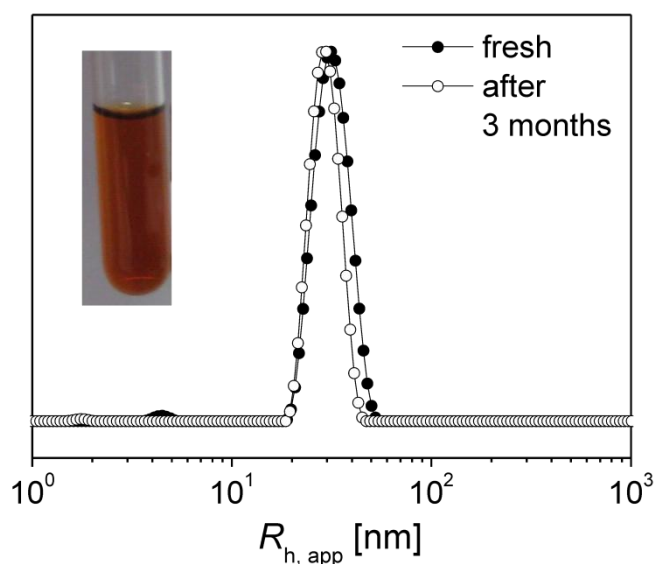


Figure 7.4. Intensity-weighted distribution of apparent hydrodynamic radii ($R_{h, app}$) for a fresh and a 3 months old solution with a γ -Fe₂O₃/TB1 ratio of 32/68 w/w (1g/L, $\theta = 90^\circ$). The photograph shows a 2 days old sample of the solution ($c = 1$ g/L).

It is emphasized, that the stability of the hybrid micelles is only provided when a quaternized triblock terpolymer is used for complexation of the negatively charged maghemite nanoparticles. Using the corresponding non-quaternized P2VP₆₀-*b*-PEO₃₉₈-*b*-

P(GME_{26-co}-EGE₂₆) triblock terpolymer at pH = 5, i.e. the P2VP block is partially protonated, the resulting solutions are stable for only 1-2 days, before significant agglomeration and subsequent precipitation occurs. Furthermore, the degree of quaternization of the P2VP block is crucial for the uniformity and stability of the produced hybrid micelles. Using a Pq2VP_{60-b}-PEO_{398-b}-P(GME_{26-co}-EGE₂₆) triblock terpolymer with a degree of quaternization of about 60 mol%, prepared by quaternization with dimethyl sulfate, results in the formation of ill-defined hybrid micelles with significantly larger nanoparticle clusters in the core (Fig. 7.12, Supporting Information). This can be attributed to the higher positive charge density at the P2VP block, possibly leading to stronger bridging effects. The corresponding solutions of the hybrid micelles are slightly turbid, and precipitation starts within a few days. As a conclusion, a moderate degree of quaternization of about 20 mol% is favourable for the formation of well-defined long term stable hybrid micelles.

7.3.4 Temperature-induced aggregation of hybrid micelles

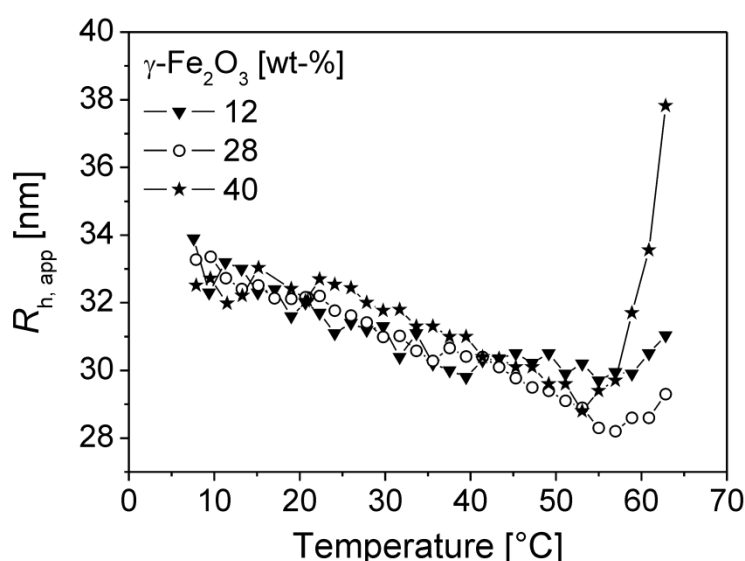


Figure 7.5. Temperature-dependent apparent hydrodynamic radii ($R_{h, app}$), obtained by cumulant analysis of the autocorrelation functions, for different γ -Fe₂O₃/TB1 ratios (1 g/L, $\theta = 90^\circ$, 2 K/step: equilibration time 10 min).

The γ -Fe₂O₃/Pq2VP-*b*-PEO-*b*-P(GME-*co*-EGE) hybrid micelles are expected to show a temperature-induced aggregation via open association, due to the thermo-responsive P(GME-*co*-EGE) corona block, that becomes hydrophobic above its cloud point (Scheme 7.1). At a sufficiently high concentration of the hybrid micelles we expect a thermo-

reversible gelation of the solution. The cloud point of the P(GME-*co*-EGE) homopolymers (50 mol% GME) is about 30 – 34 °C, depending on concentration.⁵² Our previous investigations on the temperature-induced aggregation of non-quaternized P2VP-*b*-PEO-*b*-P(GME-*co*-EGE) triblock terpolymers at low pH (i.e. P2VP block is protonated) revealed, that the cloud point of the P(GME-*co*-EGE) end block is shifted significantly to higher temperatures, as compared to the homopolymer.⁵² This was attributed to the attachment of the hydrophilic PEO and P2VP blocks, a common phenomenon already described in literature.⁶¹

First, the thermo-responsive behaviour of the hybrid micelles was investigated by temperature dependent DLS. Fig. 7.5 shows the apparent hydrodynamic radii ($R_{h, app}$) as a function of temperature for three different γ -Fe₂O₃/TB1 mixtures. Only for the sample with the highest maghemite fraction (γ -Fe₂O₃/TB1 = 40/60 w/w) a distinct increase in $R_{h, app}$ was observed at about 55 °C, i.e. aggregation of hybrid micelles into bigger clusters occurs due to the coil-to-globule transition of the P(GME-*co*-EGE) blocks. This indicates, that a critical maghemite fraction, and accordingly a critical fraction of hybrid micelles, is needed to enable aggregation. As the number of triblock terpolymer chains stabilizing the maghemite clusters in the core was found to be constant (see previous section), a higher fraction of free (non-bound) TB1 unimers is present in solution at low γ -Fe₂O₃/TB1 ratios, and the percolation of hybrid micelles upon aggregation of the P(GME-*co*-EGE) blocks is hindered. Instead, the TB1 unimers start to aggregate into core-shell-corona (CSC) micelles with a P(GME-*co*-EGE) core.⁵² As the hydrodynamic radius of the CSC micelles is expected to be similar with respect to that of the γ -Fe₂O₃/TB1 hybrid micelles, no significant change in $R_{h, app}$ was observed upon heating for the samples with low nanoparticle fractions (12 and 28 wt%). Only an increase in the intensity of scattered light was detected due to the increasing fraction of micellar aggregates (results not shown). As a conclusion, a certain minimum fraction of γ -Fe₂O₃ nanoparticles, i.e. fraction of hybrid micelles, is necessary for the temperature-induced aggregation of the hybrid micelles, and thus for the gelation in concentrated γ -Fe₂O₃/TB1 solutions.

A closer look to Fig. 7.5 reveals, that for all samples the hydrodynamic radii of the hybrid micelles decrease with increasing temperature, until the cloud point (T_{CP}) of the P(GME-*co*-EGE) block is reached. This might be attributed to the P(GME-*co*-EGE) block, starting to lose some bound water in the hydration shell already at temperatures below the cloud

point, resulting in a shrinkage of the hybrid micelles.⁵² This behaviour, being comparable to that of PEO at higher temperatures,⁶²⁻⁶⁶ is important for the discussion on the gelation behaviour of concentrated $\gamma\text{-Fe}_2\text{O}_3/\text{TB1}$ solutions in the following section.

7.3.5 Thermo-reversible gelation and rheology

We investigated the temperature-induced gelation of several micellar solutions by different methods. Initially, simple test tube inversion experiments have been performed to get a qualitative impression of the sample behaviour in dependence of temperature and concentration (see phase diagram in Fig. 7.14, Supporting Information), followed by a more detailed analysis by rheology for two representative samples. Finally, we demonstrated that the gelation can be reversibly and reproducibly induced by contactless magnetic heating of the samples in a suitable HF field.

Concentrated $\gamma\text{-Fe}_2\text{O}_3/\text{Pq2VP-}b\text{-PEO-}b\text{-P(GME-co-EGE)}$ solutions for gelation studies were prepared by mixing diluted solutions of the quaternized triblock terpolymers and the maghemite ferrofluid, followed by evaporation of the solvent under mild conditions (room temperature, 70 mbar) until the desired concentration was reached. The composition of the samples investigated by rheology and HF-magnetocalorimetry is given in Table 7.2.

Table 7.2 Composition of aqueous $\gamma\text{-Fe}_2\text{O}_3/\text{Pq2VP-}b\text{-PEO-}b\text{-P(GME-co-EGE)}$ hybrid micelle solutions for rheology and HF-magnetocalorimetry.

	triblock terpolymer content		$\gamma\text{-Fe}_2\text{O}_3$ content	$\gamma\text{-Fe}_2\text{O}_3/\text{polymer}$
	[wt%]		[wt%] ^a	[w/w]
	TB1	TB2		
S1 ^b	5	-	4	45/55
S2 ^b	10	-	8	45/55
S3 ^{b,c}	20	-	16	45/55
S4 ^c	-	14	6	30/70
S5 ^c	-	20	-	0/100

a) The given values are based on the iron oxide content of the ferrofluid, as determined by TGA (27 wt%)

b) HF-magnetocalorimetry

c) Rheology

We have learned from the temperature-dependent DLS experiments, that a certain minimum $\gamma\text{-Fe}_2\text{O}_3/\text{TB1}$ ratio is useful to induce aggregation upon heating. Consequently, for the first investigated sample a high maghemite fraction was chosen, i.e. $\gamma\text{-Fe}_2\text{O}_3/\text{TB1} =$

45/55 w/w, with an overall solids content of 36 wt% (sample S3, Table 7.2). By the test tube inversion method we found an interesting gel-sol-gel transition for sample S3 upon heating, forming free-standing hydrogels at temperatures below room temperature (7 °C) and at elevated temperatures (> 50 °C), respectively (Fig. 7.6A). The high temperature gel phase was long term stable below ca. 70 °C, without any sign of precipitation or phase separation (Fig. 7.14, Supporting Information). A comparable gel-sol-gel transition upon heating was observed for the corresponding non-quaternized P2VP-*b*-PEO-*b*-P(GME-*co*-EGE) triblock terpolymers at pH = 7, too.⁵² In contrast, for solutions with an identical concentration of TB1 (20 wt%), but a lower fraction of maghemite nanoparticles (including the pure TB1 solution), no gelation neither at low nor high temperatures was observed. This confirms the findings from DLS, that the presence of a sufficient amount of maghemite nanoparticles, i.e. minimum fraction of hybrid micelles, is crucial for a thermo-reversible gelation of the γ -Fe₂O₃/Pq2VP-*b*-PEO-*b*-P(GME-*co*-EGE) solutions. The fraction of free (non-bound) TB1 unimers, forming CSC micelles with P(GME-*co*-EGE) cores upon heating, obviously does not contribute to the gel formation.

The thermo-responsive behaviour of the γ -Fe₂O₃/TB1 based hydrogel (sample S3, Table 7.2) was investigated more systematically by rheology. We applied an oscillatory stress to the sample using a cone-plate shear cell geometry, and investigated the storage (G') and loss modulus (G'') in dependence of temperature and frequency, respectively. Regimes with $G' > G''$ are referred to as gel state, whereas the sol-state is characterized by $G'' > G'$.⁶⁷ Figure 7.6B shows G' and G'' as a function of temperature. Below 12 °C, G' exceeds G'' , i.e. the solution is in the gel state, which is consistent with the test tube inversion results. The observed crossing of the G' and G'' graphs at 12 °C points to a transition to the sole state, with G' being significantly lower compared to G'' . Interestingly, G' and G'' decrease over a broad temperature range, with a minimum around 40 °C. This is different to the behaviour of the non-quaternized triblock terpolymers, that show a sharp gel-sol transition.⁵² Finally, G' exceeds G'' again for temperatures above 50.7 °C, i.e. a second gel state is formed. This can be attributed to the thermo-responsive P(GME-*co*-EGE) corona block of the hybrid micelles, becoming hydrophobic at this point, and thus forming the network junctions (Scheme 7.1). The gel-sol-gel transition upon heating is fully reversible, as the same transition can be observed upon cooling (Fig. 7.6B). Furthermore, the gelation behaviour is not altered upon storage for several months, revealing the pronounced stability of the solution.

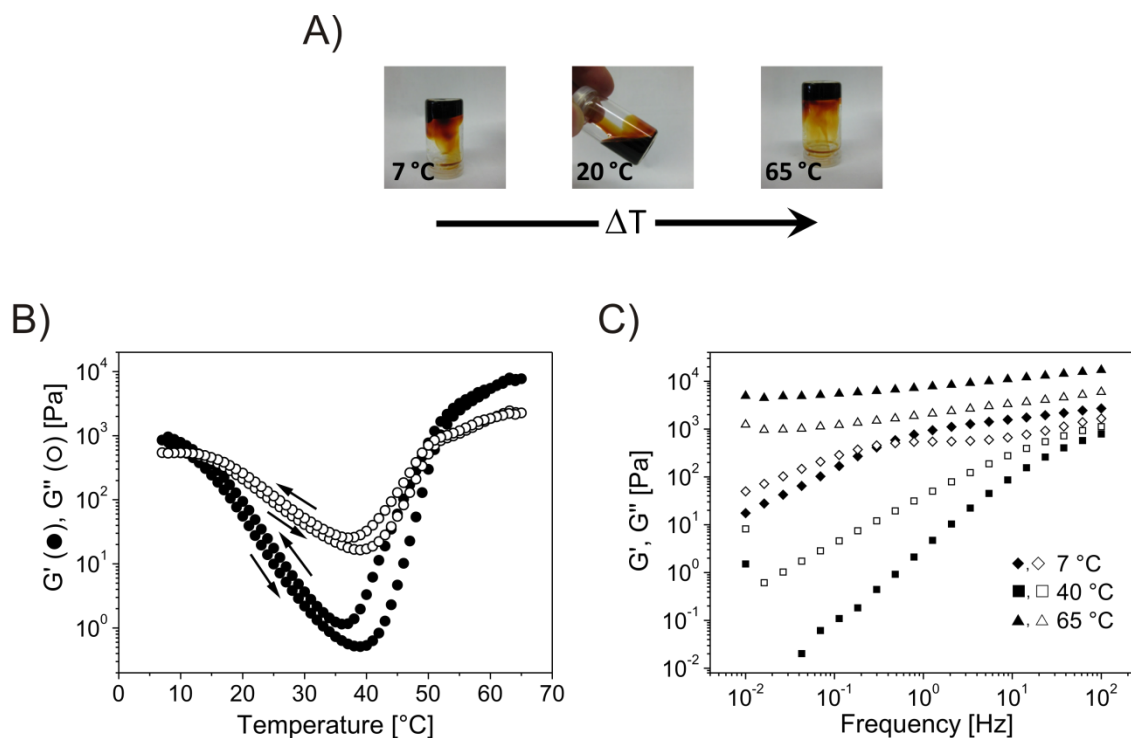


Figure 7.6. A) Photographs at different temperatures (test tube inversion method), B) temperature-dependent G' and G'' ($\gamma = 0.7\%$, $f = 1$ Hz, 0.1 K/min), and C) frequency-dependent G' (closed symbols) and G'' (open symbols) at different temperatures ($\gamma = 0.7\%$), for a 36 wt% solution with a $\gamma\text{-Fe}_2\text{O}_3/\text{TB1}$ ratio of 45/55 w/w (sample S3, Table 2).

More information about the internal structure of the corresponding gel and sol states can be deduced from frequency dependent measurements (Fig. 7.6C). For the gel state, a weak linear dependence or an independence of G' on frequency is expected, while for a viscoelastic fluid, G' is always lower than G'' , and $G' \propto \omega^2$ and $G'' \propto \omega^1$.

In the frequency sweep at $7\text{ }^\circ\text{C}$, G' exceeds G'' at high frequencies, however, both moduli show a strong dependence on frequency with a cross over at 0.3 Hz (Fig. 7.6C). Thus, the solution is in the gel state for frequencies above 0.3 Hz, indicating a short relaxation time of the low temperature gel state. In the gel state at $f > 0.3$ Hz, G'' shows a minimum, which is commonly observed for gels formed by cubic micellar phases.^{52,68-71} We therefore conclude, that the low-temperature gel is formed by a close packing of $\gamma\text{-Fe}_2\text{O}_3/\text{TB1}$ hybrid micelles, in analogy to the non-quaternized P2VP-*b*-PEO-*b*-P(GME-*co*-EGE) triblock terpolymers at $\text{pH} = 7$, forming a cubic packing of spherical CSC micelles with P2VP cores as deduced from small-angle neutron scattering.⁵² The observed gel-sol transition at $12\text{ }^\circ\text{C}$ (Fig. 7.6B) can therefore be attributed to the shrinkage of the micelles, caused by the loss of water from solvated P(GME-*co*-EGE) blocks. This behaviour is in full correspondence with the observations made by temperature-dependent

DLS (Fig. 7.5).

The frequency sweep at 40 °C reveals the typical behaviour of a viscoelastic fluid, i.e. G'' exceeds G' , and both show a strong frequency dependence (Fig. 7.6C). In the high temperature gel state at 65 °C, G' exceeds G'' over the whole frequency range, and both moduli run almost parallel with frequency in the log-log plot. Such a dynamic behaviour is expected for chemically or physically crosslinked gels, that generally follow the relation $G' \propto G'' \propto \omega^n$.^{67,72,73} This observation strongly supports the proposed open association of γ -Fe₂O₃/TB1 hybrid micelles in the high temperature gel phase, caused by the P(GME-*co*-EGE) blocks becoming hydrophobic above the cloud point, and thus providing additional physical crosslinks (Scheme 7.1).

While the gel strength of S3 at 65 °C is relatively high ($G'(1 \text{ Hz})$ ca. 8 kPa), this goes along with a comparatively high viscosity in the sol state at room temperature, as indicated by the high G'' values of about 200 Pa. We attribute this to the solids content of 36 wt% combined with the high maghemite fraction, leading to a large number of hybrid micelles. With respect to application, however, a low viscosity in the sole state is favourable. A comparable gel-sol-gel transition can be found in less concentrated solutions down to a concentration of 26 wt%, too, while keeping the γ -Fe₂O₃/TB1 ratio constant at 45/55 w/w. For even lower concentrations, the low temperature gel phase disappears and only a sol-gel transition upon heating is observed (Fig. 7.14, Supporting Information). However, dilution goes along with an unfavourable increase in the sol-gel transition temperature, i.e., the temperature range in which the high temperature gel phase is long term stable before syneresis occurs (above ca. 70 °C) is getting more narrow.

In order to realize a low-viscosity system that still allows the formation of a strong gel at comparable temperatures with respect to sample S3 (ca. 50 °C), we employed a Pq2VP-*b*-PEO-*b*-P(GME-*co*-EGE) triblock terpolymer with a longer P(GME-*co*-EGE) block (TB2, Table 7.1) for the formation of hybrid micelles. It is expected, that with increasing block length of the P(GME-*co*-EGE) block the critical concentration for hydrogel formation decreases, as found in our previous investigations on the non-quaternized analogues.⁵² After screening a series of concentrations (Fig. 7.14, Supporting Information), we found that a 20 wt% solution with a γ -Fe₂O₃/TB2 ratio of 30/70 (sample S4, Table 7.2) is sufficient to achieve a temperature-induced sol-gel transition at about 50 °C, while keeping the viscosity in the sol state low (Fig. 7.7A). Upon heating the gel state is reached

at 51.5 °C, as indicated by the cross-over of G' and G'' at that point. Despite the considerably lower solids content, the gel strength at 65 °C ($G'(1 \text{ Hz})$ ca. 4.5 kPa) is only moderately reduced compared to that for sample S3 ($G'(1 \text{ Hz})$ ca. 8 kPa). In contrast to S3, this sample does not form a low temperature gel phase, as revealed by test tube inversion. This can be attributed to the decreased solids content and the lower maghemite fraction, i.e. the volume fraction of hybrid micelles is too low to form a close packing, even for higher concentrated solutions (Fig. 7.14, Supporting Information).

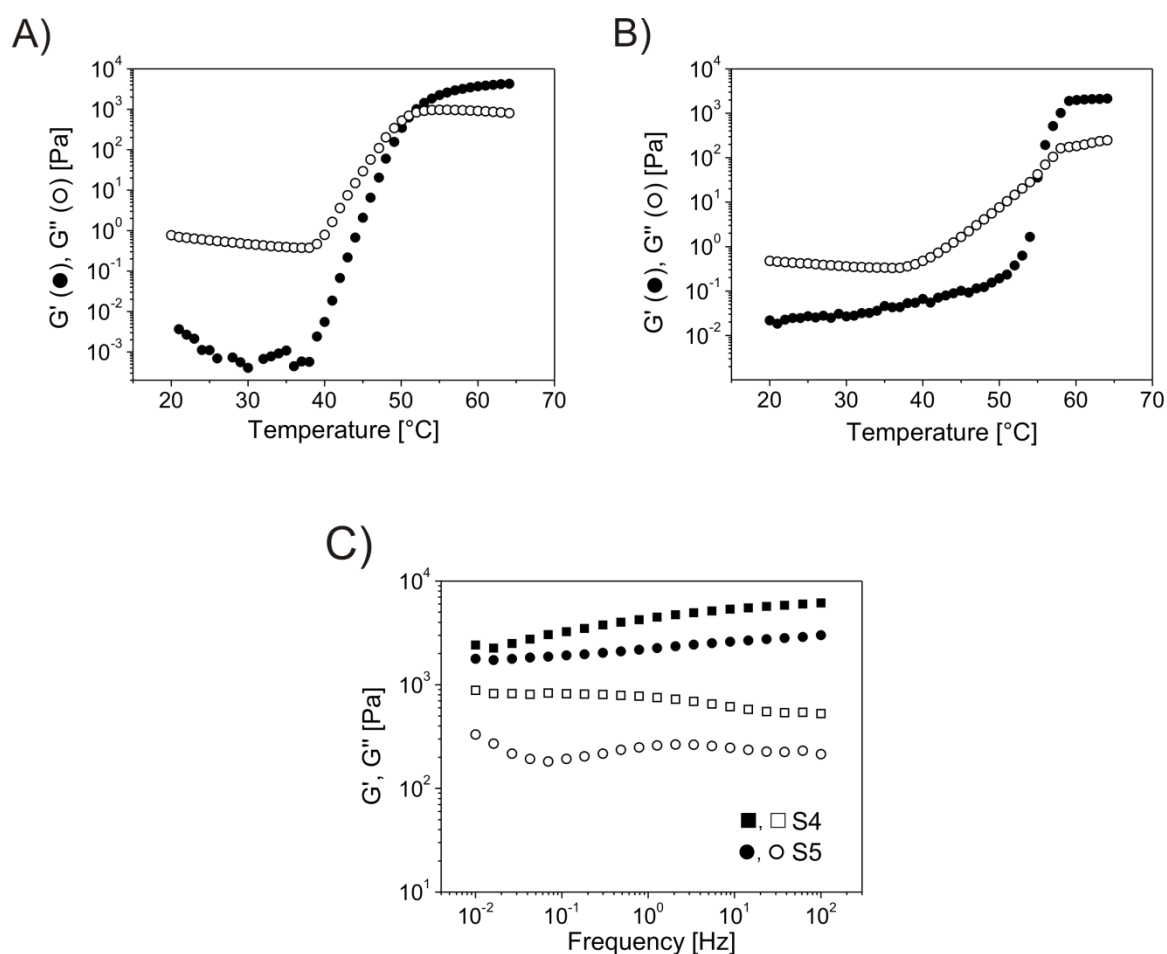


Figure 7.7. Temperature-dependent G' and G'' ($\gamma = 0.7 \%$, $f = 1 \text{ Hz}$, 0.1 K/min) for A) a 20 wt% solution with a $\gamma\text{-Fe}_2\text{O}_3/\text{TB2}$ ratio of 30/70 w/w (sample S4, Table 2), and B) a 20 wt% solution of pure TB2 triblock terpolymer (sample S5, Table 2). C) Comparison of the frequency dependent G' (closed symbols) and G'' (open symbols) at 65 °C for samples S4 and S5 ($\gamma = 0.7 \%$).

In contrast to TB1, the pure TB2 triblock terpolymer (sample S5, Table 7.2) shows a sol-gel transition upon heating for identical concentrations (20 wt%), which is ascribed to the longer P(GME-*co*-EGE) block. Compared with sample S4, the sol-gel transition is slightly shifted to higher temperatures (Fig. 7.7B). Interestingly, the gel strength of the γ -

$\text{Fe}_2\text{O}_3/\text{TB2}$ mixture at 65 °C ($G'(1 \text{ Hz})$ ca. 4.5 kPa) is higher compared to that of the pure TB2 triblock terpolymer ($G'(1 \text{ Hz})$ ca. 2.3 kPa) over the whole frequency range (Fig. 7.7C), despite the lower TB2 content in sample S4. This is attributed to the different gel structures. For the $\gamma\text{-Fe}_2\text{O}_3/\text{TB2}$ mixture (sample S4) gelation is induced by the open association of hybrid micelles, caused by the P(GME-*co*-EGE) block becoming insoluble, and thus forming physical crosslinks. In contrast, gelation of the pure TB2 triblock terpolymer (sample S5) is based on the formation of CSC micelles with a P(GME-*co*-EGE) core, analogous to the corresponding non-quaternized triblock terpolymers at low pH,⁵² i.e. in this case a close packing of CSC micelles is formed. It is noted, that a pure 14 wt% solution of TB2, i.e. equal polymer content with respect to sample S4, does not show a temperature-induced gelation.

7.3.6 Response of the hybrid micelle solutions to magnetic fields

In addition to the thermo-responsivity of the micellar solution as described above, the incorporated maghemite nanoparticles provide the access to magnetic manipulation. We investigated the performance of these new materials in static as well as in high frequency magnetic fields.

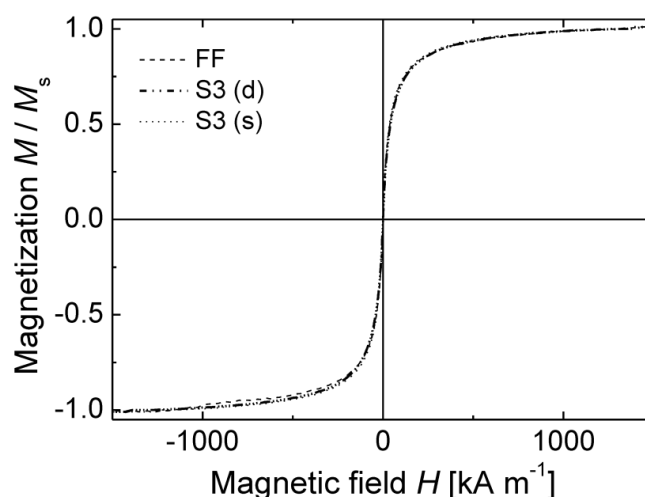


Figure 7.8. Normalized magnetization curves of the stock ferrofluid FF, and the hybrid micelle solution S3 (Table 2) before (s) and after freeze-drying (d).

In order to get information whether the incorporation of the maghemite nanoparticles into the hybrid micelles influences their magnetization behaviour, we performed quasi-static magnetization experiments (VSM). In Fig. 7.8, the magnetization graphs of the ferrofluid, the micellar solution S3 (Table 7.2), and the respective freeze-dried sample are shown, after normalizing with the saturation magnetization. The three graphs match excellently, indicating that neither the incorporation into the hybrid micelles, nor the drying process is of significant influence on the superparamagnetism and the magnetic moment distribution. These results confirm the internal remagnetization mode (Néel process) for virtually all particles. On the contrary, if particle rotation played a significant role in the field orientation of the particles, a strong influence from changes in the particles' local viscosity and immobilization of the particles by micelle formation, or even the freeze-drying process would be observed. Furthermore, we can conclude that the particle concentration, and thus particle interaction forces, do not influence the experiments significantly.

It is of upcoming interest that superparamagnetic nanoparticles offer the opportunity to develop heat in high frequency magnetic fields due to relaxational loss mechanisms. One of the great advantages is that in the kHz regime, where such particles are quite effective, many other materials, including water and tissue, are almost transparent, so that a selective local heating can be observed. In the present system, this ability can be of interest to induce a local temperature-induced gelation of the reversible hydrogels by a remote stimulus such as an electromagnetic field.

We investigated the magnetic heating performance of the ferrofluid and the micellar solutions S1 – S3 (Table 7.2) by analyzing the temperature development of the samples during application of a high frequency alternating magnetic field (high frequency magnetocalorimetry, HF-MC). In these experiments, the samples were subjected to different magnetic field amplitudes H between 3.5 kA/m and 31.5 kA/m at a frequency of about 300 kHz.

As soon as the field was switched on, all investigated samples showed a fast heat development. The actual heating rate depends on the amplitude field strength, the particle concentration, and the heat capacity of the respective sample (Fig. 7.9A). When an amplitude field strength of 13 kA/m and higher is applied, the gelation temperature (~ 50 °C) of the sample S3 (Fig. 7.6) is reached within two minutes or less. When the sample

temperature reached 65 °C, the experiments were stopped, and the gelation of the micellar solution was confirmed by test tube inversion. The sample S3 showed a good bulk gelation after the magnetic heating, and no phase separation was observed, neither in the ferrofluid nor the ferrohydrogel. After the sample cooled down to room temperature, the ferrohydrogel readily disassembled into a micellar solution again. The process can be repeated many times without the detection of any changes in the gelation behaviour or magnetic properties.

More quantitative results on the particles' heating power can be obtained from the initial slope of the heating curves. In the beginning of the measurement, the sample temperature is still close to ambient, so that heat exchange effects to the environment can be neglected. The frequency-normalized heat power P_f (the energy transferred per radiation period $\tau = 1/f$) is therefore determined at early irradiation times, and is given by

$$P_f = c_p \cdot \frac{\left(\frac{dT}{dt}\right)_{t \rightarrow 0}}{f} \quad (\text{eq. 4})$$

As can be seen in Fig. 7.9B, P_f is a linear function of the maghemite mass fraction (μ_M) at constant field amplitude. The graph combines results from the ferrofluid and from micellar solutions, indicating that the heat power is not influenced by the presence of the polymer. The linear relationship also attests a constant heat power per mass fraction, so that it is possible to extract the specific heat power $\text{SHP}_f = dP_f/d\mu_M$ from the slope.

As expected, SHP_f increases with increasing field strength, and shows a typical dependence on the field amplitude (Fig. 7.9C). This dependence has recently been described as of second order.⁷⁴ We obtain SHP_f values between 1×10^{-5} and 7×10^{-5} J/g, corresponding to SHP values between 4 and 17 W/g at 300 kHz, for field amplitudes up to 32 kA/m. The results are in the expected range, based on findings reported in literature.⁷⁴

The possibility to induce a gelation of the samples by remote heating using alternating magnetic fields is thus clearly indicated. This makes this new type of magneto-responsive hydrogels attractive for hyperthermia applications.^{21,75,76} The sol-gel transition can be easily adjusted to body temperature by adjusting the composition of the thermo-sensitive P(GME-co-EGE) block.⁵² Thus, the hybrid micelle solutions might be easily injected at

the tumour site, and in-situ gelation immobilizes the superparamagnetic nanoparticles at the desired place. Furthermore, this might be combined with a site-specific drug delivery, a promising application for injectable hydrogels.^{77,78} The possibility to induce a fast and reversible deformation/contraction by applying nonuniform magnetic fields is believed to be of interest for the construction of switches or micropumps in microfluidic devices as an alternative to thermo-responsive chemically crosslinked hydrogels showing a volume-change upon heating.⁷⁹

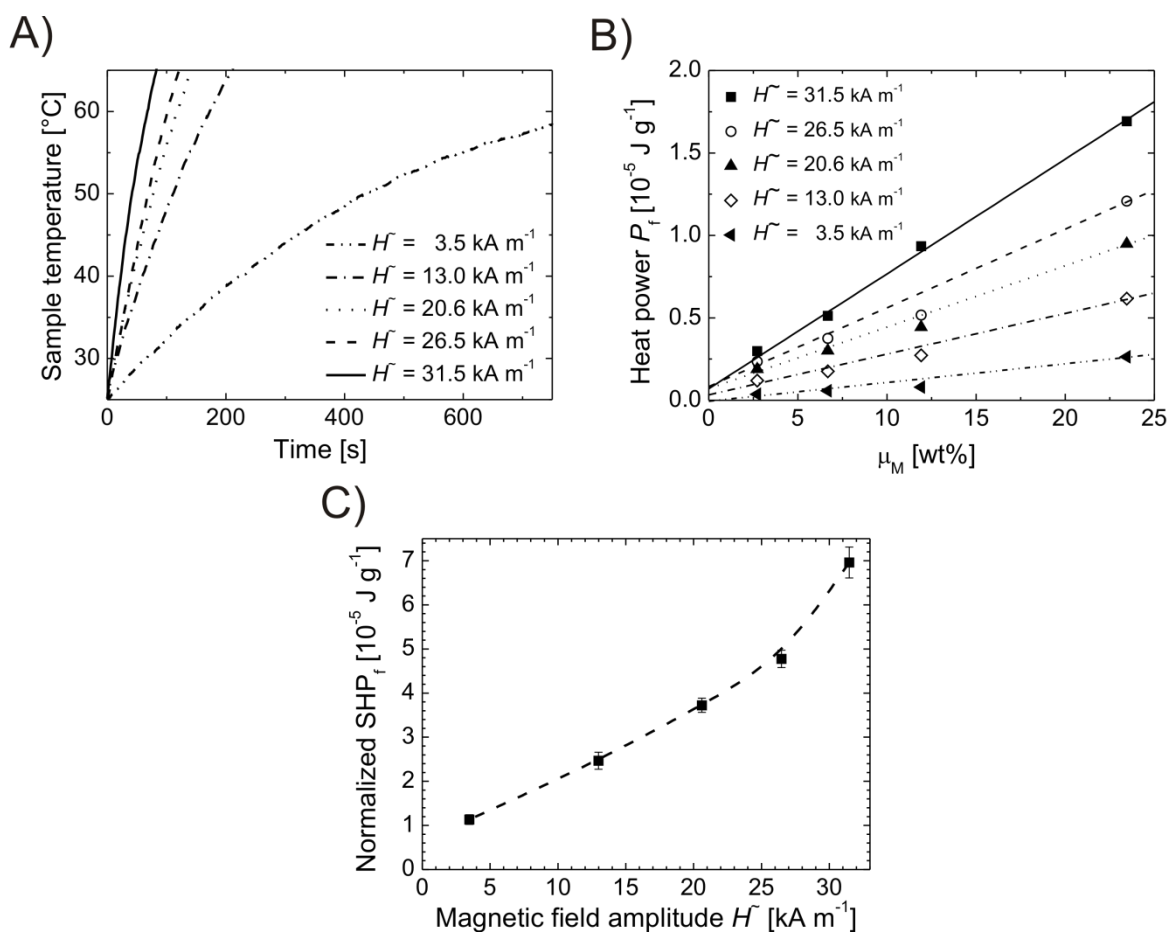


Figure 7.9. A) Heating curves obtained in HF-MC experiments at different field strengths H for the hybrid micelle solution S3 (Table 2), B) determination of the specific heat power SHP_f of the employed maghemite nanoparticles at different field amplitudes H from the slope of P_f vs. μ_M , and C) frequency normalized specific heat power (SHP_f) of the maghemite nanoparticles at different field amplitudes H .

7.4 Conclusion

Magneto-responsive hydrogels based on $\gamma\text{-Fe}_2\text{O}_3/\text{Pq2VP-}b\text{-PEO-}b\text{-P(GME-co-EGE)}$ hybrid micelles were prepared, showing a reversible temperature-induced gelation which can be remotely triggered using AC magnetic fields. Well defined hybrid micelles were formed upon mixing solutions of the triblock terpolymer and the ferrofluid, driven by electrostatic interactions between the oppositely charged quaternized Pq2VP blocks and the citrate stabilized $\gamma\text{-Fe}_2\text{O}_3$ nanoparticles. The micelles consist of a $\gamma\text{-Fe}_2\text{O}_3/\text{Pq2VP}$ complex coacervate core, a water soluble PEO shell, and a thermo-responsive P(GME-co-EGE) corona. The core of the hybrid micelles contains clusters of maghemite nanoparticles, with on average 3.5 nanoparticles.

The amount of triblock terpolymer bound to the $\gamma\text{-Fe}_2\text{O}_3$ clusters was found to be constant for sufficiently high triblock terpolymer fractions, with about 30 chains stabilizing a cluster. As a result, free (non-bound) triblock terpolymer unimers are present in solution for high polymer/maghemite ratios. Consequently, a critical maghemite fraction, and accordingly a critical fraction of hybrid micelles, was necessary to enable a temperature-induced aggregation via open association, and thus gelation, at temperatures above the cloud point of the P(GME-co-EGE) corona blocks (Scheme 7.1). This is attributed to excess non-bound unimers, forming CSC micelles with a P(GME-co-EGE) core upon heating, which hinders the percolation of hybrid micelles.

At sufficiently high concentrations and maghemite fractions, the hybrid micelle solutions show a reversible gelation upon heating. Interestingly, a gel-sol-gel transition with gel states below ($< 12\text{ }^\circ\text{C}$) and above ($> 50\text{ }^\circ\text{C}$) room temperature was found at a high solids content (36 wt%). The gel phase at low temperatures is based on a close packing of hybrid micelles, whereas the high temperature gel state is formed via an open association of hybrid micelles.

Magnetization experiments showed, that the incorporation of $\gamma\text{-Fe}_2\text{O}_3$ into the hybrid micelles has no significant influence on the superparamagnetism and the magnetic moment distribution of the nanoparticles. Inductive heating was successfully used to remotely trigger gelation by applying alternating magnetic fields. As soon as the field was switched on, a fast heat development was observed, and for sample S3 (Table 7.2) gelation could be achieved within less than 2 minutes for amplitude field strength of 13

kA/m and higher. The remote heating process can be repeated many times without any detectable changes in the gelation behaviour or magnetic properties.

Acknowledgment

We would like to thank Andreas Walther (Applied Physics, Helsinki University of Technology) and Joachim Schmelz (MCII, University of Bayreuth) for performing TEM experiments, Alexander Wittemann (Physical Chemistry I, University of Bayreuth) for the Zeta potential measurements, and Dmitry Pergushov (Polymer Science, Moscow State University) for helpful discussions. We are indebted to Ingo Rehberg and Reinhard Richter (Experimental Physics V, University of Bayreuth) for providing us with the rheology equipment. Financial support from the German Science Foundation (priority program SPP 1259 and Emmy-Noether-Program) is gratefully acknowledged.

7.5 Supporting Information

Fourier transform infrared spectroscopy (FT-IR)

FT-IR spectra were recorded on a Bruker Equinox 55/S FT-IR spectrometer using the software OPUS ViewerTM 4.2. The measurements were performed with KBr pellets, prepared after grinding a mixture of KBr (Merck) with a small amount of the sample.

The extracted wavenumber region shows four bands of interest (Figure 7.10). The bands at 1630 and 1578 cm^{-1} correspond to quaternized 2VP (q2VP) units, whereas the bands at 1590 and 1568 cm^{-1} are caused by the remaining non-quaternized 2VP units in the P2VP₆₀-*b*-PEO₃₉₈-*b*-P(GME₂₆-*co*-EGE₂₆) triblock terpolymer. The band from the q2VP units at 1630 cm^{-1} is clearly visible for both triblock terpolymers, however, the absorbance at the peak maximum is much higher for the triblock terpolymer being quaternized with Me₂SO₄, indicating a much higher degree of quaternization. In addition, the peak at 1578 cm^{-1} is only detectable when Me₂SO₄ was used for quaternization. Having in mind that the degree of quaternization of the P2VP block being quaternized with MeI was calculated to 20 mol%, by determining the amount of iodide counterions via titration with AgNO₃, we estimate from the FT-NIR spectrum that quaternization with Me₂SO₄ resulted in a degree of quaternization of about 60 mol%.

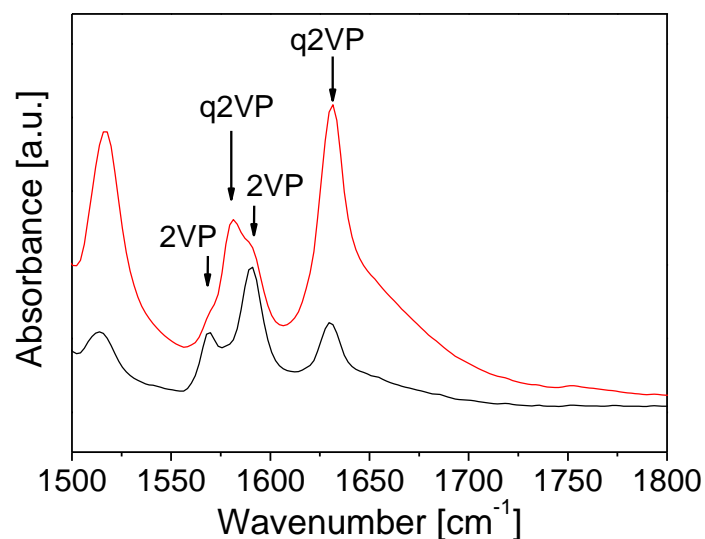


Figure 7.10 FT-IR spectra of Pq2VP₆₀-*b*-PEO₃₉₈-*b*-P(GME₂₆-*co*-EGE₂₆) quaternized with MeI (—) and Me₂SO₄ (—); KBr pellets.

TEM

For the evaluation of the maghemite nanoparticle size, the software Image Tool™ 3.00 (UTHSCSA) was used. The diameter of 150 individual particles was measured and the obtained values were averaged. The mean diameter of the nanoparticles is 8.2 nm with a standard deviation of 2.5.

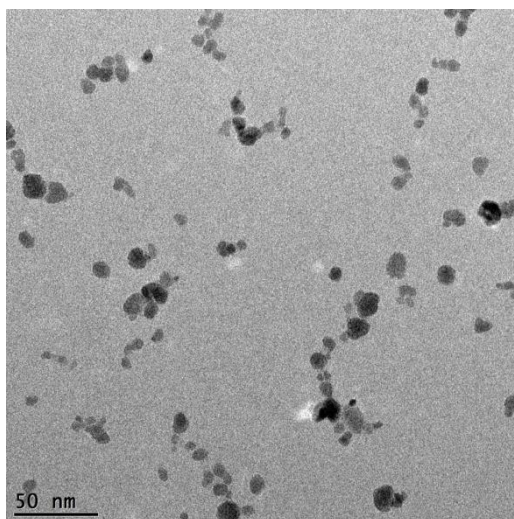


Figure 7.11. TEM image of the pure γ -Fe₂O₃ nanoparticles ($c = 1$ g/L).

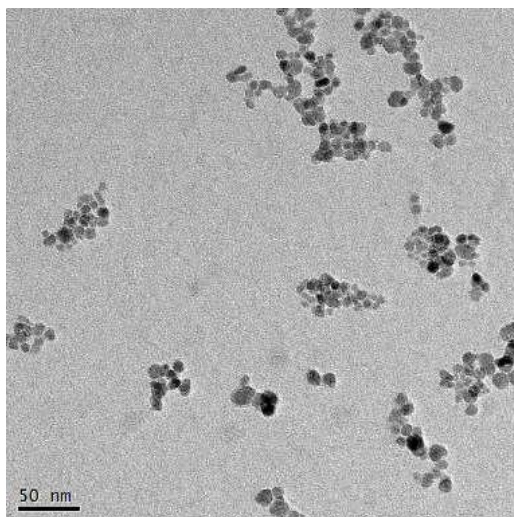


Figure 7.12. TEM image of $\gamma\text{-Fe}_2\text{O}_3/\text{PqP2VP}_{95}\text{-}b\text{-PEO}_{337}\text{-}b\text{-P}(\text{GME}_{21}\text{-}co\text{-EGE}_{21})$ hybrid clusters; degree of quaternization of the P2VP-block: 60 mol% ($c = 1$ g/L; $\gamma\text{-Fe}_2\text{O}_3/\text{polymer} = 65/35$ w/w).

pH dependent DLS

pH dependent light scattering experiments were conducted using the DLS device (see manuscript, Experimental Part) in combination with a titrator (Titrand 809, Metrohm, Herisau, Switzerland). NaOH (1M, Titrisol, Merck) was added in small portions of 2 μL . The equilibration time after each titration step was 3 min. The scattering intensity data presented in Figure 7.13 correspond to a time average of one measurement, conducted for 1 min each. The non-quaternized $\text{P2VP}_{62}\text{-}b\text{-PEO}_{452}\text{-}b\text{-P}(\text{GME}_{36}\text{-}co\text{-EGE}_{36})$ triblock terpolymer shows a strong increase of the scattering intensity at a pH of 5. Below $\text{pH} = 5$, the P2VP block is protonated and therefore hydrophilic, the polymer chains are unimolecularly dissolved. However at a pH higher than 5, P2VP is deprotonated and becomes hydrophobic which causes a formation of core-shell-corona micelles with P2VP in the core.⁵² In the case of the analogue quaternized polymer (degree of quaternization of 20 mol%), no increase in count rate is observed up to a pH of almost 10. In conclusion, a degree of quaternization of 20 mol% is already high enough to render the P2VP block water soluble at any pH.

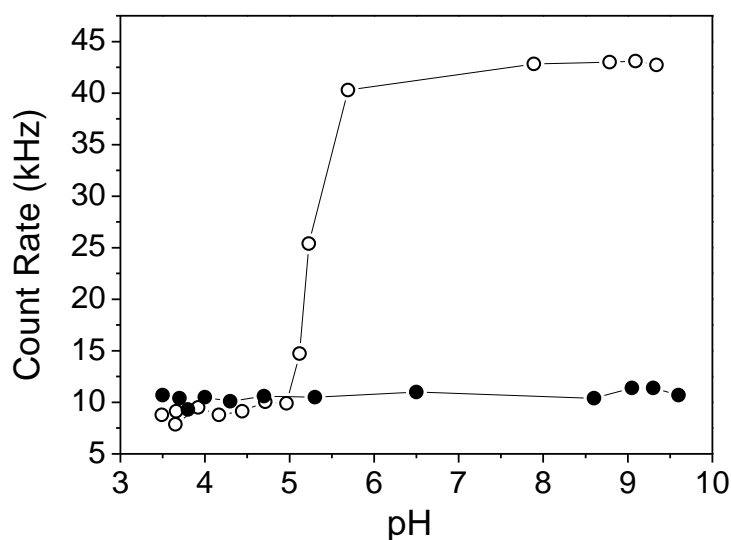


Figure 7.13. pH-dependent scattering intensity of non-quaternized (open symbols)⁵² and quaternized (closed symbols, 20 mol% quaternized q2VP units) P2VP₆₂-*b*-PEO₄₅₂-*b*-P(GME₃₆-co-EGE₃₆) at room temperature (1 g/L, $\theta = 90^\circ$, titer 1M NaOH: stepwise addition of 2 μ L with an equilibration time of 3 min).

Test tube inversion

The phase diagram (Figure 7.14) was constructed applying the test tube inversion method. The samples were heated stepwise (1 $^\circ$ C per step) using a MKR 13 thermomixer (HLC Biotech). After an equilibration time of 2 min per step, the test tubes were taken out of the mixing block, and tilted in order to check whether the samples flow or not. For the highest concentrations, the accuracy of the determined sol-gel transition temperatures is limited due to the already very high viscosity in the fluid state. At temperatures above ca. 70 $^\circ$ C, the samples show a slow phase separation (syneresis) with time (several hours). This is attributed to water getting a bad solvent for PEO at elevated temperatures, and is in accordance with observations on PluronicTM based hydrogels.

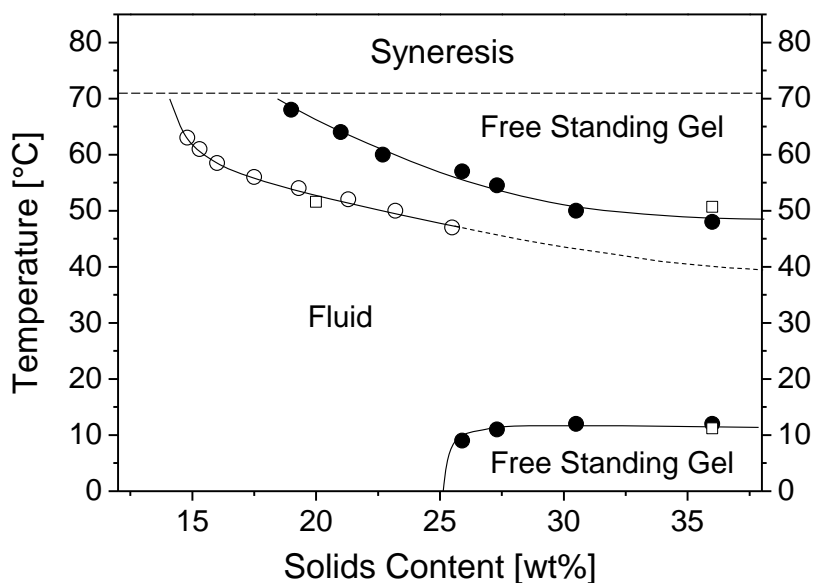


Figure 7.14. Phase diagram of $\gamma\text{-Fe}_2\text{O}_3/\text{TB1}$ (45/55 w/w, closed circles) and $\gamma\text{-Fe}_2\text{O}_3/\text{TB2}$ (30/70 w/w, open circles) mixtures, determined by the test tube inversion method. The open squares correspond to transition temperatures extracted from rheology (temperature at which $G' = G''$).

7.6 References

- [1] Yang, X. Q.; Chen, Y. H.; Yuan, R. X.; Chen, G. H.; Blanco, E.; Gao, J. M.; Shuai, X. *T. Polymer* **2008**, *49*, 3477.
- [2] Dimitrov, I.; Trzebicka, B.; Müller, A. H. E.; Dworak, A.; Tsvetanov, C. B. *Prog. Polym. Sci.* **2007**, *32*, 1275.
- [3] Gil, E. S.; Hudson, S. M. *Prog. Polym. Sci.* **2004**, *29*, 1173.
- [4] Ahn, S.-k.; Kasi, R. M.; Kim, S.-C.; Sharma, N.; Zhou, Y. *Soft Matter* **2008**, *4*, 1151.
- [5] Responsive Gels: Volume Transitions I/II. In *Adv. Polym. Sci.*; Dušek, K., Ed.; Springer: Berlin, 1993; Vol. 109/110.
- [6] Li, C.; Madsen, J.; Armes, S. P.; Lewis, A. L. *Angew. Chem. Int. Ed.* **2006**, *45*, 3510.
- [7] Vogt, A. P.; Sumerlin, B. S. *Soft Matter* **2009**, *5*, 2347.
- [8] Filipcsei, G.; Csetneki, I.; Szilágyi, A.; Zrínyi, M. *Adv. Polym. Sci.* **2007**, *206*, 137.
- [9] Zrínyi, M.; Barsi, L.; Büki, A. *Polym. Gels Netw.* **1997**, *5*, 415.
- [10] Szabo, D.; Szeghy, G.; Zrínyi, M. *Macromolecules* **1998**, *31*, 6541.
- [11] Zrínyi, M. *Colloid Polym. Sci.* **2000**, *278*, 98.
- [12] François, N. J.; Allo, S.; Jacobo, S. E.; Daraio, M. E. *J. Appl. Polym. Sci.* **2007**, *105*, 647.
- [13] Liu, T.-Y.; Hu, S.-H.; Liu, T.-Y.; Liu, D.-M.; Chen, S.-Y. *Langmuir* **2006**, *22*, 5974.

- [14] Huang, L.-Y.; Yang, M.-C. *J. Magn. Magn. Mater.* **2007**, *310*, 2874.
- [15] Liu, T. Y.; Hu, S. H.; Liu, K. H.; Liu, D. M.; Chen, S. Y. *J. Controlled Release* **2008**, *126*, 228.
- [16] Collin, D.; Auernhammer, G. K.; Gavat, O.; Martinoty, P.; Brand, H. R. *Macromol. Rapid Commun.* **2003**, *24*, 737.
- [17] Varga, Z.; Fehér, J.; Filipcsei, G.; Zrínyi, M. *Macromol. Symp.* **2003**, *200*, 93.
- [18] Varga, Z.; Filipcsei, G.; Zrínyi, M. *Polymer* **2006**, *47*, 227.
- [19] Ceylan, S.; Friese, C.; Lammel, C.; Mazac, K.; Kirschning, A. *Angew. Chem., Int. Ed.* **2008**, *47*, 8950.
- [20] Vaishnava, P. P.; Tackett, R.; Dixit, A.; Sudakar, C.; Naik, R.; Lawes, G. *J. Appl. Phys.* **2007**, *102*, 063914/1.
- [21] Lao, L. L.; Ramanujan, R. V. *J. Mater. Sci.: Mater. Med.* **2004**, *15*, 1061.
- [22] Gneveckow, U.; Jordan, A.; Scholz, S.; Brüß, V.; Waldöfner, N. *Med. Phys.* **2004**, *31*, 1444.
- [23] Schmidt, A. M. *J. Magn. Magn. Mater.* **2005**, *289*, 5.
- [24] Dong, H.; Mantha, V.; Matyjaszewski, K. *Chem. Mater.* **2009**, *21*, 3965.
- [25] Schmidt, A. M. *Macromol. Rapid Commun.* **2006**, *27*, 1168.
- [26] Kaiser, A.; Gelbrich, T.; Schmidt, A. M. *J. Phys.: Condens. Matter* **2006**, *18*, S2563.
- [27] Schmidt, A. M. *Colloid Polym. Sci.* **2007**, *285*, 953.
- [28] Mayer, C. R.; Cabuil, V.; Lalot, T.; Thouvenot, R. *Adv. Mater.* **2000**, *12*, 417.
- [29] Xulu, P. M.; Filipcsei, G.; Zrínyi, M. *Macromolecules* **2000**, *33*, 1716.
- [30] Chatterjee, J.; Haik, Y.; Chen, C. J. *Colloid Polym. Sci.* **2003**, *281*, 892.
- [31] Mitsumata, T.; Sakai, K.; Takimoto, J.-I. *J. Phys. Chem. B* **2006**, *110*, 20217.
- [32] Qin, J.; Asempah, I.; Laurent, S.; Fornara, A.; Muller, R. N.; Muhammed, M. *Adv. Mater.* **2009**, *21*, 1354.
- [33] Gelbrich, T.; Feyen, M.; Schmidt, A. M. *Macromolecules* **2006**, *39*, 3469.
- [34] Wang, Y.; Teng, X.; Wang, J.-S.; Yang, H. *Nano Lett.* **2003**, *3*, 789.
- [35] Vestal, C. R.; Zhang, Z. J. *J. Am. Chem. Soc.* **2002**, *124*, 14312.
- [36] Matsuno, R.; Yamamoto, K.; Otsuka, H.; Takahara, A. *Chem. Mater.* **2002**, *15*, 3.
- [37] Schmidt, A. M. *Macromol. Rapid Commun.* **2005**, *26*, 93.
- [38] Chanana, M.; Jahn, S.; Georgieva, R.; Lutz, J.-F.; Bäuml, H.; Wang, D. *Chem. Mater.* **2009**, *21*, 1906.
- [39] Xie, J.; Xu, C.; Kohler, N.; Hou, Y.; Sun, S. *Adv. Mater.* **2007**, *19*, 3163.

- [40] Chen, S.; Li, Y.; Guo, C.; Wang, J.; Ma, J.; Liang, X.; Yang, L. R.; Liu, H. Z. *Langmuir* **2007**, *23*, 12669.
- [41] Ai, H.; Flask, C.; Weinberg, B.; Shuai, X. T.; Pagel, M. D.; Farrell, D.; Duerk, J.; Gao, J. *Adv. Mater.* **2005**, *17*, 1949.
- [42] Kim, B. S.; Qiu, J. M.; Wang, J. P.; Taton, T. A. *Nano Lett.* **2005**, *5*, 1987.
- [43] Lecommandoux, S.; Sandre, O.; Chécot, F.; Rodriguez-Hernandez, J.; Perzynski, R. *Adv. Mater.* **2005**, *17*, 712.
- [44] Lecommandoux, S.; Sandre, O.; Chécot, F.; Perzynski, R. *Prog. Solid State Chem.* **2006**, *34*, 171.
- [45] Herdt, A. R.; Kim, B. S.; Taton, T. A. *Bioconjugate Chem.* **2007**, *18*, 183.
- [46] Zhu, J. T.; Hayward, R. C. *J. Am. Chem. Soc.* **2008**, *130*, 7496.
- [47] Sheparovych, R.; Sahoo, Y.; Motornov, M.; Wang, S.; Luo, H.; Prasad, P. N.; Sokolov, I.; Minko, S. *Chem. Mater.* **2006**, *18*, 591.
- [48] Berret, J. F.; Schonbeck, N.; Gazeau, F.; El Kharrat, D.; Sandre, O.; Vacher, A.; Airiau, M. *J. Am. Chem. Soc.* **2006**, *128*, 1755.
- [49] Lai, J. L.; Hoffman, J. M.; Ebara, M.; Hoffman, A. S.; Estournés, C.; Wattiaux, A.; Stayton, P. S. *Langmuir* **2007**, *23*, 7385.
- [50] Lutz, J.-F.; Stiller, S.; Hoth, A.; Kaufner, L.; Pison, U.; Cartier, R. *Biomacromolecules* **2006**, *7*, 3132.
- [51] Papaphilippou, P.; Loizou, L.; Popa, N. C.; Han, A.; Vekas, L.; Odysseos, A.; Krasia-Christoforou, T. *Biomacromolecules* **2009**, *10*, 2662.
- [52] Reinicke, S.; Schmelz, J.; Lapp, A.; Karg, M.; Hellweg, T.; Schmalz, H. *Soft Matter* **2009**, *5*, 2648
- [53] Massart, R. *C. R. Acad. Sci. Paris, Ser. C* **1980**, *291*, 1.
- [54] Kang, Y. S.; Risbud, S.; Fabolt, J. F.; Stroeve, P. *Chem. Mater.* **1996**, *8*, 2209.
- [55] Toy, A. A.; Reinicke, S.; Müller, A. H. E.; Schmalz, H. *Macromolecules* **2007**, *40*, 5241.
- [56] Provencher, S. W. *Comput. Phys. Commun.* **1982**, *27*, 213.
- [57] Chantrell, R.; Popplewell, J.; Charles, S. *IEEE T. Magn.* **1978**, *14*, 975.
- [58] Berkowitz, A. E.; Schuele, W. J.; Flanders, P. J. *J. Appl. Phys.* **1968**, *39*, 1261.
- [59] Magnetic and Other Properties of Oxides and Related Compounds. In *Landolt-Börnstein, Group III: Crystal and Solid State Physics*; Hellwege, K.-H., Ed.; Springer: Berlin, 1970; Vol. 4a.
- [60] Burchard, W.; Richtering, W. *Prog. Colloid Polym. Sci.* **1989**, *80*, 151.

- [61] Schilli, C. M.; Zhang, M.; Rizzardo, E.; Thang, S. H.; Chong, Y. K.; Edwards, K.; Karlsson, G.; Müller, A. H. E. *Macromolecules* **2004**, *37*, 7861.
- [62] Castelletto, V.; Hamley, I. W.; English, R. J.; Mingvanish, W. *Langmuir* **2003**, *19*, 3229.
- [63] Li, H.; Yu, G.-E.; Price, C.; Booth, C.; Hecht, E.; Hoffmann, H. *Macromolecules* **1997**, *30*, 1347.
- [64] Ogura, M.; Tokuda, H.; Imabayashi, S.-I.; Watanabe, M. *Langmuir* **2007**, *23*, 9429.
- [65] Prud'homme, R. K.; Wu, G.; Schneider, D. K. *Langmuir* **1996**, *12*, 4651.
- [66] Vamvakaki, M.; Papoutsakis, L.; Katsamanis, V.; Afchoudia, T.; Fragouli, P. G.; Iatrou, H.; Hadjichristidis, N.; Armes, S. P.; Sidorov, S.; Zhurov, D.; Zhurov, V.; Kostylev, M.; Bronstein, L. M.; Anastasiadis, S. H. *Faraday Discuss.* **2005**, *128*, 129.
- [67] Winter, H. H.; Mours, M. *Adv. Polym. Sci.* **1997**, *134*, 165.
- [68] Barbosa, S.; Cheema, M. A.; Taboada, P.; Mosquera, V. *J. Phys. Chem. B* **2007**, *111*, 10920.
- [69] Hamley, I. W. *Phil. Trans. R. Soc. Lond. A* **2001**, *359*, 1017.
- [70] Jones, J. L.; McLeish, T. C. B. *Langmuir* **1995**, *11*, 785.
- [71] Kossuth, M. B.; Morse, D. C.; Bates, F. S. *J. Rheol.* **1999**, *43*, 167.
- [72] Chambon, F.; Winter, H. H. *J. Rheol.* **1987**, *31*, 683.
- [73] Richtering, H. W.; Gagnon, K. D.; Lenz, R. W.; Fuller, R. C.; Winter, H. H. *Macromolecules* **1992**, *25*, 2429.
- [74] Hergt, R.; Hiergeist, R.; Zeisberger, M.; Glöckl, G.; Weitschies, W.; Ramirez, L. P.; Hilger, I.; Kaiser, W. A. *J. Magn. Magn. Mater.* **2004**, *280*, 358.
- [75] Ramanujan, R. V.; Ang, K. L.; Venkatraman, S. *J. Mater. Sci.* **2009**, *44*, 1381.
- [76] Schexnailder, P.; Schmidt, G. *Colloid Polym. Sci.* **2009**, *287*, 1.
- [77] He, C.; Kim, S. W.; Lee, D. S. *J. Controlled Release* **2008**, *127*, 189.
- [78] Yu, L.; Ding, J. *Chem. Soc. Rev.* **2008**, *37*, 1473.
- [79] Suzuki, H. *J. Intel. Mat. Syst. Str.* **2006**, *17*, 1091.

8 Appendix

8.1 Thermo-sensitive polymers with tunable LCST based on modified polyglycidol

In chapter 4 and 5, the synthesis of triblock terpolymers, containing P2VP, PEO and a polyglycidol derivative, was presented. The chosen monomer sequence, a vinyl monomer for the starting block and two epoxide monomers for the second and the third block, respectively, provided the opportunity to perform the whole synthesis in a one-pot reaction. Since the C block was further supposed to be thermo-sensitive, the choice of monomer was limited to two possibilities, one of which included the glycidyl ethers GME and EGE, as presented in chapter 5. Another approach however, which I followed in the beginning of my work, dealt with modified polyglycidol (PG).

The pendant OH-groups of PG can be transferred into ester or carbamate groups by treating the polymer with anhydrides or isocyanate compounds, according to the procedures described by Dworak et al.^{1,2} The reaction schemes are shown in Figure 8.1.

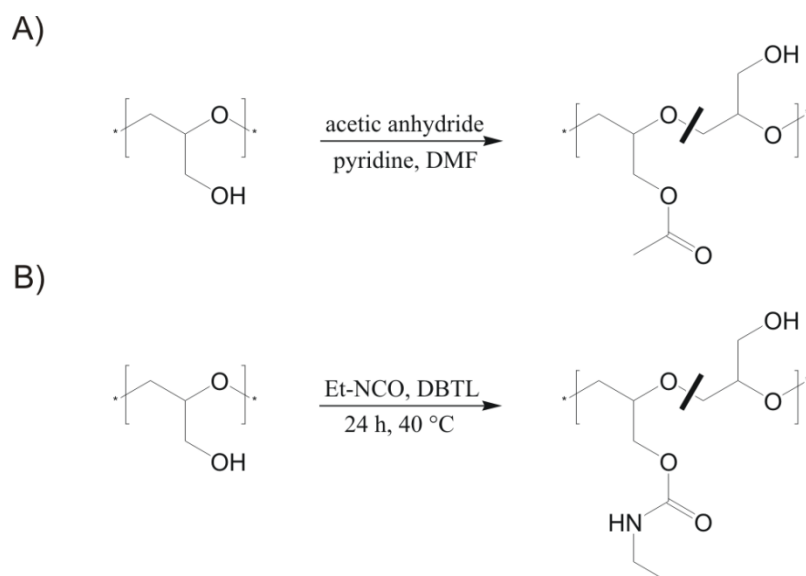


Figure 8.1. Reaction scheme of the modification of polyglycidol with A) acetic anhydride and B) ethyl isocyanate.

The resulting polymers are statistical copolymers composed of hydrophilic glycidol and hydrophobic glycidyl ester or carbamate units. The fraction of hydrophobic groups can be controlled simply by the relative amount of anhydride or isocyanate used. Since the ester

groups were reported to be prone to hydrolysis under acidic conditions¹, I was focusing on the modification of polyglycidol with ethyl isocyanate.

The reaction was carried out in dry DMF. After dissolution of the polymer precursor, addition of dibutyl tin dilaurate (DBTL) and degassing by purging with nitrogen, the desired amount of ethyl isocyanate was added. The solution was kept at 40 °C for 24 h. After that, the polymer was precipitated into cold diethyl ether and dried under reduced pressure. The extent of modification was determined by ¹H-NMR spectroscopy. Figure 8.2 shows the fraction of carbamate groups of a modified homo-PG (3000 g/mol) and the modified PG block of a P2VP₂₇-*b*-PEO₁₆₆-*b*-PG₂₆ triblock terpolymer, in dependence of the used amount of isocyanate and DBTL. It occurred that the degree of modification can indeed easily be controlled by the composition of reaction mixture in both cases.

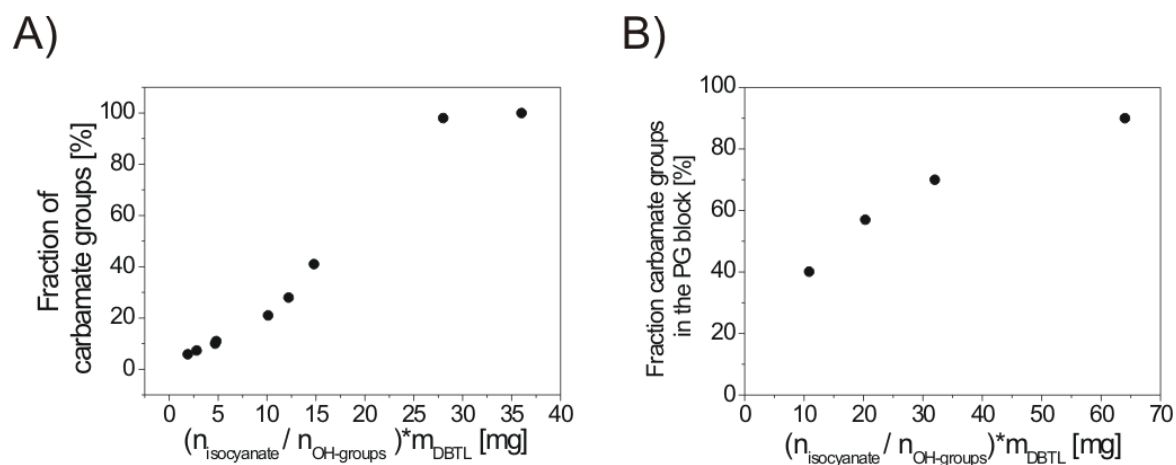


Figure 8.2. Fraction of carbamate groups in A) modified homo-PG (3000 g/mol) and B) the modified PG block of a P2VP₂₇-*b*-PEO₁₆₆-*b*-PG₂₆ triblock terpolymer; the carbamate fractions were determined via ¹H-NMR spectroscopy.

The modified homo-PG's were dissolved in Millipore water and the transmittance in dependence on temperature was monitored. Figure 8.3A shows, that the cloud point depends strongly on the degree of modification. On the other hand, each coil-to-globule transition appeared to be rather broad, as shown in Figure 8.3B. For most applications however, a sharp and quick transition is favored.

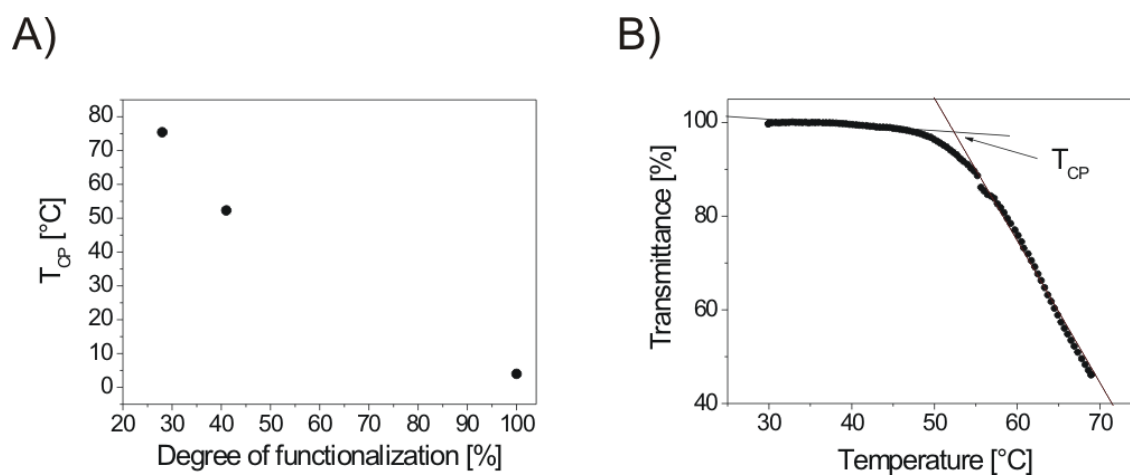


Figure 8.3. A) Dependence of the cloud point of an aqueous solution of modified PG (3000 g/mol) on the degree of modification, $c = 2.5$ g/L; B) Transmittance of an aqueous solution of modified PG in dependence on temperature, degree of modification: 40 %, $c = 2.5$ g/L, heating rate: 1 K/min.

The much better performance of PGME and PEGE with respect to thermo-sensitivity and the fact, that the deprotection and modification of the PG block basically means two more steps to be accomplished, made me finally decide to utilize GME and EGE for our hydrogel concept.

- [1] Jamróz-Piegza, M.; Utrata-Wesolek, A.; Trzebicka, B.; Dworak, A. *Eur. Polym. J.* **2006**, *42*, 2497.
- [2] Dworak, A.; Trzebicka, B.; Utrata, A.; Walach, W. *Polym. Bull.* **2003**, *50*, 47.

8.2 List of publications

Scientific journals

1. Ah Toy, A.; Reinicke, S.; Schmalz, H.; Müller, A. H. E.
One-pot synthesis of polyglycidol containing block copolymers with alkyllithium initiators using the phosphazene base *t*-BuP₄, *Macromolecules* **2007**, *40*, 5241-5244.
2. Reinicke, S.; Schmelz, J.; Schmalz, H.
pH- and Temperature-Sensitive Hydrogels Based on Triblock Terpolymers, *Polymer preprints (American Chemical Society, Division Polymer Chemistry)* **2008**, *49*, 459-460.
3. Joso, R.; Reinicke, S.; Walther, A.; Schmalz, H.; Müller, A. H. E.; Barner, L.
Facile Access to Hydroxy-Functional Core-Shell Microspheres via Grafting of Ethylene Oxide by Anionic Ring-Opening Polymerization, *Macromolecular Rapid Communications* **2009**, *30*, 1009-1014.
4. Reinicke, S.; Schmelz, J.; Lapp, A.; Karg, M.; Hellweg, T.; Schmalz, H.
Smart Hydrogels Based on Double Responsive Triblock Terpolymers, *Soft Matter*, **2009**, *5*, 2648-2657.
5. Plamper, F. A.; Reinicke, S.; Elomaa, M.; Schmalz, H.; Tenhu, H.
Pearl Necklace Architecture: Novel Threaded Star-Shaped Copolymers, *Macromolecules* **2010**, *43*, 2190-2203.
6. Reinicke, S.; Döhler, S.; Tea, S.; Krekhova, M.; Messing, R.; Schmidt, A. M.; Schmalz, H.
Magneto-responsive hydrogels based on maghemite/triblock terpolymer hybrid micelles, *Soft Matter* **2010**, *6*, 2760-2773.
7. Reinicke, S.; Karg, M.; Lapp, A.; Heymann, L.; Hellweg, T.; Schmalz, H.
Flow induced ordering in cubic gels formed by P2VP-*b*-PEO-*b*-P(GME-*co*-EGE) triblock terpolymer micelles: A rheo-SANS study, *Macromolecules* **2010**, *43*, 10045-10054.
8. Reinicke, S.; Schmalz, H.
Combination of living anionic polymerization and ATRP via “click” chemistry as a versatile route to multiple responsive triblock terpolymers and corresponding hydrogels, *Colloid and Polymer Science* **2011**, in print, DOI:10.1007/s00396-010-2359-7.

9. Karg, M.; Reinicke, S.; Lapp, A.; Hellweg, T.; Schmalz, H. Temperature-dependent gelation behaviour of double responsive P2VP-*b*-PEO-*b*-P(GME-*co*-EGE) triblock terpolymers: A SANS study, *Macromolecular Symposia* **2011**, accepted.

Book sections

1. Schacher, F.; Reinicke, S.; Walther, A.; Schmalz, H.; Müller, A. H. E. New Amphiphilic Nanostructures Based on Block Terpolymers Made by Anionic Polymerization in E. Khosravi, Y. Yagci, Eds.: *New Smart Materials via Metal Mediated Macromolecular Engineering: From Complex to Nano Structures*, NATO Science for Peace and Security Series, Springer, Dordrecht, 167, ISBN 978-90-481-3276-8, **2009**.

8.3 Contributions to national and international conferences

1. 18th IUPAC INTERNATIONAL SYMPOSIUM ON IONIC POLYMERIZATION, Kloster Banz, Germany, Sept. 2007;
Poster presentation: "Synthesis of Triblock Terpolymers Containing Glycidol and Derivatives"
2. 3rd STIPOMAT CONFERENCE, Les Diablerets, Switzerland, Oct. 2007;
Poster presentation: "Synthesis and Characterization of Stimuli Responsive Triblock Terpolymers based on Polyglycidol and its Derivatives"
3. BIOPOLYSURF – INTERNATIONAL JOINT MEETING – POLYAMPHI - BIOSONS, Biarritz, France, Feb. 2008;
Poster presentation: "Synthesis of Triblock Terpolymers Containing Glycidol and Derivatives"
4. POLYMER NETWORKS GROUP CONFERENCE, Larnaca, Cyprus, June 2008;
Poster presentation: "'Smart' Hydrogels based on Stimuli Responsive Tris-Hydrophilic Triblock Terpolymers"
5. 236th ACS NATIONAL MEETING, Philadelphia, USA, Aug. 2008;
Oral presentation: "pH- and Temperature Sensitive Hydrogels based on Triblock Terpolymers"
6. BIO & POLYMERS - BIENNIAL MEETING OF THE GDCh DIVISION MACROMOLECULAR CHEMISTRY, Aachen, Germany, Sept. 2008;
Poster presentation: "'Smart' Hydrogels based on Stimuli Responsive Trishydrophilic Triblock Terpolymers"
7. FRONTIERS IN POLYMER SCIENCE SYMPOSIUM, Mainz, Germany, June 2009;
Poster presentation: "'Smart' Hydrogels based on Tris-Hydrophilic Triblock Terpolymers: Structural Aspects"
8. 23rd CONFERENCE of the ECIS, Antalya, Turkey, Sept. 2009;
Oral presentation: "'Smart' Hydrogels Based on Double-Responsive Triblock Terpolymers"
9. MAKROMOLEKULARES KOLLOQUIUM 2010, Freiburg, Germany, Feb. 2010;
Poster presentation: "'Smart' Hydrogels Based On Double-Responsive Triblock Terpolymers"

10. 43rd WORLD POLYMER CONGRESS, Glasgow, UK, July 2010;
Poster presentation: “Magneto-responsive Hydrogels based on Maghemite/Triblock Terpolymer Hybrid Micelles”

Glossary

$\overrightarrow{\Delta v}$	shear gradient direction	d_{hkl}	distance between neighboring reticular planes
\vec{e}	vorticity vector	Dithranol	1,8,9-Trihydroxyanthracene
\vec{v}	shear direction	DLS	dynamic light scattering
$\dot{\gamma}$	shear rate	DMAc	Dimethyl acetamide
$ \eta ^*$	magnitude of complex viscosity	DP	degree of polymerization
$[A]_0$	initial concentration of compound A	DPE	diphenyl ethylene
A	peak area	DPMPLi	1,1-Diphenyl-3-methyl pentyllithium
AC	alternating current	$D_T; D_R$	translation; rotational diffusion coefficient
AF4	Assymetric flow field flow fractionation	d_v	volume average particle diameter
app.	apparent	E	energy
ATRP	atom transfer radical polymerization	EBiB	ethyl 2-bromoisobutyrate
bcc	body centered cubic	EEGE	1-ethoxyethyl glycidyl ether
BuLi	butyllithium	EGE	ethyl glycidyl ether
c_p	heat capacity	Et_3Al	triethyl aluminium
(cryo-)TEM	(cryogenic) transmission electron microscopy	F	fineman ross coefficient; Form factor
CSC	core-shell-corona	f	fineman ross coefficient; frequency
CSR	shear rate controlled mode	fcc	face centered cubic
CSS	stress controlled mode	FT-(N)IR	fourier transform – (near) infrared
DA	Diels-Alder	g	Autocorrelation function
DC	direct current		
DHB	dihydroxy benzoic acid		

G(Γ)	decay rate distribution function	$\text{Me}^{\text{II}}\text{Fe}^{\text{III}}_2\text{O}_4$	mixed ferrite
G*	complex shear modulus	$M_n; M_w$	number average; weight average molecular weight
G'	storage modulus	MWCO	molecular weight cutoff
G''	loss modulus	NaNDS	sodium 2,6-naphthalene disulfonate
G ₀	equilibrium modulus	NMP	nitroxide mediated polymerization; N-methyl pyrrolidone
GME	glycidyl methyl ether		
H	magnetic field strength		
h, k, l	Miller indices	NMR	nuclear magnetic resonance
HF-MC	high frequency magneto-calorimetry	P(M)AA	poly(meth)acrylic acid
HMTETA	N,N,N',N'',N''',N''''-hexamethyltriethylene tetraamine	P(q), K, F ²	form factors
I	intensity; initiator	P2VP	poly(2-vinylpyridine)
k	Boltzmann constant	P4VP	poly(4-vinylpyridine)
L	ligand	PAGE	poly(alkylglycidyl ether)
LCST	lower critical solution temperature	PB	polybutadiene
m	magnetic moment of a single nanoparticle	PBO	poly(butylene oxide)
M	monomer	PCL	poly(ϵ -caprolactone)
M _(s)	(saturation) magnetization	PDEAAm	poly(diethyl acrylamide)
MALDI-ToF MS	matrix assisted laser desorption ionization - time of flight mass spectrometry	PDEAEMA	poly(diethylaminoethyl methacrylate)
MALLS	multi-angle laser light scattering	PDI	polydispersity index
Me ₂ SO ₄	dimethyl sulfate	PDMAEMA	poly(dimethylaminoethyl methacrylate)
MeI	methyl iodide	PDMS	poly(dimethyl siloxane)
		PEO	poly(ethylene oxide)
		PEP	poly(ethylene- <i>co</i> -propylene)
		P_f	frequency-normalized heat power
		PG	polyglycidol

PGMA	poly(glycerol methacrylate)	R_g	radius of gyration
PHEMA	poly(hydroxyethyl methacrylate)	R_h	hydrodynamic radius
PI	polyisoprene	RI	refractive index
pK_S ; pK_B	negative, decadic logarithm of acid dissociation constant K_S and base dissociation constant K_B	RO(M)P	ring opening (methathesis) polymerization
PMDETA	N,N,N',N'',N'''-pentamethyl diethylene triamine	S	stimulus
PMEO _x MA	poly(methoxyethoxyethyl methacrylate)	S(q)	structure factor
PMMA	poly(methyl methacrylate)	SANS	small angle neutron scattering
PnB(M)A	poly(n-butyl(meth)acrylate)	SAXS	small angle x-ray scattering
PNIPAAm	poly(N-isopropyl acrylamide)	sc	simple cubic
POEGMA	poly[oligo(ethylene glycol) methacrylate]	SEC	size exclusion chromatography
Pox	polyoxazoline	SHP	specific heat power
PPO	poly(propylene oxide)	$\tan\delta$	loss factor
Pq2VP	poly(2-vinylpyridine-co-2-N-methyl-2-vinylpyridinium iodide)	<i>t</i> -BuOH	<i>tert.</i> -butanol
PS	polystyrene	<i>t</i> -BuOK	potassium <i>tert.</i> -butoxide
PVA	poly(vinyl alcohol)	<i>t</i> -BuOLi	lithium <i>tert.</i> -butoxide
PVE	poly(vinyl ether)	<i>t</i> -BuP ₄	phosphazene base
q	scattering vector	T _{CP}	cloud point
R	core radius	TEA	triethyl amine
r	reactivity ratio	TGA	thermogravimetric analysis
RAFT	reversible addition fragmentation chain transfer polymerization	THF	tetrahydrofuran
		<i>u</i>	electrophoretic mobility
		UCST	upper critical solution temperature
		VSM	vibrating sample magnetometry

X_A, x_A	molar fraction of compound A	μ_0	permeability of space
x_p	conversion	μ_M	mass fraction of maghemite particles
Γ	decay rate	v_M	maghemite content
δ	phase angle	ρ	density; shape factor; scattering length density
$\epsilon_0\epsilon$	solution permittivity	τ	shear stress
ζ	zeta-potential	Φ	azimuthal angle
$\eta_{(0)}$	(zero shear) viscosity	ω	angular frequency
θ	scattering angle		
λ	wavelength		

Acknowledgements

I would like to make use of this occasion to thank a huge number of people who provided me with support during the last three and a half years of scientific research.

First of all, I have to thank my supervisor and “Doktorvater” Prof. Axel Müller for giving me the opportunity to work in MCII. I appreciate his kindness and patience and want to thank him further for giving me numerous useful tips, contributing to the success of my research efforts. I further have to mention the generous funding for visits of national and international conferences at which I could present my research results.

I am strongly indebted to Dr. Holger Schmalz, who was contributing strongly to the success of my research. He invested a lot of time for discussions and reviewing manuscripts and posters. During my research, I had to deal a lot with the polymerization of ethylene oxide, which required a special care and lab equipment. I want to thank Holger for guiding me in the handling of ethylene oxide especially in the beginning of my thesis. I finally want to thank him for his patience and the nice working atmosphere.

I want to thank Dr. Felix Schacher and Dr. Andreas Walther for discussions, useful tips and for spending time on TEM measurements. Special thanks to Felix for the introduction to anionic polymerization techniques, the nice music in the lab and for his patience regarding the mess around him. I am sorry ;-)

I also appreciate the support from Dr. Jiayin Yuan. He was also involved in many discussions and gave the incentive to introduce “click” chemistry for the synthesis of ABC triblock terpolymers. Besides, he was always spreading a good mood in the lab.

I further want to thank Dr. Felix Plamper for discussions and especially for taking the time to review manuscripts, even when being very busy. I also want to thank him for the great time I had when I visited him in Helsinki. His kindness and hospitality are legendary.

I acknowledge the contributions given by our collaborators Prof. Thomas Hellweg and Prof. Annette Schmidt. Special thanks to Dr. Matthias Karg for his support in all SANS-related aspects and for the nice atmosphere during our stay in Saclay. I also want to thank Renate Messing for her efforts on the ferrogel part.

I want to thank Prof. Ingo Rehberg and Dr. Reinhard Richter for providing rheology equipment and Dr. Jerome Crassous for showing me how to use the rheometer.

Special thanks also to the following people:

Gaby Oliver for dealing with all bureaucratic things, Joachim Schmelz and Stefan Döhler, who were strongly contributing to the success of my research within their lab courses, Sabine Wunder and Marietta Böhm for SEC measurements, Dr. Markus Drechsler for cryo-TEM measurements and TEM related discussions and Alexander Schmalz and André Gröschel for support in all ATRP related questions.

I surely don't want to forget the rest of the recent and former MCII members and guests: Dr. Markus Burkhardt, Markus Ruppel, Dr. Manuela Schumacher, Dr. Youyong Xu, Pierre Millard, Sergey Nosov, Evis Penott-Chang, Prof. Alexander Yakimansky, Dr. Dmitry Pergushov, Dr. Anja Goldmann, Karina Möller, Jeannine Rockser, Dr. Girish Behera, Dr. Saikat Mandal, Bing Fang, Dr. Anuj Mittal, Hans-Joachim Voigtländer, Dr. Weian Zhang, Stephan Weiß, Thomas Ruhland (thank you for joining the coffee breaks), Dr. Jie Kong, Alexander Majewski, Andreas Hanisch, Melanie Förtsch, Annika Pfaffenberger, Kerstin Küspert, Christopher Synatschke, Markus Müllner, Annette Krökel, Eva Betthausen, Susanne Edinger, André Pfaff, Sandrine Tea, Dr. Michael Witt, Raymond Joso, Shohei Ida, Andrew Ah Toy, Darkeyah Reuven, Dr. Hülya Arslan, Matt Hunley, Anthony Granville, Sylvain Catrouillet, Meirav Ben-Lulu and Dr. Petar Petrov. Thank you for the nice working atmosphere, for numerous BBQ's and cake sessions, after-work-beers and for the endless number of Ossi-related jokes ;-)

Many thanks also to all people who are involved in the Chemiker Spaßgesellschaft CSG e.V. You have strongly contributed to the fact that I will remember the time in Bayreuth as a very nice one. I am convinced that the future CSG activities will motivate me to come back to Bayreuth once in a while.

I finally want to thank Andrea Wolf for resisting the musical torture in the lab ;-)

For financial support, I do appreciate the funding of the Deutsche Forschungsgemeinschaft (DFG) within the priority program SPP 1259 "Smart" Hydrogels.

Last but not least, I owe thousand thanks to Carina and my family who were supporting me throughout the whole time I spent in Bayreuth and helped me a lot to relax, when times were

Acknowledgements

tough. Thanks also to my friends from Halle. I am pleased that we managed to stay in touch throughout the last four years.

Erklärung

Die vorliegende Arbeit wurde von mir selbstständig verfasst und ich habe dabei keine anderen als die angegebenen Hilfsmittel und Quellen benutzt.

Ferner habe ich nicht versucht, anderweitig mit oder ohne Erfolg eine Dissertation einzureichen oder mich der Doktorprüfung zu unterziehen.

Bayreuth, den 28.09.2010



Stefan Reinicke